UDELAR FQ FACULTAD DE QUIMICA

UNIVERSIDAD DE LA REPÚBLICA URUGUAY

PEDECIBA MEC-UDELAR

Caracterización del tegumento de *Echinococcus granulosus* y su interacción con el sistema inmune del hospedero.

Lic. SEBASTIÁN MILES

Tesis de Doctorado

Presentada como uno de los requisitos para el título de

DOCTOR EN QUÍMICA

Programa de posgrado en Química de la Facultad de Química

Universidad de la República

Programa de Desarrollo de Ciencias Básicas

Junio 2022

Caracterización del tegumento de *Echinococcus granulosus* y su interacción con el sistema inmune del hospedero.

Tribunal:

Dra. Margot Paulino

Dr. Alejandro Chabalgoity

Dr. Uriel Koziol

Dr. Gustavo Mourglia-Ettlin

Director de Tesis

Dra. Sylvia Dematteis

Directora Académica

Tu creíste que volar era imposible, pero…

Pero todo lo que se diga antes de un "pero" no sirve

José "Piezas" Sánchez

AGRADECIMIENTOS

La realización de esta tesis ha requerido la integración de varios proyectos distintos, cada uno interactuando con muchas personas que han sido fundamentales para la finalización de la misma. Por ello, quiero manifestar mi mayor agradecimiento a cada uno:

En primer lugar, a Gus y Sylvia, por la oportunidad que me han brindado, y su rol fundamental como guía en mi formación. Además, quiero agradecer en particular el permitirme desarrollar actividades fuera de lo planeado, en ámbitos desconocidos para el grupo y mantenerse a la par con mis intereses, y sobre todo su fe en mis decisiones.

A Freddy y Marek, por invitarme y recibirme en Heidelberg, y no solo enseñarme de microscopía, sino permitirme desarrollar un proyecto tan distinto a su tema de trabajo. Agradecer también a la colaboración establecida entre los grupos de trabajo, y el futuro de la misma.

A Madelón y Rosario, por sus conocimientos de espectrometría de masas, y su confianza puesta en mi para el uso de sus equipos. A su vez por su disposición para discutir resultados e ideas, y permitirnos desarrollar una nueva línea de trabajo.

A Euge y Marce, por su disposición para la discusión de resultados, y bajarnos a tierra.

A los integrantes de la “casita de adelante”, los que están y los que han pasado. Así también como al resto de los integrantes del Laboratorio de Inmunología.

A las agencias financiadoras que han contribuido en el desarrollo de esta tesis: PEDECIBA, CSIC, ANII, CAP, SIN, Boehringer Ingelheim, Intarnational Union of Immunolgical Societies, German Academic Exchange Service y Burroughs Wellcome Fund.

Un enorme agradecimiento a mi familia, por su trabajo en silencio y sus palabras de aliento.

Un especial agradecimiento a Vero, por acompañarme a lo largo de todo este proceso, por motivarme en los malos momentos, y obligarme a disfrutar de los buenos.

Al resto de las personas que se están quedando en el tintero, por su servicio en la sombra.

Caracterización del tegumento de *Echinococcus granulosus* y su interacción con el sistema inmune del hospedero.

Sebastián Miles, Lic.

Programa de posgrado en Química de la Facultad de Química

Universidad de la República

Programa de Desarrollo de Ciencias Básicas

2022

Director de Tesis: Dr. Gustavo Mourglia-Ettlin

Directora Académica: Dra. Sylvia Dematteis

Departamento de Biociencias, Área Inmunología

Facultad de Química, Universidad de la República

RESUMEN

La equinococosis quística, o hidatidosis, es la zoonosis causada por el cestodo parásito *Echinococcus granulosus sensu lato* (s.l.). En hospederos intermediarios, se ha sugerido que la calidad de la respuesta de anticuerpos sería relevante en los fenómenos de resistencia y/o susceptibilidad a la infección. En este sentido, respuestas inmunes direccionadas hacia determinados antígenos parasitarios podrían ofrecer altos niveles de protección. Por ello, nos planteamos identificar antígenos protectores presentes en el tegumento de los protoscoleces de *E. granulosus* s.l. y diseñar péptidos derivados de los mismos como candidatos vacunales. Sin embargo, dada la escasa información disponible sobre aspectos básicos de la biología y bioquímica del parásito necesarios para cumplir con nuestro objetivo, realizamos en primer lugar, una caracterización del tegumento para luego utilizar dicha información como base del diseño vacunal. En este sentido, describimos al tegumento no solo como una barrera física frente a los componentes celulares y solubles del sistema inmune del hospedero, sino también como una estructura que participa activamente en la interacción con su sistema inmune; ya sea mediante procesos de detoxificación, de respuesta al estrés, de liberación de componentes inmunomoduladores y/o de excreción de vesículas extracelulares. Por otro lado, caracterizamos la respuesta inmune humoral desarrollada naturalmente por los ratones C57Bl/6, la cual es capaz de limitar el establecimiento de la infección. Así, mostramos que una respuesta de anticuerpos direccionada hacia un repertorio limitado de antígenos parasitarios, con una alta producción de anticuerpos IgG2a/c e IgG2b, es capaz de inducir la muerte parasitaria. A partir de estos resultados, identificamos siete de los antígenos parasitarios potencialmente protectores, y diseñamos *in silico* seis péptidos derivados de ellos como candidatos vacunales. Dos de estos péptidos mostraron la capacidad de inducir anticuerpos específicos con actividad anti-parasitaria *in vitro*, así como de generar niveles significativos de protección en el modelo murino de infección secundaria.

Characterization of the tegument in *Echinococcus granulosus* and its interaction with the host immune system.

Sebastian Miles, Lic.

Graduate Program in Chemistry, Facultad de Química

Universidad de la República

Programa de Desarrollo de Ciencias Básicas

2022

DIRECTORS: Dr. Gustavo Mourglia-Ettlin & Dra. Sylvia Dematteis

Departamento de Biociencias, Área Inmunología

Facultad de Química, Universidad de la República

ABSTRACT

Cystic echinococcosis, also known as hydatidosis, is a zoonotic infectious disease caused by the cestode parasite *Echinococcus granulosus sensu lato* (s.l.). In intermediate hosts, the quality of the antibody response has been suggested to be involved in the host resistance/susceptibility to the infection. In this sense, an immune response directed towards specific parasite antigens could offer high levels of protection. The main aim of the present thesis was to identify potentially protective antigens present on the tegument of protoscoleces from *E. granulosus* s.l., and to design peptides derived from such antigens as potential peptide-based vaccine candidates. However, due to the scarce information available regarding basic aspects of *E. granulosus* s.l. biology and biochemistry, we firstly performed an in-depth characterization of the tegument in protoscoleces, and then used the obtained information as a starting point for our vaccine development. In this sense, we described the tegument not only as a physical barrier against cellular and soluble components of the host immune system, but also as a structure actively involved in the interaction with the host. This interaction can be mediated through detoxification processes, stress-induced responses, release of immunomodulating components, and/or excretion of extracellular vesicles. With these results in mind, we then characterized an effective humoral response (naturally developed in infected C57Bl/6 mice) able to limit the infection establishment. In this sense, we showed that an antibody response directed towards a limited number of key tegumental antigens, and with a significant production of IgG2a/c and IgG2b antibodies, could induce the parasite death. Moreover, we identified seven potentially protective parasite antigens, and designed six peptides as vaccine candidates. Two of such peptides were able to induce specific antibodies with high anti-parasite activity *in vitro*, as well as to generate significant levels of protection in the murine model of secondary infection.

ÍNDICE

LISTA DE ABREVIATURAS

2DE: Electroforesis bidimensional en geles de SDS-PAGE

AgB: Antígeno B

CDC: *Centers for Disease Control and Prevention*

DRP: Proteína reconocida diferencialmente

EQ: Equinococosis quística

EV: Vesícula extracelular

FABP: Fatty acid binding protein

GO: Ontología de genes (del inglés: *Gene Ontology*)

GST1: Glutatión-S-transferasa 1

HPF: Congelación a alta presión (del inglés: *High Pressure Freezing*)

inmunoTEM: Microscopía electrónica de transmisión con inmuno-marcación

m/z: Relación masa-carga

MHC: Complejo mayor de histocompatibilidad

NTD: Enfermedad tropical desatendida (del inglés: *Neglected Tropical Disease*)

OMS: Organización mundial de la salud

PSC: Protoscolex

PTM: Modificación post-traduccional (del inglés: *Post-translational Modification*)

s.l.: *sensu lato*

s.s.: *sensu stricto*

SEM: Microscopía electrónica de barrido

SERPA: Análisis proteómico de serología (del inglés: Serological proteome analisis)

SSS: Similitud de estructura secundaria

TEM: Microscopía electrónica de transmisión

tomoEM: Tomografía electrónica

TSS: Similitud de estructura terciaria

TVB: Cuerpo tegumentario vesiculado (del inglés: *Tegumental Vesicular Body*)

CAPÍTULO 1
INTRODUCCIÓN

Las Enfermedades Tropicales Desatendidas (NTD, del inglés *Neglected Tropical Diseases*) son un grupo de diversas enfermedades que afectan en su mayoría a regiones en desarrollo como África, Asia y América del Sur (Hotez et al., 2011). Estas enfermedades pueden ser causadas por virus y bacterias, aunque en su mayoría son enfermedades parasitarias. Los helmintos parásitos son un grupo diverso y complejo de metazoarios que viven y se alimentan dentro de sus hospederos (Hotez et al., 2008).

El término helminto no tiene un valor taxonómico, ya que, si bien los organismos que lo componen comparten características morfológicas, estas no están necesariamente relacionadas a nivel evolutivo. Sin embargo, todos los helmintos parásitos son capaces de generar infecciones crónicas en sus hospederos naturales específicos, llevando a una clasificación en filos basada en la morfología externa, ciclo de vida, hospederos y órganos que infectan (Gazzinelli-Guimaraes & Nutman, 2018). Muchas de estas helmintiasis (infecciones causadas por helmintos) afectan a animales de producción, generando grandes pérdidas en áreas productivas, siendo varias de ellas enfermedades zoonóticas donde el humano es un hospedero natural o accidental. Actualmente, se estima que las helmintiasis afectan a 1 de cada 4 individuos en el planeta (Hotez et al., 2008).

1.1. *Echinococcus granulosus* y equinococosis quística.

1.1.1. *Echinococcus granulosus*: El parásito.

Echinococcus granulosus es un parásito cestodo de gran importancia para la salud humana y animal, ya que es el agente etiológico de una de las 20 NTDs listadas por la

Organización Mundial de la Salud. La infección causada por este parásito es una zoonosis cosmopolita denominada equinococosis quística (EQ) o hidatidosis (Cucher et al., 2015).

El ciclo de vida de *E. granulosus* requiere de dos hospederos mamíferos diferentes (Figura 1). El hospedero definitivo siempre es un carnívoro (principalmente perros) que se infecta al ingerir vísceras contaminadas, desarrollando el gusano adulto en su intestino delgado. Este gusano se reproduce de forma sexuada produciendo huevos -conteniendo las oncósferas- que son expulsados junto a las heces. Las oncósferas, al ser ingeridas por un hospedero intermediario (ungulados domésticos y salvajes), pueden generar una infección crónica que se manifiesta en forma de quiste unilocular de crecimiento lento pero constante (Thompson & Lymbery, 1995). Este quiste hidático, o metacestodo, se localiza mayoritariamente en el hígado o pulmón, y consiste en una cavidad llena de líquido (denominado líquido hidático) delimitada por una capa germinativa (hacia el interior del quiste), una capa laminar (capa intermedia) y una membrana periquística (hacia el exterior del quiste) formada por la respuesta inflamatoria del hospedero (Díaz et al., 2011a, 2011b).

En el interior del quiste pueden desarrollarse por reproducción asexuada miles de protoscoleces (PSC), convirtiéndolo así en un quiste fértil. Los PSC son el estadio infectivo para los hospederos definitivos al ser ingeridos, siendo capaces de desarrollarse en gusanos adultos. A su vez, si accidentalmente un quiste fértil se rompe o fisura dentro del hospedero intermediario, se produce una siembra de PSC, donde cada uno de estos es potencialmente capaz de originar un nuevo quiste en un proceso denominado infección secundaria o EQ secundaria (Heath, 1970).

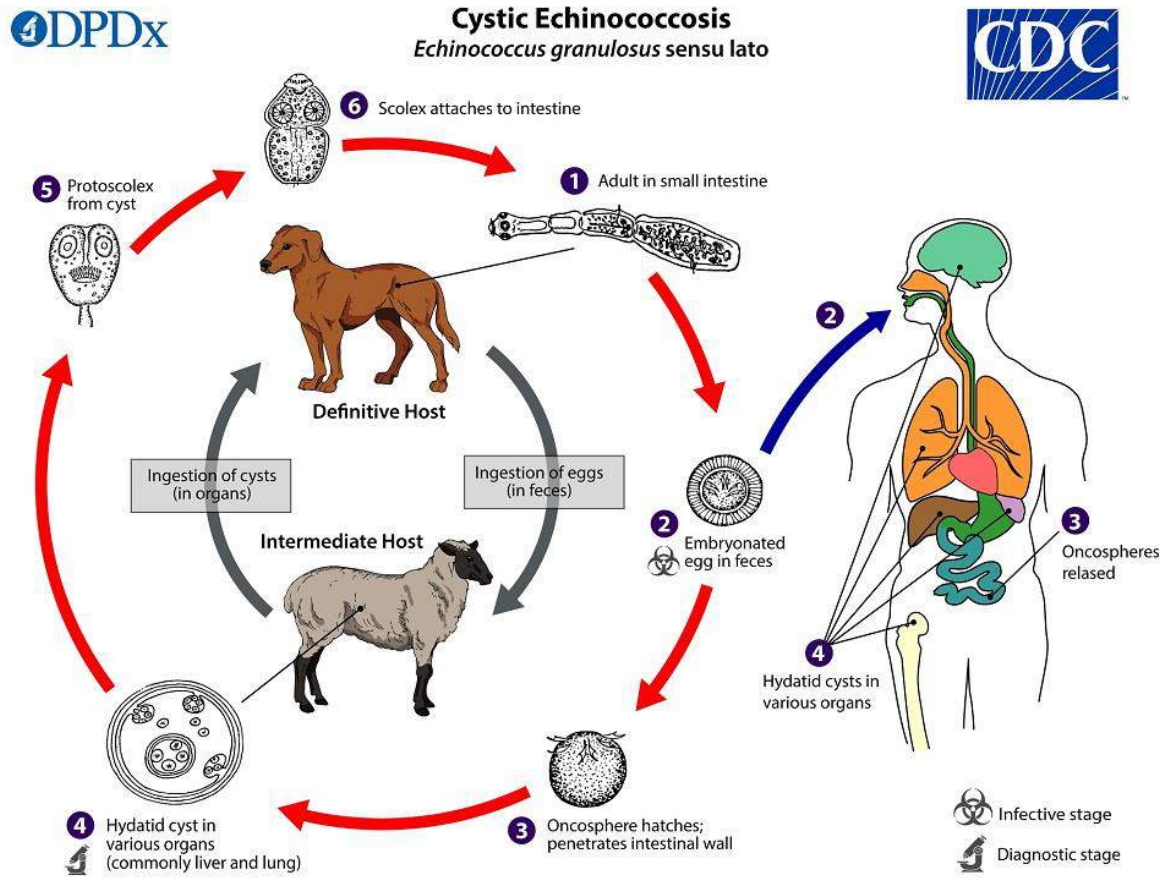

Figura 1. Ciclo de vida de *E. granulosus s.l.* (1) Gusano adulto, (2) Huevo embrionado, (3) Oncósfera, (4) Quiste hidático, (5) Protoescólex, (6) Escólex adherido a la mucosa intestinal. (Tomado del sitio oficial del Centro para el Control y Prevención de Enfermedades del gobierno de los Estados Unidos: www.cdc.gov/ /parasites/echinococcosis/biology.html).

En las últimas décadas, se ha profundizado en el estudio de *E. granulosus* observándose diferencias considerables entre diferentes aislados parasitarios, tanto en términos fenotípicos y fisiológicos como en cuanto a su variabilidad genética, las cuales han llevado a una división de *E. granulosus* en "cepas" (Cucher et al., 2015). De esta manera, se han caracterizado nueve genotipos principales (G1-G8, G10), agrupados en cuatro especies, que se correlacionan con el hospedero intermediario preferencial de cada una de ellas

(Nakao et al., 2010). Así, *E. granulosus sensu stricto* (s.s.) refiere a los genotipos G1-G3, *E. equinus* a G4, *E. ortleppi* a G5, y *E. canadensis* a G6-G8 y G10. A su vez, *E. granulosus sensu lato* (s.l.) refiere al conjunto de todas ellas.

1.1.2. Equinococosis quística: La enfermedad en hospederos intermediarios.

La equinococosis quística (EQ) es una enfermedad crónica y compleja, que afecta en gran medida a animales de producción generando enormes perjuicios económicos a nivel mundial (Budke et al., 2006). Los seres humanos pueden contraer EQ mediante la ingesta de oncósferas (por ejemplo, tras consumir vegetales contaminados), pero debido a que esta infección no permite que se complete el ciclo de vida del parásito, los humanos se consideran un hospedero intermediario accidental.

El metacestodo se establece mayoritariamente en el hígado o pulmón, donde presenta un crecimiento lento de aproximadamente 1 cm por año, pudiendo alcanzar 20 cm de diámetro en una infección hepática. En su desarrollo, los quistes pueden comprimir estructuras adyacentes, fisurarse, romperse o infectarse, provocando complicaciones clínicas. El espectro clínico de la EQ va desde infecciones asintomáticas a severas, y raramente fatales. Existen distintas aproximaciones para el manejo clínico de la EQ, desde la quimioterapia hasta las técnicas percutáneas o la cirugía (Brunetti & Junghanss, 2009; Piccoli et al., 2014; Rinaldi et al., 2014).

Las medidas de prevención se han basado, mayoritariamente, en controlar el ciclo de vida del parásito, promoviendo la faena higiénica y educando a las comunidades rurales, principalmente en el descarte de vísceras infectadas, las cuales usualmente son utilizadas como alimento para cánidos, permitiéndole así al parásito completar su ciclo de vida (Pourseif et al., 2018).

Por otro lado, también existen drogas antihelmínticas utilizadas para interrumpir el ciclo de vida del parásito, aunque estas conllevan un costo extra y son aplicadas mayoritariamente a hospederos definitivos (Deokate et al., 2014). Actualmente, existe una única vacuna veterinaria que ha alcanzado el mercado para prevenir infecciones por *E. granulosus* s.s. en ganado ovino, denominada EG95 (Heath et al., 2003; Lightowlers et al., 1999).

1.1.3. Protoscoleces de *E. granulosus*: Particularidades.

Los protoscoleces (PSC) de *E. granulosus* s.l. son el estadío infectivo para los hospederos definitivos. Una vez ingeridos, los PSC son activados en el estómago de los hospederos por medio de la acción del pH ácido y las sales biliares, desencadenando diversos cambios morfológicos en los PSC, donde la evaginación es el más evidente. Los PSC activados y evaginados pueden anclarse a las mucosas del intestino delgado de los hospederos definitivos, desarrollándose en gusanos adultos. La morfología general de los PSC está constituida por cuatro regiones diferentes, siendo estas (i) el rostelo (conteniendo el cono rostelar y los ganchos), (ii) la región de ventosas (donde se encuentran las ventosas), (iii) la región del cuello, y (iv) la región del cuerpo (Antoniou & Tselentis, 1993). El cuerpo y el cuello forman el denominado soma de los PSC, mientras que el rostelo y la región de ventosas forman el escólex. En PSC invaginados, solo el soma es visible, ya que el escólex se encuentra dentro del cuerpo del mismo (Figura 2).

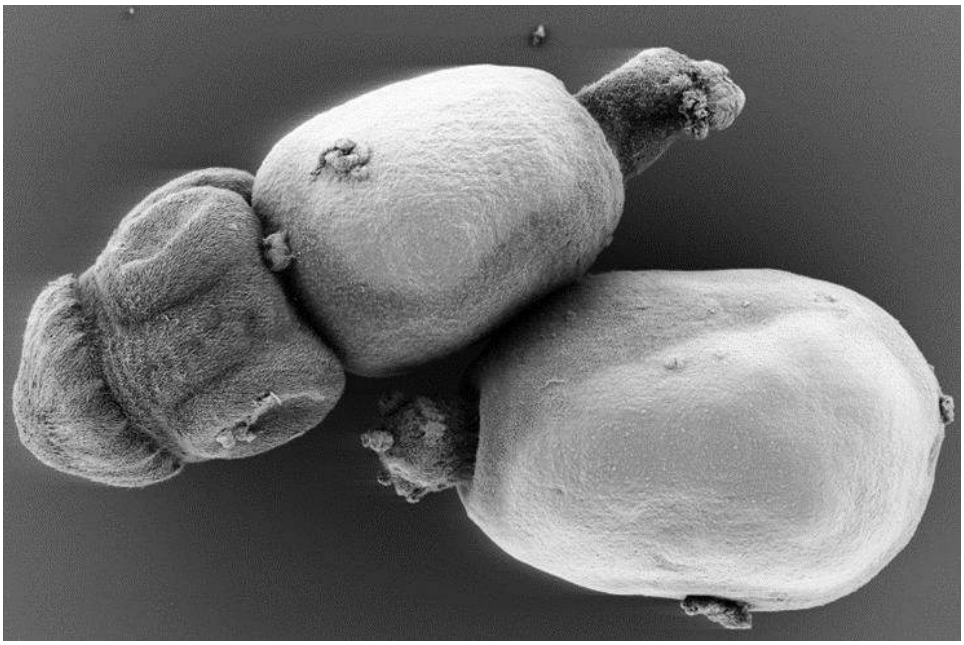

Figura 2. Morfología de los protoscoleces de *E. granulosus* s.l. Morfología general de los protoscoleces de *E. granulosus* s.l. evaginados (arriba) e invaginados (abajo). En los evaginados se observa el rostelo, la región de ventosas, el cuello y el cuerpo; mientras que en protoscoleces invaginados solo se observa el cuerpo.

1.1.4. El tegumento de los PSC de *E. granulosus*.

Una característica interesante de los cestodos es la existencia de un sincitio, o sincicio, multinucleado y sin límites celulares que cubre la totalidad del parásito, denominado tegumento (Jha & Smyth, 1971; Morseth, 1967). En los PSC existen diferencias considerables entre el tegumento del soma y el del escólex. Por ejemplo, mientras que el tegumento del escólex suele ser fino y posee espinas tegumentales en la parte exterior (Figura 3A), el tegumento del soma es de mayor tamaño y está cubierto por una capa de mucinas denominadas glicocálix (Figura 3B) (Galindo et al., 2008).

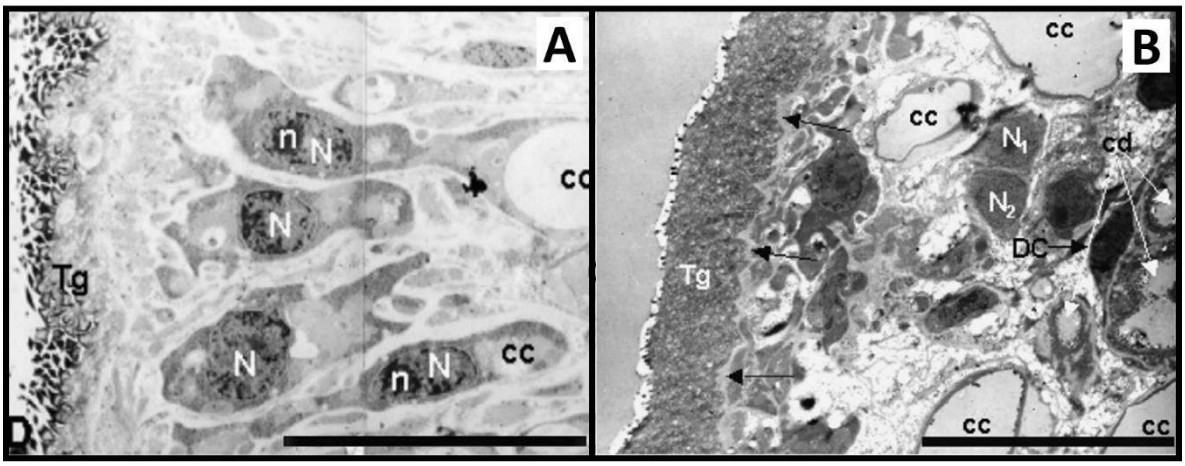

Figura 3. Tegumento de protoscoleces de *E. granulosus s.l.* Microscopía electrónica de transmisión de protoscoleces de *E. granulosus* s.l., enfocado en el tegumento (a la izquierda de cada imagen) del (A) escólex y (B) soma. *Tg*: tegumento, *N*: núcleo; *n*: nucléolo, *cc*: corpúsculos calcáreos (imagen modificada de Galindo et al., 2008).

Dentro de las funciones del tegumento destacan la absorción de nutrientes y la defensa respecto al medio externo parasitario. Por un lado, ya que los cestodos carecen de un canal alimentario, el tegumento es la ruta principal de absorción de sustancias y nutrientes. A su vez, el tegumento está involucrado en actividades de detoxificación y antioxidación, y participa en rutas de excreción/secreción de sustancias, incluyendo la liberación de componentes inmunomoduladores (Cheng, 1986).

1.1.5. Modelo murino de EQ secundaria.

Una característica interesante de los PSC de *E. granulosus* s.l. es su plasticidad para poder desarrollarse en nuevos quistes hidáticos en caso de ocurrir una siembra de PSC dentro del hospedero intermediario, por ejemplo, tras la fisura de un quiste fértil. Este fenómeno, denominado infección secundaria, puede ser replicado mediante la inoculación de PSC viables en la cavidad peritoneal de ratones inmunocompetentes, considerándose este un modelo experimental de EQ secundaria (Heath, 1970).

Este modelo ha sido ampliamente utilizado para el estudio de diversos aspectos relacionados a la inmunobiología de la infección por *E. granulosus* s.l., ya sea para aspectos básicos de la misma (Barrios et al., 2019; Baz et al., 2006; Cucher et al., 2013; Dematteis et al., 2003; Mourglia-Ettlin et al., 2011), para ensayos pre-clínicos de nuevos agentes quimioterapéuticos (Breijo et al., 2011; Ceballos et al., 2010; Cumino et al., 2012), para estudios de potenciales candidatos vacunales (Burgu et al., 2007; Hashemitabar et al., 2005; Hernández & Nieto, 1994), o para estudios de nuevas herramientas de diagnóstico y/o seguimiento (Denegri et al., 1995; Ferragut et al., 1998; Mamuti et al., 2002).

Por otro lado, el modelo de EQ secundaria ofrece una ventaja enorme sobre el modelo de infección primaria, ya que permite utilizar estadíos parasitarios no-infectivos para el ser humano (como es el caso de las oncósferas), simplificando así las condiciones de bioseguridad en el trabajo.

La EQ secundaria experimental puede dividirse en dos etapas, al menos cuando se trabaja con ratones de la cepa Balb/c: una etapa temprana o de pre-enquistamiento (hasta los días 20-30 p.i. aproximadamente), durante la cual se establece la infección al diferenciarse los PSC en quistes; seguida de una etapa tardía, crónica o de post-enquistamiento, durante la cual los quistes establecidos crecen en tamaño y eventualmente pueden volverse fértiles (Richards et al., 1983). Así, se asume que las respuestas inmune efectivas para limitar la infección deberían ocurrir principalmente en la etapa de pre-enquistamiento, durante la cual la respuesta de anticuerpos, las respuestas celulares y de citoquinas jugarían un papel relevante (Mourglia-Ettlin et al., 2016a, 2016b).

1.1.6. Susceptibilidad diferencial en el modelo murino de EQ secundaria.

La selección de cepas murinas en el trabajo con modelos experimentales debe ser cuidadosamente considerada, ya que distintas cepas de ratones pueden generar respuestas inmunes diferentes contra numerosas enfermedades, lo que conlleva a que existan

diferencias en susceptibilidad entre las mismas. Por ejemplo, entre las dos cepas de ratones más utilizadas (Balb/c y C57Bl/6), se han reportado diferencias para enfermedades autoinmunes (Matsuo et al., 2019; Qiao et al., 2010), cáncer (Díaz-Zaragoza et al., 2017; Maronpot, 2009; Ponnaiya et al., 2006), infecciones virales (Henderson et al., 2015; Kulcsar et al., 2015; Xiang et al., 2016), infecciones bacterianas (Cheers et al., 1978; Chiodini & Buergelt, 1993; Fornefett et al., 2018a; Liu et al., 2002), infecciones por protozoarios (Ferreira et al., 2018; Mols-Vorstermans et al., 2013), e infecciones por helmintos (Anthony et al., 2007; Pereira et al., 2016; Zhang et al., 2005).

En este sentido, nuestro grupo reportó recientemente que las cepas Balb/c y C57Bl/6 presentan alta y baja susceptibilidad a la EQ secundaria experimental, respectivamente, si bien ambas cepas desarrollan la infección (Mourglia-Ettlin et al., 2016a). Así, para un mismo lote de parásitos, los ratones C57Bl/6 no solo presentan un porcentaje de animales infectados menor que los ratones Balb/c, sino que también en los animales infectados se genera un número menor de quistes, siendo estos usualmente de menor tamaño (Figura 4). Esta diferencia de susceptibilidad está parcialmente asociada a tres factores complementarios: (i) las cepas Balb/c y C57Bl/6 polarizan sus respuestas inmunes adaptativas hacia perfiles predominantemente de tipo Th2 y Th1, respectivamente (Mourglia-Ettlin et al., 2016b); (ii) dichas cepas difieren en sus haplotipos de moléculas MHC-II, lo cual genera una presentación diferencial de antígenos haciendo que el espectro de especificidades de los anticuerpos inducidos sea diferente (Sofron et al., 2016); y (iii) los ratones C57Bl/6 presentan mayores niveles de anticuerpos activadores del sistema de complemento, ya sea en términos de IgG2b natural como IgM, IgG2b e IgG2c inducidos (Mourglia-Ettlin et al., 2016a).

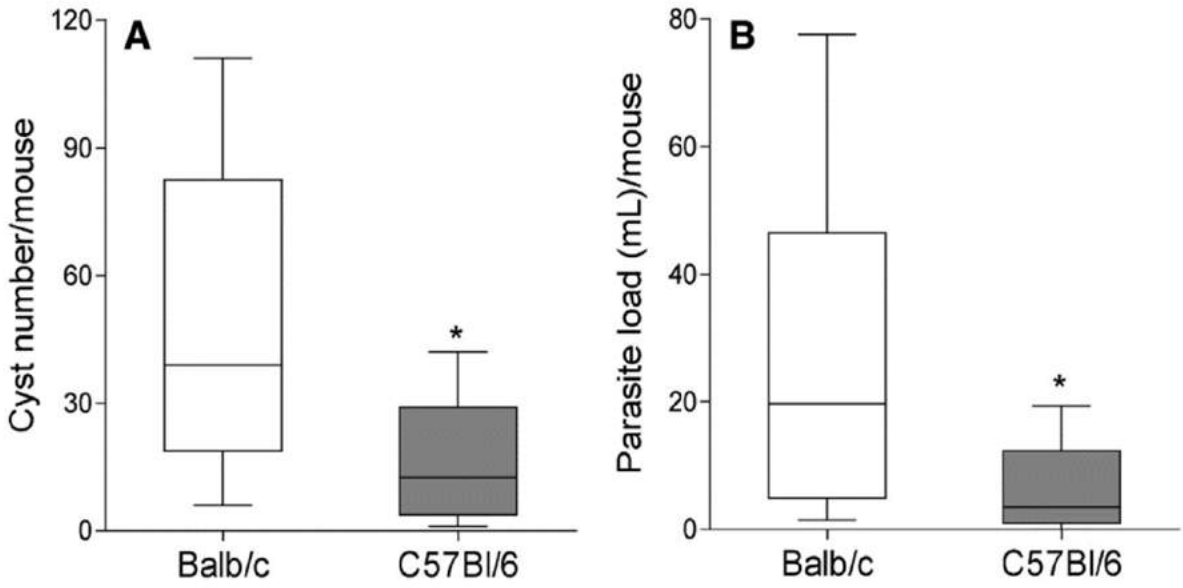

lFigura 4. Diferencia de susceptibilidad frente a la equinococosis quística secundaria en ratones Balb/c y C57Bl/6. Los ratones de la cepa Balb/c (blanco) presentan una mayor susceptibilidad a la EQ secundaria experimental que los ratones de la cepa C57Bl/6 (gris). Esta diferencia se observa tanto en (A) el número de quistes desarrollados en cada ratón, como en (B) la carga total parasitaria por ratón (expresada como la sumatoria de los volúmenes quísticos). (Imagen modificada de Mourglia-Ettlin et al., 2016a).

1.2. Antígenos parasitarios protectores.

1.2.1. EG95: Un caso de éxito.

La vacuna EG95 contiene un antígeno recombinante de 17 kDa derivado de oncósferas de *E. granulosus* s.s. Esta vacuna ha mostrado ser capaz de inducir niveles de protección, en ovejas, entre 95-100% frente a la infección natural según diversos estudios (Heath et al., 2003; Lightowlers et al., 1999, 1996). De manera interesante, EG95 tiene como correlato de protección la capacidad de inducir anticuerpos protectores en hospederos intermediarios naturales (Chow et al., 2008; Heath et al., 2003; Heath & Koolaard, 2012), los cuales se ha demostrado que, al menos *in vitro*, son capaces de activar el sistema complemento en la superficie de las oncósferas, llevándolas así a la muerte.

Desafortunadamente, el gen *eg95-1* (codificante para el antígeno EG95) es altamente polimórfico e inmunológicamente diferente entre genotipos parasitarios (Alvarez Rojas et al., 2013, 2012; Chow et al., 2008; Haag et al., 2009). En este sentido, no existen en la actualidad estudios que demuestren la eficacia de EG95 contra otros genotipos de *E. granulosus* distintos a G1-G3 (*E. granulosus* s.s.). Asimismo, no se han reportado estudios que demuestren la eficacia de EG95 en otros hospederos intermediarios distintos a los ovinos (por ejemplo: bovinos, porcinos, etc.).

1.2.2. Otros antígenos protectores.

Debido a las posibles limitantes de EG95 como antígeno vacunal universal frente a la infección por *E. granulosus* s.l., diversas proteínas parasitarias han sido estudiadas como posibles antígenos protectores, reportándose resultados prometedores en varios casos. De manera general, los antígenos protectores son aquellas estructuras moleculares específicas de un patógeno que pueden desencadenar respuestas inmunes eficientes para impedir o limitar la infección.

Así, proteínas como EgA31, EgDf1, Antígeno 5, Eg14-3-3 y EgM han mostrado ser inmunogénicas y capaces de inducir altos niveles de anticuerpos específicos en hospederos definitivos y/o intermediarios inmunizados, a la vez que han demostrado generar altos niveles de protección en modelos murinos de infección (Pourseif et al., 2018). Sin embargo, hasta el momento ninguna de estas proteínas ha sido evaluada en ensayos clínicos veterinarios frente a infecciones naturales.

1.2.3. Antígenos tegumentarios protectores.

Además de los antígenos recombinantes estudiados como candidatos vacunales, existe una fracción de proteínas tegumentarias de PSC de *E. granulosus* s.l. -denominada

PSEx- que ha mostrados altos niveles de protección en el modelo murino de EQ secundaria (Hernández & Nieto, 1994). Además, la inmunización con PSEx ha mostrado ser capaz de inducir altos niveles de anticuerpos específicos tanto en hospederos intermediarios (Valizadeh et al., 2017), como en hospederos definitivos (Carol & Nieto, 1998); naturales en ambos casos.

La fracción antigénica PSEx se obtiene mediante la incubación de PSC viables con un detergente iónico suave, capaz de solubilizar las proteínas de membrana (del tegumento) sin dañar la estructura general de los PSC (Hernández & Nieto, 1994). A pesar de los resultados prometedores obtenidos PSEx, es prácticamente nula la información disponible relacionada con su composición proteica, lo cual habría limitado la continuación de estudios que hicieran uso de la misma.

1.2.4. Disponibilidad de datos proteómico para *E. granulosus*.

Pese a la limitada información generalmente disponible sobre diversos aspectos de la biología y bioquímica de *E. granulosus* s.l., existen varios estudios proteómicos realizados sobre (casi) todos sus estadíos parasitarios. Estos se basan principalmente en dos estudios que proponen el proteoma completo de *E. granulosus* s.l. deducido a partir de su transcriptoma (Tsai et al., 2013; Zheng et al., 2013).

Mediante el uso de dichos proteomas como referencia, se ha realizado la caracterización proteómica de líquido hidático, productos de excreción/secreción de PSC y de fracciones antigénicas obtenidas a partir de la capa germinativa y los PSC de *E. granulosus* s.l. (Hidalgo et al., 2016; Monteiro et al., 2010; Sedaghat et al., 2021; Y. Wang et al., 2015; Wu et al., 2019). Además, se ha analizado el cambio en la expresión de proteínas entre los estadíos de PSC y gusano adulto (Cui et al., 2013).

1.2.5. Modificaciones post-traduccionales en *E. granulosus*.

Las modificaciones post-traduccionales (PTMs, del inglés: *Post-translational modifications*) son modificaciones covalentes, y generalmente derivadas de procesos enzimáticos, que se realizan en las proteínas luego de su traducción ribosómica. Muchas veces la presencia de estas PTMs permite obtener finalmente el producto proteico maduro y funcional.

Las PTMs pueden ocurrir en las cadenas laterales de los aminoácidos o en los extremos C- y N-terminales de las proteínas, promoviendo así el correcto plegamiento de estas, y mejorando su estabilidad o participación en diversas funciones regulatorias y de señalización celular (Voet et al., 2016). Hasta el momento se han identificado cientos de PTMs distintas, siendo algunas producidas exclusivamente por algunos organismos (Walsh, 2010). Esta diferencia en la producción de PTMs puede tener implicaciones importantes en el desarrollo de productos bioterapéuticos, donde la selección apropiada del sistema de producciones es fundamental.

Hasta el momento, no existe un análisis sistemático de las PTMs presentes en proteínas de *E. granulosus* s.l., ni de ningún otro cestodo. Sin embargo, existen algunos trabajos que reportan la existencia de glicosilación (Alvarez Errico et al., 2001; Khoo et al., 1997), acetilación (Virginio et al., 2012) y amidación (McVeigh et al., 2005) en proteínas de *E. granulosus*. A su vez, existen reportes sobre la presencia de geranil-geranilación (Spiliotis & Brehm, 2004) y S-farnesilación (Spiliotis et al., 2005) en proteínas de *E. multilocularis*, así como de manosilación en proteínas de *Taenia solium* (Plancarte et al., 1999).

1.3. Vacunas.

Una vacuna es una preparación biológica que confiere inmunidad activa frente a una enfermedad en particular. Existen vacunas profilácticas con el objetivo de proteger al

individuo de enfermedades, así como vacunas terapéuticas que buscan tratar una enfermedad ya existente -usualmente crónica- en un individuo dado.

1.3.1. Importancia de las vacunas.

Las vacunas son el avance medico más importante de la historia del ser humano, siendo secundando solo, quizás, por los antibióticos. Las vacunas permiten manipular la extraordinaria habilidad del sistema inmune para responder y recordar encuentros con patógenos y sus antígenos (Clem, 2011). Así, desde que se implementaron los primeros programas masivos de vacunación, se ha transformado la salud pública a nivel mundial, prácticamente desapareciendo las enfermedades infecciosas responsable de la muerte de la mayoría de los niños e infantes en países con altas tasas de vacunación (Pollard & Bijker, 2021). La OMS estima que las vacunas evitan, anualmente, entre 2 y 3 millones de muertes, reduciéndose en los últimos 30 años a un tercio la tasa global de muerte en niños menores de 5 años. Además, las vacunas han permitido lograr la erradicación casi completa de 14 enfermedades infecciosas según la CDC, destacando notablemente la viruela, la peste bovina y la polio (Pollard & Bijker, 2021).

1.3.2. Composición general de una vacuna.

Si bien existen numerosos tipos de vacunas, la formulación general, y el objetivo de cada uno de sus componentes, es esencialmente el mismo. Una vacuna en su forma más básica está compuesta por tres ingredientes principales: el diluyente, el adyuvante y el antígeno (D'Amico et al., 2021). El diluyente es el vehículo que permite la administración inyectable de la preparación, en él el resto de los componentes se disuelven o se mantienen en suspensión. El adyuvante es un componente usualmente químico (por ejemplo, sales de aluminio) que induce inflamación en el sitio de inyección, fenómeno necesario para el

desarrollo de una respuesta inmune adaptativa. Por último, el antígeno es el elemento derivado del patógeno contra el cual se induce la respuesta inmune. Independientemente de si la respuesta inducida es de tipo celular, humoral o mixta, la misma estará dirigida hacia el antígeno. Así, en caso de una infección natural, el sistema inmune está preparado para limitar y controlar la infección.

1.3.3. Tipos de vacunas.

Desde la primera vacuna creada por Edward Jenner en 1796 hasta el presente, estas han sufrido cambios radicales, principalmente en la naturaleza del antígeno utilizado, que permitieron optimizar su fabricación, almacenamiento y distribución (D'Amico et al., 2021). A su vez, cambios fundamentales en la formulación vacunal permitieron el desarrollo de vacunas contra nuevas enfermedades infecciosas y no infecciosas.

Las vacunas clásicas, también llamadas de primera generación, son vacunas cuyo antígeno es un microorganismo entero -ya sea vivo, atenuado o inactivado- que generan usualmente respuestas fuertes con larga memoria inmunológica.

Las vacunas de segunda generación, o vacunas de subunidades, poseen como antígeno un único componente del patógeno (por ejemplo, una proteína, un polisacárido o un toxoide). Estos componentes pueden ser obtenidos tras la purificación de un extracto patogénico natural, o ser antígenos recombinantes. Las vacunas de segunda generación suelen generar una respuesta inmune menos fuerte y duradera que las de primera generación, haciendo necesario el uso de dosis de refuerzo. No obstante, al ser respuestas menos agresivas, estas vacunas pueden ser administradas a la mayoría de la población, incluidas personas con un sistema inmune débil o problemas crónicos de salud.

Las vacunas de tercera generación no contienen al antígeno *per se*, sino que utilizan material genético (ADN o ARNm) que codifica para la proteína antigénica. Tras la

inmunización, las propias células del individuo inoculado generan dichas proteínas, y estas son reconocidas por su sistema inmune (Clem, 2011; D'Amico et al., 2021; Pollard & Bijker, 2021). Las vacunas de tercera generación han ganado notoriedad en los últimos años, presentando grandes ventajas y desventajas. Por un lado, los costos y tiempos de producción suelen ser mucho menores para este tipo de vacunas, pero suelen presentar una pobre estabilidad, y generar respuestas inmunes débiles y de relativa corta duración, requiriéndose refuerzos periódicos (Wadhwa et al., 2020).

1.3.4. Vacunas basadas en péptidos.

Además de las tres generaciones de vacunas utilizadas actualmente para uso humano, existen otros tipos de vacunas aún en desarrollo. Un ejemplo de estas son las vacunas basadas en péptidos, donde el antígeno es un fragmento pequeño de una proteína del patógeno, que induce respuestas inmunes con reactividad cruzada contra el antígeno nativo (Malonis et al., 2020; Nelde et al., 2021).

Siguiendo la lógica reduccionista que llevó a la creación de las vacunas de segunda generación, donde se buscó limitar la respuesta inmune solamente hacia los componentes del patógeno que confieren protección, en las vacunas basadas en péptidos se busca direccionar la respuesta inmune únicamente contra porciones de esos antígenos protectores. Así, con el uso de péptidos cortos (5-50 aminoácidos) usualmente producidos de forma sintética, se pueden generar respuestas de células B (anticuerpos) o células T (inmunidad celular) -o combinación de ellas-, generando una memoria inmunológica capaz de proteger frente a una infección natural. Estas vacunas se basan en el principio que los receptores inmunes BCR y TCR reconocen únicamente un fragmento de la proteína antigénica, ya sea por interacción directa, o mediante presentación por MHC.

Aunque en la actualidad no existe aún ninguna vacuna basada en péptidos en el mercado, existe un gran interés en el desarrollo de este tipo de vacunas, tanto para

enfermedades infecciosas como no infeccionas (Malonis et al., 2020). En este sentido, son varias las vacunas peptídicas contra cáncer que se encuentran en fases clínicas de investigación (II y III), y varias vacunas basadas en péptidos contra enfermedades infeccionas están siendo evaluadas en fase clínica I (Di Natale et al., 2020).

Por otro lado, estudios pre-clínicos de vacunas peptídicas contra infecciones por helmintos han mostrado resultados promisorios; incluidas infecciones por *Trichinella spiralis* (McGuire et al., 2002), *T. solium* (Huerta et al., 2001; Toledo et al., 1999), *Fasciola gigantica* (Jezek et al., 2008), y *F. hepática* (Rojas-Caraballo et al., 2014). En el caso de *E. granulosus* s.l., aunque varios péptidos han sido propuestos como candidatos vacunales de interés (Li et al., 2021; Pan et al., 2017; L. Wang et al., 2019), no existen reportes que demuestren su eficiencia *in vivo* hasta el momento.

1.4. Diseño de vacunas.

El diseño de vacunas es un proceso complejo y costoso que consiste no solo en la correcta selección del antígeno, sino también en el adyuvante, la ruta de administración y el esquema de vacunación. Sumado a los ensayos pre-clínicos y clínicos necesarios, el tiempo medio para que una vacuna alcance el mercado suele variar entre 8-15 años (Gouglas et al., 2018).

1.4.1. Selección clásica de antígenos.

El desarrollo de las primeras vacunas de segunda generación consistía en estudiar el posible uso de los antígenos más abundantes presentes en el patógeno como candidatos vacunales. Esto se debía a que, en la mayoría de los casos, para obtener cantidades de antígenos suficientes para los estudios de inmunogenicidad y protección, era necesario realizar cultivos de patógenos en el laboratorio, y purificación de sus antígenos, donde solo

unos pocos antígenos eran obtenidos (Mora et al., 2003). Además de representar una metodología costosa y que requiere de mucho tiempo, tiene la gran limitante adicional de no ser aplicable a organismos no-cultivables, limitando enormemente el espectro de patógenos que pueden ser analizados.

1.4.2. Vacunología Reversa.

Con la disponibilidad de los genomas completos de patógenos, y el avances en las herramientas bioinformáticas, el campo de la vacunología cambió drásticamente a principios del siglo XXI mediante la introducción de la vacunología reversa (Rappuoli, 2001, 2000). Esta estrategia se basa en el análisis de los genomas completos mediante algoritmos informáticos, que permiten la selección de secuencias con potencial capacidad protectora, de manera fácil, rápida y barata.

Los distintos algoritmos permiten, por ejemplo, filtrar las proteínas superficiales o secretadas (las cuales suelen ser las que principalmente interaccionan con el sistema inmune del hospedero) (Bendtsen et al., 2004; Käll et al., 2004; Krogh et al., 2001; Petersen et al., 2011), analizar la antigenicidad, alergenicidad y toxicidad de las mismas (Gupta et al., 2013; Magnan et al., 2010; Saha & Raghava, 2006), evaluar el grado de similitud con las proteínas del hospedero (Altschul et al., 1990), y evaluar la presencia de epítopes B y T en las mismas (Larsen et al., 2006; Nielsen & Lund, 2009), entre muchas otras características.

El campo de la vacunología reversa está en avance continuo, tanto mediante la introducción de nuevos algoritmos que permitan analizar propiedades inexploradas, así como mediante la mejora constante en la calidad y fiabilidad de las predicciones.

1.4.3. Diseño de vacunas basadas en péptidos.

Mediante el uso de la vacunología reversa, es posible identificar péptidos como candidatos vacunales. El uso de algoritmos bioinformáticos permite seleccionar únicamente los epítopes B y/o T de proteínas con baja antigenicidad, generando respuestas efectivas que no ocurrirían en el caso del uso de dichas proteínas en forma recombinante. Estos epítopes pueden ser producidos de forma automatizada, no biológica, a gran escala y con excelentes niveles de pureza, reduciendo los costos que involucra la producción de antígenos recombinantes.

La eficacia pre-clínica de las vacunas basadas en péptidos ha sido evaluada en combinación con el uso de diversos tipos de adyuvantes (sales de aluminio, emulsiones, liposomas, virosomas y saponinas), permitiendo una gran flexibilidad en la generación de la formulación vacunal (Azmi et al., 2014).

HIPÓTESIS

La hipótesis central de la presente tesis se basa en que el tegumento de los PSC de *E. granulosus* s.l. juega un papel importante en el establecimiento y desarrollo de la EQ secundaria, y que el reconocimiento de ciertos antígenos tegumentarios por parte del sistema inmune del hospedero es capaz de generar protección en el modelo murino de infección secundaria experimental.

OBJETIVOS

Objetivo general. Caracterizar el tegumento de los PSC de *E. granulosus* s.l., en términos de su estructura, organización y composición; así como analizar su papel -y el de sus antígenos protectores- en el desarrollo de la infección secundaria.

Objetivos específicos:

1. Caracterizar la ultraestructura y organización de los distintos componentes celulares y subcelulares que conforman el tegumento de los PSC de *E. granulosus* s.l.

2. Caracterizar a nivel proteómico y bioinformático los componentes proteicos presentes en el tegumento de los PSC de *E. granulosus* s.l.

3. Evaluar el papel de los componentes tegumentarios de PSC de *E. granulosus* s.l. en el establecimiento de la EQ secundaria experimental.

4. Diseñar péptidos antigénicos derivados de proteínas tegumentarias de PSC de *E. granulosus* s.l. y evaluar su potencial vacunal en el modelo murino de EQ secundaria.

CAPÍTULO 2

Objetivo específico #1: *Caracterizar la ultraestructura y organización de los distintos componentes celulares y subcelulares que conforman el tegumento de los PSC de E. granulosus s.l.*

En el presente capítulo se presenta una descripción detallada de la organización celular y subcelular de los componentes presentes en el tegumento del soma de PSC de *E. ortleppi,* y en menor medida, de *E. granulosus* s.s. En este sentido, y mediante el uso de diversas técnicas de microscopía electrónica, se presenta un análisis y reconstrucción tridimensional del tegumento de los PSC, así como un estudio del tránsito de componentes a través del mismo. Por ello, el presente capítulo se divide en dos secciones:

1) Organización celular del tegumento de los PSC.
2) Rutas de excreción/secreción e internalización a través del tegumento de los PSC.

La mayoría de estos resultados están contenidos en la publicación adjunta:

Art. 1

"*Ultrastructural characterization of the tegument in protoscoleces of Echinococcus ortleppi*"

Miles S, Cyrklaff M, Magnone J, García-Luna J, Ancarola ME, Cucher M, Dematteis S, Frischknecht F, Mourglia-Ettlin G.

International Journal for Parasitology (2021)

doi:10.1016/j.ijpara.2021.05.004

CAPÍTULO 2

SECCIÓN 1

Organización celular del tegumento de los PSC.

Los primeros estudios sobre el tegumento de *E. granulosus* s.l. se remontan a las décadas de 1960 y 1970 (Jha & Smyth, 1971; Morseth, 1967), todos realizados usando técnicas clásicas de microscopia electrónica. El estudio más nuevo y completo sobre el tegumento de los PSC fue publicado en 2008 por Galindo y colaboradores, donde utilizan microscopía electrónica de trasmisión (TEM) y de barrido (SEM) para realizar una descripción básica de las células que componen el tegumento y sus alrededores; resaltando las diferencias existentes entre el tegumento del soma y del escólex.

Avances en las técnicas de microscopía electrónica permiten obtener información aún más detallada, mejorando la resolución y nitidez de las imágenes obtenidas. Asimismo, permiten generar reconstrucciones tridimensionales de los componentes observados. En este sentido, y mediante el uso de microscopios *state-of-the-art*, hemos analizado el tegumento de PSC de *E. ortleppi* (genotipo G5), y en menor medida de *E. granulosus* s.s. (genotipo G1), obteniendo por primera vez una visión tridimensional general de su ultraestructura y de la distribución de los distintos componentes celulares que lo componen. Además, describimos y caracterizamos por primera vez, una estructura con alto contenido de vesículas encontrada dentro del tegumento.

Los estudios de microscopía fueron realizados con PSC viables de *E. granulosus* s.l. obtenidos de quistes pulmonares bovinos provenientes de infecciones naturales. El genotipo de cada lote de parásitos (correspondiente cada uno a un quiste hidático diferente) fue analizado mediante la secuenciación del fragmento génico codificante para la ciclo-oxigenasa 1 (*cox1*) mitocondrial (Cucher et al., 2011), correspondiendo en la mayoría de los casos a la especie *E. ortleppi* (genotipo G5), y en menor medida a la especie

E. granulosus s.s. (genotipo G1). Los parásitos de cada lote fueron fijados siguiendo el procedimiento estándar con paraformaldehído y glutaraldehído (2,0% y 2,5%, respectivamente), y almacenados a 4°C hasta su uso.

La morfología general de los PSC, tanto del genotipo G5 como G1, fue analizada mediante SEM, observándose la morfología clásicamente reportada (Figura 5) (Antoniou & Tselentis, 1993). Por un lado, en PSC evaginados, se identificaron cuatro regiones: 1) el rostelo, 2) la región de ventosas, 3) el cuello, y 4) el cuerpo. Así, se identificaron el escólex (rostelo junto a la región de ventosas) y el soma (cuello junto a cuerpo) de los PSC. A su vez, en la región opuesta al escólex, se pudo observar el tallo de unión de los PSC a la capa germinativa. Por su parte, en PSC invaginados, únicamente se observó el cuerpo de los PSC. Estos resultados también mostraron que la morfología general de los PSC de *E. ortleppi* y *E. granulosus* s.s. es muy similar. Cabe destacar que este el primer estudio utilizando SEM para caracterizar PSC de *E. ortleppi*.

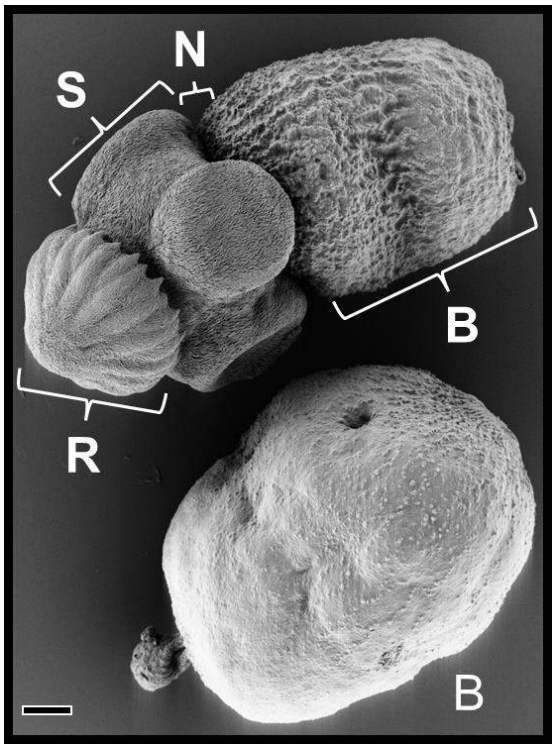

Figura 5. Morfología general de protoscoleces de *E. ortleppi*. La morfología general de protoscoleces de *E. ortleppi* fue analizada mediante microscopía electrónica de barrido. En

la imagen se observa un protoscolex evaginado (arriba) e invaginado (abajo). *R*: rostelo; S: región de ventosas; *N*: cuello; *B*: cuerpo; *T*: tallo. Barra de escala = 10 µm. (Imagen modificada de Miles et al., 2021; Art. 1).

Luego de confirmar la estructura general de los PSC, así como su integridad, se procedió a analizar la parte más externa de su soma (considerada esta como el tegumento). La misma está constituida por el citoplasma distal y los distintos tipos celulares encontrados inmediatamente por debajo del mismo (Galindo et al., 2008). Para este estudio, se utilizaron dos métodos distintos de preparación de las muestras para TEM: por un lado el método clásico de muestras embebidas en resina, y por el otro, la congelación a alta presión (HPF, del inglés *high-pressure freezing*) seguida de sustitución por congelación (en inglés: *freeze substitution*). Luego, se obtuvieron secciones ultra-finas (70 nm) de cada muestra y estas fueron analizadas por TEM. La distribución de los territorios celulares observada fue concordante con los datos previamente reportados (Galindo et al., 2008), sin observarse diferencias importantes entre el tegumento del soma de PSC de *E. ortleppi* y de *E. granulosus* s.s.

Por su parte, en la Figura 6 se muestra la distribución de componentes en el tegumento del soma de PSC de *E. ortleppi*, analizada mediante dos preparaciones de muestra distintas. En ambas se observa el parénquima, la zona fibrosa, el citoplasma distal y el glicocálix, así como las células musculares y tegumentales. A su vez, y aunque no se muestran en la Figura 6, se observaron también las células flamígeras y sus cilias correspondientes. A pesar de que las imágenes obtenidas por ambas preparaciones fueron prácticamente idénticas, el resto de los estudios se realizaron utilizando PSC preparados por HPF, ya que estos mostraron imágenes más nítidas.

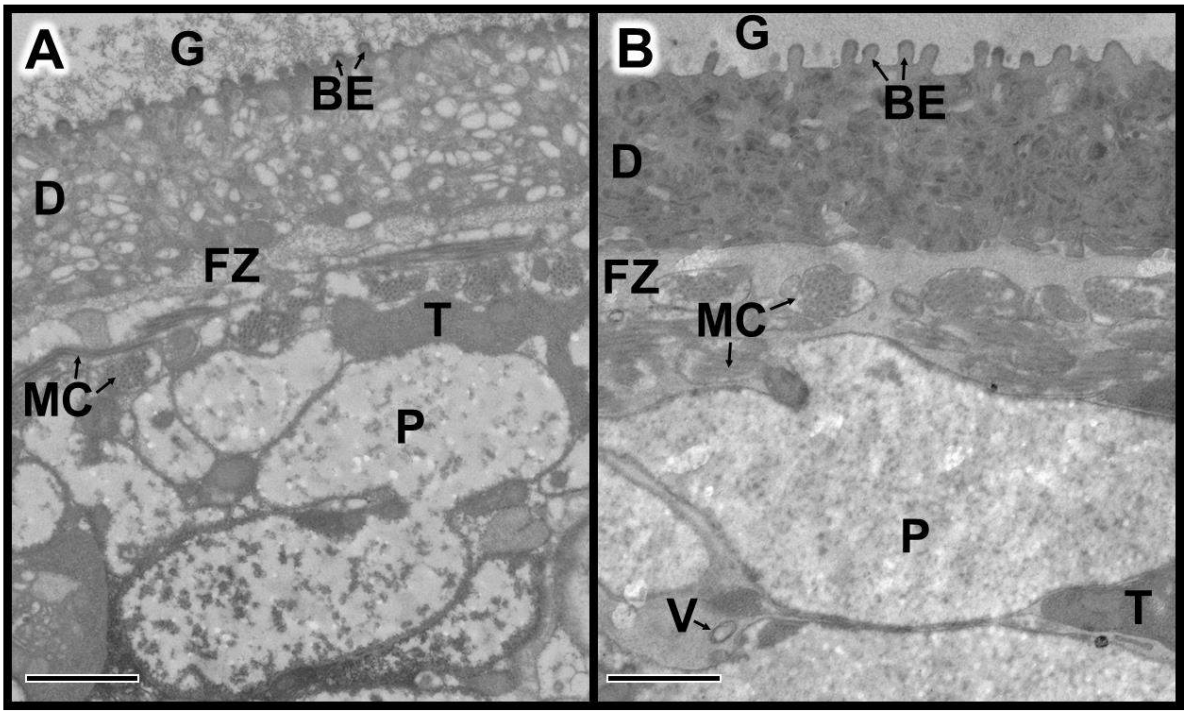

Figura 6. Tegumento del soma de protoscoleces. El tegumento del soma de protoscoleces de *E. ortleppi* fue analizado mediante microscopía electrónica de transmisión en secciones ultra finas (70 nm) de protoscoleces. (A) protoscoleces embebidos en resina por metodología clásica. (B) protoscoleces embebidos en resina por congelación a alta presión seguidos por substitución en frio (HPF seguido de *Freeze substitution*). *G*: glicocálix; *D*: citoplasma distal; *FZ*: zona fibrosa; *MC*: células musculares; *T*: células tegumentales; *P*: parénquima; *BE*: elevaciones romas; *V*: vesículas. Barra de escala = 500 nm. (Imagen modificada de Miles et al., 2021; Art. 1).

A continuación, se amplió el estudio de la distribución de los componentes tegumentarios mediante la reconstrucción 3D de su ultraestructura. Para ello, se obtuvieron secciones gruesas (500 nm) de los PSC preparados mediante HPF, las cuales fueron analizadas mediante tomografía electrónica (tomoEM). Este estudio se realizó utilizando un microscopio electrónico de transmisión capaz de girar la muestra de -60° a +60°, obteniéndose así imágenes cada 2° de rotación. A su vez, se obtuvieron 6 imágenes tomográficas seriadas de cada muestra, con las cuales se generó un tomograma mediante el uso del software etomo (Kremer et al., 1996), y la distribución tridimensional de sus

componentes se analizó utilizando el software IMOD (Kremer et al., 1996). Al unir los tomogamas de las 6 secciones seriadas obtenidas, se generó una reconstrucción 3D de una sección de 10 µm en las direcciones X e Y, y de 3 µm de grosor en el tegumento de los PSC de *E. ortleppi*, siendo ésta la primera reconstrucción 3D realizada para el tegumento de PSC de *E. granulosus* s.l. En la Figura 7 se muestran los resultados 3D, donde se señalan cada uno de los componentes mencionados anteriormente. Cabe destacar que los corpúsculos calcáreos y el núcleo y la membrana nuclear de estos, las únicas estructuras no mostradas en la Figura 6.

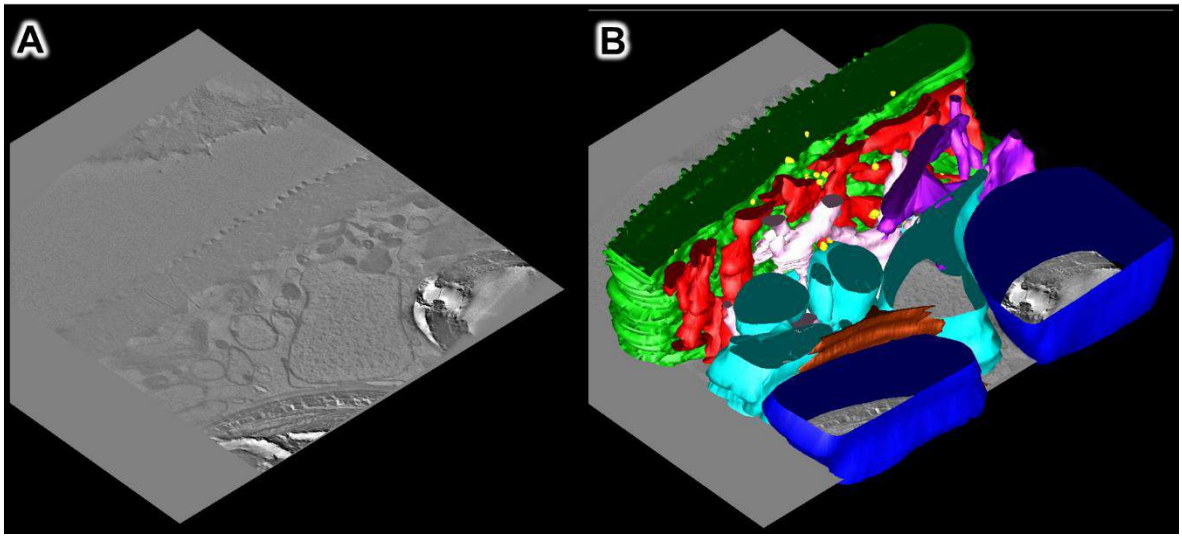

Figura 7. Reconstrucción 3D del Tegumento. (A) Imagen tomográfica del tegumento de protoscoleces obtenidas por tomografía electrónica. (B) Reconstrucción tridimensional de estructuras tegumentales obtenidas de seis tomografías seriadas de 500 nm. Citoplasma distal (verde); células musculares (rojo); células tegumentarias (blanco); parénquima (celeste); células flamígeras (violeta); corpúsculo calcáreo (azul); núcleo y membrana nuclear del corpúsculo calcáreo (marrón); vesículas (amarillo). (Imagen modificada de Miles et al., 2021; Art. 1).

De manera interesante, nuestros resultados permitieron identificar una estructura novedosa, situada entre el citoplasma distal y la zona fibrosa (Figura 8). Esta estructura electrón-lucida y acelular, fue observada a lo largo de todo el tegumento del soma de los

PSC (Figura 8C), conteniendo en su interior vesículas discretas de 75 a 250 nm de diámetro, así como otras estructuras limitadas por membranas. Debido a su ubicación y contenido vesicular, se la nombró como Cuerpo Tegumentario Vesiculado (TVB, del inglés: *Tegumental Vesicular Body*).

La reconstrucción 3D del TVB mostró que es una estructura única, si bien se observa como estructuras independientes en secciones individuales (Figura 8D). Además, el TVB se observó tanto en los PSC de *E. ortleppi* como en lo de *E. granulosus* s.s. (Figura suplementaria 1 de Miles et al., 2021; Art. 1), y por ambos métodos de preparación de muestra, reduciendo así drásticamente la posibilidad de que esta sea un artefacto generado por la metodología de trabajo.

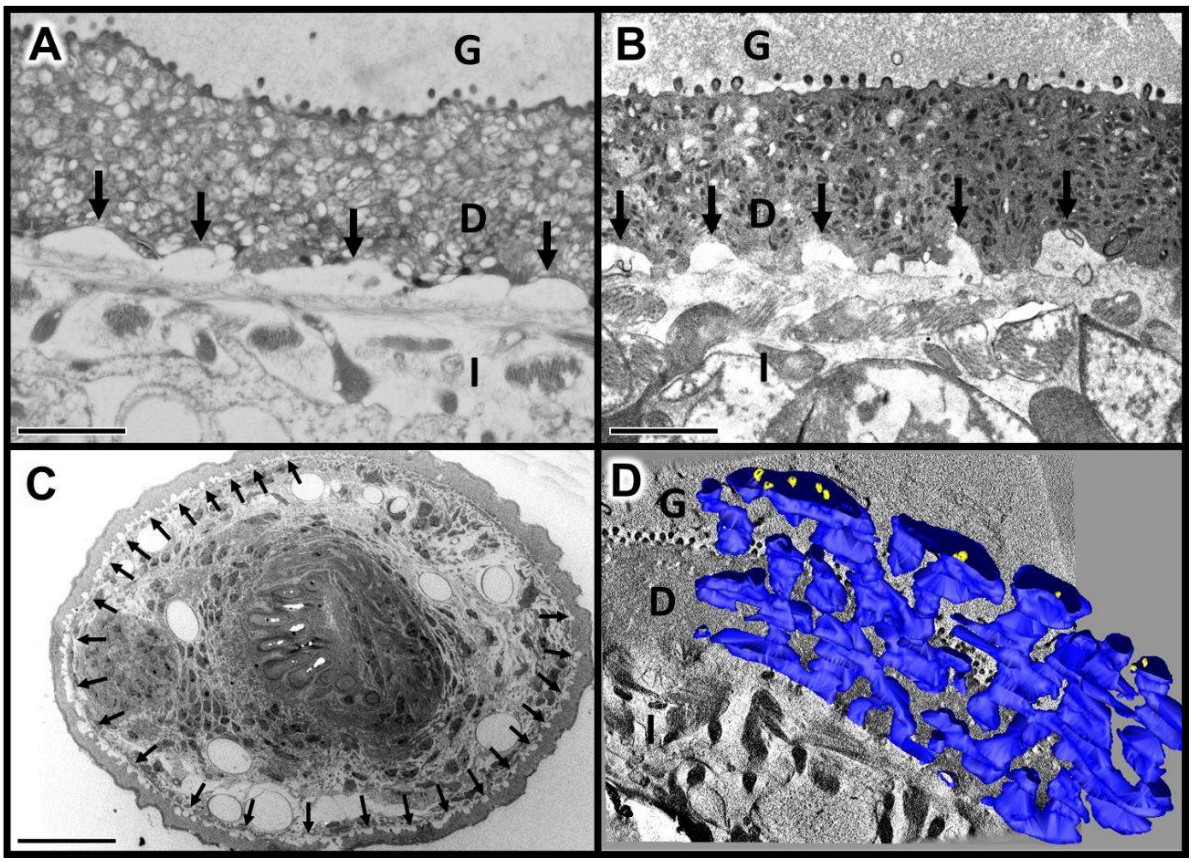

Figura 8. Cuerpo Tegumentario Vesiculado. Caracterización ultraestructural de una estructura novedosa en protoscoleces de *E. granulosus* s.l. observada entre el citoplasma distal y la zona fibrosa. Esta estructura, denominada Cuerpo Tegumentario Vesiculado (TVB;

del inglés: *Tegumental Vesicular Body*) contienen vesículas discretas en su interior. (A) TVB (flechas) observado mediante TEM en protoscoleces embebidos de forma clásica. (B) TVB (flechas) observado mediante TEM en protoscoleces preparados por HPF. (C) TVB (flechas) cubriendo casi la totalidad del cuerpo del protoscolex. (D) Reconstrucción tridimensional de TBV, mostrando el contenido vesicular. *I*: Interior inmediato; *D*: Citoplasma Distal; *G*: Glicocálix; *V*: vesículas. Barra de escala: (A y B) = 500 nm; (C) = 10 µm. (Imagen tomada de Miles et al., 2021; Art. 1).

CAPÍTULO 2

SECCIÓN 2

Rutas de excreción/secreción e internalización a través del tegumento de los PSC.

En el tegumento de los PSC de *E. granulosus* s.l. se han reportado 6 tipos de vesículas (V1-V6) (Bui et al., 1999). Las vesículas V1 (también conocidas como T3) son ovoides, electrón-lúcidas y de origen desconocido. Las vesículas V2 (también conocidas como T1) tienen forma de cometa, y son electrón-lúcidas pero con un centro electrón-denso. Las vesículas V3 poseen una morfología de disco plano, o mancuerna, con un centro electrón-denso amorfo. Las vesículas V4 y V5 (también conocidas como T2) están presentes mayoritariamente en el tegumento del escólex, presentan una forma redonda delimitada por una doble membrana, y muestran un centro electrón-lúcido (V4) o electrón-denso (V5). Finalmente, las vesículas V6 son similares a las V1, pero solo se observan solo en muestras preparadas mediante HPF.

En nuestro estudio, y mediante TEM, se identificaron consistentemente las vesículas V1, V2 y V3 dentro del citoplasma distal del soma de los PSC de *E. ortleppi* y *E. granulosus* s.s. (Figura 9). Asimismo, estas fueron observadas tanto en muestras embebidas en resina de forma clásica, así como en las muestras preparadas por HPF.

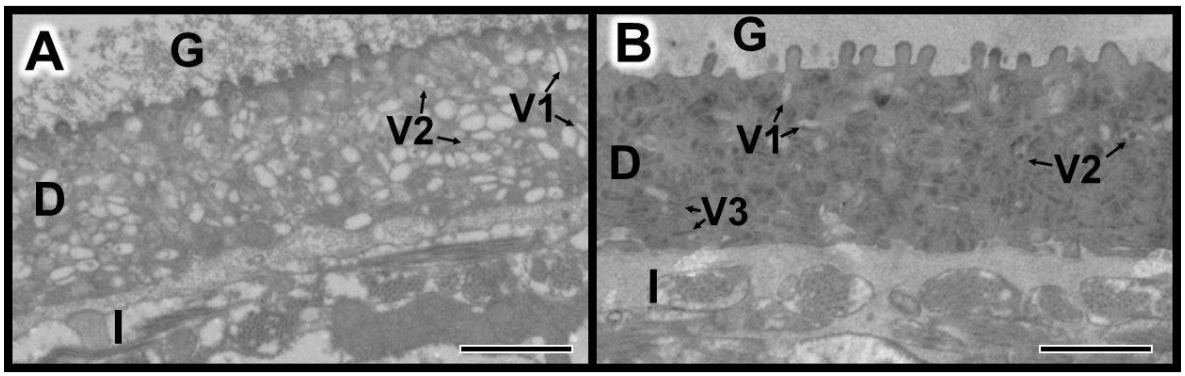

Figura 9. Vesículas clásicas en el tegumento. Vesículas clásicas V1, V2 y V3 fueron identificadas mediante microscopía electrónica de transmisión en secciones ultra finas (70

nm) de protoscoleces de *E. ortleppi* embebidos en resina tanto por metodología clásica (A) como por congelación a alta presión (B). *G*: glicocálix; *D*: citoplasma distal; *I*: Interior inmediato. Barra de escala = 500 nm. (Imagen modificada de Miles et al., 2021; Art. 1).

Por otro lado, dentro del área denominada "interior inmediato" (2,5 µm por debajo del citoplasma distal), se observaron vesículas no clásicas, es decir, que no fueron consistentes con la clasificación V1-V6; ya que fueron electrón-lúcidas, de mayor tamaño y con morfología semi-esférica (Figura 7). Estas vesículas no clásicas comparten su morfología y tamaño con las vesículas encontradas dentro del TVB. Además, y mediante un análisis exhaustivo de imágenes obtenidas mediante TEM, estas vesículas también se identificaron en todos los puntos de una posible ruta de secreción y/o internalización (Figura 10), que incluye al interior inmediato, la zona fibrosa, todo el citoplasma distal y el glicocálix. De manera interesante, cabe mencionar que las vesículas no clásicas observadas dentro del citoplasma distal están contenidas dentro de una estructura electrón-lúcida de mayor tamaño (Figura 10C-F).

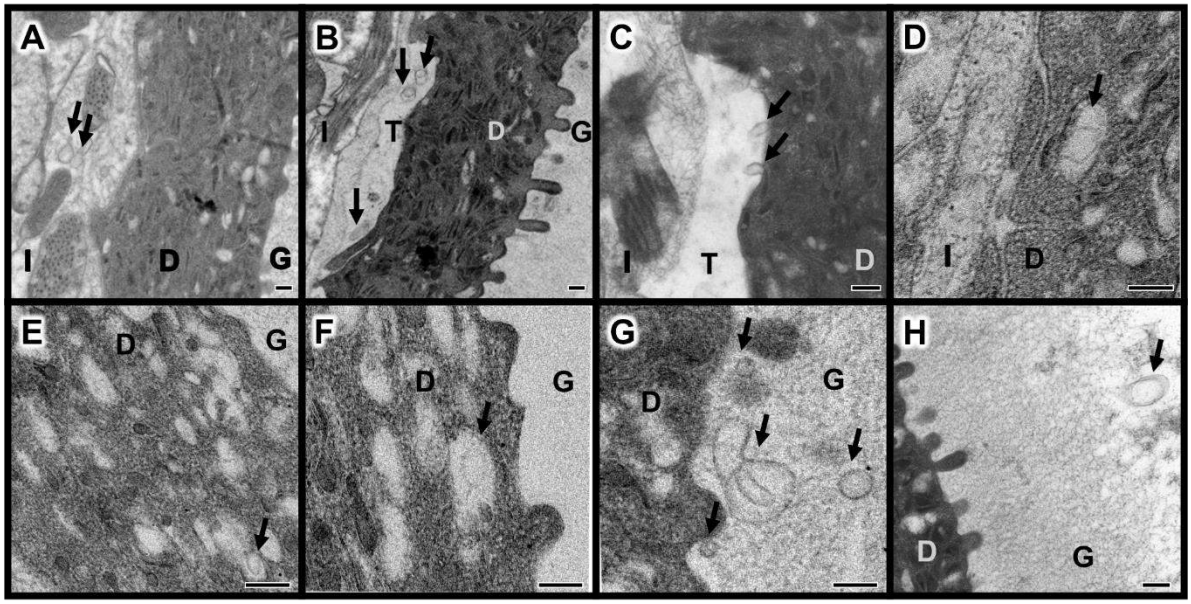

Figura 10. Vesículas no clásicas en el tegumento. Se considera vesículas no clásicas a aquellas no consistentes con V1-V6, con características electrón-lúcidas encontradas a lo

largo del tegumento del soma de protoscoleces. Estas vesículas no clásicas (señaladas con flechas) fueron identificadas en: (A) interior inmediato por debajo de la zona fibrosa, (B) dentro del TVB, (C) en la interface entre el TVB y el citoplasma distal, (D) en la cara más interna del citoplasma distal, (E) dentro del citoplasma distal, (F) en la cara más externa del citoplasma distal, (G) en la cara más interna del glicocálix, (H) en la cara más externa del glicocálix. *I*: interior inmediato; *D*: citoplasma distal; *G*: glicocálix; *T*: TVB. Barra de escala = 200 nm. (Imagen tomada de Miles et al., 2021; Art. 1).

La extensa localización de estas vesículas no clásicas, desde el glicocálix hasta el interior inmediato, sugiere que estarían involucradas en rutas de internalización (si el movimiento de las mismas es desde el glicocálix hacia el interior) y/o externalización (si el movimiento de las mismas es desde el interior hacia el glicocálix). En este sentido, el tegumento de los PSC se ha reportado como una región de alto tránsito molecular, mediante el cual el parásito es capaz que absorber nutrientes y componentes del hospedero, a la vez que participa de la excreción/secreción de componentes inmunomoduladores, y la liberación de exosomas (Nicolao et al., 2019; Pan et al., 2018; Wu et al., 2019; Zhou et al., 2019). Por ello, y para evaluar si las vesículas no clásicas descritas están involucradas en el tránsito de componentes a través del tegumento, se estudió mediante TEM con inmuno-marcación (inmunoTEM) la localización de tres antígenos parasitarios (GST1, FABP y AgB) y de una proteína del hospedero altamente presente en el líquido hidático (IgG bovinas).

En primer lugar, se analizó la localización de la proteína GST1 (glutatión S-transferasa 1). Esta enzima parasitaria está involucrada en la protección celular frente al estrés oxidativo, la modulación de procesos de señalización y la detoxificación de xenobióticos -incluyendo antihelmíntico-, entre otras funciones (Arbildi et al., 2017). Debido a que el tegumento es la interface entre el PSC y posibles componentes del sistema inmune del hospedero, la presencia de GSTs en el mismo podría ser útil para la sobrevida del parásito. En efecto, existen reportes que muestran la presencia de GST-1 en la superficie

de los PSC de *E. granulosus* s.l. (Arbildi et al., 2021), aunque su localización exacta no fue descrita. Por ello, analizamos la distribución de GST-1 en el tegumento mediante inmunoTEM sobre secciones ultrafinas (70 nm) de PSC de *E. ortleppi.* Para esto se incubaron las secciones con anticuerpos de ratón anti-GST-1, luego fueron incubadas con anticuerpos de conejo anti-ratón, y finalmente fueron incubadas con anticuerpos de cabra anti-conejo conjugados a nanopartículas (10 nm) de oro. Para el análisis de datos, las imágenes del tegumento del soma de los PSC fueron divididas en tres zonas, distinguiendo así entre glicocálix, citoplasma distal e interior inmediato. El área de cada zona fue calculada y el número de marcas en cada zona (círculos electrón-densos correspondientes a las nanopartículas de oro), se contó de forma manual; obteniéndose un valor de densidad de marcas en cada zona. En la Figura 11 se muestra una imagen representativa, donde cada marca representaría una molécula de GST-1 reconocida por un anticuerpo. Como se observa, la GST-1 se halló mayoritariamente presente en el glicocálix de los PSC. De manera interesante, cabe destacar que también se observó la co-localización de GST-1 en las vesículas contenidas en el TVB (Figura 11C), indicando que esta enzima formaría parte del cargamento vesicular.

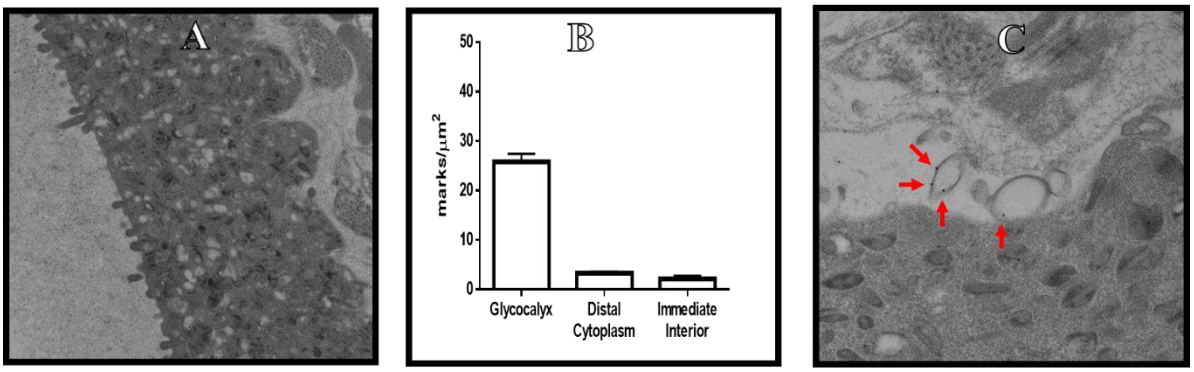

Figura 11. Análisis de GST-1 mediante inmunoTEM. La presencia de GST-1 en el tegumento del soma (A) y sobre las vesículas presentes dentro del TVB (C, indicadas mediante flechas) fue analizada mediante inmunoTEM en secciones ultrafinas (70 nm) de protoscoleces preparados mediante HPF. La abundancia de GST-1 a través del tegumento fue analizada en términos de densidad (número de marcas por μm^2), dividiendo al tegumento en

glicocálix, citoplasma distal e interior inmediato. La densidad de marcas para cada zona se observa en B. (Imagen modificada de Miles et al., 2021; Art. 1).

La presencia de la proteína parasitaria FABP (del inglés: *fatty acid binding protein*) a lo largo del tegumento, se analizó de forma análoga al estudio de la GST-1. Las FABP son proteínas pequeñas de unión reversible a ácidos grasos y otros ligandos hidrofóbicos (Xu et al., 2019). En particular, *E. granulosus* s.l. presenta un alto requerimiento de lípidos provenientes del hospedero para el mantenimiento y crecimiento del quiste hidático (Pórfido et al., 2020). En este sentido, la FABP se observó mayoritariamente presente en el glicocálix; y al igual que la GST-1, también se observó su co-localización en las vesículas presentes dentro del TVB (Figura 12).

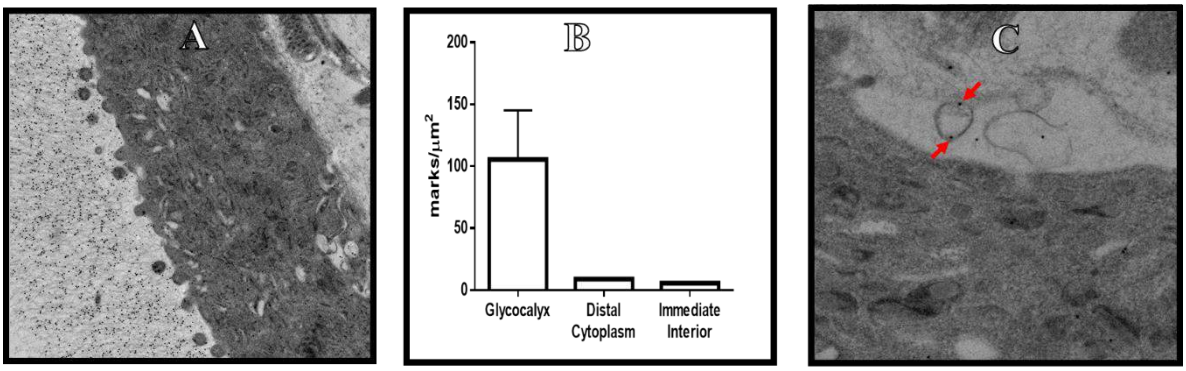

Figura 12. Análisis de FABP mediante inmunoTEM. La presencia de FABP en el tegumento del soma (A) y sobre las vesículas presentes dentro del TVB (C, indicadas mediante flechas) fue analizada mediante inmunoTEM en secciones ultrafinas (70 nm) de protoscoleces preparados mediante HPF. La abundancia de FABP a través del tegumento fue analizada en términos de densidad (número de marcas por μm^2), dividiendo al tegumento en glicocálix, citoplasma distal e interior inmediato. La densidad de marcas para cada zona puede ser observada en B. (Resultados no publicados).

Por otro lado, la presencia del antígeno B (AgB, subunidad 8/1) fue analizada de la misma manera que la GST-1 y la FABP. El AgB es una lipoproteína oligomérica compuesta

por subunidades relacionadas (de AgB8/1 a AgB8/5) de 8 kDa cada una (Chemale et al., 2001). Este antígeno es la proteína parasitaria más abundante en el líquido hidático, y está involucrada en diversas interacciones entre el parásito y el hospedero; fomentando el establecimiento de la infección así como la sobrevida del parásito en el hospedero intermediario (Monteiro et al., 2012; Riganò et al., 2007). Los resultados mostraron que la presencia del AgB en el tegumento de los PSC se observó mayoritariamente en el citoplasma distal; estando co-localizado dentro de las vesículas presentes en el TVB (Figura 13).

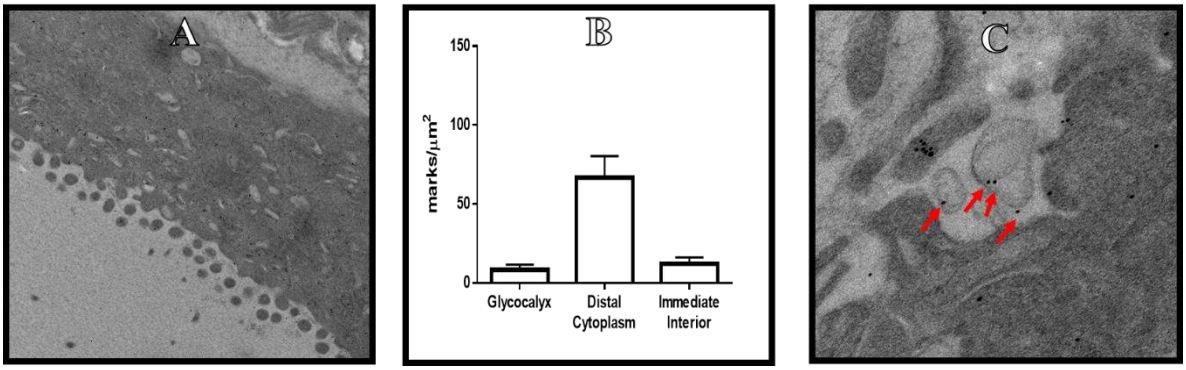

Figura 13. Análisis de AgB mediante inmunoTEM. La presencia de AgB en el tegumento del soma (A) y sobre las vesículas presentes dentro del TVB (C, indicadas mediante flechas) fue analizada mediante inmunoTEM en secciones ultrafinas (70 nm) de protoscoleces preparados mediante HPF. La abundancia de AgB a través del tegumento fue analizada en términos de densidad (número de marcas por μm^2), dividiendo al tegumento en glicocálix, citoplasma distal e interior inmediato. La densidad de marcas para cada zona puede ser observada en B. (Imagen modificada de Miles et al., 2021; Art. 1).

Finalmente, se analizó la presencia de proteínas del hospedero en el tegumento de los PSC, la cual estaría directamente relacionada con posibles vías de internalización. Para ello, se examinó la presencia de IgG bovina mediante inmunoTEM, ya que las IgG son de las proteínas del hospedero más abundantes dentro del líquido hidático (Aziz et al., 2011). En este sentido, y de manera interesante, se observó que la distribución de las IgG bovinas no fue uniforme a través del tegumento, a diferencia de lo observado para las moléculas parasitarias (GST-1, FABP y AgB). En el caso de las IgG bovinas, su presencia se observó en

forma de cúmulos, tanto en el glicocálix como en el citoplasma distal e interior inmediato (Figura 14). Además, una alta presencia de cúmulos de IgG bovinas fue observada en las células tegumentarias así como en sus extensiones citoplasmáticas, sugiriendo que los PSC serían capaces de internalizar proteínas del hospedero desde el líquido hidático. Esta internalización podría ser un proceso activo que concentra y transporta las proteínas del hospedero, de manera independiente a las vesículas no clásicas, ya que ningún cumulo de IgG bovinas se observó en asociación con dichas vesículas.

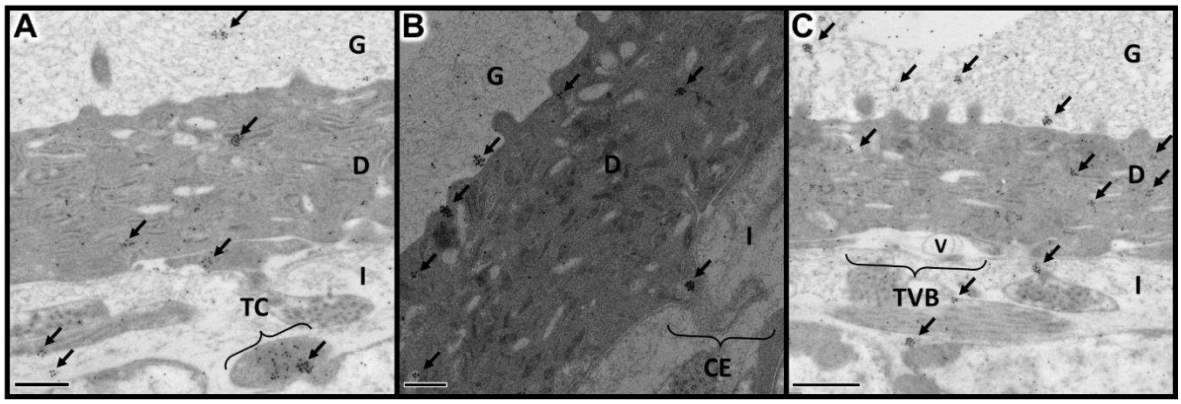

Figura 14. Inmunolocalización de antígenos del hospedero. La presencia de IgG bovinas en el tegumento del soma fue analizada mediante inmunoTEM en secciones ultrafinas (70 nm) de protoscoleces preparados mediante HPF. Cúmulos de marcas (flechas) fueron identificados a lo largo del glicocálix (G), citoplasma distal (D) e interior inmediato (I) de protoscoleces. Las figuras muestran diferentes imágenes de la misma sección mostrando estructuras interesantes. Una alta cantidad de marcas fue observada dentro de las células tegumentales (TC), y cúmulos de marcas fueron observados en sus correspondientes extensiones citoplasmáticas (CE). No se observaron marcas asociadas a vesículas presentes en TVB. Barra de escala = 500 nm. (Imagen tomada de Miles et al., 2021; Art. 1).

CAPÍTULO 2

CONCLUSIONES

La EQ es una enfermedad zoonótica cosmopolita que genera grandes pérdidas económicas y de salud a nivel mundial. A pesar de esto, aún es limitada la información sobre diversos aspectos de la biología y bioquímica del parásito que la causa. La gran complejidad de este parásito se evidencia en parte, en la alta plasticidad de desarrollo que presenta el estadío de PSC, ya que estos pueden desarrollarse tanto en gusanos adultos en el hospedero definitivo, como en metacestodes en el hospedero intermediario. En este sentido, en los PSC, la mayor barrera de interacción entre el parásito y el sistema inmune del hospedero es el tegumento, un sincicio celular que posee diversas actividades.

En el presente capítulo de la tesis, se realizó una caracterización detallada del tegumento de los PSC de *E. ortleppi* mediante el uso de diversas técnicas avanzadas de microscopía electrónica. Así, se obtuvo una reconstrucción 3D de los componentes tegumentarios clásicos, y se identificó, por primera vez, una novedosa estructura parasitaria -denominada TVB- que presenta un alto contenido de vesículas discretas en su interior. A su vez, se observaron vesículas similares en el glicocálix, citoplasma distal e interior inmediato, conteniendo antígenos parasitarios (GST-1, FABP y AgB) como carga vesicular. Estos antígenos parasitarios fueron localizados uniformemente en las estructuras tegumentarias. De manera interesante, la presencia de antígenos del hospedero (IgG bovinas) se observó bajo la forma de cúmulos, sugiriendo una posible ruta de internalización activa en el tegumento de los PSC de *E. granulosus* s.l.

CAPÍTULO 3

Objetivo específico #2: *Caracterizar a nivel proteómico y bioinformático los componentes proteicos presentes en el tegumento de los PSC de E. granulosus s.l.*

En este capítulo se presenta una descripción detallada de los componentes proteicos del tegumento de los PSC de *E. granulosus* s.l., así como un estudio de las modificaciones post-traduccionales asociadas a los mismos. Para ello, se utilizó una fracción de antígenos tegumentarios denominada PSEx, la cual fue analizada mediante dos técnicas distintas y complementarias de espectrometría de masas (MALDI-TOF/TOF y nanoLC-MS/MS); y los componentes identificados fueron luego analizados a nivel bioinformático. Así, el presente capítulo se divide en dos secciones:

3) Composición proteica del tegumento de PSC de *E. granulosus* s.l.
4) Modificaciones post-traduccionales presentes en proteínas tegumentarias de PSC de *E. granulosus* s.l.

La mayoría de estos resultados están contenidos en las siguientes publicaciones adjuntas:

Art. 2

"Combining proteomics and bioinformatics to explore novel tegumental antigens as vaccine candidates against Echinococcus granulosus infection"

Miles S, Portela M, Cyrklaff M, Ancarola ME, Frischknecht F, Durán R, Dematteis S, Mourglia-Ettlin G.

Journal of cellular biochemistry (2019)

doi: 10.1002/jcb.28799

Art. 3

"Unraveling post-translational modifications in Echinococcus granulosus sensu lato"

Miles S, Magnone J, García-Luna J, Dematteis S, Mourglia-Ettlin G.

Acta Tropica (2022)

doi: 10.1016/j.actatropica.2022.106410

A su vez, los resultados correspondientes al análisis proteómico de PSEx mediante espectrometría de masas nanoLC-MS/MS, sobre los cuales se basa parcialmente el estudio de modificaciones post-traduccionales, están contenidos en la siguiente publicación adjunta:

Anexo 1

"*Interactome analysis of CD5 and CD6 ectodomains with tegumental antigens from the helminth parasite Echinococcus granulosus*"

Miles S, Velasco-de-Andrés M, Lozano F, Mourglia-Ettlin G.

International Journal of Biological Macromolecules (2020)

doi: 10.1016/j.ijbiomac.2020.08.219

CAPÍTULO 3

SECCIÓN 3

Composición proteica del tegumento de PSC de E. granulosus s.l.

El tegumento de los PSC de *E. granulosus* s.l. es una zona compleja, compuesta por varias y diversas estructuras y células, que está involucrado en el tránsito de moléculas desde y hacia el interior del parásito. De esta forma, y a través del tegumento, el parásito no solo es capaz de internalizar los nutrientes necesarios para su sobrevida, sino que también es capaz de liberar, mediante excreción/secreción de componentes solubles y asociados a vesículas, diversos antígenos con potenciales actividades inmunomoduladoras (Nicolao et al., 2019; Pan et al., 2018; Wu et al., 2019; Zhou et al., 2019).

Por otro lado, el tegumento de los PSC constituye la primera línea de defensa del parásito, siendo sus componentes los primeros en interactuar con el sistema inmune del hospedero. En este sentido, se ha reportado que ciertos antígenos aún no identificados, presentes en el tegumento de los PSC de *E. granulosus* s.l., son capaces de inducir protección en el modelo murino de EQ secundaria. Parte de esta evidencia fue obtenida mediante estudios donde, tras la inoculación con PSC íntegros pero no viables (obtenidos mediante irradiación con luz UV), se genera un 100% de protección frente a posteriores desafíos con PSC viables en modelo murino de infección (Molan & Saeed, 1988). Por el contrario, si se inoculan PSC físicamente dañados (es decir, exponiendo antígenos no tegumentarios), no se observaba protección frente a una infección secundaria experimental (Molan & Saeed, 1988). Por otro lado, y en línea con estos resultados, si se inmuniza ratones con un extracto de proteínas tegumentarias, se logra inducir hasta un 80% de protección en el modelo murino de EQ secundaria (Hernández & Nieto, 1994).

Por ello, y para lograr una descripción más detallada del tegumento de los PSC de *E. granulosus* s.l., y poder analizar además su papel en el desarrollo de la infección, realizamos

una caracterización de su composición proteica. Para esto, nos centramos en analizar el extracto de proteínas tegumentarias capaz de inducir protección en el modelo murino de EQ secundaria (Hernández & Nieto, 1994). Dicho extracto, denominado PSEx, se obtuvo tras la incubación de PSC viables con un detergente suave no iónico (MEGA-10), seguido de una diálisis exhaustiva de la fracción soluble -contra PBS- para eliminar los restos de detergente (Hernández & Nieto, 1994). Así, obtuvimos un gran lote de PSEx utilizado a lo largo de toda la tesis, cuya concentración proteica fue de 3,8 mg/mL, y con relaciones (masa/masa) proteínas/carbohidratos y proteínas/lípidos de 7,2 y 1,3, respectivamente. Estas determinaciones se realizaron siguiendo los protocolos generales reportados por Miguez et al. (1996).

Por otro lado, y previo al análisis proteómico de PSEx, nos propusimos confirmar que la extracción con MEGA-10 solubilizó principalmente proteínas del citoplasma distal y del glicocálix de los PSC de *E. granulosus* s.l., y no otros componentes del interior parasitario. Para ello, y haciendo uso de las técnicas de microscopía electrónica descritas en el capítulo anterior, analizamos el tegumento de los PSC pre- y post-incubación con MEGA-10. Así, observamos que el tratamiento indujo la completa desaparición del citoplasma distal junto al glicocálix, sin afectar significativamente las estructuras internaras de los PSC de *E. granulosus* s.l. (Figura 15).

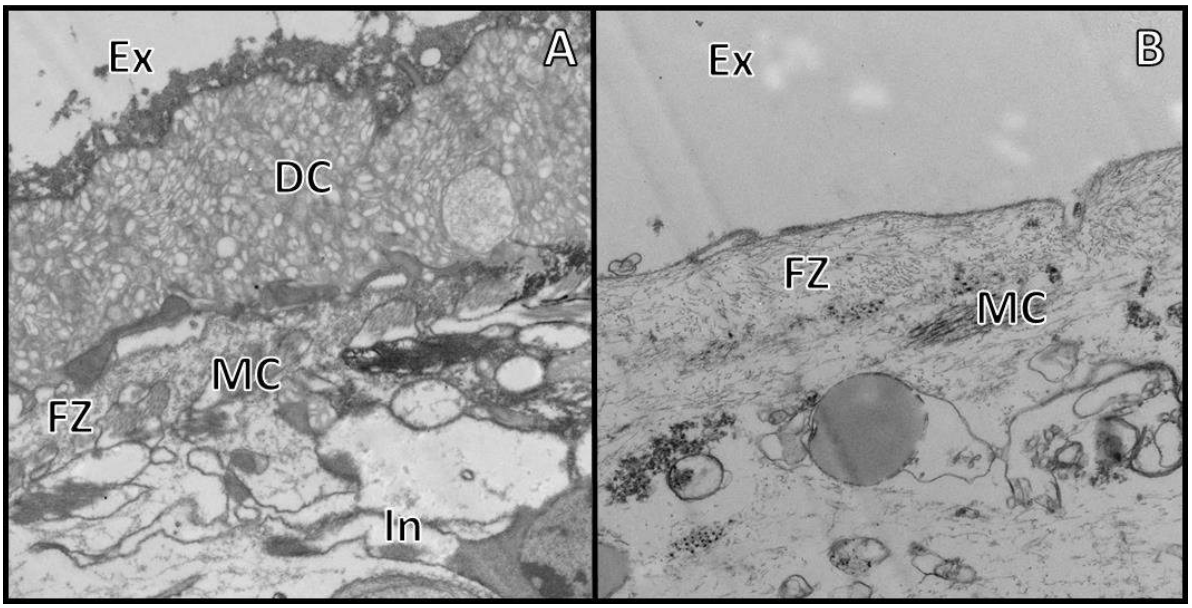

Figura 15. Tegumento pre y post extracción de PSEx. El tegumento de protoscoleces fue analizado mediante TEM antes (A) y después (B) de realizar la extracción de PSEx con el detergente MEGA-10. La estructura del interior inmediato se mantiene intacta tras la extracción, mientras que el citoplasma distal y la glicocálix desaparece por completo. (Imagen modificada de Miles et al., 2019; Art. 2).

Luego de confirmar que la fracción antigénica PSEx se compone principalmente de sustancias presentes en el tegumento (glicocálix y citoplasma distal) de los PSC de *E. granulosus* s.l., procedimos a analizar su proteoma mediante resolución bidimensional en geles de electroforesis (2DE) (Mourglia-Ettlin et al., 2018), seguida de identificación mediante espectrometría de masas de cada uno de los spots observados. Para ello, las proteínas de PSEx se sometieron, en primer lugar, a un isoelectroenfoque en un gradiente lineal de pH de 3 a 10; previa eliminación de lípidos y lipoproteínas que potencialmente interfirieran en este proceso. Luego, los componentes de PSEx se resolvieron según su peso molecular en un gel desnaturalizante SDS-PAGE al 10%.

Los geles 2DE obtenidos fueron teñidos con Azul de Coomassie o nitrato de plata, y los spots individuales observados fueron recortados y analizados mediante espectrometría de masas MALDI-TOF/TOF. En total, se colectaron 96 spots de ambos geles (50 spots del gel teñido con Azul de Coomassie, y 46 spots del gel teñido con nitrato de plata), los cuales fueron desteñidos y sometidos a digestión tríptica compatible con espectrometría de masas. Finalmente, se logró identificar 58 proteínas diferentes presentes en 63 spots (Figura 16): 27 proteínas identificadas solamente en los geles teñidos con Azul de Coomassie, 20 proteínas identificadas solamente en los geles teñidos con nitrato de plata, y 11 proteínas identificadas en ambos geles. Es interesante destacar que, mediante esta estrategia, no se identificaron proteínas del hospedero (*Bos taurus*).

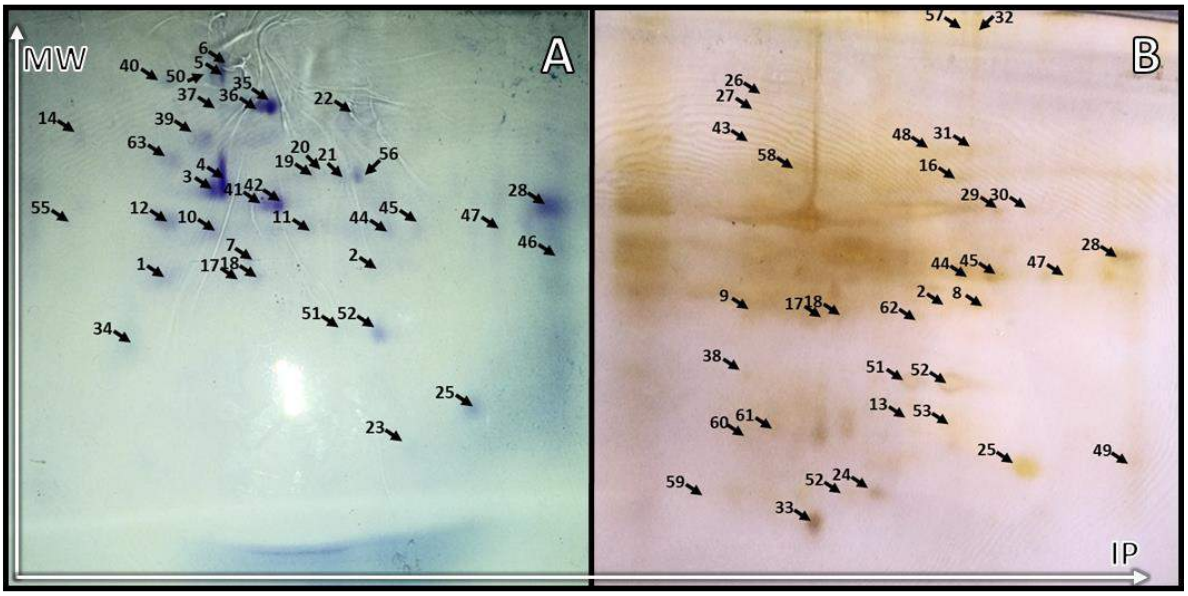

Figura 16. Resolución bidimensional de PSEx. Las proteínas presentes en PSEx fueron separadas según su punto isoeléctrico en un rango lineal de 3-10 (de izquierda a derecha), y luego según su masa molecular en un gel de SDS-PAGE. Los geles 2D-PAGE fueron teñidos con Azul de Coomassie (A) o nitrato de plata (B), y los spots individuales observados fueron colectados para análisis por espectrometría de masas. Las flechas indican la localización de las proteínas identificadas. (Imagen modificada de Miles et al., 2019; Art. 2).

Una vez obtenido el proteoma de PSEx, se procedió a analizarlo mediante Ontología de Genes (GO, del inglés: *Gene Ontology*), la cual es una iniciativa bioinformática que busca unificar la representación de genes y sus productos mediante un vocabulario controlado, permitiendo así analizar genomas y proteomas en base a características de cada uno de sus componentes (Harris et al., 2008). En el caso de proteínas, GO permite asociar términos a 3 categorías generales: Procesos Biológicos, Funciones Moleculares, y Componente Celular. Para realizar este análisis con el proteoma de PSEx, primero se obtuvieron los términos de GO asociados a cada una de las 58 proteínas encontrados en la base de datos de UniProt, y luego se realizó una predicción complementaria de términos de GO a cada proteína mediante el uso del programa FFPred3 (Cozzetto et al., 2016). Así, se obtuvieron 711 términos asociado a 56 proteínas, existiendo dos proteínas del proteoma cuyo gran tamaño no permitió la realización de este análisis bioinformático, siendo 184 de estos términos únicos en el proteoma. Finalmente, se realizó una primera reducción en dos niveles de jerarquía, seguido por una agrupación en "superclusters" de términos vagamente relacionados (Supek et al., 2011) para ser mostrados como gráficos de torta (Figura 17).

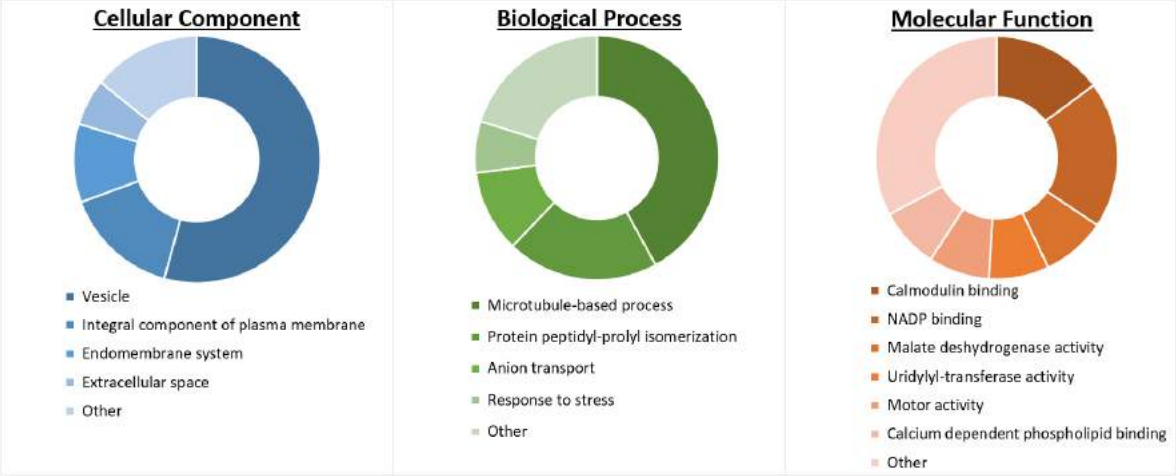

Figura 17. Estudio de *Gene Ontology* del proteoma de PSEx. El análisis de GO de las proteínas de PSEx se muestra dividido en Componentes Celulares, Procesos Biológicos y Funciones Moleculares. Para cada categoría, los términos únicos fueron reducidos en 2 niveles de jerarquía y los términos vagamente relacionados fueron agrupados en "superclusters" y mostrados como gráficos de torta. (Imagen modificada de Miles et al., 2019; Art. 2).

Los resultados obtenidos mostraron que PSEx es una fracción compleja compuesta por proteínas principalmente localizadas en el citoplasma distal. En este sentido, los análisis de GO son consistentes con esta afirmación, ya que se observó que la mayoría de las proteínas están asociadas a vesículas, siendo el citoplasma distal un sincicio celular altamente vesiculado como se mostró en el capítulo anterior. Además, el análisis de GO mostró que las proteínas presentes en PSEx están involucradas en diversas funciones metabólicas; así como en procesos basados en microtúbulos, como puede ser el tránsito de moléculas a través del citoplasma distal o el movimiento parasitario, ambas funciones asociadas al tegumento de los PSC de *E. granulosus* s.l.

CAPÍTULO 3

SECCIÓN 4

Modificaciones post-traduccionales presentes en proteínas tegumentarias de PSC de E. granulosus s.l.

Conocer el proteoma de una fracción antigénica con capacidad protectora puede constituir el primer paso para desarrollar nuevas herramientas de diagnóstico y/o estrategias de vacunación frente a un agente infeccioso. Sin embargo, existen características particulares de cada proteína que tienen que ser tomadas en cuenta previo al uso de las mismas como candidatos para inmunodiagnóstico y/o inmunoterapias. Una de estas características es la presencia de modificaciones post-traduccionales (PTMs, del inglés: *Post-Translational Modifications*), las cuales son usualmente modificaciones covalentes, generadas comúnmente mediante procesos enzimáticos, que ocurren en las proteínas luego de la síntesis ribosómica. Las PTMs influyen en la señalización celular, permiten la activación/desactivación de enzimas, ayudan al correcto plegamiento y estabilidad de las proteínas, entre muchas otras funciones (Voet et al., 2016). Las PTMs se localizan tanto en las cadenas laterales de los aminoácidos, así como en los extremos C- y N- terminales de las proteínas. Estas modificaciones suelen generar cambios conformacionales e introducir posibles impedimentos estéricos para el desarrollo de algunos tipos de respuesta inmune, principalmente el reconocimiento mediante anticuerpos. En este sentido, las PTMs pueden afectar negativamente la reactividad cruzada de anticuerpos inducidos en respuesta a un antígeno recombinante (usualmente carente de PTMs) presente en una formulación vacunal, afectando así el reconocimiento de la proteína nativa en el contexto de una infección natural (Walsh, 2010).

Hasta la fecha, se han caracterizado más de 400 PTMs distintas, presentes en organismos procariotas y eucariotas (Walsh, 2010). Sin embargo, el estudio de las PTMs en *E. granulosus* s.l., y en cestodos en general, ha sido muy limitado. Por ello, en esta sección

del capítulo se profundizó en la identificación de posibles PTMs presentes en proteínas del tegumento de los PSC de *E. granulosus* s.l.

En primer lugar, partiendo de los espectros obtenidos por MALDI-TOF/TOF para cada uno de los 63 spots identificados en PSEx, y analizados en la sección anterior de este capítulo, y haciendo uso del programa FindMod (Wilkins et al., 1999), se identificaron 27 posibles PTMs enzimáticas presentes en las 58 proteínas identificadas en PSEx (Tabla 1). Este programa reanaliza los espectros de masas usados para identificar una proteína, generando una sub-lista de valores m/z a los cuales se les restó la masa teórica de cada una de las PTMs analizadas. Así, si existe un nuevo valor de m/z que coincide con uno de los fragmentos peptídicos de la digestión teórica de la proteína, se sugiere que el valor de m/z original corresponde a dicho fragmento peptídico unido a dicha PTM.

Por otro lado, y mediante una búsqueda manual en la base de datos de UniProt, se encontraron proteínas de *E. granulosus* s.l. anotadas que contenían 5 de las 27 posibles PTMs identificadas por FindMod (Tabla 1). Además, 8 PTMs adicionales fueron encontradas anotadas en proteínas de otros platelmintos (Tabla 1). En paralelo, y dado que solo se analizaron PTMs enzimáticas, se procedió a examinar si las enzimas que catalizan cada una de las 27 modificaciones identificadas por FindMod estaban presentes en el genoma de *E. granulosus* s.l. Así, primero se obtuvo una lista de la/s enzima(s) necesarias para realizar cada modificación, y luego se las buscó en la base de datos de proteínas *E. granulosus* s.l.; identificando las enzimas necesarias para realizar 22 PTMs, incluyendo aquellas 13 PTMs anotadas en proteínas de platelmintos (Tabla 1).

La presencia de 19 de estas 22 PTMs fue además identificada en las proteínas de PSEx mediante el uso de espectrometría de masas de alta resolución (nanoLC-MS/MS). Para ello, se utilizaron espectros previamente obtenidos para PSEx por nuestro grupo de trabajo (Miles et al., 2020, Anexo 1). El espectrómetro de masas nanoLC-MS/MS analiza todos los fragmentos obtenidos de la digestión tríptica de una fracción proteica a la vez, en contraposición con MALDI-TOF/TOF donde se analizan spots individuales, lo cual aumenta

la sensibilidad de la técnica en gran medida. Para este análisis, se generó una base de datos personalizada compuesta únicamente por las 58 proteínas identificadas por MALDI-TOF/TOF, y se identificaron las proteínas modificadas para cada una de las PTMs descritas anteriormente. Además, y ya que las PTMs se encuentran ancladas a la cadena lateral de un aminoácido (o extremos C- y N- terminales de las proteínas), y tanto los análisis de FindMod como la identificación por nanoLC-MS/MS permite identificar el punto de anclaje de las PTMs, se identificaron aquellas PTMs unidas al mismo aminoácido en cada péptido por ambas metodologías. Así, 9 PTMs en las proteínas de PSEx fueron identificadas con una muy alta confianza, correspondiendo a acetilación, metilación, fosforilación, deamidación, deamidación seguida por metilación, *S*-nitrosilación, di-hidroxilación y di-metilación. De manera interesante, cabe destacar que estas 5 últimas PTMs fueron identificadas por primera vez en este estudio, tanto en proteínas de *E. granulosus* s.l. así como en platelmintos en general.

Tabla 1. Identificación de modificaciones post-traduccionales. 27 posibles PTMs fueron identificadas en las proteínas de PSEx mediante el software FindMod a partir de espectros de masas obtenidos por MALDI-TOF/TOF. La búsqueda de proteínas de *E. granulosus* s.l., u otros Platelmintos anotadas con alguna de estas PTMs en la base de datos de UniProt resultó en la identificación de 5 y 13 proteínas previamente reportadas respectivamente. La búsqueda de las enzimas claves necesarias para que se realicen las PTMs estudiadas en el genoma de *E. granulosus* s.l. fue exitosa para 22 PTMs. De estas, 19 fueron identificadas tras analizar el PSEx mediante nanoLC-MS/MS. Los tics (✓) indican que al menos una proteína fue identificada presentando la PTM analizada, o que la enzima(s) clave(s) se encuentran presentes en el genoma de *E. granulosus* s.l. (Tabla modificada de Miles et al., 2022; Art. 3).

Abreviación	Modificaciones Post Traduccionales	Masa monoisotópica (Da)	Identificado por MALDI-TOF/TOF	Reportado en		Enzimas claves en E. granulosus s.l.	Identificado por nanoLC-MS/MS
				E. granulosus s.l.	Otros platelmintos		
ACET	*Acetylation*	42.0106	✓	✓	✓	✓	✓
ADP	*ADP-ribosylation*	541.061	✓	-	-	✓	-
AMID	*Amidation*	-0.9847	✓	-	✓	✓	-
BROM	*Bromination*	77.9105	✓	-	-	-	-
CSEA	*Cysteine sulfenic acid (-SOH)*	15.9949	✓	✓	✓	✓	✓
CSIA	*Cysteine sulfinic acid (-SO2H)*	31.9898	✓	-	-	-	-
CYSP	*Cysteine persulfide*	31.9721	✓	-	✓	✓	✓
DEAM	*Deamidation*	0.984	✓	-	-	✓	✓
DEAME	*Deamidation followed by a methylation*	14.9997	✓	-	-	✓	✓
DIHYDR	*Dihydroxylation*	31.9898	✓	-	-	✓	✓
DIMETH	*Dimethylation*	28.0314	✓	-	-	✓	✓
FARN	*S-farnesyl cysteine*	204.1878	✓	-	✓	✓	✓
FORM	*Formylation*	27.9949	✓	-	-	-	-
GERA	*Geranyl-geranylation*	272.2504	✓	-	✓	✓	✓
GGLU	*Gamma-carboxyglutamic acid*	43.9898	✓	-	-	-	-
GLCN	*O-GlcNac*	203.0794	✓	✓	✓	✓	✓
GLUT	*Glutathionylation*	305.0681	✓	-	-	✓	-
HYDR	*Hydroxylation*	15.9949	✓	-	✓	✓	✓
METH	*Methylation*	14.0157	✓	-	✓	✓	✓
MYRI	*Myristoylation*	210.1984	✓	-	✓	✓	✓
NTRY	*S-Nitrosylation*	28.9902	✓	-	-	✓	✓
OCTA	*n-Octanoate*	126.1044	✓	-	-	✓	✓
PALM	*Palmitoylation*	238.2297	✓	-	✓	✓	✓
PHOS	*Phosphorylation*	79.9663	✓	✓	✓	✓	✓
SULF	*Sulfation*	79.9568	✓	✓	✓	✓	✓
TRIMETH	*Trimethylation*	42.047	✓	-	-	✓	✓
TRIMETK	*N6,N6,N6-Trimethyl-5-hydroxylysine*	59.0497	✓	-	-	-	-

CAPÍTULO 3

CONCLUSIONES

La escasa información disponible acerca de varios aspectos de la biología y bioquímica de *E. granulosus* s.l., contribuye a que existan pocos avances biotecnológicos aplicados al control de la infección. Por ello, en el presente capítulo de la tesis se realizó una caracterización proteómica completa de una fracción de proteínas tegumentarias obtenidas principalmente del citoplasma distal de PSC de *E. granulosus* s.l.

En primer lugar, se corroboró mediante microscopía electrónica, que PSEx estuviese compuesto principalmente por proteínas tegumentarias. Luego, se analizó su contenido proteico, glucídico y lipídico, y se realizó su resolución proteica en geles bidimensionales. Posteriormente, se realizó una caracterización proteómica de los componentes identificados, a partir de los spots individuales observados en los geles 2DE. Así, se obtuvo un proteoma aproximado de PSEx compuesto por 58 proteínas.

Luego, y partiendo de este estudio, se analizó la presencia de posibles PTMs en las proteínas de PSEx, identificándose 22 posibles PTMs; nueve de las cuales fueron identificadas con una muy alta confianza. Este estudio complementó la caracterización proteómica del tegumento de los PSC de *E. granulosus* s.l., y permitió expandir la escasa información disponible sobre la existencia de PTMs en proteínas de platelmintos.

CAPÍTULO 4

Objetivo específico #3: *Evaluar el papel de los componentes tegumentarios de PSC de E. granulosus s.l. en el establecimiento de la EQ secundaria experimental.*

En este capítulo se presenta una descripción de la respuesta inmune humoral generada por el hospedero en el modelo murino de EQ secundaria, contra componentes tegumentarios de PSC de *E. granulosus* s.l. En primer lugar, se analizó la respuesta de anticuerpos generadas en dos cepas de ratones con diferentes niveles de susceptibilidad natural a la infección experimental. Luego, se identificaron aquellos antígenos parasitarios diferencialmente reconocidos por los anticuerpos generados entra ambas cepas de ratones. Así, el presente capítulo se divide en 2 secciones:

5) Respuesta inmune humoral contra componentes del tegumento de PSC de *E. granulosus* s.l. en el modelo murino de EQ secundaria.
6) Reconocimiento diferencial de antígenos tegumentarios de PSC de *E. granulosus* s.l. por parte de anticuerpos de ratones Balb/c y C57Bl/6.

La mayoría de estos resultados están contenidos en la siguiente publicación adjunta:

Art. 4

"Linking murine resistance to secondary cystic echinococcosis with antibody responses targeting Echinococcus granulosus tegumental antigens"

Miles S, Magnone J, Cyrklaff M, Arbildi P, Frischknecht F, Dematteis S, Mourglia-Ettlin G.

Immunobiology (2020)

doi: 10.1016/j.imbio.2020.151916

CAPÍTULO 4

SECCIÓN 5

Respuesta inmune humoral contra componentes del tegumento de PSC de E. granulosus s.l. en el modelo murino de EQ secundaria.

Los modelos animales son esenciales para el estudio de enfermedades infecciosas, siendo los modelos murinos los más utilizados debido al tamaño de los animales, su bajo costo, facilidad de manejo, y diversidad de cepas exo- y endogámicas; muchas de las cuales pueden, además, ser modificadas genéticamente con facilidad. Además, el sistema inmune de los ratones está bien caracterizado, y muestra grandes similitudes con el sistema inmune de los humanos; haciendo que los ratones sean susceptibles a muchos patógenos, sin ser necesariamente sus hospederos naturales (Colby et al., 2017).

Sin embargo, las distintas cepas de ratones existentes suelen mostrar grandes diferencias en la respuesta inmune montada frente en el contexto de una enfermedad determinada, sea esta infecciosa o no. En este sentido, existen reportes sobre diferencias en la respuesta inmune entre ratones de las cepas Balb/c y C57Bl/6 -las dos más ampliamente utilizadas en modelos murinos de infección- frente a virus, bacterias, protozoarios y helmintos parásitos (Anthony et al., 2007; Cheers et al., 1978; Chiodini & Buergelt, 1993; Ferreira et al., 2018; Fornefett et al., 2018b; Henderson et al., 2015; Kulcsar et al., 2015; Liu et al., 2002; Mols-Vorstermans et al., 2013; Mourglia-Ettlin et al., 2016a; Pereira et al., 2016; Xiang et al., 2016; Zhang et al., 2005). En particular, también se han hallado estas diferencias frente a la infección experimental con *E. granulosus* s.l., las cuales se han asociado con diferencias en la susceptibilidad al desarrollo de la EQ secundaria (Mourglia-Ettlin et al., 2016a). En este sentido, se ha reportado que los ratones de la cepa C57Bl/6, presentan anticuerpos naturales -e inducidos- con mayor capacidad de limitar el establecimiento de la infección; a la vez que presentan un mayor número de macrófagos

peritoneales y células B, y una respuesta de citoquinas del tipo Th2 menos intensa, que genera en su conjunto una baja susceptibilidad a la infección secundaria experimental (Mourglia-Ettlin et al., 2016a, 2016b).

En el presente capítulo analizamos en detalle la respuesta inmune humoral desarrollada por ratones Balb/c y C57Bl/6 frente a antígenos tegumentarios de PSC de *E. granulosus* s.l. en el modelo de EQ secundaria. Para esto, se obtuvo el suero de ratones Balb/c y C57Bl/6 infectados (21 días p.i.), y de sus controles sin infectar; para luego, mediante ELISA, evaluar el título de cada isotipo (IgM, IgA e IgE) -y subclase (IgG1, IgG2b, IgG2a/c e IgG3)- de anticuerpos contra PSEx. Además, se analizó el índice de avidez para cada isotipo/subclase de anticuerpos. Los resultados obtenidos mostraron que, los ratones Balb/c normales, presentan un título de anticuerpos naturales capaces de reconocer componentes de PSEx, mayor que los ratones C57Bl/6 normales (Figura 18). Además, y de manera interesante, los ratones Balb/c presentaron mayores títulos de anticuerpos IgE, tanto en ratones normales como infectados, con respecto a los ratones C57Bl/6. La inducción de anticuerpos IgE suele ser la respuesta clásica en las infecciones por helmintos parásitos, mediando el reconocimiento y degranulación de eosinófilos y mastocitos con el fin de eliminar al parásito (Fitzsimmons et al., 2014).

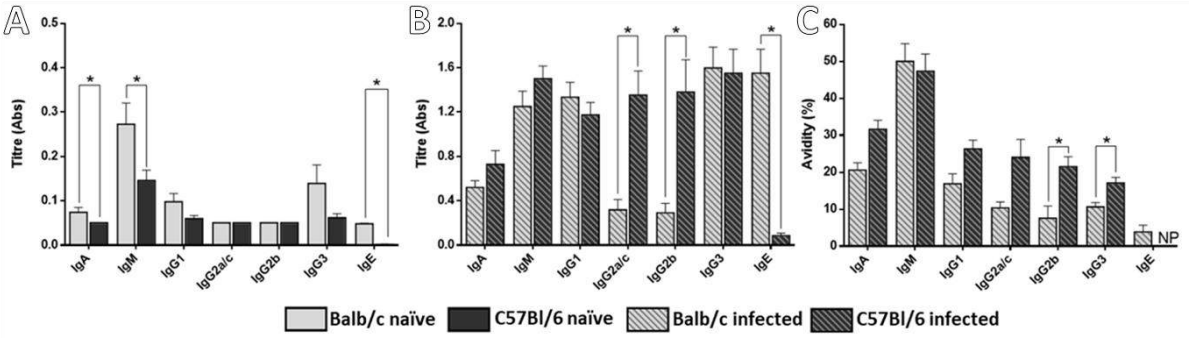

Figura 18. Respuesta de anticuerpos contra antígenos tegumentarios. El título de anticuerpos específicos contra PSEx fue analizado mediante ELISA en suero de ratones Balb/c y C57Bl/6 normals (A) e infectados (B). Los títulos fueron expresados como la absorbancia detectada a la mayor dilución no saturante analizada. El índice de avidez (C) de

los anticuerpos anti-PSEx fue analizado mediante ELISA en suero de ratones infectados. Estadística: test U de Mann-Whitney-Wilcoxon. Los resultados se muestran como media ± SEM. Las diferencias fueron consideradas como significativas con $p < 0.05$, y mostradas con un asterisco. (Imagen modificada de Miles et al., 2020; Art. 4).

Por su parte, los ratones de la cepa C57Bl/6 infectados, generaron altos títulos -y con alta avidez- de anticuerpos IgG2b e IgG2c específicos (Figura 18). Estos anticuerpos, podrían ser capaces de inducir la activación del sistema complemento sobre la superficie de los PSC, induciendo así la muerte de los mismos. Para confirmar esto, se analizó mediante ensayos *in vitro*, la activación del sistema complemento por vía clásica, y la consecuente muerte de los PSC, por parte de los anticuerpos presentes en el suero de ratones Balb/c y C57Bl/6. Para ello, en primer lugar, se purificaron las γ-globulinas del suero de ratones Balb/c y C57Bl/6 -infectados y controles- mediante precipitación con sulfato de amonio. Luego, se incubaron PSC viables de *E. granulosus* s.l. con las γ-globulinas purificadas suplementadas con suero fresco de ratones normales, Balb/c o C57Bl/6 según fuese el caso, como fuente de complemento. Tras 4 horas de incubación, se evaluó la viabilidad de los PSC, observándose que únicamente las γ-globulinas procedentes de ratones C57Bl/6 infectados fueron capaces de aumentar significativamente la tasa de muerte de los parásitos, inducida por el suero fresco (Figura 19).

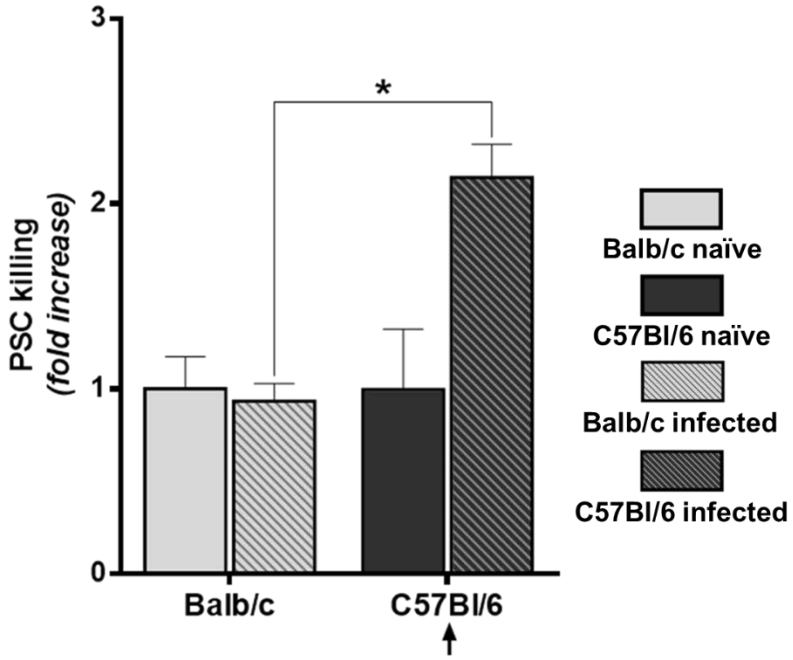

Figura 19. Activación del sistema de complemento dependiente de anticuerpos. La actividad protoscolicida de los anticuerpos dependiente de la activación del sistema del complemento fue analizada *in vitro.* Para esto se utilizaron γ-globulinas purificadas del suero de ratones Balb/c y C57Bl/6 normales e infectados, las cuales fueron complementadas -o no- con suero de ratones normales de la misma cepa. El gráfico muestra el *fold-increase* de la muerte de protoscoleces con respecto a la misma condición no complementada. Estadística: *2-way* ANOVA. Los resultados se muestran como media ± SEM. Las diferencias fueron consideradas como significativas con $p < 0.05$, y mostradas con una flecha (comparaciones entre una misma cepa) o asterisco (comparaciones entre cepas). (Imagen modificada de Miles et al., 2020; Art. 4).

A continuación, y para confirmar que los anticuerpos involucrados en la muerte de los PSC sean específicos para sus antígenos tegumentarios, se analizó el perfil de estructuras parasitarias reconocidas por los anticuerpos de cada cepa de ratones. Para ello, se realizaron estudios de inmunoTEM, donde se incubaron secciones ultrafinas (70 nm) de PSC frescos preparados mediante HPF, con el suero de ratones Balb/c y C57Bl/6 -infectados y sus controles- y se evaluó la densidad de marcas en forma análoga a los procedimientos descritos en el Capítulo 2 de esta tesis (Figura 20).

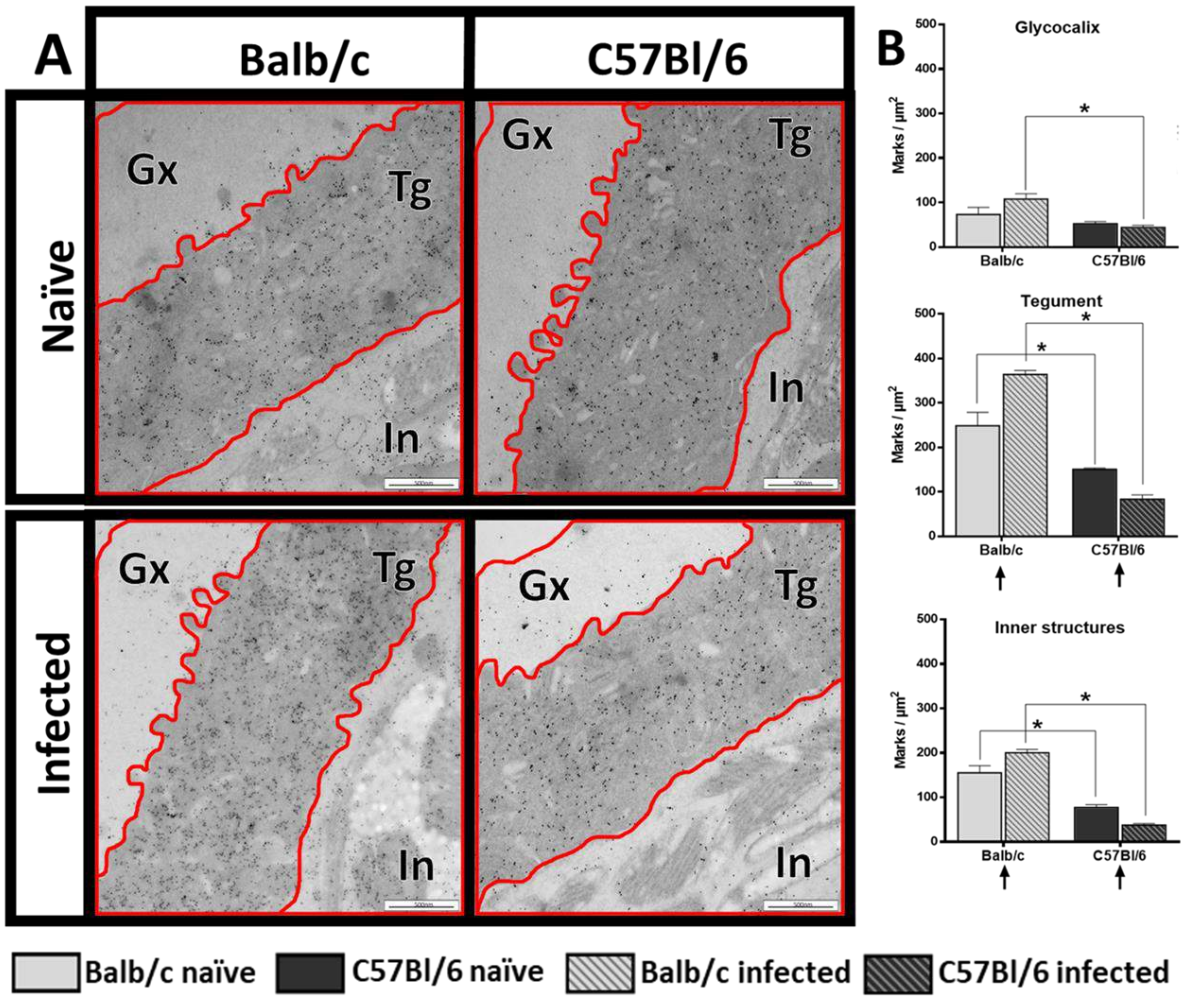

Figura 20. Reconocimiento de antígenos en el tegumento de protoscoleces. El reconocimiento de antígenos en el tegumento de protoscoleces por parte de los anticuerpos de ratones Balb/c y C57Bl/6 normales e infectados fue analizado mediante inmunoTEM y análisis de densidad de marcas. En (A) se muestran imágenes representativas de las condiciones analizadas mediante inmunoTEM, donde los bordes de cada estructura parasitaria analizada se marcan en rojo, dividiendo las secciones en glicocálix (Gx), citoplasma distal (Tg) e interior inmediato (In). Para cada estructura, el número de marcas fue obtenido de forma manual, y el área correspondiente fue calculada, obteniéndose un valor de densidad de marca (B), a partir de 6 réplicas para cada condición. Los resultados se muestran como media ± SEM. Las diferencias fueron consideradas como significativas con $p < 0.05$, y mostradas con una flecha (comparaciones entre una misma cepa) o asterisco (comparaciones entre cepas). (Imagen modificada de Miles et al., 2020; Art. 4).

Los resultados mostraron que, generalmente, se observaron valores mayores de densidad de marca con los sueros de ratones Balb/c respecto a los C57Bl/6; y en todas las regiones parasitarias estudiadas. Más interesante aún, mientras que los sueros de los ratones Balb/c infectados mostraron un aumento respecto a los sueros Balb/c normales en la densidad de marcas sobre el tegumento y las estructuras del interior inmediato de los PSC; lo opuesto se observó para ratones C57Bl/6. Esta disminución en los valores de densidad de marca por parte de los anticuerpos del suero de ratones C57Bl/6 infectados, sumado al aumento en su título de anticuerpos específicos para PSEx y al incremento de su capacidad protoscolicida *in vitro*, previamente discutidos; sugiere que los ratones C57Bl/6 generarían una respuesta inmune humoral intensa contra un número limitado de antígenos tegumentarios. Así, este hecho podría estar involucrado en la menor susceptibilidad de los ratones de la cepa C57Bl/6 al desarrollo de la EQ secundaria.

Además, es interesante destacar que, si se inmunizan ratones Balb/c y C57Bl/6 con PSEx (en ausencia de adyuvante), la respuesta humoral temprana desarrollada es muy similar a la generada en el contexto de la infección experimental. Estos resultados fueron obtenidos tras realizar, primero, una inmunización con PSEx en ratones Balb/c y C57Bl/6 a los días 0 (*priming*) y 10 (*booster*), y obtener el suero de los mismos al día 17 post-*priming*. Luego, repetimos las actividades realizadas anteriormente, pero utilizando los sueros obtenidos mediante inmunización con PSEx (Figura 21). Así, observamos que el reconocimiento de antígenos en el tegumento de los PSC (en términos de densidad de marcas) fue menor en los sueros provenientes de ratones C57Bl/6 inmunizados que en su contraparte Balb/c. A su vez, el reconocimiento de antígenos en el tegumento disminuyó en ratones C57Bl/6 inmunizados con PSEx (Figura 21A); de manera análoga a lo ocurrido en el contexto de la infección experimental. Más interesante aún, la actividad protoscolicida *in vitro* de los sueros de ratones C57Bl/6 aumentó tras la inmunización con PSEx (con respecto a ratones C57Bl/6 normales); a la vez que esta fue mayor que la de los sueros obtenidos de ratones Balb/c inmunizados con PSEx (Figura 21C). En términos de títulos e índice de avidez de los anticuerpos específicos contra PSEx generados tras inmunización, el perfil de los

mismos fue similar al de los generados en la infección experimental (Figura 21B). Así, se observó un mayor título de anticuerpos de la subclase IgG2a/c en ratones C57Bl/6, y un mayor título de anticuerpos IgE en ratones Balb/c; aunque este parecería ser menor en ratones inmunizados con respecto a ratones infectados.

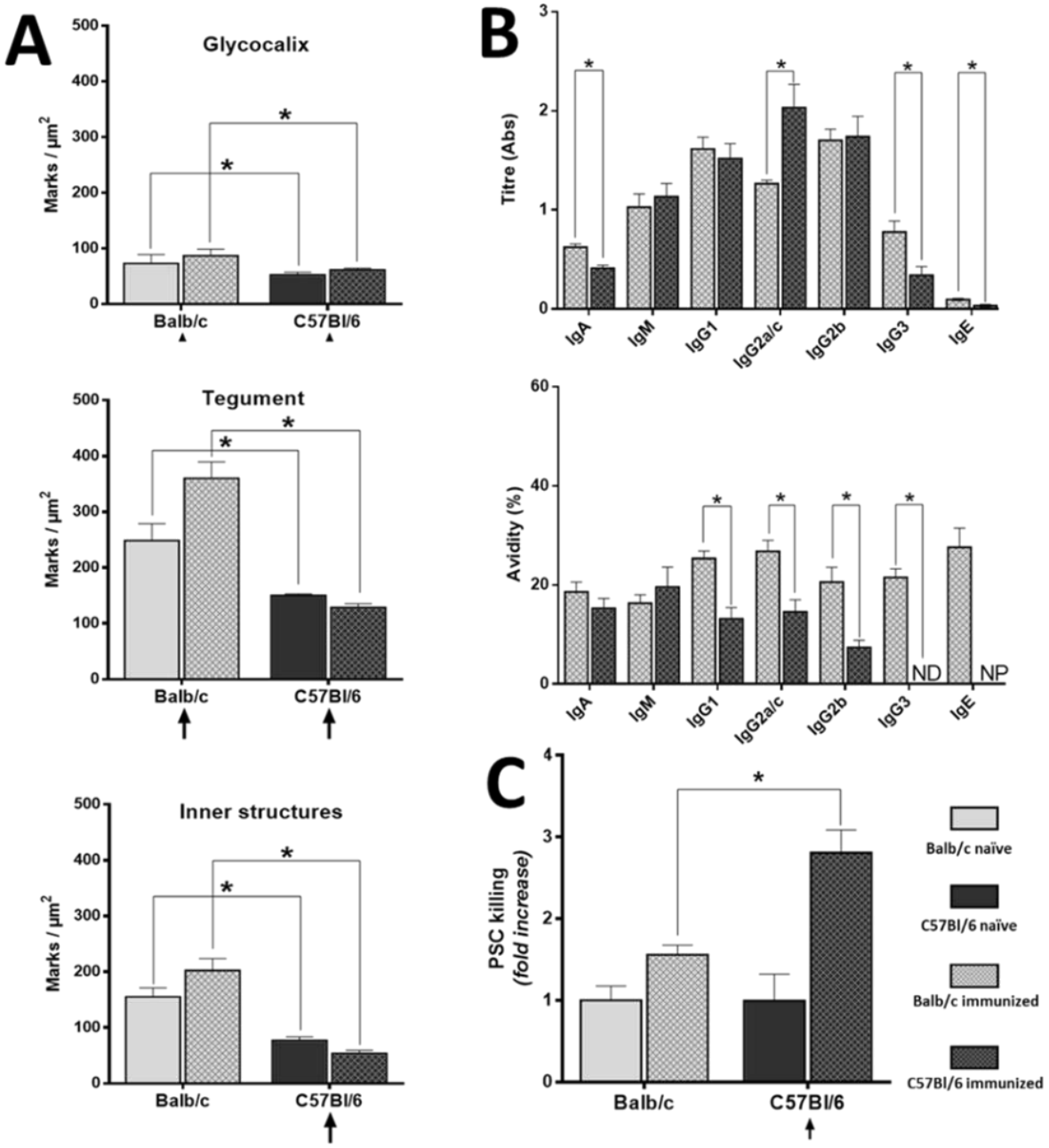

Figura 21. Respuesta inmune humoral en ratones Balb/c y C57Bl/6 inmunizados con PSEx.
(A) El análisis por inmunoTEM fue análogo al mostrado en la Figura 20, incubando las

secciones ultra-finas de PSC con suero de ratones Balb/c y C57Bl/6; normales o inmunizados con PSEx. El reconocimiento de antígenos sobre el tegumento de PSC se muestra en términos de densidad de marcas para el glicocálix (Gx), citoplasma distal (Tg) e interior inmediato (In); obtenida a partir de 6 réplicas para cada condición. Estadística: test de Student. (B) El título de anticuerpos específicos en ratones Balb/c y C57Bl/6 inmunizados con PSEx, y la avidez de los mismos, fue analizado mediante ELISA. Estadística: Mann-Whitney-Wilcoxon. (C) La actividad protoscolicida de los anticuerpos dependiente de la activación del sistema del complemento fue analizada *in vitro* utilizando suero homólogo normal suplementado con γ-globulinas purificadas del suero de ratones Balb/c y C57Bl/6; normales o inmunizados con PSEx. Estadística: *2-way* ANOVA. En todos los casos, los resultados se muestran como media ± SEM. Las diferencias fueron consideradas como significativas con $p < 0.05$, y mostradas con una flecha (comparaciones entre una misma cepa) o asterisco (comparaciones entre cepas). (Imagen tomada de Miles et al., 2020; Art. 4).

La similitud entre la respuesta humoral desarrollada por ambas cepas de ratones, tanto en el contexto de la infección experimental, como luego de la inmunización con PSEx, sugiere que existe una predisposición genética por parte de ambas cepas para el desarrollo de sus respuestas de anticuerpos específicas para antígenos parasitarios. Es decir, no sería necesaria una actividad inmunomoduladora activa por parte del parásito que desvíe la respuesta inmune hacia una respuesta humoral ineficiente en el caso de ratones Balb/c; sino que los ratones C57Bl/6 estarían genéticamente predispuestos a desarrollar anticuerpos específicos contra antígenos de mayor relevancia para el parásito. Esto podría deberse, al menos en parte, por la presencia diferencial de alelos del MHC-II presentes en ambas cepas de ratones (Sofron et al., 2016).

CAPÍTULO 4

SECCIÓN 6

Reconocimiento diferencial de antígenos tegumentarios de PSC de E. granulosus s.l. por parte de anticuerpos de ratones Balb/c y C57Bl/6.

Los resultados descritos en la sección anterior, mostraron que los ratones C57Bl/6 generan anticuerpos específicos contra antígenos tegumentarios con un repertorio de reconocimiento limitado, pero con alta capacidad protoscolicida *in vitro*. Esto implica, necesariamente, que existe una diferencia en los antígenos reconocidos por parte de los anticuerpos de cada una de las cepas de ratones. Esta diferencia en reconocimiento podría explicar -al menos parcialmente- la diferencia reportada en los niveles de susceptibilidad de las cepas de ratones Balb/c y C57Bl/6 al desarrollo de la EQ secundaria; ya sea que los anticuerpos de los ratones más resistentes (C57Bl/6) podrían estar reconociendo antígenos con capacidad protectora.

Por ello, en esta sección nos propusimos identificar aquellos antígenos reconocidos únicamente por anticuerpos de ratones con baja susceptibilidad (C57Bl/6) a la EQ secundaria. Este análisis fue realizado mediante una estrategia SERPA (del inglés: *Serological Proteome Analysis*), la cual se basa en la identificación proteica por espectrometría de masas (MALDI-TOF/TOF) de antígenos identificados, mediante *Western blots*, por parte de anticuerpos séricos. Para ello, y muy brevemente, se realizó una separación bidimensional de las proteínas presentes en PSEx (siguiendo los protocolos descritos en el Capítulo 3), las cuales fueron electro-transferidas a membranas de PDVF. Luego, las membranas fueron incubadas con el suero de los ratones correspondientes (ratones Balb/c y C57Bl/6, infectados y controles), bloqueadas con BSA y posteriormente incubadas con anticuerpos conjugados a peroxidasa, específicos contra anticuerpos de ratón. El suero de los ratones normales fue analizado en términos de IgM, IgA, IgG e IgE;

mientras que para los ratones infectados se analizaron adicionalmente todas las subclases de IgG. Finalmente, las membranas fueron reveladas mediante quimioluminiscencia, y los spots desarrollados únicamente en los *Western blots* correspondientes a ratones C57Bl/6; fueron mapeados en los geles 2DE, colectados y analizados mediante espectrometría de masas; siguiendo los protocolos y estrategias previamente descritos en el Capítulo 3.

Este análisis SERPA nos permitió obtener dos resultados interesantes. Por un lado, se obtuvo información sobre la diversidad de epítopes B lineales reconocidos por los anticuerpos séricos de cada condición. En este sentido, cabe resaltar que el estudio de SERPA, al basarse en una separación desnaturalizante de proteínas en geles de SDS-PAGE, permite la identificación únicamente de antígenos que presenten epítopes lineales reconocidos por anticuerpos. A pesar de esta limitante, los resultados obtenidos son concordantes con los expuestos en la sección previa de este capítulo, ya que se observó un bajo número de antígenos reconocidos por anticuerpos naturales de ambas cepas, y un aumento en el reconocimiento específico por parte de los anticuerpos de ratones infectados (Figura 22). Este aumento fue observado principalmente para las subclases de IgG, donde se destaca una gran diferencia en el número de antígenos reconocidos por anticuerpos IgG2b e IgG2a/c entre ambas cepas de ratones. Así, nuevamente se observó que los ratones C57Bl/6 infectados generaron una respuesta de anticuerpos restringida hacia un menor número de antígenos/epítopes en relación a los ratones Balb/c (Figura 22).

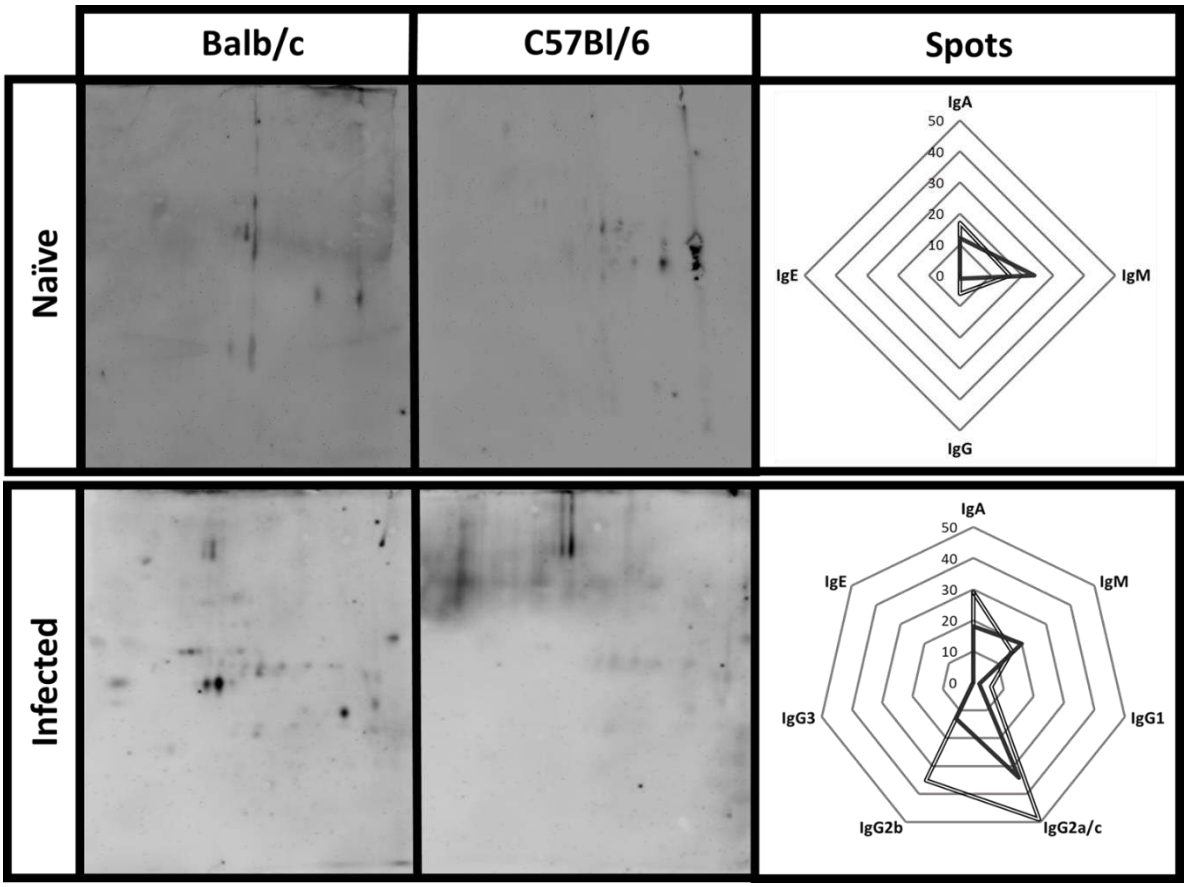

Figura 22. Diversidad de reconocimiento de epítopes B lineales. El análisis por SERPA fue realizado a partir de la separación bidimensional de PSEx en geles 2DE seguido por la eletrotransferencia a membranas PDVF. Luego, estas fueron analizadas mediante *Western blots* detectando los perfiles de reconocimiento por cada clase y subclase de anticuerpos presentes en el suero de ratones Balb/c y C57Bl/6 normales e infectados. Para cada clase/subclase de anticuerpos, el número de *spots* desarrollados fue contado manualmente, y representado en diagramas esquemáticos. En los diagramas, cada línea concéntrica representa un valor de 10 *spots*. Las líneas huecas y sólidas representan los resultados de Balb/c y C57Bl/6, respectivamente. MW (masa molecular, en KDa), IP (punto isoeléctrico). (Imagen tomada de Miles et al., 2020; Art. 4).

Por otro lado, el análisis por SERPA nos permitió identificar a nivel proteómico aquellos antígenos reconocidos únicamente por anticuerpos de ratones con baja susceptibilidad a la infección (C57Bl/6), los cuales podrían corresponder potencialmente a

antígenos protectores. Así, los ratones C57Bl/6 inducirían respuestas de anticuerpos más eficientes a la hora de limitar el establecimiento de la infección por *E. granulosus* s.l., respecto a los ratones Balb/c. La identificación por SERPA fue realizada tanto para anticuerpos naturales como inducidos; identificándose un total de 13 proteínas diferencialmente reconocidas (DRP) por los anticuerpos de ratones C57Bl/6 (Figura 23).

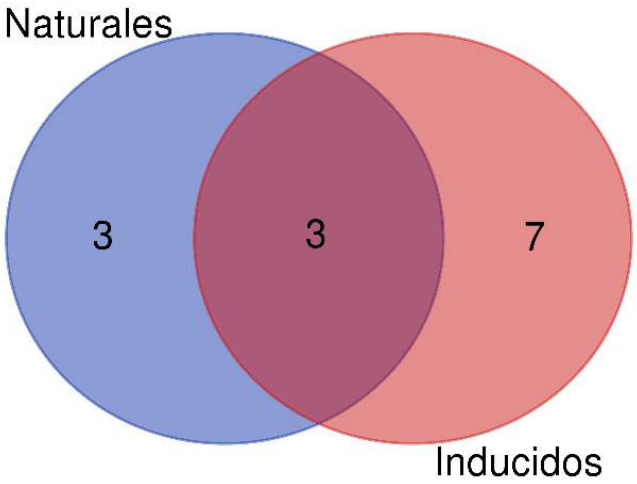

Figura 23. Proteínas reconocidas diferencialmente mediante SERPA. El número de antígenos de PSEx reconocidos únicamente por anticuerpos presentes en el suero de ratones C57Bl/6. Los resultados se muestran como diagrama de Venn, resaltando los antígenos reconocidos solamente por anticuerpos naturales (n=3), solamente por anticuerpos inducidos (n=7), o por anticuerpos naturales e inducidos (n=3).

Entre las DRP identificadas, aquellas reconocidas únicamente por anticuerpos inducidos (7 DRP) serían las de mayor interés para nuestro trabajo; ya que podrían servir a futuro para generar potenciales productos biotecnológicos que ayuden al combate de la EQ. Por ello, analizamos si existen características intrínsecas de dichas DRP, o características genéticas de las cepas de ratones utilizadas, que resulten en que estas 7 proteínas parasitarias sean diferencialmente reconocidas. Para esto, primero se analizaron tres características de las proteínas necesarias para la generación de anticuerpos específicos: 1) la capacidad del antígeno para producir una respuesta inmune (antigenicidad) fue predicha

en base a la secuencia aminoacídica mediante el software ANTIGENpro (Magnan et al., 2010); 2) la abundancia de regiones antigénicas (del inglés: *Abundance of Antigenic Regions*, AAR) fue analizada mediante el software Secret-AAR (Cornejo-Granados et al., 2018); y 3) el valor de unicidad (del inglés: *Uniqueness Score*, US) fue calculado como el producto entre el valor de "*Query coverage"* y "*Identity percentages"* para la proteína con mayor homología identificada tras realizar un BlastP contra todas las proteínas no-helmínticas en la base de datos no-redundante de NCBI (excluyendo las taxonomías de Cestodos, Trematodos y Nematodos). Estos resultados se encuentran en la Tabla 2.

Tabla 2. Caracterización inmunoinformática de las DRPs seleccionadas. Las DRPs reconocidas únicamente por los anticuerpos inducidos en ratones C57Bl/6 tras la infección experimental fueron caracterizadas mediante tres herramientas bioinformáticas. Las columnas "Antigenicidad" y "AAR" muestran los valores predichos obtenidos mediante el uso del software ANTIGENpro y Secret-AAR, respectivamente. La columna "Unicidad" refiere al valor del producto entre el valor de "*Query coverage"* y "*Identity percentages"* para la proteína no-helmíntica con mayor homología identificada. (Tabla modificada de Miles et al., 2020; Art. 4).

DRP	Protein Name	Antigenicity	AAR	US
1	Malate dehydrogenase mitochondrial	0.45	41.6	0.57
2	Nucleoside diphosphate kinase A 2	0.24	150	0.39
3	Actin	0.43	32.8	0.92
4	Severin/Gelosin	0.82	33.2	0.24
5	Malate dehydrogenase cytoplasmatic	0.43	37.7	0.57
6	Vesicular amine transporter	0.72	24.7	0.09
7	Peptidyl-prolyl cis-trans isomerase	0.92	32.6	0.70

Por otro lado, y en base a la información genética disponible sobre las cepas de ratones Balb/c y C57Bl/6 que indican que cada cepa posee un haplotipo de MHC-II distinto (H-2-IA^{d} y H-2-IA^{b}, respectivamente) (Sofron et al., 2016), se analizó la presencia de epítopes T teóricos presentes en cada una de las 7 DRP para los haplotipos de MHC-II

correspondientes a cada cepa; utilizando para ello el software NetMHCII (Nielsen & Lund, 2009). Este software predice la fuerza de unión de cada posible péptido de 15 aminoácidos provenientes de una proteína dada, con la molécula de MHC-II; representando esta unión en términos de IC_{50} (nM). De esta manera, se obtuvo tanto el número total, como el valor de IC_{50}, para cada uno de los posibles epítopes T (Figura 24A), así como los "*cores*" de los mismos (Figura 24B). Ambas métricas mostraron que las 7 DRP poseen una mayor capacidad de unión con el haplotipo de MHC-II presente en ratones C57Bl/6.

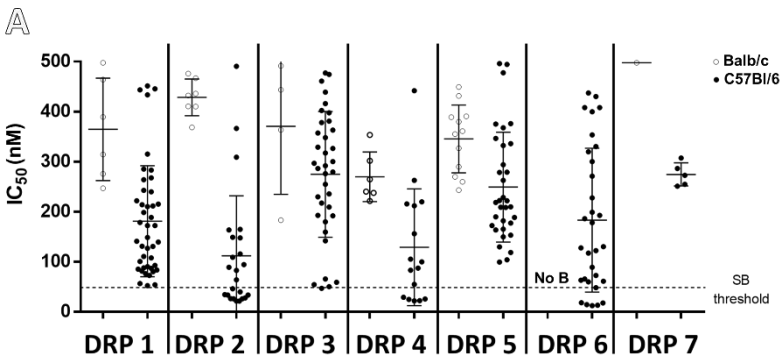

B

DRP	Different MHC-II binding cores	
	Balb/c (H-2-IAd)	C57Bl/6 (H-2-IAb)
1	4	12
2	2	8
3	3	12
4	1	7
5	3	11
6	0	9
7	1	1

Figura 24. Caracterización inmunoinformática de los potenciales epítopes T presentes en las DRPs. Para las 7 DRPs reconocidas únicamente por los anticuerpos inducidos en ratones C57Bl/6 tras la infección experimental, la afinidad de unión de cada posible péptido de 15aa de largo fue analizada contra los haplotipos de MHC-II presentes en ratones Balb/c y C57Bl/6. En (A) se muestran todos los posibles epítopes T con una afinidad de unión (IC_{50}) ≤ 500 nM contra el haplotipo de MHC-II H-2-IA^d (Balb/c, círculos huecos), o H-2-IA^b (C57Bl/6, círculos sólidos). La línea punteada representa el *threshold* que define a los epítopes T de alta unión (IC50 ≤50 nM). En (B) se muestra el número de *cores* distintos presentes en cada DRP capaces de unirse a las moléculas de MHC-II analizadas. No B (no existe un péptido predicho con IC50 ≤ 500 nM). Los rangos representan los valores de la media±SEM. (Imagen modificada de Miles et al., 2020; Art. 4).

CAPITULO 4

CONCLUSIONES

El éxito del establecimiento de una infección depende, en gran medida, de la susceptibilidad intrínseca que posee el hospedero hacia el patógeno. En el modelo murino de EQ secundaria, el resultado de la infección varía según la cepa de ratones utilizada. Así, se ha reportado que los ratones de las cepas Balb/c y C57Bl/6 presentan una susceptibilidad diferencial a la infección, siendo los ratones C57Bl/6 menos permisivos al desarrollo de la EQ secundaria.

Por ello, en el presente capítulo se comparó la respuesta humoral desarrollada en ambas cepas de ratones; observándose que solo los ratones C57Bl/6 mostraron un aumento significativo, durante la etapa temprana de la EQ secundaria, en la actividad anti-parasitaria *in vitro* de sus anticuerpos. Esto correlacionó con que los ratones C57Bl/6 generaron una respuesta humoral con un repertorio de reconocimiento limitado, direccionando la respuesta hacia un menor número de componentes parasitarios; aunque probablemente de mayor relevancia. A su vez, tanto el perfil de anticuerpos generados, como el reconocimiento antigénico y la actividad protoscolicida *in vitro* de los mismos, fueron reproducidas mediante la inmunización con PSEx en ausencia de adyuvante. Todo esto sugeriría que, la respuesta de anticuerpos contra antígenos de PSC de *E. granulosus* s.l. estaría influenciada en gran medida, por diferencias genéticas existentes entre los ratones de las cepas Balb/c y C57Bl/6.

Por otro lado, se analizaron aquellos antígenos reconocidos únicamente por anticuerpos de ratones C57Bl/6. Así, mediante estudios SERPA, se identificaron 13 antígenos diferencialmente reconocidos (DRP) entre ambas cepas de ratones; 7 de los cuales fueron reconocidos únicamente por anticuerpos inducidos en ratones C57Bl/6 infectados. El estudio de los epítopes T teóricos en estas DRP, sugirió que los mismos son

capaces de unirse de forma más eficiente al haplotipo de MHC-II presente en ratones C57Bl/6. Esto sugeriría entonces, que la existencia de una predisposición genética para producir mejores respuestas de anticuerpos de tipo T-dependientes contra ciertos antígenos tegumentarios de PSC de *E. granulosus* s.l., influiría positivamente en la resistencia al desarrollo de la EQ secundaria en ratones de la cepa C57Bl/6.

CAPÍTULO 5

Objetivo específico #4: *Diseñar péptidos antigénicos derivados de proteínas tegumentarias de PSC de E. granulosus s.l. y evaluar su potencial vacunal en el modelo murino de EQ secundaria.*

En este capítulo se presenta el diseño *in silico* y la evaluación experimental de péptidos derivados de proteínas tegumentarias de PSC de *E. granulosus* s.l., como candidatos vacunales frente a la EQ secundaria experimental. Para ello, se realizó una etapa previa de trabajo, consistente en adquirir experiencia en el uso de herramientas bio-inmuno-informáticas aplicadas al diseño de péptidos de interés inmuno-tecnológico. Luego, se propuso un *workflow* novedoso para el diseño de péptidos con potencial uso biotecnológico, mediante el uso combinado de herramientas bio-inmuno-informáticas. Seguidamente, se estudió la respuesta de anticuerpos desencadenada tras inmunización con dichos péptidos. Finalmente, se estudió el potencial anti-parasitario *in vitro* de los anticuerpos generados, así como se evaluó la protección *in vivo* inducida mediante inmunización con los péptidos diseñados. Así, el presente capítulo se divide en 4 secciones:

7) Obtención de experiencia en el uso de herramientas bio-inmuno-informáticas para el diseño de péptidos de interés inmuno-tecnológico.

8) Diseño y optimización bio-inmuno-informática de péptidos como candidatos vacunales frente a la EQ secundaria.

9) Evaluación *in vitro* e *in vivo* del potencial vacunal contra la EQ secundaria de péptidos sintéticos de diseño bio-inmuno-informático.

La mayoría de estos resultados están contenidos en las siguientes publicaciones adjuntas:

Art. 2

"Combining proteomics and bioinformatics to explore novel tegumental antigens as vaccine candidates against Echinococcus granulosus infection"

Miles S, Portela M, Cyrklaff M, Ancarola ME, Frischknecht F, Durán R, Dematteis S, Mourglia-Ettlin G.

Journal of cellular biochemistry (2019)

doi: 10.1002/jcb.28799

Art. 5

"Identification of universal diagnostic peptide candidates for neglected tropical diseases caused by cestodes through the integration of multi-genome-wide analyses and immunoinformatic predictions"

Miles S, Navatta M, Dematteis S, Mourglia-Ettlin G.

Infection, Genetics and Evolution (2017)

doi: 10.1016/j.meegid.2017.07.020

Art. 6

"In silico design and experimental evaluation of peptide-based vaccines against secondary cystic echinococcosis"

Miles S, Dematteis S, Mourglia-Ettlin G.

Biologicals (2022, *submitted*)

CAPÍTULO 5

SECCIÓN 7

Obtención de experiencia en el uso de herramientas bio-inmuno-informáticas para el diseño de péptidos de interés inmuno-tecnológico.

Hasta aquí, hemos analizado diversos aspectos de la biología y bioquímica del parásito *E. granulosus* s.l., centrándonos en el tegumento de los PSC y en su interacción con el sistema inmune del hospedero. En su conjunto, los resultados obtenidos mostraron que una respuesta inmune adecuada contra ciertos componentes tegumentarios, es potencialmente capaz de limitar el establecimiento de la infección en el modelo murino de EQ secundaria. A su vez, se identificaron satisfactoriamente no solo las proteínas parasitarias que componen el tegumento de los PSC, sino también aquellas proteínas antigénicas reconocidas únicamente por anticuerpos generados en ratones infectados que presentan una baja susceptibilidad intrínseca al desarrollo de la EQ secundaria (cepa C57Bl/6). En base a estos resultados, nos propusimos diseñar *in silico*, y evaluar experimentalmente, vacunas peptídicas derivadas de las proteínas identificadas como reconocidas diferencialmente.

Sin embargo, el diseño de péptidos como candidatos vacunales involucra una gran componente de estudios bio-inmuno-informáticos; y por ello, previo al diseño de vacunas peptídicas *per se*, nos propusimos generar experiencia en el uso de las herramientas informática de utilidad. En este sentido, primero decidimos diseñar péptidos potencialmente útiles para el diagnóstico "universal" de las tres enfermedades tropicales desatendidas causadas por especies de parásitos cestodos: *E. granulosus* s.l., *E. multilocularis* y *Taenia solium* (Tsai et al., 2013).

En primer lugar, a partir del proteoma deducido del genoma de cada cestodo, se predijeron las proteínas secretadas por cada parásito (secretoma). Esto fue logrado

siguiendo el flujo de trabajo propuesto por S. Wang et al., (2015) y X. Wang et al., (2015) con algunas modificaciones (Figura 24); seleccionando primero las proteínas que no poseían regiones transmembrana (mediante los softwares TMHMM y Phobius) (Käll et al., 2004; Krogh et al., 2001), pero que presentaban péptidos señal de secreción clásica o no clásica (mediante los softwares SignalP y SecretomeP, respectivamente) (Bendtsen et al., 2004; Petersen et al., 2011). Seguidamente, se descartaron aquellas proteínas con localización mitocondrial (mediante el software TargetP) (Emanuelsson et al., 2000) o en el retículo endoplasmático (mediante los softwares PS-Scan y PredGPI) (de Castro et al., 2006; Pierleoni et al., 2008). Las proteínas seleccionadas fueron consideradas como el secretoma predicho para cada cestodo; constituyendo un 13,7%, 10,0% y 7,2% del total de proteínas para *E. granulosus* s.l., *E. multilocularis* y *T. solium*; respectivamente.

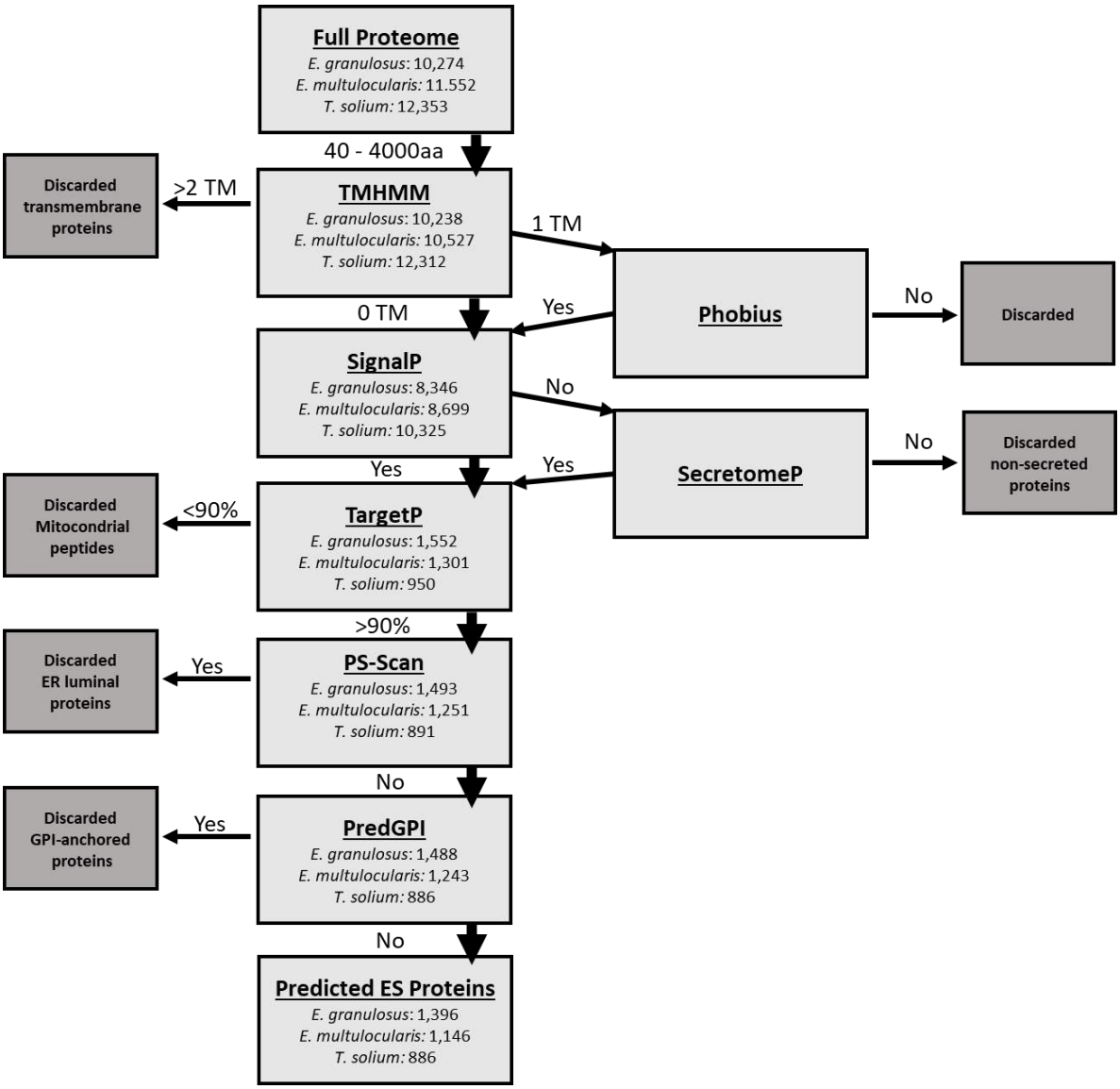

Figura 25. Predicción in silico de secretomas. Flujo de trabajo bioinformático utilizado para predecir los secretoma partiendo del proteoma completo reportado para cada cestodo. (Imagen modificada de Miles et al., 2017; Art. 5).

A partir de los secretomas predichos, se procedió a identificar las proteínas con alta similitud presentes en los tres secretomas. Esto se realizó mediante análisis de BlastP, seleccionando únicamente aquellas proteínas que presentaban una identidad mayor al 90%

entre ellas; resultando en un total de 25 proteínas secretadas comunes a los tres cestodos (Figura 26).

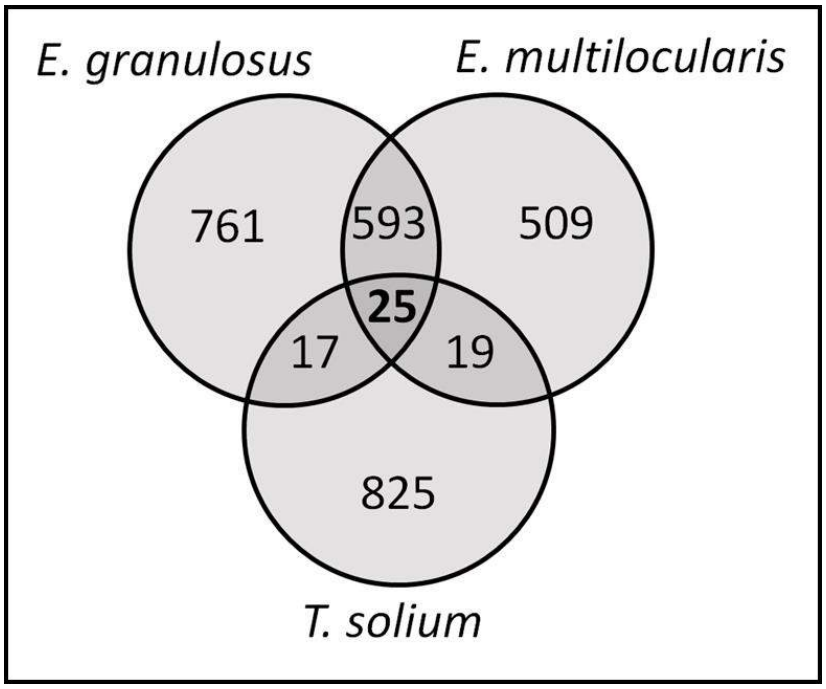

Figura 26. Proteínas secretadas comunes a los cestodos. A partir del secretoma obtenido para cada cestodo, se identificaron aquellas proteínas con una identidad mayor al 90% entre secretomas BlastP. El diagrama de Venn muestra el número de proteínas compartidas por cada secretoma, siendo 25 proteínas compartidas entre los 3 cestodos. (Imagen modificada de Miles et al., 2017; Art. 5).

A continuación, se conformaron 25 sets de proteínas, compuestos cada uno por las proteínas comunes correspondientes a cada uno de los tres cestodos. Para analizar el posible uso de al menos uno de estos sets en el desarrollo de un potencial test de diagnóstico universal para NTD causadas por cestodos, se analizaron 4 características clave de manera secuencial para predecir si son capaces de inducir respuestas de anticuerpos en el contexto de una posible infección natural: *(i)* se descartaron las proteínas parasitarias con alta similitud a proteínas de *Homo sapiens*, de manera de maximizar las probabilidades de generar respuestas inmunes contra las proteínas parasitarias tras una infección natural

(Figura 27A); *(ii)* se seleccionaron aquellas proteínas con alta antigenicidad (predicha mediante el software ANTIGENpro) (Magnan et al., 2010) (Figura 27B); *(iii)* se seleccionaron las proteínas que presentaban posibles péptidos (epítopes T) con alta fuerza de unión en -al menos- 20 moléculas distintas de MHC-II humanas (Nielsen & Lund, 2009) (Figura 27C); y *(iv)* se analizó la presencia de epítopes B lineales cuyas secuencias aminoacídicas estuviese presente en las tres proteínas del set (Larsen et al., 2006) (Figura 28).

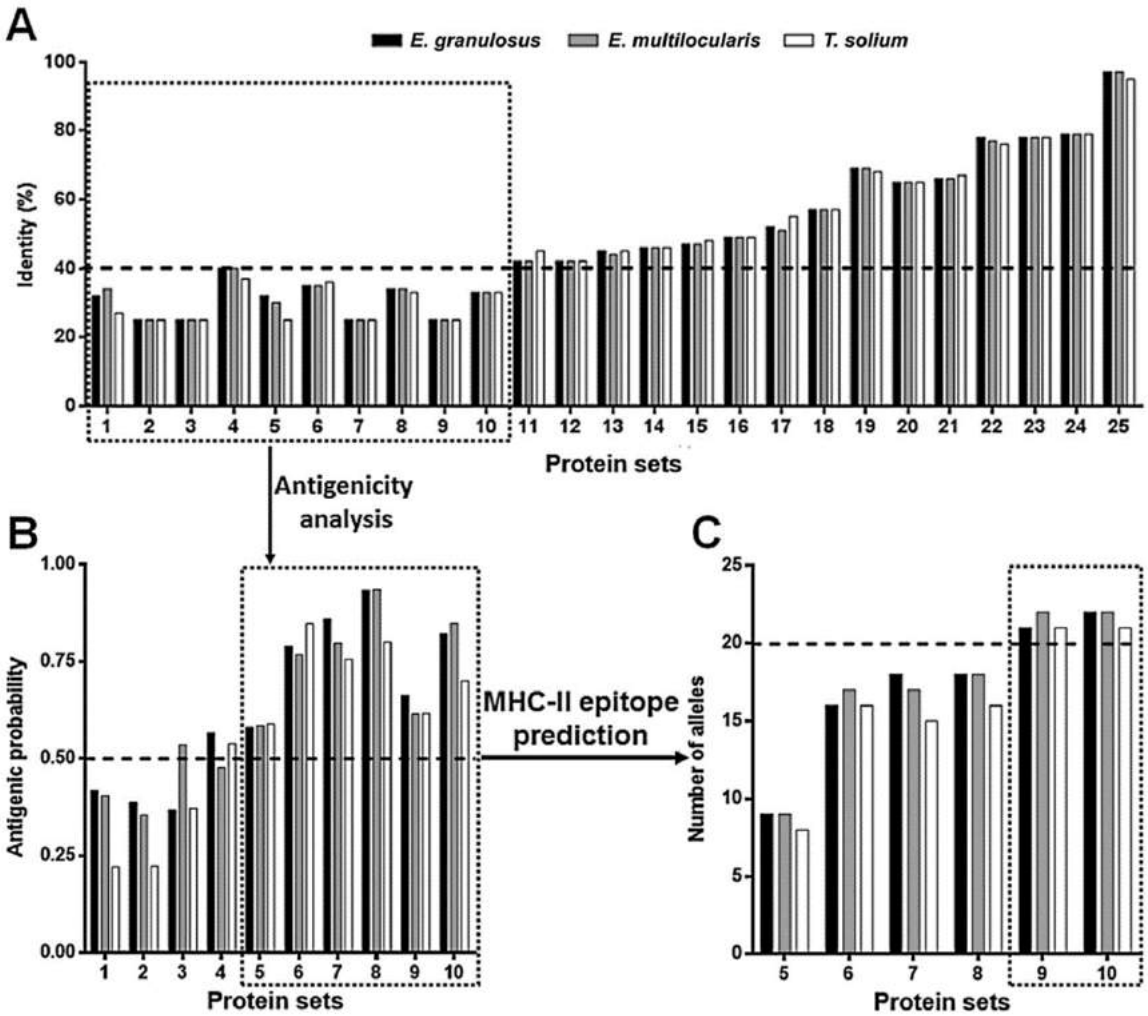

Figura 27. Análisis inmunoinformáticos de las proteínas secretadas. Se identificaron posibles candidatos para test de diagnóstico a partir de las proteínas secretadas comunes entre los cestodos. En (A) se comparó la secuencia aminoacídica de las proteínas secretadas contra el proteoma completo de *Homo sapiens* mediante BlastP, mostrando el score de identidad (%) más alto para cada proteína de los 25 sets. En (B) se calculó la probabilidad

de que las proteínas que mostraron una identidad menor al 40% contra proteínas de *H. sapiens* sean antigénicas. En (C) se analizó la presencia de posibles epítopes T contra 26 alelos de MHC-II distintos dentro de las proteínas antigénicas. Aquellos sets que las 3 proteínas mostraban baja homología con proteínas de *H. sapiens*, alta probabilidad de ser antigénicas, y al menos un péptido de 15aa con alta fuerza de unión (IC_{50} < 50nM) para 20 o más moléculas de MHC-II diferentes fueron seleccionadas (Imagen tomada de Miles et al., 2017; Art. 5).

Para que se desarrollen fuertes respuestas de anticuerpos T-dependientes específicas contra una proteína, esta no solo debe ser antigénica y "diferente" a las del hospedero, sino que también deberían poseer tanto epítopes T como epítopes B. El estudio de los epítopes T presentes en una proteína es complejo, ya que estos no solo deben ser reconocidos por los TCR de los linfocitos T, sino que este reconocimiento debe darse en el contexto de una interacción entre el epítope (en forma de péptido) y una molécula de MHC-II. A su vez, las moléculas de MHC-ll son altamente polimórficas en la población humana, pudiendo hacer que dos individuos generen respuestas de anticuerpos distintas tras una infección natural con el mismo patógeno. Este fenómeno, puede influir negativamente sobre la performance de cualquier test de inmuno-diagnóstico basado en la detección de anticuerpos específicos. Por ello, en este estudio, realizamos un abordaje minimalista de la presencia de epítopes T en los 6 sets seleccionados. Además, creemos importante mencionar que este análisis no tomó en cuenta la abundancia de cada MHC-II en la población humana, ni la posibilidad del uso de péptidos de distinto tamaño; ya que el mismo es un ejercicio teórico, por lo tanto, una validación experimental sería finalmente necesaria para el diseño final de un posible test de inmuno-diagnóstico.

Por otro lado, en un test de inmuno-diagnóstico clásico, se analiza la presencia de anticuerpos, específicos contra un antígeno determinado, presentes en el suero del individuo. Estos anticuerpos, se unen a regiones concretas del antígeno llamados epítopes B, los cuales pueden ser lineales (una secuencia de aminoácidos continuos) o conformacionales (aminoácidos distantes en la secuencia aminoacídica, pero próximos

espacialmente debido al plegamiento proteico). Poder identificar exactamente las regiones reconocidas por los anticuerpos, y generar test de inmuno-diagnóstico utilizando los péptidos correspondientes a los epítopes B lineales, permitiría reducir enormemente los costos de producción.

Sin embargo, es importante destacar que los epítopes B lineales deben estar accesibles para que ocurra el reconocimiento mediante anticuerpos. En este sentido, las posibles PTMs presentes en los antígenos, podrían generar impedimentos estéricos, limitando así su reconocimiento. Dado que las proteínas de los sets 9 y 10 son proteínas secretadas, y no se encontraron dentro de las proteínas identificadas en PSEx, no pudimos hacer uso de la información obtenida para proteínas tegumentarias (Capítulo 3). Para subsanar este impedimento, realizamos una predicción bioinformática de 14 PTMs distintas sobre las proteínas de los sets 9 y 10, co-localizándolas en la secuencia de aminoácidos correspondientes a los epítopes B lineales predichos. Finalmente, 3 epítopes B lineales fueron identificados como “limpios”, al carecer de posibles PTMs en su secuencia (Figura 28).

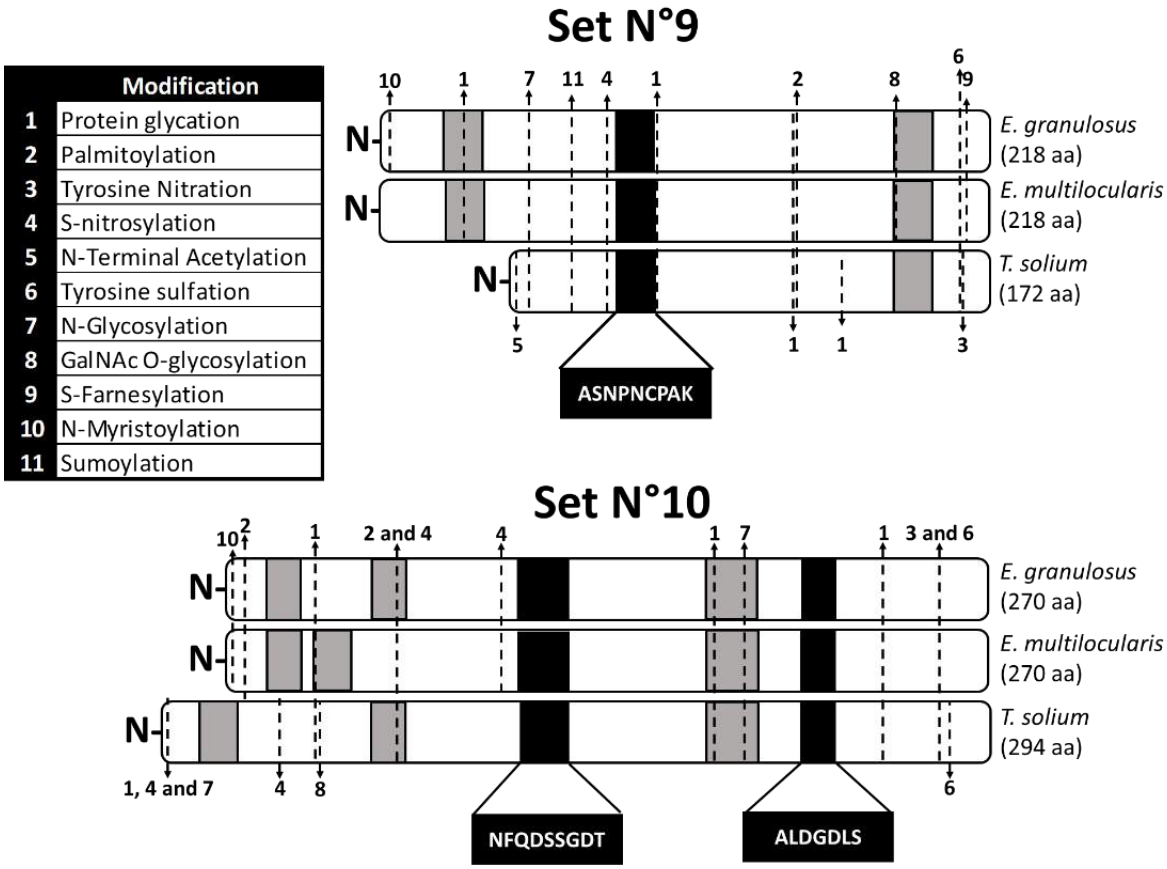

Figura 28. Identificación de epítopes B limpios. Los epítopes B lineales presentes en las proteínas de los sets que presentaban epítopes T contra al menos 20 MHC-II distintos (sets #9 y #10) fueron predichos mediante el software Bepipred 1.0. Los sitios de PTMs fueron analizados usando los servidores de GPS y CBS, donde las líneas punteadas muestran la localización de cada una de las 11 PTMs predichas. Los epítopes B predichos en cada proteína se muestran en gris, mientras que los epítopes B limpios y compartidos entre las 3 proteínas del set se muestran en negro. (Imagen tomada de Miles et al., 2017; Art. 5).

Por último, y dado que los epítopes B lineales deben localizarse en la superficie de la proteína para que sean accesible al reconocimiento por anticuerpos, analizamos la exposición de los 3 epítopes B lineales limpios. Para ello, primero se realizó una predicción de la estructura tridimensional de cada una de las proteínas correspondientes a los sets 9 y 10, mediante el uso del software RaptorX (Källberg et al., 2012). Luego, se mapearon

manualmente los epítopes en estudio sobre las estructuras 3D, realizándose una evaluación de la exposición superficial de los mismos. Finalmente, se obtuvo un péptido de cada set proteico como candidato para un potencial test de inmuno-diagnóstico "universal" para las NTD causada por cestodos (Figura 29).

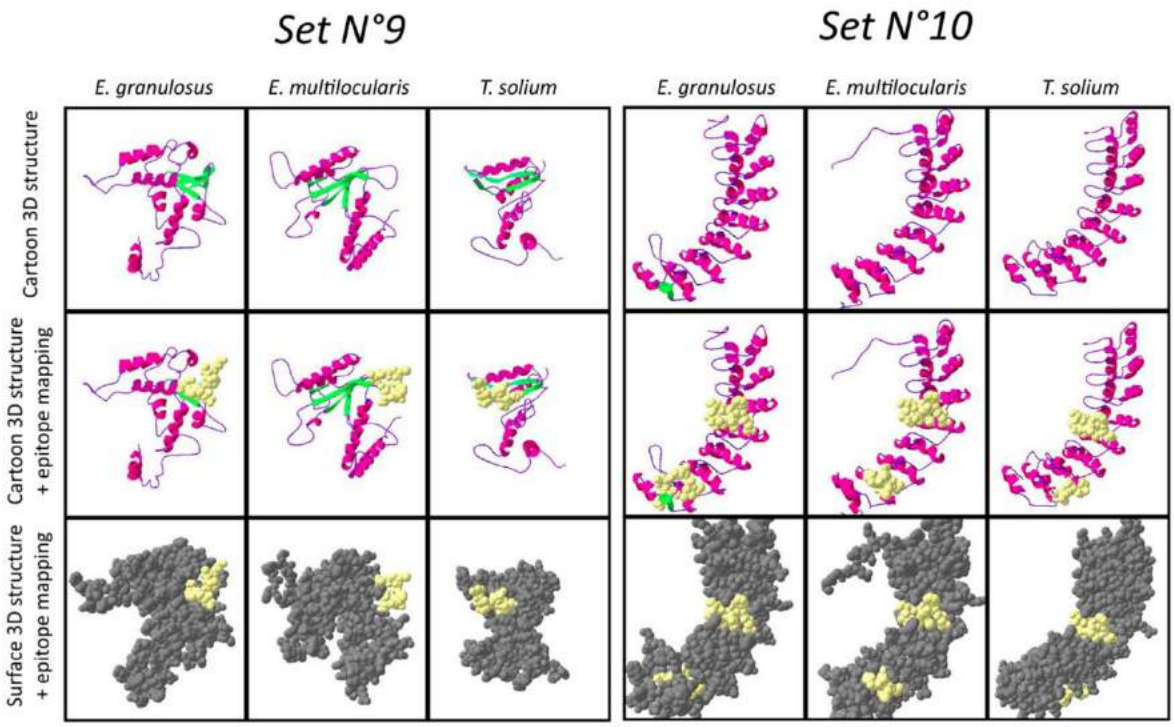

Figura 29. Mapeo de los epítopes B limpios en los modelos 3D de las proteínas. Para cada proteína en los sets #9 y #10, se realizó una predicción de la estructura 3D mediante el software RaptorX. Los epítopes B limpios fueron localizados en los modelos utilizando el software DeepView. Las estructuras secundarias se muestran en magenta (α-helices) y verde (hojas-β), mientras que la estructura 3D se representa en gris. Los epítopes B limpios se representan en amarillo. (Imagen tomada de Miles et al., 2017; Art. 5).

El presente flujo de trabajo diseñado para la selección de epítopes B lineales con posible aplicación biotecnológica, es de especial interés cuando se parte de genomas completos. Sin embargo, la selección de péptidos con éxito biotecnológico puede ser mejorada si se dispone de información experimental adicional. En particular, si se parte de proteínas identificadas mediante espectrometría de masas, la selección de epítopes B

lineales "limpios" puede ser analizada mediante co-localización de epítopes B lineales predichos sobre los fragmentos m/z utilizados para la identificación proteica, siguiendo lo expuesto en el Capítulo 3.

Por ello, se aplicó una variación a este flujo de trabajo con las proteínas de PSEx identificadas en el Capítulo 3, obteniéndose péptidos con potencial uso como candidatos vacunales frente a la EQ secundaria experimental (Figura 30). En primer lugar, se predijeron los epítopes B lineales presentes en las proteínas de PSEx identificadas, y se seleccionaron aquellos epítopes B lineales que co-localizaban con los fragmentos m/z utilizados en espectrometría de masas para identificar la proteína parental. Esto permite seleccionar epítopes B limpios, ya que estos fragmentos m/z usados en espectrometría de masas, están necesariamente libres de PTMs.

A continuación, se descartaron aquellos péptidos presentes en proteínas de organismos no-helmintos, y se realizó un estudio de similitud de estructura secundaria (SSS, del inglés: *Secondary Structure Similarity*). Al comprar las estructuras secundarias obtenidas mediante predicción *in silico* con el software SOPMA (Geourjon & Deléage, 1995), la SSS permite comparar la estructura secundaria adoptada por un péptido sintético en solución vs. el mismo péptido dentro de su proteína parental. Así, se seleccionaron aquellos péptidos que compartían al menos un 80% de los aminoácidos en la misma conformación (hélices-α, hojas-β o *coils*). Finalmente, se analizó la toxicidad (Gupta et al., 2013) y alergenicidad (Saha & Raghava, 2006) de los péptidos, seleccionándose 16 péptidos -no tóxicos ni alergénicos- provenientes de 15 proteínas distintas presentes PSEx, como posibles candidatos vacunales de tipo peptídicos.

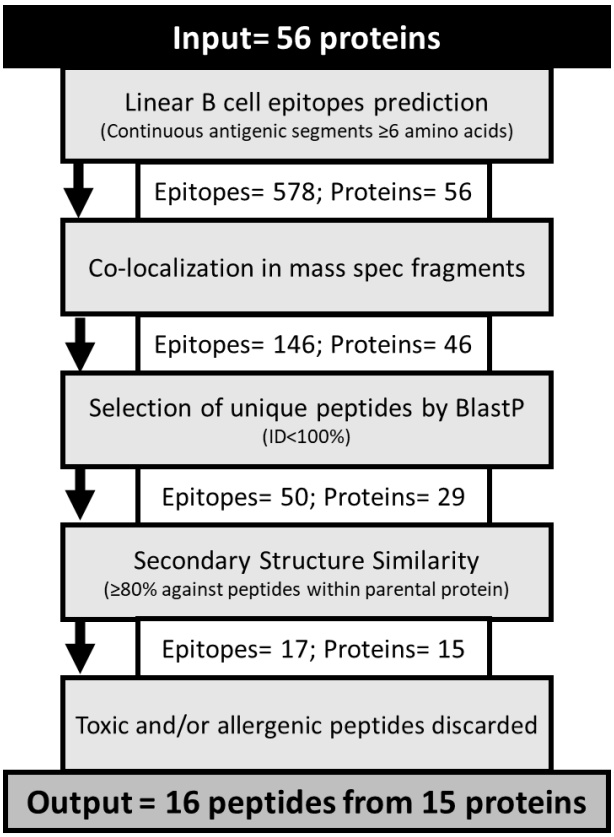

Figura 30. Predicción in silico de candidatos vacunales peptídicos. Flujo de trabajo bioinformático diseñado y utilizado para la predicción de péptidos con potencial uso inmunoterapéutico. A partir del proteoma de PSEx identificado mediante MALDI-TOF/TOF, se seleccionaron epítopes B lineales limpios, únicos, con estructura secundaria similar entre el péptido en solución y el péptido dentro de la proteína nativa. Luego se descartaron los péptidos tóxicos o alergénicos, y se seleccionaron 16 péptidos derivados de 15 proteínas para posibles aplicaciones biotecnológicas. (Imagen modificada de Miles et al., 2019; Art. 4).

Así, mediante la aplicación de más de 25 softwares diferentes, se realizaron estudios de proteomas completos, secuencias aminoacídicas discretas, y estructuras tridimensionales; obteniéndose experiencia en el uso de herramientas bio-inmuno-informáticas, y de manejo de bases de datos. Esta experiencia permitió luego, realizar la selección de péptidos con capacidad protectora descrita a continuación en este capítulo.

CAPÍTULO 5

SECCIÓN 8

Diseño y optimización bio-inmuno-informática de péptidos como candidatos vacunales frente a la EQ secundaria.

A partir de la experiencia adquirida en el uso de herramientas bio-inmuno-informáticas, desarrollamos un flujo de trabajo optimizado para el diseño y selección de péptidos como candidatos vacunales frente a la EQ secundaria experimental. Mediante la introducción de dos pasos clave, el flujo de trabajo propuesto permitió la selección de epítopes B lineales con alta probabilidad de éxito para uso biotecnológico. Estos pasos consistieron en seleccionar péptidos con evidencia proteómica de estar libres de PTMs, y evaluar *in silico* la potencial reactividad cruzada de los anticuerpos inducidos por los mismos frente al péptido en solución vs. en su proteína parental nativa.

Así, consideramos que el flujo de trabajo planteado podría ser aplicable a candidatos vacunales nativos, para los cuales se disponga de información espectral obtenida a través de espectrometría de masas. En este caso, se partió de las 7 proteínas identificadas en el capítulo anterior; es decir, aquellas únicamente reconocidas a través de epítopes B lineales, por parte de los anticuerpos de ratones C57Bl/6 infectados. De esta manera, primero, se predijeron todos los posibles epítopes B lineales (>7 aminoácidos de largo), presentes en las proteínas.

Luego, la presencia de PTMs en dichos epítopes dentro de la proteína parental nativa fue analizada mediante dos estrategias sucesivas y complementarias, seleccionado únicamente los epítopes B lineales limpios: *(i)* selección de epítopes que co-localizan con los fragmentos peptídicos utilizados para la identificación proteica mediante MALDI-TOF/TOF, y *(ii)* análisis de co-localización para los epítopes no selecciones respecto a las 22 PTMs identificadas en las proteínas de PSEx (Capítulo 3). Así, solo aquellos epítopes B

lineales carentes de PTMs, ya sea por evidencia proteómica o PTMómica, fueron seleccionados.

A continuación, se descararon aquellos epítopes B lineales limpios cuya secuencia aminoacídica se halló presente en proteínas de mamíferos; de manera de maximizar la antigenicidad de los mismos y reducir los posibles inconvenientes relacionados con fenómenos de auto-reactividad. Así, 21 epítopes fueron seleccionados, derivados únicamente de 5 de las 7 proteínas iniciales (Tabla 3).

Por otro lado, y ya que los epítopes B lineales deben ser accesibles para el reconocimiento por anticuerpos dentro de su(s) proteína(s) nativa(s), se seleccionaron únicamente aquellos epítopes superficiales, mediante la predicción tridimensional de los antígenos y el mapeo manual de los epítopes sobre las estructuras 3D; siguiendo las estrategias descritas en la sección anterior. Además, se realizó un análisis similar al SSS discutido anteriormente, pero comparando, en lugar de su estructura secundaria, la estructura terciaria de los péptidos en solución vs. en su proteína parental nativa. Este nuevo análisis, denominado TSS (del ingés: *Tertiary Structure Similarity*), consistió en obtener la estructura 3D del péptido dentro de la proteína nativa a partir de la estructura proteica obtenida previamente. Luego, se predijo *de novo* la estructura del péptido en solución, mediante el software PEPFold3 (Lamiable et al., 2016). Una vez obtenidas ambas estructuras, la posición tridimensional de cada aminoácido fue comparada entre el péptido nativo y el péptido en solución mediante el software TM-align (Zhang & Skolnick, 2005); seleccionado así cuatro péptidos con estructuras altamente similares. A su vez, a partir de aquellos péptidos largos (≥13 aminoácidos) con estructura tridimensional similar solamente en una fracción del péptido (cobertura no menor a 7 aminoácidos), se generaron péptidos modificados seleccionando únicamente los aminoácidos con estructura compartida. Luego, la estructura 3D de los péptidos modificados fue obtenida y la TSS fue analizada, seleccionándose así dos péptidos adicionales (Tabla 3).

Tabla 3. Diseño de los candidatos vacunales peptídicos. A partir de las 7 DRPs identificadas en el capítulo 4, se diseñaron candidatos vacunales peptídicos siguiendo un flujo de trabajo bioinformático propuesto por nuestro grupo. Las columnas "código de la proteína", "nombre de la proteína" y "código de acceso" refieren a la proteína parental analizada, mientras que el resto de las columnas reflejan el número de péptidos seleccionados luego de cada paso. "Epítopes B lineales" corresponde al número de epítopes identificados por el software Bepipred. Los epítopes limpios por "MS/MS" y "PTMómica" corresponden a los péptidos que no presentan ninguna PTMs en su secuencia aminoacídica. "Epítopes únicos" corresponden a los péptidos cuya secuencia de aminoácidos no se encuentra presente en ninguna proteína de mamífero. "Epítopes superficiales" corresponde a los epítopes expuestos en la superficie de la proteína parental. Los epítopes con alto TSS, tanto "original" como "modificado" corresponden a los epítopes que muestran una alta similitud en la estructura terciara entre el péptido en solución y el péptido dentro de la proteína nativa. "Péptidos seleccionados" corresponden al número final de epítopes seleccionados de cada proteína, usando en análisis posteriores. (Tabla modificada de Miles et al., *submitted;* Art. 6).

Protein Code	Protein Name	Accession Number	Linear B-cell epitopes	Clean epitopes		Unique Epitope	Superficial Epitopes	High TSS epitopes		Selected peptides
				MS/MS	PTMomics			Original	Modified	
P1	Severin/Gelsolin	U6IX85	11	3	3	6	6	1	1	2
P2	Malate dehydrogenase mitochondrial	A0A068X1L3	5	2	0	2	2	2	0	2
P3	Malate dehydrogenase cyotplasmatic	A0A068WYB8	7	0	5	4	4	1	1	2
P4	Actin	W6UMH9	8	4	2	2	2	0	0	-
P5	Vesicular amine transporter	A0A068X307	11	5	3	7	7	0	0	-
P6	Nucleoside diphosphate kinase	A0A068WL30	3	1	0	0	-	-	-	-
P7	Peptidyl-prolyl cis-trans isomerase	P14088	3	1	1	0	-	-	-	-

Como resultado del flujo de trabajo descrito, finalmente se seleccionaron 6 péptidos como candidatos vacunales peptídicos, derivados de 3 de las 7 proteínas parasitarias iniciales. Para simplificar la escritura, se nombraron dichos péptidos como P1A y P1B (derivados de la proteína P1), P2A y P2B (derivados de la proteína P2), y P3A y P3B (derivados de la proteína P3) (Figura 31).

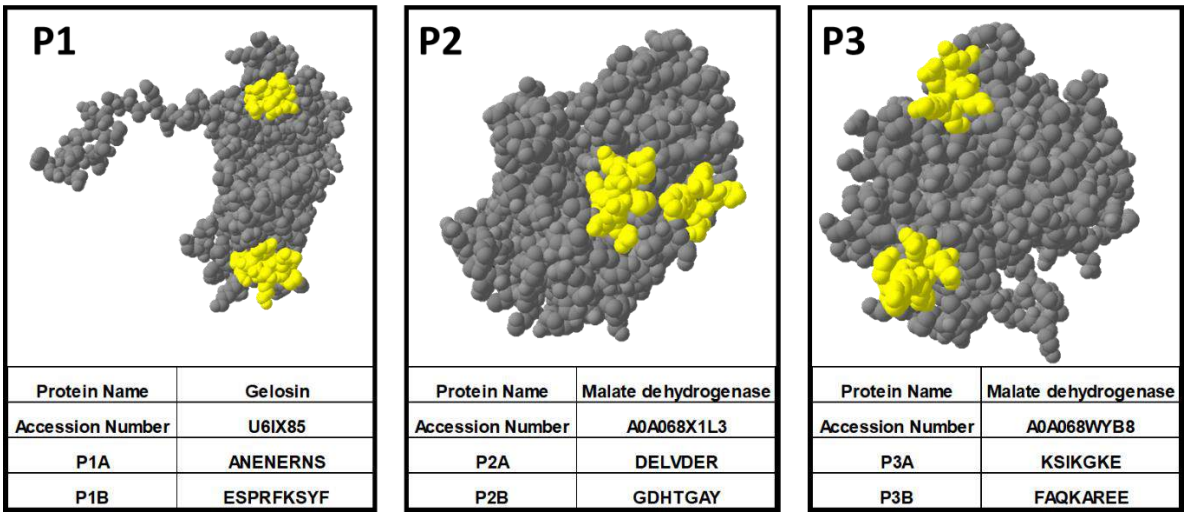

Protein Name	Gelosin
Accession Number	U6IX85
P1A	ANENERNS
P1B	ESPRFKSYF

Protein Name	Malate dehydrogenase
Accession Number	A0A068X1L3
P2A	DELVDER
P2B	GDHTGAY

Protein Name	Malate dehydrogenase
Accession Number	A0A068WYB8
P3A	KSIKGKE
P3B	FAQKAREE

Figura 31. Candidatos vacunales peptídicos. Los péptidos sugeridos como candidatos vacunales fueron seleccionados siguiendo el flujo de trabajo propuesto. En cada figura se muestra la estructura tridimensional predicha de cada proteína parental (P1, P2 y P3), resaltándose los péptidos seleccionados de cada proteína en amarillo. El nombre de la proteína, el código de acceso, y la secuencia aminoacídica de los péptidos seleccionados se muestran en las tablas correspondientes. (Imagen tomada de Miles et al., *submitted;* Art. 6).

CAPÍTULO 5

SECCIÓN 9

Evaluación in vitro e in vivo del potencial vacunal contra la EQ secundaria de péptidos sintéticos de diseño bio-inmuno-informático.

La generación de anticuerpos específicos contra los 6 péptidos seleccionados en la sección anterior, fue evaluada mediante inmunización de ratones CD1 con cada uno de ellos. Para esto, se solicitó la síntesis comercial de los péptidos seleccionados (síntesis automatizada, no biológica y con alto nivel de pureza), en formato "libre" y "acoplado a la proteína KLH". Cabe destacar que, dado que los péptidos exhiben únicamente propiedades del tipo epítope B, se requiere de su conjugación covalente a una proteína *carrier* (o transportadora), para conferirles epítopes T y así poder desarrollar respuestas humorales con características T-dependientes.

Así, seis grupos de ratones CD1 fueron inmunizados con cada uno de los conjugados péptido-KLH, usando QuillA® como adyuvante y siguiendo un esquema de inmunización del tipo *priming-booster-booster* (días 0, 15 y 30). En paralelo, se inmunizaron dos grupos adicionales de ratones CD1, uno solo con QuillA® (control de adyuvante) y otro con KLH comercial formulada en QuillA® (control de especificidad). En el día 45 post-*priming*, los ratones de todos los grupos fueron sangrados, y la respuesta de anticuerpos específicos desarrollada fue analizada mediante ELISA utilizando el formato "libre" de cada péptido como agente sensibilizante.

En primer lugar, el éxito de la inmunización fue confirmado mediante el análisis del título de anticuerpos IgG específicos para KLH, ya que todos los grupos inmunizados (salvo el control de adyuvante) recibieron KLH con sus formulaciones vacunales (Figura 32).

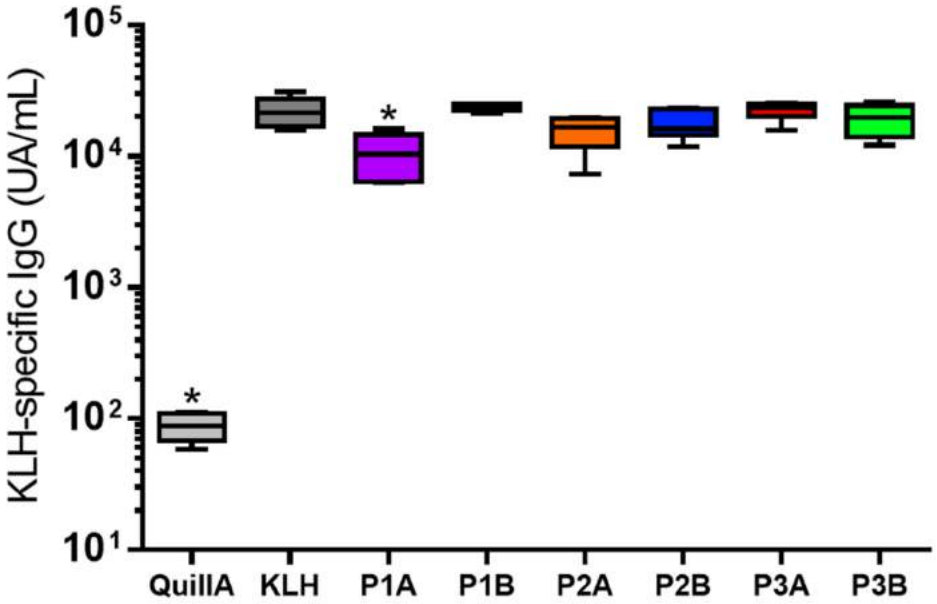

Figura 32. Respuesta de anticuerpos anti-KLH. El título de anticuerpos IgG específicos contra KLH en el suero de los ratones inmunizados con péptidos conjugados a KLH, y sus respectivos controles, fue analizado mediante ELISA. Los títulos de IgG específicos son reportados como el valor de absorbancia detectado normalizado por el factor de dilución. Los resultados se muestran como *box-and-whiskers*, comparando las diferencias con el grupo inmunizado con KLH comercial mediante la aplicación del test no-paramétrico Kruskal-Wallis, considerándose diferencias significativas para valores de $p<0,05$. (Imagen modificada de Miles et al., *submitted;* Art. 6).

Luego de confirmar el correcto proceso de inmunización, se procedió a analizar la respuesta específica contra los péptidos seleccionados. Para ello, se sensibilizaron placas de ELISA, directamente con cada uno de los péptidos sintéticos (en formato "libre"), y luego se determinó el título de anticuerpos IgG específicos para cada péptido. Los resultados obtenidos mostraron que se indujeron altos niveles de anticuerpos IgG específicos para los péptidos P2A y P2B, a la vez que niveles relativamente bajos de anticuerpos IgG específicos para los péptidos P3A y P3B; en ambos casos en comparación con los anticuerpos IgG inducidos en el grupo inmunizado con KLH/QuilIA® (control de especificidad). Cabe destacar

que no se observaron niveles significativos de anticuerpos IgG específicos para los péptidos P1A y P1B (Figura 33).

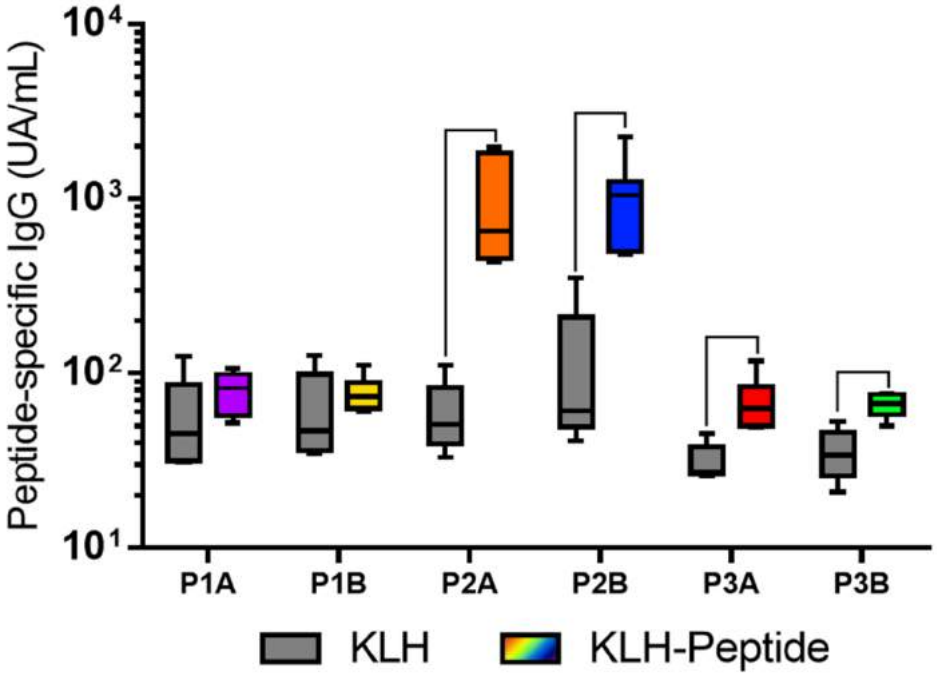

Figura 33. Respuesta de anticuerpos anti-péptidos. El título de anticuerpos IgG específicos contra cada uno de los péptidos sintéticos en el suero de los ratones inmunizados con péptidos conjugados a KLH, y sus respectivos controles, fue analizado mediante ELISA. Los títulos de IgG específicos son reportados como el valor de absorbancia detectado normalizado por el factor de dilución. Los resultados se muestran como *box-and-whiskers*, comparando las diferencias con el grupo inmunizado con KLH comercial mediante la aplicación del test no paramétrico Mann Whitney-Wilcoxon, considerándose diferencias significativas para valores de $p < 0.05$. (Imagen modificada de Miles et al., *submitted;* Art. 6).

En paralelo, se analizó la reactividad cruzada con las proteínas parentales nativas, por parte de los anticuerpos inducidos tras inmunización. En este sentido, y dado que las 3 proteínas de las cuales derivan los 6 péptidos en estudio, fueron identificadas en PSEx con altos valores de abundancia relativa (2,58%, 1,79% y 0,51%, para P1, P2 y P3; respectivamente), analizamos la reactividad cruzada de los anticuerpos inducidos mediante ELISA sobre placas sensibilizadas con PSEx. De manera interesante, los anticuerpos

inducidos tras inmunización con los péptidos derivados de las proteínas P2 y P3, reconocieron claramente estructuras presentes en PSEx; probablemente sus proteínas parentales nativas (Figura 34).

Por otro lado, cabe destacar que los ratones inmunizados con P1A-KLH, fueron los únicos que no mostraron niveles significativos de anticuerpos IgG específicos para el péptido en formato "libre" (Figura 33), así como tampoco mostraron anticuerpos IgG con evidente reactividad cruzada contra componentes presentes en PSEx (Figura 34). Estos resultados sugieren entonces, que los anticuerpos IgG inducidos en el grupo de ratones inmunizados con P1A-KLH/QuillA® no poseerían capacidad protectora. Por ello, y dado que la formulación P1A-KLH/QuillA® es altamente similar a las demás formulaciones, en términos de *carrier* y adyuvante, decidimos utilizar a este grupo experimental como un control de referencia interno en el resto de estudio.

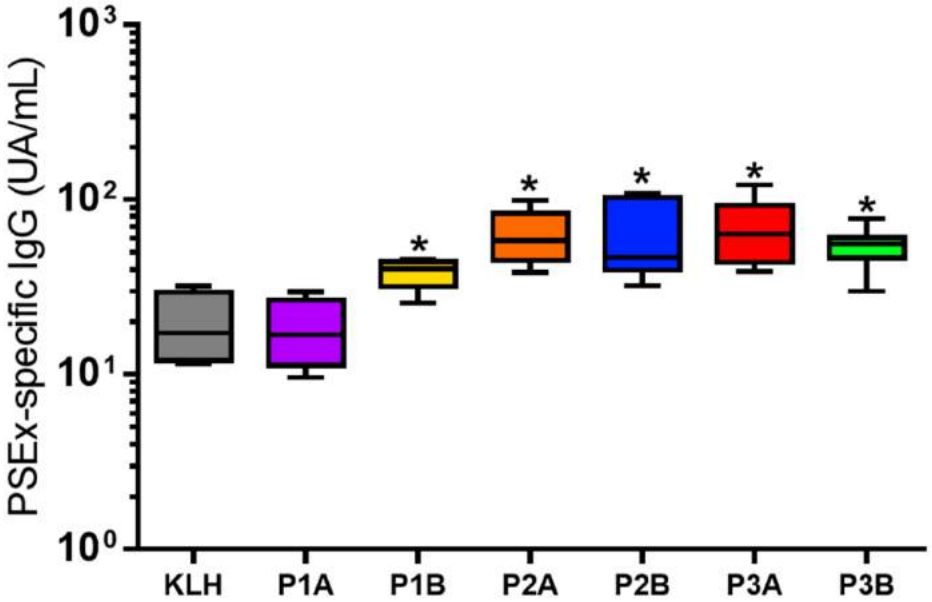

Figura 34. Respuesta de anticuerpos anti-PSEx. El título de anticuerpos IgG específicos contra PSEx en el suero de los ratones inmunizados con péptidos conjugados a KLH, y sus respectivos controles, fue analizado mediante ELISA. Los títulos de IgG específicos son reportados como el valor de absorbancia detectado normalizado por el factor de dilución. Los resultados se muestran como *box-and-whiskers*, comparando las diferencias con el

grupo inmunizado con KLH comercial mediante la aplicación del test no paramétrico Kruskal-Wallis, considerándose diferencias significativas para valores de $p < 0.05$. (Imagen modificada de Miles et al., *submitted;* Art. 6).

A continuación, se realizó un estudio exploratorio *in vitro* de la actividad anti-parasitaria de los anticuerpos inducidos tras la inmunización con los péptidos seleccionados acoplados a KLH. Para ello, se utilizaron tres ensayos distintos y complementarios.; cada uno buscando evidenciar un posible mecanismo de acción de los anticuerpos inducidos. Así, en primer lugar, se analizó si la interacción directa de los anticuerpos con PSC de *E. granulosus* s.l. es capaz de inducir la muerte parasitaria (Figura 35A). Luego, se evaluó si la interacción de los anticuerpos influye en los procesos metabólicos de los PSC; por ejemplo, en la absorción de nutrientes (Figura 35B). En tercer y último lugar, se evaluó la capacidad de los anticuerpos inducidos para activar el complemento por vía clásica, sobre la superficie de los PSC de *E. granulosus* s.l., desencadenando así la muerte de los mismos (Figura 35C). En los tres ensayos realizados, los resultados del incremento en el porcentaje de PSC no viables, se reportó normalizados respecto del resultado obtenido para los anticuerpos específicos contra P1A (control interno).

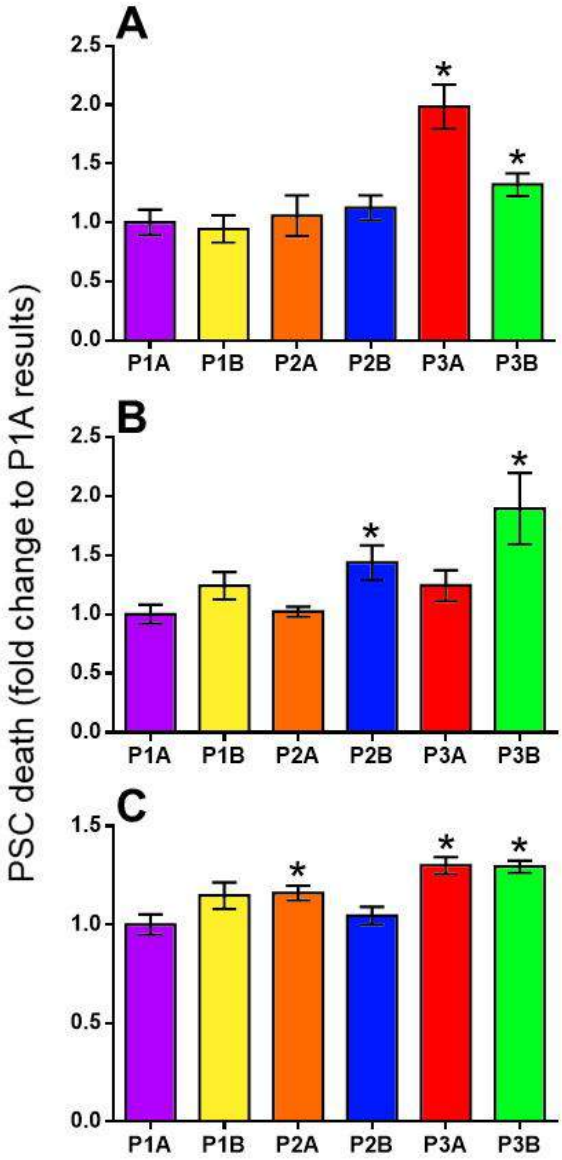

Figura 35. Evaluación in vitro de la actividad antiparasitaria de los anticuerpos específicos contra péptidos. El incremento en la muerte parasitaria inducida por los anticuerpos específicos contra los péptidos fue analizada *in vitro* y normalizada a los resultados obtenidos con los anticuerpos α-P1A. (A) Muerte parasitaria inducida por la interacción directa entre los anticuerpos y los protoscoleces cultivados en PBS durante 48hs. (B) Muerte parasitaria inducida por la interferencia metabólica de los anticuerpos con protoscoleces cultivados en RPMI durante 120hs. (C) Muerte parasitaria inducida por la activación clásica del sistema del complemento mediada por anticuerpos en la superficie de protoscoleces cultivados en PBS con suero normal de ratón durante 48hs. Los resultados se muestran como la media±SEM, y la estadística fue realizada usando el test de Student. Las diferencias

respecto a los resultados obtenidos con los anticuerpos específicos conta P1A fueron consideradas significativas con un p <0.05. (Imagen tomada de Miles et al., *submitted;* Art. 6).

En este sentido, los resultados mostraron que, en los tres ensayos realizado, los anticuerpos inducidos mediante inmunización con P1B-KLH/QuillA® fueron similares a los obtenidos con el control interno (P1A-KLH/QuillA®) (Figura 35). Por otro lado, los anticuerpos específicos inducidos tras inmunización con P2A-KLH/QuillA®, mostraron un incremento en la muerte parasitaria mediante la activación clásica del sistema complemento (Figura 35C), mientras que los anticuerpos específicos obtenidos tras inmunización con P2B-KLH/QuillA® fueron capaces de interferir con rutas metabólicas parasitarias relevantes (Figura 35B). De manera interesante, los anticuerpos generados mediante inmunización con los 2 péptidos derivados de la proteína P3 (acoplados a KLH y formulados junto a QuillA®), mostraron los mejores perfiles de actividad anti-parasitaria *in vitro*. En este sentido, los anticuerpos específicos para P3A mostraron la mayor actividad anti-parasitaria intrínseca observada, así como un incremento en la muerte de PSC mediante activación del sistema complemento (Figura 35C); mientras que los anticuerpos específicos para P3B, indujeron la muerte parasitaria *in vitro* en los 3 ensayos realizados (Figura 35).

Finalmente, los resultados obtenidos de las actividades anti-parasitarias *in vitro*, mostraron que los anticuerpos generados tras la inmunización de ratones CD1 con -algunos- conjugados péptidos-KLH formulados junto a QuillA®, fueron capaces de inducir la muerte parasitaria. En base a estos resultados prometedores, nos propusimos analizar la capacidad protectora de los péptidos tras la inmunización activa con los mismos, seguida de un desafío experimental con PSC de *E. granulosus* s.l. viables. Para esto, ensayamos tres formulaciones vacunales diferentes -además del grupo control- compuestas cada una de ellas, por pares de péptidos conjugados a KLH, formulados junto a QuillA® como adyuvante. Los dos péptidos conjugados a KLH que indujeron anticuerpos sin actividad anti-parasitaria *in vitro*,

fueron formulados como "Vacuna 1" (P1A-KLH + P2A-KLH). Por otro lado, el par de péptidos que mostró inducción de anticuerpos con actividad anti-parasitaria *in vitro* solamente en uno de los tres ensayos realizados, fueron formulados como "Vacuna 2" (P2A-KLH + P2B-KLH). Finalmente, los péptidos que indujeron anticuerpos capaces de realizar al menos dos actividades anti-parasitarias cada uno, fueron combinados como "Vacuna 3" (P3A-KLH + P3B-KLH).

La evaluación de la protección inducida por cada una de las formulaciones vacunales fue analizada en el modelo murino de EQ secundaria. En primer lugar, se realizó una inmunización sub-cutánea de ratones CD1, siguiendo el esquema de *priming-booster-booster* ya mencionado (días 0, 15 y 30). Luego, al día 45 post-*priming*, los ratones de todos los grupos, se desafiaron mediante inoculación intraperitoneal de 2,000 PSC viables de *E. granulosus* s.l.; y 6 meses post-infección, a todos los ratones se les realizó eutanasia y el resultado de la infección se evaluó en términos de porcentaje de ratones infectados (Figura 36A) y de número de quistes desarrollados (Figura 36B).

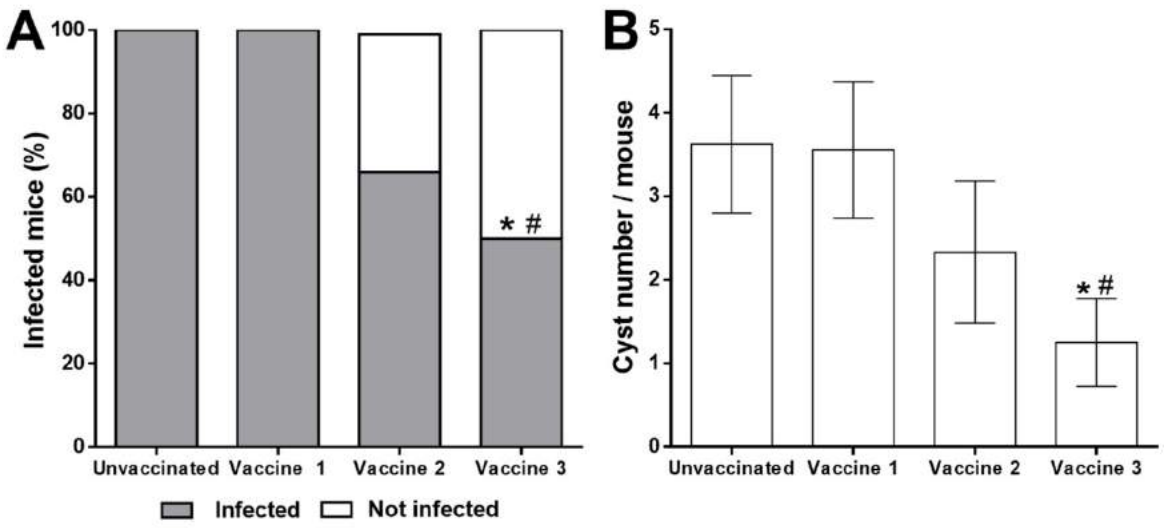

Figura 36. Eficacia de las vacunas peptídicas en el modelo de infección secundaria. La protección generada por las formulaciones "Vacuna 1", "Vacuna 2" y "Vacuna 3" fue evaluada *in vivo* en el modelo murino de EQ secundaria. Grupos de ratones CD1 fueron inmunizados por la vía s.c. con cada una de las formulaciones siguiendo un esquema de *priming-booster-booster* (días 0, 15 y 30). Luego, cada ratón fue inoculado en la cavidad

peritoneal con 2000 protoscoleces viables al día 45 *post-priming*. Seis meses post-infección todos los ratones fueron sacrificados y los quistes hidáticos desarrollados en cada ratón fueron contados. Los resultados se muestran en términos del porcentaje de ratones infectados (A), y el número (media±SEM) de quistes hidáticos peritoneales por ratón (B). En (A), el test exacto de Fisher fue usado para evaluar la significancia de la protección, tanto con respecto al grupo no vacunado como al "Vacuna 1", mientras que en (B) la estadística fue evaluada usando el test no paramétrico de Mann Whitney-Wilcoxon. Los asteriscos y numerales corresponden a diferencias significativas contra el grupo no vacunado y "Vacuna 1", respectivamente. En todos los casos, las diferencias significativas corresponden a $p<0.05$. (Imagen tomada de Miles et al., *submitted;* Art. 6).

Como se mencionó previamente, y basándonos en los resultados obtenidos *in vitro*, la "Vacuna 1" fue utilizada como un grupo de control interno. De esta forma, el grupo "Vacuna 1" incluyó todos los posibles efectos inducidos inespecíficamente por la respuesta inmune generada contra KLH. En línea con lo esperado, el grupo inmunizado con la "Vacuna 1" no mostró diferencias significativas respecto al grupo no vacunado; tanto en términos de porcentaje de ratones infectados, como en relación al número de quistes desarrollados por ratón (Figura 36). Por su parte, la "Vacuna 2", si bien mostró una reducción del 33% en el número de ratones infectados (Figura 36), estos resultados no fueron estadísticamente significativos al compararlos con el grupo no vacunado o con el grupo inmunizado con la "Vacuna 1". Por último, la "Vacuna 3" mostró una protección significativa del 50% de los individuos frente a la infección secundaria por *E. granulosus* s.l.; tanto al comparar los resultados con el grupo no vacunado como con el grupo inmunizado con la "Vacuna 1" (Figura 36A). Además, los ratones inmunizados con la "Vacuna 3", desarrollaron en la cavidad peritoneal, un número de quistes significativamente menor al observado en los grupos control (no vacuna y "Vacuna 1") (Figura 36B).

CAPÍTULO 5

CONCLUSIONES

Las vacunas son uno de los avances en la medicina más importantes en la historia de la humanidad. Sin embargo, el diseño y la producción de vacunas convencionales, suele requerir mucho tiempo y esfuerzo, a la vez que una gran inversión económica. Además, las vacunas convencionales suelen incluir cargas antigénicas innecesarias, que pueden desencadenar respuestas inmunes no-eficientes, o incluso perjudiciales. Por ello, las vacunas basadas en péptidos, son una alternativa interesante a las vacunas convencionales, ya que pueden ser diseñadas *in silico* casi en su totalidad, su producción es segura y barata, y son capaces de inducir respuestas inmunes exclusivamente hacia epítopes protectores. Sin embargo, es necesario un diseño adecuado de los péptidos a usarse en las formulaciones vacunales, ya que no solo se debe desarrollar una respuesta inmune contra el péptido sintético, sino que ésta tiene que ser capaz de reconocer a las proteínas nativas en el contexto de una infección natural.

En el presente capítulo se propuso un flujo de trabajo optimizado para el diseño de péptidos vacunales a partir de candidatos identificados por técnicas proteómicas. De esta manera, introdujimos dos pasos críticos para el diseño de péptidos con alta probabilidad de generar anticuerpos eficientes tras inmunización. En primer lugar, nos aseguramos de seleccionar únicamente epítopes B lineales libres de modificaciones post-traduccionales; y luego, seleccionamos únicamente aquellos epítopes (péptidos) cuya estructura en solución fuese altamente similar a la estructura dentro de la proteína nativa. Así, maximizamos la posibilidad de generar anticuerpos con reactividad cruzada entre ambos. Aplicando este flujo de trabajo a siete proteínas previamente sugeridas como potenciales candidatos vacunales, obtuvimos 6 péptidos candidatos, dos de los cuales mostraron ser capaces de inducir anticuerpos con actividad anti-parasitaria *in vitro*, así como protección significativa en el modelo murino de EQ secundaria.

CAPÍTULO 6
DISCUSIÓN

La equinococosis quística (EQ) es una enfermedad zoonótica cosmopolita causada por la infección con el parásito cestodo *E. granulosus* s.l., que genera grandes impactos negativos en las economías regionales, debido a sus efectos sobre la salud humana y animal (Budke et al., 2006). La OMS clasifica a la EQ como una de las 20 enfermedades tropicales desatendidas, existiendo escasa información disponible sobre la biología de este parásito.

En este sentido, el objetivo original de la presente tesis, fue la identificación de antígenos protectores contra *E. granulosus* s.l. -y la generación de candidatos vacunales peptídicos derivados de los mismos- partiendo de una fracción antigénica de PSC con capacidad de inducir protección en el modelo murino de EQ secundaria (Hernández & Nieto, 1994). Sin embargo, la escasa información sobre diversos aspectos de la biología y bioquímica básica del parásito, limitaban el desarrollo inicial de nuestro estudio.

Por ello, fue necesario obtener información detallada de la biología básica de los PSC de *E. granulosus* s.l.; en particular, en relación a su tegumento. Así, en primer lugar, realizamos una caracterización exhaustiva del tegumento, tanto en términos de su ultraestructura, como en relación a su composición proteica y presencia de PTM. Luego, estudiamos la interacción entre el sistema inmune del hospedero y componentes tegumentarios, diseccionando y comparando la repuesta humoral desarrollada por ratones infectados pertenecientes a cepas con alta y baja susceptibilidad a la EQ secundaria experimental. Finalmente, identificamos potenciales antígenos protectores, y a partir de ellos, diseñamos péptidos como potenciales candidatos vacunales. Dos de estos péptidos fueron capaces de inducir anticuerpos con actividad anti-parasitaria *in vitro*, así como niveles significativos de protección en el modelo murino de EQ secundaria.

Hasta la fecha, los estudios estructurales enfocados en el tegumento de PSC de *E. granulosus* s.l. (Galindo et al., 2008; Jha & Smyth, 1971; Morseth, 1967), fueron realizados utilizando técnicas clásicas de microcopia electrónica, principalmente TEM y SEM. Por ello, en el Capítulo 2 de la presente tesis, se estudió el tegumento y las estructuras internas adyacentes, mediante la aplicación combinada de técnicas de microscopía electrónica de última generación. Esta combinación, que incluyó preparación de muestras mediante HPF, análisis por inmuno-marcación y tomografía electrónica seriada seguida por reconstrucción 3D; no solo permite obtener información novedosa sobre la estructura de los patógenos, sino que también permite analizar la relación existente entre las estructuras y sus funciones (Cyrklaff et al., 2017).

Por ello, nos planteamos como primero objetivo estudiar la ultraestructura y organización de los distintos componentes y células que conforman el tegumento de los PSC; y analizar las posibles rutas de excreción/secreción y/o internalización presentes en el tegumento. Así, en primer lugar, analizamos mediante SEM (Figura 5) y TEM (Figura 6), la estructura clásica de los PSC (Antoniou & Tselentis, 1993) y el tegumento de su soma (Galindo et al., 2008), siendo ambos consistentes con los reportes previos disponibles. Además, reportamos que la organización celular de PSC de *E. ortleppi* es similar a la de *E. granulosus* s.s.; sugiriendo así que dicha organización sería común a todo el complejo *E. granulosus* s.l.

La ultraestructura del tegumento del soma fue luego analizada mediante tomografía electrónica generando una reconstrucción 3D del citoplasma distal y de estructuras parasitarias internas adyacentes (Figura 7). De esta reconstrucción 3D destacamos la intrincada disposición adoptada por las fibras musculares en alternancia con fibras longitudinales y circulares (Coutelen et al., 1952), que cubren por completo el cuerpo del parásito. Por otro lado, los análisis mediante TEM y tomoEM permitieron la identificación y caracterización, de una estructura acelular nunca antes descrita. Esta estructura, que denominamos TVB, es electrón-lúcida y se ubica entre el citoplasma distal y la zona fibrosa

(Figura 8), conteniendo en su interior vesículas discretas. Si bien existen reportes previos donde se observaron, mediante TEM, estructuras similares a TVB en PSC de *E. granulosus* s.l. (Hu et al., 2011; B. Wang et al., 2015), las mismas fueron completamente ignoradas al tratárselas como vacuolas. La existencia del TVB fue observado en todos los lotes de parásitos frescos analizados -tanto PSC de *E. ortleppi* (Figura 8) como de *E. granulosus* s.s. (Figura suplementaria 1 del manuscrito Adjunto 1); a la vez que también se lo observó de manera independiente del método utilizado en la preparación de la muestra (Figura 8A y B). De manera interesante, destacamos que el TVB fue observado cubriendo gran parte del soma del parásito, como estructuras discretas (Figura 8C), las cuales se conectan en distintos planos Z formando una única macro-estructura; tal y como se observó mediante tomoEM (Figura 8D). A su vez, identificamos estructuras semiesféricas dentro del TVB, con características de vesículas en el rango de tamaño desde 75 a 250 nm de diámetro.

El tegumento de los PSC de *E. granulosus* s.l. cumple funciones en el metabolismo parasitario, así como en la defensa contra -y la comunicación con- el hospedero. En este sentido, los PSC son capaces de excretar/secretar diversos componente parasitarios, tanto de manera soluble (Díaz et al., 2011a, 2011b), como mediante vesículas extracelulares (EV) (Nicolao et al., 2019; W. Wang et al., 2019; Wu et al., 2021; Zhang et al., 2020). En las enfermedades parasitarias, la liberación de EVs cumple funciones de inter-comunicación parasitaria, y de comunicación parásito-hospedero, siendo las EVs capaces de intervenir en los sistemas regulatorios del hospedero (Marcilla et al., 2014).

Por ello, analizamos la existencia de posibles rutas de exo- y/o endocitosis a través del tegumento. Así, en primer lugar estudiamos la presencia de estructuras vesiculares (con tamaño y morfología similar a EVs) en el tegumento de PSC de *E. ortleppi*; identificando -mediante TEM- cuerpos vesiculares compatibles con EVs en todos los pasos de un posible proceso de exo- o endocitosis (Figura 10). Al analizar las imágenes desde una perspectiva exocítica, las vesículas podrían ser formadas por células especializadas en el interior del parásito (Figura 10A), desplazándose luego hacia el exterior mediante su cargado en el TVB

(Figura 10B) y pasando finalmente al citoplasma distal (Figura 10C); o entrando directamente al citoplasma distal (Figura 10D). Una vez allí dentro, las vesículas podrían ser transportadas hacia el exterior parasitario (Figura 10E y F), pasando por el glicocálix (Figura 10G), para finalmente ser excretadas (Figura 10H). El proceso inverso podría resultar en la endocitosis de EVs presentes en el líquido hidático. En este sentido, una característica interesante observada en las vesículas presentes en el citoplasma distal, fue el hecho que las mismas estaban contenidas en una estructura de mayor tamaño -probablemente involucrada en los procesos de transporte vesicular- limitada por membranas (Figura 10D-F).

En paralelo, y para poder discriminar entre posibles rutas exo- y endocíticas de las vesículas, analizamos la localización de componentes parasitarios (GST-1, FABP y AgB) y componentes del hospedero (IgG bovinas), en el tegumento del soma de los PSC de *E. granulosus* s.l. Además, evaluamos la presencia de dichos componentes en el cargamento de las vesículas. En este sentido, la enzima GST-1 parasitaria fue identificada mayoritariamente en el glicocálix de los PSC (Figura 11). Esta enzima está involucrada en la protección parasitaria frente a fenómenos de oxidación inducidos por el hospedero, así como en la detoxificación pasiva de xenobióticos del tipo drogas antihelmínticas (Arbildi et al., 2017). La alta presencia de GST-1 en el glicocálix podría estar relacionada con su actividad de protección parasitaria, ya que el glicocálix es la estructura parasitaria más externa, y por lo tanto, en mayor contacto con los sistemas de defensa del hospedero.

De manera análoga a lo observado para GST-1, la alta presencia de FABPs en el glicocálix del tegumento (Figura 12), podría estar involucrada en los fenómenos parasitarios de absorción lipídica; ya que *E. granulosus* s.l. requiere de una gran cantidad de lípidos del hospedero para su crecimiento y para el mantenimiento de la integridad y funcionalidad del quiste hidático (Pórfido et al., 2020); y probablemente también para la sobrevida de los PSC. Por otro lado, las FABPs de *F. hepática* han mostrado ser capaces de suprimir la respuesta inmune del hospedero, inhibiendo la activación de TLR4 (Martin et al., 2015), y de fomentar

la activación alternativa de los macrófagos, resultando en una regulación a la baja en la producción de citoquinas pro-inflamatorias y de óxido nítrico (Figueroa-Santiago & Espino, 2014). Así, y en caso que las FABPs de *E. granulosus* s.l. exhibiesen funciones similares a las reportadas para *F. hepatica*, la alta presencia de FABPs en el glicocálix del tegumento podría influir también en los fenómenos de inmunomodulación y protección parasitaria. Por otro lado, el AgB fue identificado mayoritariamente en el citoplasma distal del tegumento de los PSC (Figura 13) ; y de manera análoga a las FABPs parasitarias, se lo ha involucrado en interacciones patógeno-hospedero que promueven el establecimiento y sobrevida del parásito en hospederos intermediarios (Monteiro et al., 2012; Riganò et al., 2007).

Además, y siguiendo una metodología similar aplicada para el análisis del cargamento proteico en EVs de helmintos (Marcilla et al., 2012), nuestros resultados mostraron que los tres antígenos parasitarios analizados se encuentran también asociados a las vesículas presentes dentro del TBV (Figura 11, 12 y 13); lo cual sugeriría que esta estructura subcelular estaría involucrada en procesos de exocitosis tegumentaria en los PSC de *E. granulosus* s.l.

Por otro lado, y aunque aún existen dudas sobre cómo los componentes del hospedero atraviesan la capa germinativa y laminar del quiste hidático, es conocida la alta presencia de proteínas del hospedero en el líquido hidático de quistes íntegros; dentro de las cuales destacan los anticuerpos IgG del hospedero. En este sentido, se ha propuesto que los PSC de *E. granulosus* s.l. serían capaces de internalizar proteínas del hospedero como fuente de nutrientes (Aziz et al., 2011), limitando así los efectos de la respuesta inmune del hospedero dentro de los quistes. Nuestros resultados obtenidos mediante immunoTEM, mostraron que las IgG del hospedero (*B. taurus*) se encuentran presentes en el tegumento del soma de los PSC, mayoritariamente formando agrupaciones o cúmulos (Figura 14); evidenciando así la existencia de procesos endocíticos a través del tegumento. Estos cúmulos fueron observados, en gran medida, dentro de las células tegumentarias (Figura 14A) y en sus extensiones citoplasmáticas (Figura 14B), sugiriendo que los PSC serían

capaces de internalizar las IgG del hospedero mediante procesos activos que concentrarían y transportarían proteínas hacia el interior parasitario. Esta internalización, parecería ocurrir de manera independiente a las vesículas, ya que ningún cúmulo de marcas fue observado asociado a vesículas.

Tomados en su conjunto, los resultados reportados en el Capítulo 2 de la presente tesis, mostraron que el tegumento de los PSC de *E. granulosus* s.l. es una estructura parasitaria compleja, involucrada en motilidad parasitaria, absorción de nutrientes, secreción de antígenos parasitarios -y de EVs-, y en fenómenos de inmunomodulación y protección frente a la respuesta inmune del hospedero. Así, diferentes estructuras y territorios celulares fueron caracterizados por primera vez mediante reconstrucción 3D del tegumento, e inmuno-localización de componentes específicos presentes en el mismo. Además, se obtuvo evidencia relacionada al tránsito vesicular a través del tegumento de los PSC de *E. granulosus* s.l., y se describió -por primera vez- una nueva estructura subcelular que contiene vesículas cargadas de componentes parasitarios con potenciales funciones inmunomoduladoras.

A continuación, y dada la gran complejidad estructural y de funciones en las que interviene el tegumento de los PSC de *E. granulosus* s.l., en el Capítulo 3 de la presente tesis realizamos una caracterización bioquímica de sus componentes proteicos. Si bien existen numerosos estudios previos sobre la composición de diversas fracciones antigénicas provenientes de distintos estadíos parasitarios de *E. granulosus* s.l. (Ahn et al., 2017; Cui et al., 2013; Hidalgo et al., 2016; Lorenzatto et al., 2015; Mourglia-Ettlin et al., 2018; Santos et al., 2016; Siles-Lucas et al., 2017; Virginio et al., 2012; Zeghir-Bouteldja et al., 2017), en ninguno de ellos se analizaron las proteínas tegumentarias específicamente. Por ello, centramos nuestro análisis en la caracterización proteómica -y bioinformática- de los componentes parasitarios presentes en el tegumento de los PSC. Además, estudiamos en detalle, las posibles modificaciones post-traduccionales presentes en los mismos.

Para realizar dicho análisis, trabajamos con una fracción de proteínas tegumentarias de PSC de *E. granulosus* s.l., denominada PSEx (Hernández & Nieto, 1994), obtenida mediante incubación de PSC viables con un detergente suave. De esta manera, el tratamiento utilizado solubiliza las proteínas presentes en el citoplasma distal y en el glicocálix, sin generar grandes cambios morfológicos en las estructuras internas del parásito (Figura 15). La identificación de proteínas tegumentarias fue realizada mediante espectrometría de masas (MALDI-TOF/TOF), a partir de los spots individuales obtenidos tras resolución bidimensional de PSEx en geles de SDS-PAGE. De esta manera, se identificaron 58 proteínas parasitarias distintas, listadas en la Tabla 1 del artículo Adjunto 2. Resulta interesante mencionar que, 22 de las proteínas identificadas fueron reportadas a nivel proteómico en este estudio por primera vez.

Una vez obtenido el proteoma de PSEx, analizamos sus componentes mediante una estrategia de *Gene Ontology* (GO). En este sentido, es importante destacar que, debido a que el proteoma fue obtenido mediante separación en geles 2DE seguido por MALDI-TOF/TOF, y a que esta metodología no permite obtener información sobre la abundancia relativa de cada proteína dentro del proteoma; no se pudo realizar un análisis clásico de enriquecimiento de GO. Sin embargo, nuestro estudio de GO permitió analizar los términos únicos presentes en el proteoma de PSEx, describiendo así las características generales de la fracción antigénica. Así, nuestros resultados mostraron que las proteínas presentes en PSEx están mayoritariamente involucradas en procesos asociados a microtúbulos -potencialmente relacionados con estructuras vesiculares- exhibiendo diversas funciones metabólicas (Figura 17). Estos resultados estarían en línea con los resultados obtenidos en el Capítulo 2 de la presente tesis, así como con las funciones previamente reportadas para el tegumento (Morseth, 1967). El citoplasma distal de los PSC está compuesto, en gran medida, por estructuras vesiculares; las cuales estarían relacionadas con el tránsito de moléculas/vesículas a través del tegumento, muy probablemente involucrando procesos de rearreglo dinámica de microtúbulos. Además, nuestro análisis de GO también sugirió que el tegumento de los PSC estaría involucrado en mecanismos parasitarios de defensa y de

respuestas al estrés oxidativo inducido por el hospedero. Así, estos resultados estarían en línea con los descritos en el Capítulo 2 de la presente tesis; por ejemplo, la alta presencia de GST-1 parasitaria en el glicocálix de los PSC.

La caracterización bioquímica del tegumento, se profundizó mediante la identificación de posibles PTMs presentes en las proteínas de contenidas en PSEx. El estudio de las PTMs en organismos eucariotas, no solo permite obtener información básica sobre la bioquímica del organismo, sino que además es importante para el desarrollo de posibles productos biotecnológicos de interés. Sin embargo, el estudio de las PTMs en proteínas de *E. granulosus* s.l., al igual que en la mayoría de los helmintos parásitos, ha sido escaso; restringiéndose a un pequeño número de trabajos publicados (Alvarez Errico et al., 2001; McVeigh et al., 2005; Plancarte et al., 1999; Spiliotis et al., 2005; Spiliotis & Brehm, 2004; Virginio et al., 2012). Esto se debe, en parte, a lo engorroso del proceso de identificación de las PTMs presentes en una proteína en particular; lo cual se vuelve extremadamente complejo al trabajar con una mezcla proteica. Sin embargo, y mediante una combinación de técnicas de espectrometría de masas y de análisis genómico, en la presente tesis logramos obtener evidencia empírica de calidad, relacionada con la presencia de posibles PTMs presentes en proteínas tegumentarias de PSC de *E. granulosus* s.l.

Para ello, en primer lugar, re-analizamos los espectros obtenidos mediante MALDI-TOF/TOF con el software FindMod, obteniendo así una lista inicial de 27 PTMs -de modificación enzimática- cuyas masas eran compatibles con ciertos fragmentos m/z obtenidos. De manera interesante, cabe mencionar que solamente 13 de las 27 PTMs identificadas por FindMod, se encontraron anotadas en proteínas de platelmintos en la base de datos de UniProt; estando solo 7 de ellas anotadas en proteínas de *E. granulosus* s.l. (Tabla 1).

Sin embargo, al ser modificaciones introducidas mediante procesos enzimáticas, procedimos a realizar la búsqueda en el genoma de *E. granulosus* s.l. de las enzimas clave involucradas en su generación. De esta manera, identificamos las enzimas claves necesarias

para la realización de 22 PTMs; incluidas las 13 PTMs anotadas en proteínas de platelmintos (Tabla 1). Tres de las 9 PTMs para las cuales existen las enzimas claves en el genoma de *E. granulosus* s.l., pero que no se encontraron anotadas en ninguna proteína de platelminto, correspondieron a múltiplos de modificaciones simples (por ejemplo: di-hidroxilación, di-metilación y tri-metilación). A su vez, 19 de las 22 PTMs fueron identificadas mediante espectrometría de masas de alta resolución, en proteínas presentes en PSEx. Cabe destacar que, 9 de ellas se encontraron asociadas al mismo fragmento m/z por ambas técnicas proteómicas, aumentando así la probabilidad de que estas PTMs estén presentes en la proteína correspondiente. Entre ellas, 5 PTMs (deamidación, deamidación seguida por metilación, *S*-nitrosilación, di-hidroxilación y di-metilación) fueron identificadas aquí por primera vez; tanto sobre proteínas de *E. granulosus* s.l. así como en proteínas de otros platelmintos.

De esta manera, la caracterización bioquímica de las proteínas presentes en el tegumento de los PSC de *E. granulosus* s.l. reportada en el Capítulo 3 de esta tesis, mostró que PSEx es una fracción proteica compleja, compuesta por -al menos- 58 proteínas parasitarias distintas. Asimismo, estas proteínas estarían -mayoritariamente- involucradas en procesos de motilidad parasitaria, de defensa contra componentes inmunes del hospedero, y de transporte de antígenos parasitarios. Además, existiría una alta variedad de PTMs asociadas a dichas proteínas. En particular, logramos sugerir la existencia de 22 PTMs diferentes; 9 de ellas identificadas con una muy alta confianza. De esta manera, nuestros resultados permitieron complementar los estudios proteómicos realizados hasta la fecha para *E. granulosus* s.l., incrementando también la escasa información disponible en relación a las posibles PTMs presentes en proteínas de organismos platelmintos.

Luego de estudiar la ultraestructura y la composición proteica del tegumento de los PSC de *E. granulosus* s.l., analizamos el papel del tegumento en el proceso de establecimiento de la EQ secundaria experimental. Para ello, en el Capítulo 4 de la presente tesis, se analizó la respuesta inmune humoral desarrollada, en dos cepas distintas de

ratones, contra componentes tegumentarios. Asimismo, se evaluó si las diferencias en las respuestas de anticuerpos desarrolladas, podrían influir sobre el éxito o fracaso del establecimiento de la infección en el modelo murino de EQ secundaria. Estos estudios se basaron en reportes recientes de nuestro grupo de trabajo, donde se reportó la susceptibilidad diferencial de las cepas Balb/c y C57Bl/6 frente al desarrollo de la EQ secundaria (Mourglia-Ettlin et al., 2016a, 2016b). En particular, focalizamos nuestro estudio, en el papel de los anticuerpos específicamente inducidos contra antígenos tegumentarios de PSC de *E. granulosus* s.l.

La calidad de una respuesta de anticuerpos, y la protección que esta genera, no solo dependen del isotipo, título y avidez de los anticuerpos, sino también de los antígenos particulares que estos reconocen. Así, de manera de analizar la calidad de la respuesta de anticuerpos desarrollada por los ratones Balb/c y C57Bl/6 infectados, estudiamos cada uno de estos factores de forma independiente; realizando comparaciones tanto entre cepas, como dentro de una misma cepa pre- y post-inoculación de PSC. Por un lado, se analizó el título de los anticuerpos específicos contra antígenos parasitarios (anti-PSEx), observándose que los ratones C57Bl/6 infectados generaron títulos de anticuerpos de las subclases IgG2c e IgG2b, mayores que los ratones Balb/c. Además, la avidez de dichos anticuerpos también fue mayor en los ratones C57Bl/6 (Figura 18).

Por otro lado, se observó -mediante immunoTEM- que el citoplasma distal de los PSC es la zona de mayor reconocimiento por parte de los anticuerpos inducidos en ambas cepas de ratones (Figura 20). Sin embargo, resultó de gran interés el hecho que, mientras en ratones Balb/c aumenta el repertorio de antígenos reconocidos sobre el citoplasma distal parasitario por parte de los anticuerpos inducidos tras inoculación de PSC, el fenómeno contrario se observó en ratones de la cepa C57Bl/6 (Figura 20). Cabe aclarar que, esta observación asume que los antígenos parasitarios estrían homogéneamente distribuidos en todo el citoplasma distal, haciendo que la densidad de marcas fuese proporcional (aunque no necesariamente de forma lineal) al número de antígenos

reconocidos por los anticuerpos. Por otro lado, y en línea con lo previamente descrito, la inmunización de ratones Balb/c y C57Bl/6 con PSEx -en ausencia de adyuvante- generó respuestas de anticuerpos muy similares a las inducidas en el contexto de la infección experimental. De esta manera, nuestros resultados sugerirían que los ratones C57Bl/6, tanto infectados como inmunizados con PSEx, reducirían el repertorio de antígenos reconocidos por parte de sus anticuerpos IgG; direccionando así la respuesta humoral hacia un menor número de componentes parasitarios, pero probablemente de mayor relevancia. Esta hipótesis, además estaría sustentada por el hecho que los anticuerpos generados en ratones C57Bl/6 poseen una mayor actividad anti-parasitaria *in vitro* que aquellos inducidos en ratones Balb/c (Figura 19).

En base a estos resultados, identificamos a continuación cuáles eran los antígenos parasitarios reconocidos diferencialmente por los anticuerpos inducidos en ratones infectados pertenecientes a las cepas Balb/c y C57Bl/6. Para ello, mediante una estrategia de SERPA, observamos que los anticuerpos de ratones Balb/c infectados reconocen un mayor número de antígenos que los de su contraparte C57Bl/6 (Figura 22); principalmente a través de los isotipos IgG2a e IgG2b (Figura 18). Creemos importante destacar que la estrategia SERPA solamente permite cuantificar el número de epítopes B lineales (debido a las condiciones desnaturalizantes del estudio), y que las respuestas inmunes desarrolladas hacia epítopes B lineales usualmente corresponden al 10% de todos los anticuerpos inducidos (Sanchez-Trincado et al., 2017). Sin embargo, estos resultados estarían en línea con aquellos previamente discutidos, obtenidos mediante inmunoTEM (Figura 20); donde podrían estar incluidos posible epítopes B conformacionales.

La estrategia de análisis de SERPA, también nos permitió identificar -a nivel proteómico- cuáles son aquellos antígenos parasitarios reconocidos únicamente por anticuerpos inducidos en ratones C57Bl/6 infectados (DRPs); los cuales podrían constituir potenciales antígenos protectores. Así, identificamos exitosamente 13 DRPs (Figura 23), 7 de los cuales fueron previamente sugeridos y/o analizados como blancos moleculares para

el control de infecciones causadas por parásitos cestodos (Chabalgoity et al., 1997, 2000; Colebrook et al., 2002; Li et al., 2004; Mourglia-Ettlin et al., 2018; Müller-Schollenberger et al., 2001; Salinas et al., 1998; Shi et al., 2009; Vessal & Bagher Tabei, 1996; Wang et al., 2016; Xiao et al., 1994). Creemos importante destacar que, una de las DRPs identificadas correspondió a la FABP de *E. granulosus* s.l., proteína cuya localización en el tegumento fue analizada previamente a través de inmunoTEM en el Capítulo 2 de la presenta tesis (Figura 12). Esta proteína, ha sido sugerida como un interesante candidato vacunal frente a la infección por *E. granulosus* s.l. (Chabalgoity et al., 1997, 2000). Por otro lado, la vacunación con el antígeno P-29 -otra de las DRPs identificados- ha mostrado ser capaz de inducir altos niveles de protección, tanto en el modelo murino de EQ secundaria (Shi et al., 2009), como en ovejas inmunizadas y desafiadas en forma primaria (Wang et al., 2016). Asimismo, la tioredoxina peroxidasa -otra DRP identificada- es una enzima clave en *E. granulosus* s.l., involucrada en los mecanismos de detoxificación parasitaria contra especies reactivas del oxígeno; cuyo bloqueo ha sido sugerido como un interesante blanco para la prevención y/o el tratamiento de la EQ (Li et al., 2004; Salinas et al., 1998). Además, estas últimas dos proteínas, al igual que la peptidil-prolil cis-trans isomerasa, fueron recientemente identificadas por nuestro grupo, como ligandos de los receptores *scavanger* CD5 y CD6; e interesantemente, la infusión de los ectodominios recombinantes de CD5 o CD6 mostró ser capaz de inducir niveles significativos de protección en el modelo murino de EQ secundaria (Mourglia-Ettlin et al., 2018).

La información discutida sobre la identidad de algunas DRPs identificadas, sugiere el bloqueo de las mismas sería beneficioso para el hospedero intermediaron, por lo que *a priori* podrían ser consideradas como potenciales antígenos protectores. Por ello, realizamos una caracterización bioinformática de las 7 DRPs identificadas, para indagar si la diferencia en reconocimiento se debe a factores genéticos que diferencien ambas cepas de ratones. Este análisis mostró que, las 7 DRPs son proteínas mayoritariamente antigénicas, cuya secuencia aminoacídica difiere notoriamente del resto de las proteínas murinas (Figura 23); permitiendo el desarrollo de respuestas humorales contra las mismas. Sin embargo, el

análisis más relevante consistió en la identificación de epítopes T dentro de cada una de las DRPs; ya que para que ocurra una respuesta de anticuerpos T-dependiente óptima, sería necesaria su presentación antigénica a células T colaboradoras, mediante la presentación en moléculas del MHC-II. En este sentido, los ratones Balb/c y C57Bl/6 poseen distintas moléculas de MHC-II (H-2-IA^{d} y H-2-IA^{b}, respectivamente) (Sofron et al., 2016), las cuales presentarían diferencias en los perfiles de péptidos que son capaces de unir, así como en la afinidad de dicha unión. Así, para las 7 DRPs, se observó que la molécula de MHC-II presente en la cepa C57Bl/6, es capaz de unir un mayor número de posibles epítopes T, y con mayor fuerza de unión global, que la molécula de MHC-II presente en los ratones Balb/c (Figura24). Esto sugeriría la existencia de una predisposición genética en los ratones C57Bl/6 para producir mejores respuestas de anticuerpos contra las 7 DRPs identificadas (tanto tras la infección experimental como tras la inmunización con PSEx); contribuyendo así a la mayor resistencia observada para dicha cepa en el desarrollo de la EQ secundaria experimental.

Tomados en su conjunto, los resultados reportados en el Capítulo 4 de la presente tesis, mostraron que la respuesta de anticuerpos contra antígenos tegumentarios de PSC de *E. granulosus* s.l., desarrollada en ratones Balb/c y C57Bl/6 infectados, presenta grandes variaciones según la cepa murina. En este sentido, los ratones Balb/c infectados se caracterizaron por desarrollar una respuesta humoral anti-helmíntica clásica -con una alta inducción de IgE específica- contra un extenso repertorio de antígenos reconocidos por sus anticuerpos IgG. Por el contrario, los ratones C57Bl/6 infectados generaron una respuesta humoral contra un repertorio de antígenos más limitado (Figura 20), aunque probablemente de mayor relevancia para la fisiología parasitaria. Además, la respuesta de anticuerpos en estos ratones resultó estar enriquecida en subclases de IgG (Figura 18) con buena capacidad para activar el sistema complemento por vía clásica (IgG2b e IgG2c), mostrando una respuesta *in vitro* potencialmente más efectiva (Figura 19). En paralelo, los anticuerpos generados en ratones C57Bl/6 infectados, reconocen en forma única -es decir, a diferencia de los generados en ratones Balb/c infectados- al menos 13 antígenos parasitarios presentes en el tegumento de los PSC; 7 de los cuales fueron previamente

sugeridos como blancos terapéuticos contra parásitos de la especie *Echinococcus*. Mediante el análisis bioinformático de estos 7 DRPs, pudimos reportar que los mismos serían mejor presentados por la molécula de MHC-II presente exclusivamente en la cepa de ratones C57Bl/6; sugiriendo así que estos ratones estarían genéticamente predispuestos a desarrollar anticuerpos T-dependientes contra los mencionados antígenos tegumentarios.

Los resultados obtenidos hasta aquí, sugieren que las 7 DRPs identificadas podrían ser consideradas como potenciales antígenos parasitarios protectores; por lo que serían de interés inmunoterapéutico. Por ello, en el Capítulo 5 de la presente tesis, diseñamos péptidos derivados de dichas DRPs y los evaluamos como posibles candidatos vacunales en el modelo murino de EQ secundaria. El diseño realizado consistió en un uso alternativo de la vacunología reversa, aplicando de forma secuencial diversos algoritmos bio-inmuno-informáticos en un flujo de trabajo optimizado por nuestro grupo. Así, y luego de obtener experiencia en el uso de las herramientas bio-inmuno-informáticas necesarias, diseñamos 6 péptidos como potenciales antígenos vacunales. La utilidad de dichos péptidos fue luego evaluada en términos del análisis *in vitro* de la actividad anti-parasitaria de los anticuerpos específicos inducidos, así como mediante estudios de protección *in vivo* haciendo uso del modelo murino de EQ secundaria.

La mayoría de las herramientas informáticas utilizadas en este capítulo se basan en el análisis de la secuencia aminoacídica de proteínas, ya sea por reconocimiento de patrones específicos o identificación de característica fisicoquímicas de los aminoácidos. De esta manera, se puede utilizar estas herramientas para analizar tanto proteínas individuales como genomas enteros. Por ello, en primer lugar, se adquirió experiencia en su uso, realizando la identificación de candidatos peptídicos con potencial valor inmunodiagnóstico para las tres enfermedades tropicales desatendidas causadas por parásitos cestodos (Art. 5). En segundo lugar, se realizó el diseño de péptidos con potencial capacidad protectora contra *E. granulosus* s.l., partiendo de las 58 proteínas identificadas en la fracción PSEx (Art. 4). De esta forma, obtuvimos experiencia en el uso de más de 25 herramientas bio-inmuno-

informáticas, así como en el manejo de base de datos genómicas y proteómicas; analizando propiedades fisicoquímicas, secuencias aminoacídicas y estructuras tridimensionales.

Esta experiencia, nos permitió generar y optimizar un flujo de trabajo para el diseño de péptidos con potencial aplicación biotecnológica, introduciendo dos pasos claves en el análisis bio-inmuno-informático que aumentaron notoriamente la probabilidad de éxito. En primer lugar, la selección de epítopes B lineales "limpios" (carentes de PTMs), basada en evidencia obtenida por espectrometría de masas; ya sea mediante análisis de co-localización en los fragmentos m/z obtenidos por MALDI-TOF/TOF, o por carecer de las PTMs sugeridas a partir de los espectros. En segundo lugar, la selección de epítopes B lineales cuya estructura terciaria en solución fuese altamente similar a su estructura terciaria dentro de la proteína parental nativa; favoreciendo así la reactividad cruzada de los anticuerpos generados contra el péptido sintético sobre la proteína nativa.

De esta forma, y siguiendo el flujo de trabajo expuesto en la Tabla 3, diseñamos 6 péptidos antigénicos derivados de las 7 DRPs reconocidas únicamente por anticuerpos inducidos en ratones C57Bl/6 infectados (Figura 31). Luego, la validación del uso de estos péptidos como candidatos vacunales frente a la infección secundaria por *E. granulosus* s.l., fue realizada mediante estrategias *in vitro*, seguidas de estudios de protección *in vivo*.

Para los ensayos *in vitro*, primero se generaron anticuerpos específicos contra los péptidos diseñados, mediante la inmunización de ratones CD1 con cada péptido conjugado a KLH, y usando QuillA® como adyuvante. El éxito de la inmunización fue confirmado al titular los sueros obtenidos contra KLH mediante ELISA (Figura 32), y la respuesta humoral específica para los péptidos fue analizada mediante titulación de los anticuerpos IgG específicos contra cada péptido (Figura 33). Así, se observaron títulos de IgG bajos, pero significativos, específicos para los péptidos P2A, P2B, P3A y P3B. A su vez, la reactividad cruzada de los anticuerpos inducidos contra las proteínas de PSEx (presumiblemente contra cada una de las proteínas parentales correspondientes) fue analizada mediante ELISA, observándose una reactividad significativa para la mayoría de los péptidos (Figura 34). En

particular, la titulación de los sueros obtenidos tras inmunización con P1A-KLH, mostró que los anticuerpos generados no fueron capaces de reconocer el péptido sintético, a la vez que no mostraron reactividad cruzada con los componentes presentes en PSEx; sugiriendo entonces que el péptido P1A no sería capaz de inducir anticuerpos con capacidad protectora. Por ello, y dado que la preparación P1A-KLH fue muy similar al resto de las preparaciones (en términos del adyuvante y del *carrier* utilizados), esta fue utilizada como un control interno para el resto de los estudios; tanto *in vitro* como *in vivo*.

La actividad anti-parasitaria *in vitro* de los anticuerpos inducidos tras inmunización con los péptidos acoplados a KLH, se analizó por medio de tres estrategias complementarias, analizando en cada una, un posible mecanismo de acción. Los anticuerpos generados contra los péptidos P3A y P3B mostraron los mejores resultados, siendo capaces de inducir la muerte de los parásitos mediante interacción directa (Figura 35A), por activación clásica del sistema complemento (Figura 35C). Además, los anticuerpos específicos contra P3B, fueron capaces de interferir con procesos metabólicos de los PSC, aumentando la tasa de muerte de los mismos (Figura 35B).

La protección *in vivo* generada mediante inmunización activa con los péptidos, fue evaluada analizando tres formulaciones vacunales; agrupando los péptidos de a pares según los resultados obtenidos *in vitro*. Así, las formulaciones “Vacuna 1”, “Vacuna 2” y “Vacuna 3”, correspondieron a baja, media y alta actividad anti-parasitaria *in vitro* por parte de los anticuerpos específicamente inducidos; respectivamente. Cabe destacar que, nuevamente, la “Vacuna 1” actuó como un control negativo donde no se observó inducción de protección respecto al grupo de ratones no vacunado (Figura 36). A su vez, este resultado sugirió que la respuesta inmune desarrollada contra KLH no influiría significativamente en el resultado de la infección. Por otro lado, la “Vacuna 3” generó una protección del 50% en los ratones inmunizados (Figura 36A), así como una reducción significativa en el número de quistes hidáticos presentes en cavidad peritoneal (Figura 36B).

Resulta interesante destacar que, el par de péptidos utilizados en cada una de las formulaciones vacunales analizadas, correspondió a una única proteína parental. En el caso de las formulaciones que mostraron cierto nivel de protección ("Vacuna 2" y "Vacuna 3"), cada una derivó de una malato deshidrogenasa parasitaria; las cuales a pesar de ser una citoplasmática (P3) y la otra mitocondrial (P2), exhiben solo un 25% de identidad entre ellas. En este sentido, existen reportes pre-clínicos del uso de malato deshidrogenasas como candidatos vacunales contra diversos patógenos, incluyendo bacterias (Arayan et al., 2019), hongos (Shibasaki et al., 2014) y parásitos unicelulares (Liu et al., 2016). A su vez, esta proteína también ha sido propuesta como un blanco molecular para drogas antihelmínticas (Kayamba et al., 2021; Probert et al., 1981; Sanchez-Moreno et al., 1987). Nuestros resultados de actividad anti-parasitaria *in vitro*, y protección *in vivo*, por parte de anticuerpos específicos contra péptidos derivados de malato deshidrogenasas, permiten consolidar a esta proteína como un candidato vacunal frente a la infección por *E. granulosus* s.l.; así como sugerir el uso de -al menos- P3A y P3B como candidatos para vacunas basadas en péptidos. Cabe señalar también, que otros mecanismos distingos a la inducción de anticuerpos, podrían estar involucrados en la protección observada tras inmunización con la "Vacuna 3".

Tomados en su conjunto, los resultados reportados en el Capítulo 5 de esta tesis, permitieron el diseño de vacunas peptídicas promisorias contra *E. granulosus* s.l. a partir de candidatos vacunales identificados por técnicas proteómicas. Esto se logró mediante la optimización de un flujo de trabajo bio-inmuno-informático, que incluyó la introducción de dos pasos clave. Estos permitieron aumentar la probabilidad de generar respuestas humorales eficientes tras la vacunación, desarrollándose anticuerpos específicos contra el péptido y su proteína parental en 4 de los 6 de los péptidos diseñados (66%). A su vez, los anticuerpos inducidos mostraron diversas actividades anti-parasitarias *in vitro*; y, finalmente, 2 de los 6 péptidos (33%), fueron capaces de generar respuestas inmunes eficientes para limitar el establecimiento de la infección secundaria experimental en el modelo murino. Si bien creemos que sería necesario optimizar la formulación "Vacuna 3"

para alcanzar mejores niveles de protección, proponemos el presente flujo de trabajo como una herramienta útil para ser aplicada a otros patógenos; reduciendo en gran medida los costos y tiempos de I+D para productos de interés biotecnológico.

En suma, y a modo de comentario global, podemos decir que los resultados derivados de la presente tesis -y comunicados en los seis artículos adjuntos más uno anexo- sugieren que el tegumento de los PSC de *E. granulosus* s.l. jugaría un papel de relevancia en el establecimiento de la infección secundaria. En este sentido, el tegumento actuaría no solo como una barrera física frente a la respuesta inmune del hospedero, sino que también la contrarrestaría activamente; ya sea mediante procesos de detoxificación de xenobióticos y/o por medio de la liberación de componentes -y EVs- inmunomoduladores; entre otros. Así, el tegumento de los PSC debe ser entendido como una región anatómica de alta complejidad, tanto estructural y funcional, como en términos de su composición. Sin embargo, también debemos tener presente que, el desarrollo de una respuesta inmune humoral de calidad contra componentes tegumentarios, podría ser capaz de limitar el establecimiento de la infección en etapas tempranas. De esta manera, la inducción de anticuerpos específicos contra ciertos antígenos tegumentarios -ya sea de forma natural o mediante inmunización con péptidos derivados de dichos antígenos- sería capaz de inducir la muerte parasitaria. En base a estos resultados, confiamos en que será posible diseñar formulaciones vacunales basadas en péptidos, que induzcan niveles óptimos de protección frente a la infección por *E. granulosus* s.l. en diversos hospederos.

CAPÍTULO 7 I

BIBLIOGRAFÍA

Ahn, C.S., Kim, J.G., Han, X., Kang, I., Kong, Y., 2017. Comparison of *Echinococcus multilocularis* and *Echinococcus granulosus* hydatid fluid proteome provides molecular strategies for specialized host-parasite interactions. Oncotarget 8, 97009–97024. https://doi.org/10.18632/oncotarget.20761

Altschul, S.F., Gish, W., Miller, W., Myers, E.W., Lipman, D.J., 1990. Basic local alignment search tool. J. Mol. Biol. 215, 403–410. https://doi.org/10.1016/S0022-2836(05)80360-2

Alvarez Errico, D., Medeiros, A., Míguez, M., Casaravilla, C., Malgor, R., Carmona, C., Nieto, A., Osinaga, E., 2001. O-glycosylation in *Echinococcus granulosus*: Identification and characterization of the carcinoma-associated Tn antigen. Exp. Parasitol. 98, 100–109. https://doi.org/10.1006/expr.2001.4620

Alvarez Rojas, C.A., Gauci, C.G., Lightowlers, M.W., 2013. Antigenic differences between the EG95-related proteins from *Echinococcus granulosus* G1 and G6 genotypes: implications for vaccination. Parasite Immunol. 35, 99–102. https://doi.org/10.1111/pim.12009

Alvarez Rojas, C.A., Gauci, C.G., Nolan, M.J., Harandi, M.F., Lightowlers, M.W., 2012. Characterization of the eg95 gene family in the G6 genotype of *Echinococcus granulosus*. Mol. Biochem. Parasitol. 183, 115–121. https://doi.org/10.1016/j.molbiopara.2012.02.005

Anthony, R.M., Rutitzky, L.I., Urban, J.F., Stadecker, M.J., Gause, W.C., 2007. Protective immune mechanisms in helminth infection. Nat. Rev. Immunol. 7, 975–987. https://doi.org/10.1038/nri2199

Antoniou, M., Tselentis, Y., 1993. Studies on *Echinococcus granulosus* using the scanning electron microscope - I. Preparations of the parasite for infection of the final host. Parasitol. Res. 79, 537–542. https://doi.org/10.1007/BF00932236

Arayan, L.T., Huy, T.X.N., Reyes, A.W.B., Hop, H.T., Son, V.H., Min, W., Lee, H.J., Kim, S., 2019. Substantial protective immunity conferred by a combination of *Brucella abortus* recombinant proteins against *Brucella abortus* infection in BALB/c mice. J. Microbiol. Biotechnol. 29, 330–338. https://doi.org/10.4014/jmb.1811.10066

Arbildi, P., La-Rocca, S., Kun, A., Lorenzatto, K.R., Monteiro, K.M., Zaha, A., Mourglia-Ettlin, G., Ferreira, H.B., Fernández, V., 2021. Expression and distribution of glutathione transferases in protoscoleces of *Echinococcus granulosus sensu lato*. Acta Trop. 221, 105991. https://doi.org/10.1016/j.actatropica.2021.105991

Arbildi, P., Turell, L., López, V., Alvarez, B., Fernández, V., 2017. Mechanistic insights into EgGST1, a Mu class glutathione S-transferase from the cestode parasite *Echinococcus granulosus*. Arch. Biochem. Biophys. 633, 15–22. https://doi.org/10.1016/j.abb.2017.08.014

Aziz, A., Zhang, W., Li, J., Loukas, A., McManus, D.P., Mulvenna, J., 2011. Proteomic characterisation of *Echinococcus granulosus* hydatid cyst fluid from sheep, cattle and humans. J. Proteomics 74, 1560–1572. https://doi.org/10.1016/j.jprot.2011.02.021

Azmi, F., Al, A., Ahmad, H., Skwarczynski, M., Toth, I., 2014. Recent progress in adjuvant discovery for peptide-based subunit vaccines. Hum. Vaccin. Immunother. 778–796. https://doi.org/10.4161/hv.27332ferr

Barrios, A.A., Grezzi, L., Miles, S., Mariconti, M., Mourglia-Ettlin, G., Seoane, P.I., Díaz, A., 2019. Inefficient and abortive classical complement pathway activation by the calcium inositol hexakisphosphate component of the *Echinococcus granulosus* laminated layer. Immunobiology 224, 710–719. https://doi.org/10.1016/j.imbio.2019.05.009

Baz, A., Mourglia-Ettlin, G, Dematteis, S., 2006. Complexity and function of cytokine responses in experimental infection by *Echinococcus granulosus*. Immunobiology 211, 3–9. https://doi.org/10.1016/j.imbio.2005.09.001

Bendtsen, J.D., Jensen, L.J., Blom, N., Von Heijne, G., Brunak, S., 2004. Feature-based prediction of non-classical and leaderless protein secretion. Protein Eng. Des. Sel. 17, 349–356. https://doi.org/10.1093/protein/gzh037

Breijo, M., Isnardi, F., Brauer, M., Schenker, R., Ferrari, M., Ferreira, A.M., 2011. An insect growth inhibitor - lufenuron - enhances albendazole activity against hydatid cyst. Vet. Parasitol. 181, 341–344. https://doi.org/10.1016/j.vetpar.2011.04.011

Brunetti, E., Junghanss, T., 2009. Update on cystic hydatid disease. Curr. Opin. Infect. Dis. 22, 497–502. https://doi.org/10.1097/QCO.0b013e328330331c

Budke, C.M., Deplazes, P., Torgerson, P.R., 2006. Global socioeconomic impact of cystic echinococcosis. Emerg. Infect. Dis. 12, 296–303. https://doi.org/10.3201/eid1202.050499

Bui, L.T., Stenzel, D.J., Jones, M.K., 1999. Reappraisal of vesicular types in the syncytial tegument of the *Echinococcus granulosus* protoscolex. Parasitol. Res. 85, 35–40. https://doi.org/10.1007/s004360050504

Burgu, A., Sarimehmetoglu, O., Gonenc, B., Oge, H., Sahin, G., Aypak, S., 2007. Effects of immunization with purified specific proteins on the formation of secondary hydatid cysts in mice. Dtsch. Tierarztl. Wochenschr. 114, 349–353.

Carol, H., Nieto, A., 1998. A mucosal IgA response, but no systemic antibody response, is evoked by intranasal immunisation of dogs with *Echinococcus granulosus* surface

antigens iscoms. Vet. Immunol. Immunopathol. 65, 29–41.

Ceballos, L., Elissondo, C., Sánchez Bruni, S., Confalonieri, A., Denegri, G., Alvarez, L., Lanusse, C., 2010. Chemoprophylactic activity of flubendazole in cystic echinococcosis. Chemotherapy 56, 386–392. https://doi.org/10.1159/000316827

Chabalgoity, J.A., Harrison, J.A., Esteves, A., Demarco de Hormaeche, R., Ehrlich, R., Khan, C.M., Hormaeche, C.E., 1997. Expression and immunogenicity of an *Echinococcus granulosus* fatty acid-binding protein in live attenuated Salmonella vaccine strains. Infect. Immun. 65, 2402–2412. https://doi.org/10.1128/iai.65.6.2402-2412.1997

Chabalgoity, J.A., Moreno, M., Carol, H., Dougan, G., Hormaeche, C.E., 2000. *Salmonella typhimurium* as a basis for a live oral *Echinococcus granulosus* vaccine. Vaccine 19, 460–469. https://doi.org/10.1016/s0264-410x(00)00197-3

Cheers, C., McKenzie, I.F., Pavlov, H., Waid, C., York, J., 1978. Resistance and susceptibility of mice to bacterial infection: course of listeriosis in resistant or susceptible mice. Infect. Immun. 19, 763–770.

Chemale, G., Haag, K.L., Ferreira, H.B., Zaha, A., 2001. *Echinococcus granulosus* antigen B is encoded by a gene family. Mol. Biochem. Parasitol. 116, 233–237. https://doi.org/10.1016/S0166-6851(01)00316-4

Cheng, T., 1986. General Parasitology, 2nd edition. Parasitology 93, 611. https://doi.org/DOI: 10.1017/S0031182000081312

Chiodini, R.J., Buergelt, C.D., 1993. Susceptibility of Balb/c, C57/B6 and C57/B10 mice to infection with *Mycobacterium paratuberculosis*. J. Comp. Pathol. 109, 309–319. https://doi.org/10.1016/S0021-9975(08)80295-2

Chow, C., Gauci, C.G., Vural, G., Jenkins, D.J., Heath, D.D., Rosenzvit, M.C., Harandi, M.F., Lightowlers, M.W., 2008. *Echinococcus granulosus*: variability of the host-protective EG95 vaccine antigen in G6 and G7 genotypic variants. Exp. Parasitol. 119, 499–505. https://doi.org/10.1016/j.exppara.2008.01.004

Clem, A.S., 2011. Fundamentals of vaccine immunology. J. Glob. Infect. Dis. 3, 73–78. https://doi.org/10.4103/0974-777X.77299

Colby, L.A., Quenee, L.E., Zitzow, L.A., 2017. Considerations for infectious disease research studies using animals. Comp. Med. 67, 222–231.

Colebrook, A.L., Jenkins, D.D., Lightowlers, M.W., 2002. Anti-parasitic effect of cyclosporin A on *Echinococcus granulosus* and characterization of the associated cyclophilin protein. Parasitology 125, 485–493. https://doi.org/DOI: 10.1017/S0031182002002330

Cornejo-Granados, F., Hurtado-Ramirez, J.M., Hernandez-Pando, R., Ochoa-Leyva, A., 2018.

Secret-AAR: a web server to assess the antigenic density of proteins and homology search against bacterial and parasite secretome proteins. Genomics. https://doi.org/10.1016/j.ygeno.2018.10.007

Coutelen, F., Biquet, J., Doby, J.-M., 1952. Le système musculaire du scolex echinococcique-Mécanismes de dévagination et d'invagination du rostre et des ventouses. Ann. Parasitol. Hum. Comparée 27, 86–94.

Cozzetto, D., Minneci, F., Currant, H., Jones, D.T., 2016. FFPred 3: Feature-based function prediction for all Gene Ontology domains. Sci. Rep. 6, 1–11. https://doi.org/10.1038/srep31865

Cucher, M., Mourglia-Ettlin, G., Prada, L., Costa, H., Kamenetzky, L., Poncini, C., Dematteis, S., Rosenzvit, M.C., 2013. *Echinococcus granulosus* pig strain (G7 genotype) protoscoleces did not develop secondary hydatid cysts in mice. Vet. Parasitol. 193, 185–192. https://doi.org/10.1016/j.vetpar.2012.11.027

Cucher, M., Prada, L., Mourglia-Ettlin, G., Dematteis, S., Camicia, F., Asurmendi, S., Rosenzvit, M., 2011. Identification of *Echinococcus granulosus* microRNAs and their expression in different life cycle stages and parasite genotypes. Int. J. Parasitol. 41, 439–448. https://doi.org/10.1016/j.ijpara.2010.11.010

Cucher, M.A., Macchiaroli, N., Baldi, G., Camicia, F., Prada, L., Maldonado, L., Avila, H.G., Fox, A., Gutiérrez, A., Negro, P., López, R., Jensen, O., Rosenzvit, M., Kamenetzky, L., 2015. Cystic echinococcosis in South America: systematic review of species and genotypes of *Echinococcus granulosus sensu lato* in humans and natural domestic hosts. Trop. Med. Int. Heal. 21, 166–175. https://doi.org/10.1111/tmi.12647

Cui, S.J., Xu, L.L., Zhang, T., Xu, M., Yao, J., Fang, C.Y., Feng, Z., Yang, P.Y., Hu, W., Liu, F., 2013. Proteomic characterization of larval and adult developmental stages in *Echinococcus granulosus* reveals novel insight into host-parasite interactions. J. Proteomics 84, 158–175. https://doi.org/10.1016/j.jprot.2013.04.013

Cumino, A.C., Nicolao, M.C., Loos, J.A., Denegri, G., Elissondo, M.C., 2012. E*chinococcus granulosus* tegumental enzymes as in vitro markers of pharmacological damage: A biochemical and molecular approach. Parasitol. Int. 61, 579–585. https://doi.org/10.1016/j.parint.2012.05.007

Cyrklaff, M., Frischknecht, F., Kudryashev, M., 2017. Functional insights into pathogen biology from 3D electron microscopy. FEMS Microbiol. Rev. 41, 828–853. https://doi.org/10.1093/femsre/fux041

D'Amico, C., Fontana, F., Cheng, R., Santos, H.A., 2021. Development of vaccine formulations: past, present, and future. Drug Deliv. Transl. Res. 11, 353–372. https://doi.org/10.1007/s13346-021-00924-7

de Castro, E., Sigrist, C.J.A., Gattiker, A., Bulliard, V., Langendijk-Genevaux, P.S., Gasteiger, E., Bairoch, A., Hulo, N., 2006. ScanProsite: Detection of PROSITE signature matches and ProRule-associated functional and structural residues in proteins. Nucleic Acids Res. 34, 362–365. https://doi.org/10.1093/nar/gkl124

Dematteis, S., Rottenberg, M., Baz, A., 2003. Cytokine response and outcome of infection depends on the infective dose of parasites in experimental infection by *Echinococcus granulosus*. Parasite Immunol. 25, 189–197. https://doi.org/10.1046/j.1365-3024.2003.00620.x

Denegri, G., Perez-Serrano, J., Casado, N., Rodriguez-Caabeiro, F., 1995. [13C]-nuclear magnetic resonance spectral profiles of serum from normal and *Echinococcus granulosus*-infected mice: a kinetic study. Parasitol. Res. 81, 170–172.

Deokate, U.A., Lahane, S.B., Sujeetkumar, A., 2014. Review on anthelmintic drugs. Int. J. Pharm. Res. 6, 1–7.

Di Natale, C., La Manna, S., De Benedictis, I., Brandi, P., Marasco, D., 2020. Perspectives in Peptide-Based Vaccination Strategies for Syndrome Coronavirus 2 Pandemic. Front. Pharmacol. 11, 1–16. https://doi.org/10.3389/fphar.2020.578382

Díaz-Zaragoza, M., Hernández-Ávila, R., Ostoa-Saloma, P., 2017. Recognition of tumor antigens in 4T1 cells by natural IgM from three strains of mice with different susceptibilities to spontaneous breast cancer. Oncol. Lett. 13, 271–274. https://doi.org/10.3892/ol.2016.5427

Díaz, A., Casaravilla, C., Irigoín, F., Lin, G., Previato, J.O., Ferreira, F., 2011a. Understanding the laminated layer of larval *Echinococcus* I: Structure. Trends Parasitol. 27, 204–213. https://doi.org/10.1016/j.pt.2010.12.012

Díaz, A., Casaravilla, C., Allen, J.E., Sim, R.B., Ferreira, A.M., 2011b. Understanding the laminated layer of larval *Echinococcus* II: Immunology. Trends Parasitol. 27, 264–273. https://doi.org/10.1016/j.pt.2011.01.008

Emanuelsson, O., Nielsen, H., Brunak, S., Von Heijne, G., 2000. Predicting subcellular localization of proteins based on their N-terminal amino acid sequence. J. Mol. Biol. 300, 1005–1016. https://doi.org/10.1006/jmbi.2000.3903

Ferragut, G., Ljungstrom, I., Nieto, A., 1998. Relevance of circulating antigen detection to follow-up experimental and human cystic hydatid infections. Parasite Immunol. 20, 541–549.

Ferreira, B.L., Ferreira, É.R., de Brito, M. V., Salu, B.R., Oliva, M.L.V., Mortara, R.A., Orikaza, C.M., 2018. BALB/c and C57BL/6 mice cytokine responses to *Trypanosoma cruzi* infection are independent of parasite strain infectivity. Front. Microbiol. 9, 1–12. https://doi.org/10.3389/fmicb.2018.00553

Figueroa-Santiago, O., Espino, A.M., 2014. *Fasciola hepatica* fatty acid binding protein induces the alternative activation of human macrophages. Infect. Immun. 82, 5005–5012. https://doi.org/10.1128/IAI.02541-14

Fitzsimmons, C.M., Falcone, F.H., Dunne, D.W., 2014. Helminth allergens, parasite-specific IgE, and its protective role in human immunity. Front. Immunol. 5, 1–12. https://doi.org/10.3389/fimmu.2014.00061

Fornefett, J., Krause, J., Klose, K., Fingas, F., Hassert, R., Eisenberg, T., Schrödl, W., Grunwald, T., Müller, U., Baums, C.G., 2018a. Comparative analysis of clinics, pathologies and immune responses in BALB/c and C57BL/6 mice infected with *Streptobacillus moniliformis*. Microbes Infect. 20, 101–110. https://doi.org/10.1016/j.micinf.2017.10.001

Fornefett, J., Krause, J., Klose, K., Fingas, F., Hassert, R., Benga, L., Grunwald, T., Müller, U., Schrödl, W., Baums, C.G., 2018b. Comparative analysis of humoral immune responses and pathologies of BALB/c and C57BL/6 wildtype mice experimentally infected with a highly virulent *Rodentibacter pneumotropicus* (*Pasteurella pneumotropica*) strain. BMC Microbiol. 18, 1–11. https://doi.org/10.1186/s12866-018-1186-8

Galindo, M., Schadebrodt, G., Galanti, N., 2008. *Echinococcus granulosus*: Cellular territories and morphological regions in mature protoscoleces. Exp. Parasitol. 119, 524–533. https://doi.org/10.1016/j.exppara.2008.04.013

Gazzinelli-Guimaraes, P.H., Nutman, T.B., 2018. Helminth parasites and immune regulation. F1000Research 7. https://doi.org/10.12688/F1000RESEARCH.15596.1

Geourjon, C., Deléage, G., 1995. Sopma: Significant improvements in protein secondary structure prediction by consensus prediction from multiple alignments. Bioinformatics 11, 681–684. https://doi.org/10.1093/bioinformatics/11.6.681

Gouglas, D., Thanh Le, T., Henderson, K., Kaloudis, A., Danielsen, T., Hammersland, N.C., Robinson, J.M., Heaton, P.M., Røttingen, J.A., 2018. Estimating the cost of vaccine development against epidemic infectious diseases: a cost minimisation study. Lancet Glob. Heal. 6, e1386–e1396. https://doi.org/10.1016/S2214-109X(18)30346-2

Gupta, S., Kapoor, P., Chaudhary, K., Gautam, A., Kumar, R., Raghava, G.P.S., 2013. *In Silico* Approach for Predicting Toxicity of Peptides and Proteins. PLoS One 8. https://doi.org/10.1371/journal.pone.0073957

Haag, K.L., Gottstein, B., Ayala, F.J., 2009. The EG95 antigen of *Echinococcus spp*. contains positively selected amino acids, which may influence host specificity and vaccine efficacy. PLoS One 4. https://doi.org/10.1371/journal.pone.0005362

Harris, M.A., Deegan, J.I., Ireland, A., Lomax, J., Ashburner, M., Tweedie, S., Carbon, S., Lewis, S., Mungall, C., Day-Richter, J., Eilbeck, K., Blake, J.A., Bult, C., Diehl, A.D., Dolan,

M., Drabkin, H., Eppig, J.T., Hill, D.P., Ni, L., Ringwald, M., Balakrishnan, R., Binkley, G., Cherry, J.M., Christie, K.R., Costanzo, M.C., Dong, Q., Engel, S.R., Fisk, D.G., Hirschman, J.E., Hitz, B.C., Hong, E.L., Krieger, C.J., Miyasato, S.R., Nash, R.S., Park, J., Skrzypek, M.S., Weng, S., Wong, E.D., Zhu, K.K., Botstein, D., Dolinski, K., Livstone, M.S., Oughtred, R., Berardini, T., Li, D., Rhee, S.Y., Apweiler, R., Barrell, D., Camon, E., Dimmer, E., Huntley, R., Mulder, N., Khodiyar, V.K., Lovering, R.C., Povey, S., Chisholm, R., Fey, P., Gaudet, P., Kibbe, W., Kishore, R., Schwarz, E.M., Sternberg, P., Van Auken, K., Giglio, M.G., Hannick, L., Wortman, J., Aslett, M., Berriman, M., Wood, V., Jacob, H., Lauledeerkind, S., Petri, V., Shimoyama, M., Smith, J., Twigger, S., Jaiswal, P., Seigfried, T., Howe, D., Westerfield, M., Collmer, C., Torto-Alalibo, T., Feltrin, E., Valle, G., Bromberg, S., Burgess, S., McCarthy, F., 2008. The Gene Ontology project in 2008. Nucleic Acids Res. 36, 440–444. https://doi.org/10.1093/nar/gkm883

Hashemitabar, G.R., Razmi, G.R., Naghibi, A., 2005. Trials to induce protective immunity in mice and sheep by application of protoscolex and hydatid fluid antigen or whole body antigen of *Echinococcus granulosus*. J. Vet. Med. B. Infect. Dis. Vet. Public Health 52, 243–245. https://doi.org/10.1111/j.1439-0450.2005.00847.x

Heath, D.D., 1970. The development of *Echinococcus granulosus* larvae in laboratory animals. Parasitology 60, 449–456. https://doi.org/10.1017/S0031182000078252

Heath, D.D., Jensen, O., Lightowlers, M.W., 2003. Progress in control of hydatidosis using vaccination - A review of formulation and delivery of the vaccine and recommendations for practical use in control programmes. Acta Trop. 85, 133–143. https://doi.org/10.1016/S0001-706X(02)00219-X

Heath, D.D., Koolaard, J., 2012. Serological monitoring of protection of sheep against *Echinococcus granulosus* induced by the EG95 vaccine. Parasite Immunol. 34, 40–44. https://doi.org/10.1111/j.1365-3024.2011.01341.x

Henderson, K.S., Pritchett-Corning, K.R., Perkins, C.L., Banu, L.A., Jennings, S.M., Francis, B.C., Shek, W.R., 2015. A comparison of mouse parvovirus 1 infection in BALB/c and C57BL/6 mice: Susceptibility, replication, shedding, and seroconversion. Comp. Med. 65, 5–14.

Hernández, A., Nieto, A., 1994. Induction of protective immunity against murine secondary hydatidosis. Parasite Immunol. 16, 537–544. https://doi.org/10.1111/j.1365-3024.1994.tb00308.x

Hidalgo, C., García, M.P., Stoore, C., Ramírez, J.P., Monteiro, K.M., Hellman, U., Zaha, A., Ferreira, H.B., Galanti, N., Landerer, E., Paredes, R., 2016. Proteomics analysis of *Echinococcus granulosus* protoscolex stage. Vet. Parasitol. 218, 43–45. https://doi.org/10.1016/j.vetpar.2015.12.026

Hotez, PJ; Mistry, N; Rubinstein, J; Sachs, J., 2011. Integrating Neglected Tropical Diseases

into AIDS ,. N. Engl. J. Med. 2086–2089.

Hotez, P.J., Brindley, P.J., Bethony, J.M., King, C.H., Pearce, E.J., Jacobson, J., 2008. Helminth infections: the great neglected tropical diseases. J. Clin. Invest. 118, 1311–1321. https://doi.org/10.1172/JCI34261

Hu, H., Kang, J., Chen, R., Mamuti, W., Wu, G., Yuan, W., 2011. Drug-induced apoptosis of *Echinococcus granulosus* protoscoleces. Parasitol. Res. 109, 453–459. https://doi.org/10.1007/s00436-011-2276-9

Huerta, M., De Aluja, A.S., Fragoso, G., Toledo, A., Villalobos, N., Hernández, M., Gevorkian, G., Acero, G., Díaz, A., Alvarez, I., Avila, R., Beltrán, C., Garcia, G., Martinez, J.J., Larralde, C., Sciutto, E., 2001. Synthetic peptide vaccine against *Taenia solium* pig cysticercosis: Successful vaccination in a controlled field trial in rural Mexico. Vaccine 20, 262–266. https://doi.org/10.1016/S0264-410X(01)00249-3

Jezek, J., El Ridi, R., Salah, M., Wagih, A., Aziz, H.W., Tallima, H., El Shafie, M.H., Khalek, T.A., Abo Ammou, F.F., Strongylis, C., Moussis, V., Tsikaris, V., 2008. *Fasciola gigantica* cathepsin L proteinase-based synthetic peptide for immunodiagnosis and prevention of sheep fasciolosis. Biopolym. - Pept. Sci. Sect. 90, 349–357. https://doi.org/10.1002/bip.20788

Jha, R.K., Smyth, J.D., 1971. Ultrastructure of the rostellar tegument of *Echinococcus granulosus* with special reference to biogenesis of mitochondria. Int. J. Parasitol. 1. https://doi.org/10.1016/0020-7519(71)90012-9

Käll, L., Krogh, A., Sonnhammer, E.L.L., 2004. A combined transmembrane topology and signal peptide prediction method. J. Mol. Biol. 338, 1027–1036. https://doi.org/10.1016/j.jmb.2004.03.016

Källberg, M., Wang, H., Wang, S., Peng, J., Wang, Z., Lu, H., Xu, J., 2012. Template-based protein structure modeling using the RaptorX web server. Nat. Protoc. 7, 1511–1522. https://doi.org/10.1038/nprot.2012.085

Kayamba, F., Faya, M., Pooe, O.J., Kushwaha, B., Kushwaha, N.D., Obakachi, V.A., Nyamori, V.O., Karpoormath, R., 2021. Lactate dehydrogenase and malate dehydrogenase: Potential antiparasitic targets for drug development studies. Bioorg. Med. Chem. 50, 116458. https://doi.org/10.1016/j.bmc.2021.116458

Khoo, K.H., Nieto, A., Morris, H.R., Dell, A., 1997. Structural characterization of the N-glycans from *Echinococcus granulosus* hydatid cyst membrane and protoscoleces. Mol. Biochem. Parasitol. 86, 237–248. https://doi.org/10.1016/S0166-6851(97)00036-4

Kremer, J.R., Mastronarde, D.N., McIntosh, J.R., 1996. Computer visualization of three-dimensional image data using IMOD. J. Struct. Biol. 116, 71–6.

Krogh, A., Larsson, B., Von Heijne, G., Sonnhammer, E.L.L., 2001. Predicting transmembrane

protein topology with a hidden Markov model: Application to complete genomes. J. Mol. Biol. 305, 567–580. https://doi.org/10.1006/jmbi.2000.4315

Kulcsar, K.A., Baxter, V.K., Abraham, R., Nelson, A., Griffin, D.E., 2015. Distinct Immune Responses in Resistant and Susceptible Strains of Mice during *Neurovirulent Alphavirus* Encephalomyelitis. J. Virol. 89, 8280–8291. https://doi.org/10.1128/jvi.00173-15

Lamiable, A., Thévenet, P., Rey, J., Vavrusa, M., Derreumaux, P., Tufféry, P., 2016. PEP-FOLD3: faster de novo structure prediction for linear peptides in solution and in complex. Nucleic Acids Res. 44, W449–W454. https://doi.org/10.1093/nar/gkw329

Larsen, J.E.P., Lund, O., Nielsen, M., 2006. Improved method for predicting linear B-cell epitopes. Immunome Res. 2, 2. https://doi.org/10.1186/1745-7580-2-2

Li, J., Zhang, W.-B., Loukas, A., Lin, R.-Y., Ito, A., Zhang, L.-H., Jones, M., McManus, D.P., 2004. Functional expression and characterization of *Echinococcus granulosus* thioredoxin peroxidase suggests a role in protection against oxidative damage. Gene 326, 157–165. https://doi.org/https://doi.org/10.1016/j.gene.2003.10.027

Li, Y., Zhu, Y., Sha, T., Chen, Z., Yu, M., Zhang, F., Ding, J., 2021. A Multi-Epitope Chitosan Nanoparticles Vaccine of Canine Against *Echinococcus granulosus*. J. Biomed. Nanotechnol. 17, 910–920. https://doi.org/10.1166/jbn.2021.3065

Lightowlers, M.W., Jensen, O., Fernandez, E., Iriarte, J.A., Woollard, D.J., Gauci, C.G., Jenkins, D.J., Heath, D.D., 1999. Vaccination trials in Australia and Argentina confirm the effectiveness of the EG95 hydatid vaccine in sheep. Int. J. Parasitol. 29, 531–534. https://doi.org/10.1016/S0020-7519(99)00003-X

Lightowlers, M.W., Lawrence, S.B., Gauci, C.G., Young, J., Ralston, M.J., Maas, D., Heath, D.D., 1996. Vaccination against hydatidosis using a defined recombinant antigen. Parasite Immunol. 18, 457–462. https://doi.org/10.1111/j.1365-3024.1996.tb01029.x

Liu, B., Koo, G.C., Yap, E.H., Chua, K.L., Gan, Y.H., 2002. Model of differential susceptibility to mucosal *Burkholderia pseudomallei* infection. Infect. Immun. 70, 504–511. https://doi.org/10.1128/IAI.70.2.504-511.2002

Liu, Z., Yuan, F., Yang, Y., Yin, L., Liu, Y., Wang, Y., Zheng, K., Cao, J., 2016. Partial protective immunity against toxoplasmosis in mice elicited by recombinant *Toxoplasma gondii* malate dehydrogenase. Vaccine 34, 989–994. https://doi.org/10.1016/j.vaccine.2015.10.067

Lorenzatto, K.R., Kim, K., Ntai, I., Paludo, G.P., Camargo de Lima, J., Thomas, P.M., Kelleher, N.L., Ferreira, H.B., 2015. Top Down Proteomics Reveals Mature Proteoforms Expressed in Subcellular Fractions of the *Echinococcus granulosus* Preadult Stage. J. Proteome Res. 14, 4805–4814. https://doi.org/10.1021/acs.jproteome.5b00642

Magnan, C.N., Zeller, M., Kayala, M.A., Vigil, A., Randall, A., Felgner, P.L., Baldi, P., 2010.

High-throughput prediction of protein antigenicity using protein microarray data. Bioinformatics 26, 2936–2943. https://doi.org/10.1093/bioinformatics/btq551

Malonis, R.J., Lai, J.R., Vergnolle, O., 2020. Peptide-Based Vaccines: Current Progress and Future Challenges. Chem. Rev. 120, 3210–3229. https://doi.org/10.1021/acs.chemrev.9b00472

Mamuti, W., Yamasaki, H., Sako, Y., Nakaya, K., Nakao, M., Lightowlers, M.W., Ito, A., 2002. Usefulness of Hydatid Cyst Fluid of *Echinococcus granulosus* Developed in Mice with Secondary Infection for Serodiagnosis of Cystic Echinococcosis in Humans 9, 573–576. https://doi.org/10.1128/CDLI.9.3.573

Marcilla, A., Martin-Jaular, L., Trelis, M., de Menezes-Neto, A., Osuna, A., Bernal, D., Fernandez-Becerra, C., Almeida, I.C., del Portillo, H.A., 2014. Extracellular vesicles in parasitic diseases. J. Extracell. Vesicles 3. https://doi.org/10.3402/jev.v3.25040

Marcilla, A., Trelis, M., Cortés, A., Sotillo, J., Cantalapiedra, F., Minguez, M.T., Valero, M.L., Sánchez del Pino, M.M., Muñoz-Antoli, C., Toledo, R., Bernal, D., 2012. Extracellular Vesicles from Parasitic Helminths Contain Specific Excretory/Secretory Proteins and Are Internalized in Intestinal Host Cells. PLoS One 7. https://doi.org/10.1371/journal.pone.0045974

Maronpot, R.R., 2009. Biological Basis of Differential Susceptibility to Hepatocarcinogenesis among Mouse Strains. J. Toxicol. Pathol. 22, 11–33. https://doi.org/10.1293/tox.22.11

Martin, I., Cabán-Hernández, K., Figueroa-Santiago, O., Espino, A.M., 2015. *Fasciola hepatica* fatty acid binding protein inhibits TLR4 activation and suppresses the inflammatory cytokines induced by lipopolysaccharide in vitro and in vivo. J. Immunol. 194, 3924–3936. https://doi.org/10.4049/jimmunol.1401182

Matsuo, T., Hashimoto, M., Sakaguchi, S., Sakaguchi, N., Ito, Y., Hikida, M., Tsuruyama, T., Sakai, K., Yokoi, H., Shirakashi, M., Tanaka, M., Ito, H., Yoshifuji, H., Ohmura, K., Fujii, T., Mimori, T., 2019. Strain-Specific Manifestation of Lupus-like Systemic Autoimmunity Caused by Zap70 Mutation. J. Immunol. https://doi.org/10.4049/jimmunol.1801159

McGuire, C., Chan, W.C., Wakelin, D., 2002. Nasal immunization with homogenate and peptide antigens induces protective immunity against *Trichinella spiralis*. Infect. Immun. 70, 7149–7152. https://doi.org/10.1128/IAI.70.12.7149-7152.2002

McVeigh, P., Kimber, M.J., Novozhilova, E., Day, T.A., 2005. Neuropeptide signalling systems in flatworms. Parasitology 131. https://doi.org/10.1017/S0031182005008851

Miguez, M., Baz, A., Nieto, A., 1996. Carbohydrates on the surface of *Echinococcus granulosus* protoscoleces are immunodominant in mice. Parasite Immunol. 18, 559–569.

Miles, S., Navatta, M., Dematteis, S., Mourglia-Ettlin, G., 2017. Identification of universal diagnostic peptide candidates for neglected tropical diseases caused by cestodes through the integration of multi-genome-wide analyses and immunoinformatic predictions. Infect. Genet. Evol. 54. https://doi.org/10.1016/j.meegid.2017.07.020

Miles, S., Portela, M., Cyrklaff, M., Ancarola, M.E., Frischknecht, F., Durán, R., Dematteis, S., Mourglia-Ettlin, G., 2019. Combining proteomics and bioinformatics to explore novel tegumental antigens as vaccine candidates against *Echinococcus granulosus* infection. J. Cell. Biochem. 120, 15320–15336. https://doi.org/10.1002/jcb.28799

Miles, S., Magnone, J., Cyrklaff, M., Arbildi, P., Frischknecht, F., Dematteis, S., Mourglia-Ettlin, G., 2020a. Linking murine resistance to secondary cystic echinococcosis with antibody responses targeting *Echinococcus granulosus* tegumental antigens. Immunobiology 225. https://doi.org/10.1016/j.imbio.2020.151916

Miles, S., Velasco-de-Andrés, M., Lozano, F., Mourglia-Ettlin, G., 2020b. Interactome analysis of CD5 and CD6 ectodomains with tegumental antigens from the helminth parasite *Echinococcus granulosus sensu lato*. Int. J. Biol. Macromol. 164, 3718–3728. https://doi.org/10.1016/j.ijbiomac.2020.08.219

Miles, S., Magnone, J., García-Luna, J., Ancarola, M.E., Cucher, M., Dematteis, S., Frischknecht, F., Cyrklaff, M., Mourglia-Ettlin, G., 2021. Ultrastructural characterization of the tegument in protoscoleces of *Echinococcus ortleppi*. Int. J. Parasitol. 51, 989–997. https://doi.org/10.1016/j.ijpara.2021.05.004

Miles, S., Magnone, J., García-Luna, J., Dematteis, S., Mourglia-Ettlin, G., 2022. Unraveling post-translational modifications in *Echinococcus granulosus sensu lato*. Acta Trop. 230, 106410. https://doi.org/10.1016/j.actatropica.2022.106410

Molan, A.L., Saeed, I.S., 1988. Protection of mice against *Echinococcus granulosus* by previous inoculation with protoscoleces exposed to ultraviolet irradiation. Japanese J. Parasitol. 37, 203–208.

Mols-Vorstermans, T., Hemphill, A., Monney, T., Schaap, D., Boerhout, E., 2013. Differential Effects on Survival, Humoral Immune Responses and Brain Lesions in Inbred BALB/C, CBA/CA, and C57BL/6 Mice Experimentally Infected with *Neospora caninum* Tachyzoites . ISRN Parasitol. 2013, 1–11. https://doi.org/10.5402/2013/830980

Monteiro, K.M., Cardoso, M.B., Follmer, C., da Silveira, N.P., Vargas, D.M., Kitajima, E.W., Zaha, A., Ferreira, H.B., 2012. *Echinococcus granulosus* Antigen B structure: Subunit composition and oligomeric states. PLoS Negl. Trop. Dis. 6. https://doi.org/10.1371/journal.pntd.0001551

Monteiro, K.M., De Carvalho, M.O., Zaha, A., Ferreira, H.B., 2010. Proteomic analysis of the *Echinococcus granulosus* metacestode during infection of its intermediate host. Proteomics 10, 1985–1999. https://doi.org/10.1002/pmic.200900506

Mora, M., Veggi, D., Santini, L., Pizza, M., Rappuoli, R., 2003. Reverse vaccinology. Drug Discov. Today 8, 459–464. https://doi.org/10.1016/S1359-6446(03)02689-8

Morseth, D.J., 1967. Fine structure of the hydatid cyst and protoscolex of *Echinococcus granulosus*. J. Parasitol. 53, 312–325. https://doi.org/10.2307/3276582

Mourglia-Ettlin, G., Marqués, J.M., Chabalgoity, J.A., Dematteis, S., 2011. Early peritoneal immune response during *Echinococcus granulosus* establishment displays a biphasic behavior. PLoS Negl. Trop. Dis. 5, 1–11. https://doi.org/10.1371/journal.pntd.0001293

Mourglia-Ettlin, G., Cucher, M., Arbildi, P., Rosenzvit, M., Dematteis, S., 2016a. Natural and induced antibodies contribute to differential susceptibility to secondary cystic echinococcosis of Balb/c and C57Bl/6 mice. Immunobiology. https://doi.org/10.1016/j.imbio.2015.07.016

Mourglia-Ettlin, G., Merlino, A., Capurro, R., Dematteis, S., 2016b. Associations between mouse strains and early peritoneal immune responses. Immunobiology. https://doi.org/10.1016/j.imbio.2015.11.012

Mourglia-Ettlin, G., Miles, S., Velasco-De-Andrés, M., Armiger-Borràs, N., Cucher, M., Dematteis, S., Lozano, F., 2018. The ectodomains of the lymphocyte scavenger receptors CD5 and CD6 interact with tegumental antigens from *Echinococcus granulosus sensu lato* and protect mice against secondary cystic echinococcosis. PLoS Negl. Trop. Dis. 12. https://doi.org/10.1371/journal.pntd.0006891

Müller-Schollenberger, V., Beyer, W., Schnitzler, P., Merckelbach, A., Roth, S., Kalinna, B.H., Lucius, R., 2001. Immunisation with *Salmonella typhimurium*-delivered glyceraldehyde-3-phosphate dehydrogenase protects mice against challenge infection with *Echinococcus multilocularis* eggs. Int. J. Parasitol. 31, 1441–1449. https://doi.org/https://doi.org/10.1016/S0020-7519(01)00244-2

Nakao, M., Yanagida, T., Okamoto, M., Knapp, J., Nkouawa, A., Sako, Y., Ito, A., 2010. State-of-the-art Echinococcus and Taenia: Phylogenetic taxonomy of human-pathogenic tapeworms and its application to molecular diagnosis. Infect. Genet. Evol. 10, 444–452. https://doi.org/10.1016/j.meegid.2010.01.011

Nelde, A., Rammensee, H.G., Walz, J.S., 2021. The peptide vaccine of the future. Mol. Cell. Proteomics 20, 100022. https://doi.org/10.1074/MCP.R120.002309

Nicolao, M.C., Rodriguez Rodrigues, C., Cumino, A.C., 2019. Extracellular vesicles from *Echinococcus granulosus* larval stage: Isolation, characterization and uptake by dendritic cells. PLoS Negl. Trop. Dis. 13, 1–24. https://doi.org/10.1371/journal.pntd.0007032

Nielsen, M., Lund, O., 2009. NN-align. An artificial neural network-based alignment algorithm for MHC class II peptide binding prediction. BMC Bioinformatics 10, 296.

https://doi.org/10.1186/1471-2105-10-296

Pan, W., Chen, D.-S., Lu, Y.-J., Sun, F.-F., Xu, H.-W., Zhang, Y.-W., Yan, C., Fu, L.-L., Zheng, K.-Y., Tang, R.-X., 2017. Bioinformatic prediction of the epitopes of *Echinococcus granulosus* antigen 5. Biomed. Reports 6, 181–187. https://doi.org/10.3892/br.2016.827

Pan, W., Xu, H.W., Hao, W.T., Sun, F.F., Qin, Y.F., Hao, S.S., Liu, H., Cao, J.P., Shen, Y.J., Zheng, K.Y., 2018. The excretory-secretory products of *Echinococcus granulosus* protoscoleces stimulated IL-10 production in B cells via TLR-2 signaling. BMC Immunol. 19, 1–9. https://doi.org/10.1186/s12865-018-0267-7

Pereira, Í.M., Lima, S.B., Freitas, A. de A., Vinaud, M.C., Lino Junior, R. de S., 2016. Experimental subcutaneous cysticercosis by *Taenia crassiceps* in BALB/c and C57BL/6 mice. Rev. Inst. Med. Trop. Sao Paulo 58. https://doi.org/10.1590/S1678-9946201658055

Petersen, T.N., Brunak, S., Von Heijne, G., Nielsen, H., 2011. SignalP 4.0: Discriminating signal peptides from transmembrane regions. Nat. Methods 8, 785–786. https://doi.org/10.1038/nmeth.1701

Piccoli, L., Tamarozzi, F., Cattaneo, F., Mariconti, M., Filice, C., Bruno, A., Brunetti, E., 2014. Long-term Sonographic and Serological Follow-up of Inactive Echinococcal Cysts of the Liver: Hints for a "Watch-and-Wait" Approach. PLoS Negl. Trop. Dis. 8. https://doi.org/10.1371/journal.pntd.0003057

Pierleoni, A., Martelli, P., Casadio, R., 2008. PredGPI: A GPI-anchor predictor. BMC Bioinformatics 9, 1–11. https://doi.org/10.1186/1471-2105-9-392

Plancarte, A., Hirota, C., Martínez-Ocaña, J., Mendoza-Hernández, G., Zenteno, E., Flisser, A., 1999. Characterization of GP39-42 and GP24 antigens from *Taena solium* cysticerci and of their antigenic GP10 subunit. Parasitol. Res. 85, 680–684. https://doi.org/10.1007/s004360050615

Pollard, A.J., Bijker, E.M., 2021. A guide to vaccinology: from basic principles to new developments. Nat. Rev. Immunol. 21, 83–100. https://doi.org/10.1038/s41577-020-00479-7

Ponnaiya, B., Cornforth, M.N., Ullrich, R.L., 2006. Radiation-Induced Chromosomal Instability in BALB/c and C57BL/6 Mice: The Difference Is as Clear as Black and White. Radiat. Res. 147, 121. https://doi.org/10.2307/3579411

Pórfido, J.L., Herz, M., Kiss, F., Kamenetzky, L., Brehm, K., Rosenzvit, M.C., Córsico, B., Franchini, G.R., 2020. Fatty acid-binding proteins in *Echinococcus spp*.: the family has grown. Parasitol. Res. 119, 1401–1408. https://doi.org/10.1007/s00436-020-06631-5

Pourseif, M.M., Moghaddam, G., Saeedi, N., Barzegari, A., Dehghani, J., Omidi, Y., 2018.

Current status and future prospective of vaccine development against *Echinococcus granulosus*. Biologicals 51, 1–11. https://doi.org/10.1016/j.biologicals.2017.10.003

Probert, A.J., Sharma, R.K., Singh, K., Saxena, R., 1981. The effect of five fasciolicides on malate dehydrogenase activity and mortality of *Fasciola gigantica*, *Fasciolopsis buski* and P*aramphistomum explanatum*. J. Helminthol. 55, 115–122. https://doi.org/10.1017/s0022149x0002558x

Qiao, G., Li, Z., Minto, A.W., Shia, J., Yang, L., Bao, L., Tschopp, J., Gao, J., Wang, J., Quigg, R.J., Zhang, J., Cytokines, B., Corporation, I., 2010. Inhibitory Protein in T Cells Causes Lupus-like Syndrome in 17, 522–533. https://doi.org/10.1038/cdd.2009.143.Altered

Rappuoli, R., 2000. Reverse vaccinology. Curr. Opin. Microbiol. 3, 445–450. https://doi.org/10.1016/s1369-5274(00)00119-3

Rappuoli, R., 2001. Reverse vaccinology, a genome-based approach to vaccine development. Vaccine 19, 2688–2691. https://doi.org/10.1016/s0264-410x(00)00554-5

Richards, K.S., Arme, C., Bridges, J., 1983. *Echinococcus granulosus equinus*: An Ultrastructural Study of Murine Tissue Response to Hydatid Cysts. Parasitology 86, 407–417. https://doi.org/10.1017/S0031182000050605

Riganò, R., Buttari, B., Profumo, E., Ortona, E., Delunardo, F., Margutti, P., Mattei, V., Teggi, A., Sorice, M., Siracusano, A., 2007. *Echinococcus granulosus* antigen B impairs human dendritic cell differentiation and polarizes immature dendritic cell maturation towards a Th2 cell response. Infect. Immun. 75, 1667–1678. https://doi.org/10.1128/IAI.01156-06

Rinaldi, F., De Silvestri, A., Tamarozzi, F., Cattaneo, F., Lissandrin, R., Brunetti, E., 2014. Medical treatment versus "Watch and Wait" in the clinical management of CE3b echinococcal cysts of the liver. BMC Infect. Dis. 14, 1–7. https://doi.org/10.1186/1471-2334-14-492

Rojas-Caraballo, J., López-Abán, J., Pérez Del Villar, L., Vizcaíno, C., Vicente, B., Fernández-Soto, P., Del Olmo, E., Patarroyo, M.A., Muro, A., 2014. In vitro and in vivo studies for assessing the immune response and protection-inducing ability conferred by *Fasciola hepatica*-derived synthetic peptides containing B- and T-cell epitopes. PLoS One 9. https://doi.org/10.1371/journal.pone.0105323

Saha, S., Raghava, G.P.S., 2006. AlgPred: Prediction of allergenic proteins and mapping of IgE epitopes. Nucleic Acids Res. 34, 202–209. https://doi.org/10.1093/nar/gkl343

Salinas, G., Fernández, V., Fernández, C., Selkirk, M.E., 1998. *Echinococcus granulosus*:Cloning of a Thioredoxin Peroxidase. Exp. Parasitol. 90, 298–301. https://doi.org/https://doi.org/10.1006/expr.1998.4339

Sanchez-Moreno, M., Salas Peregrin, J.M., Leon, P., Garcia-Ruiz, M.A., Lemaur, M., Monteoliva, M., 1987. Malate dehydrogenase in helminth parasites. Inhibition by benzimidazoles and pyrimidine derivatives. Arzneimittel-Forschung/Drug Res. 37, 1327–1331.

Sanchez-Trincado, J.L., Gomez-Perosanz, M., Reche, P.A., 2017. Fundamentals and Methods for T- and B-Cell Epitope Prediction. J. Immunol. Res. 2017. https://doi.org/10.1155/2017/2680160

Santos, G.B. Dos, Monteiro, K.M., da Silva, E.D., Battistella, M.E., Ferreira, H.B., Zaha, A., 2016. Excretory/secretory products in the *Echinococcus granulosus* metacestode: is the intermediate host complacent with infection caused by the larval form of the parasite? Int. J. Parasitol. 46, 843–856. https://doi.org/10.1016/j.ijpara.2016.07.009

Sedaghat, B., Hajjaran, H., Sadjjadi, F.S., Heidari, S., Sadjjadi, S.M., 2021. Proteomic characterization of hydatid cyst fluid: two-dimensional electrophoresis (2-DE) setup through optimizing protein extraction. BMC Res. Notes 14, 22. https://doi.org/10.1186/s13104-020-05433-3

Shi, Z., Wang, Y., Li, Zongji, Li, Zhaoyu, Bo, Y., Ma, R., Zhao, W., 2009. Cloning, expression, and protective immunity in mice of a gene encoding the diagnostic antigen P-29 of *Echinococcus granulosus*. Acta Biochim. Biophys. Sin. (Shanghai). 41, 79–85. https://doi.org/10.1093/abbs/gmn009

Shibasaki, S., Aoki, W., Nomura, T., Karasaki, M., Sewaki, T., Ueda, M., 2014. Evaluation of Mdh1 protein as an antigenic candidate for a vaccine against candidiasis. Biocontrol Sci. 19, 51–55. https://doi.org/10.4265/bio.19.51

Siles-Lucas, M., Sánchez-Ovejero, C., González-Sánchez, M., González, E., Falcón-Pérez, J.M., Boufana, B., Fratini, F., Casulli, A., Manzano-Román, R., 2017. Isolation and characterization of exosomes derived from fertile sheep hydatid cysts. Vet. Parasitol. 236, 22–33. https://doi.org/10.1016/j.vetpar.2017.01.022

Sofron, A., Ritz, D., Neri, D., Fugmann, T., 2016. High-resolution analysis of the murine MHC class II immunopeptidome. Eur. J. Immunol. 46, 319–328. https://doi.org/10.1002/eji.201545930

Spiliotis, M., Brehm, K., 2004. *Echinococcus multilocularis*: Identification and molecular characterization of a Ral-like small GTP-binding protein. Exp. Parasitol. 107, 163–172. https://doi.org/10.1016/j.exppara.2004.05.006

Spiliotis, M., Tappe, D., Brückner, S., Mösch, H.-U., Brehm, K., 2005. Molecular cloning and characterization of Ras- and Raf-homologues from the fox-tapeworm *Echinococcus multilocularis*. Mol. Biochem. Parasitol. 139, 225–237. https://doi.org/10.1016/j.molbiopara.2004.11.013

Supek, F., Bošnjak, M., Škunca, N., Šmuc, T., 2011. Revigo summarizes and visualizes long lists of gene ontology terms. PLoS One 6. https://doi.org/10.1371/journal.pone.0021800

Thompson, R., Lymbery, A., 1995. Echinococcus and hydatid disease. Wallingford: CAB International.

Toledo, A., Larralde, C., Fragoso, G., Gevorkian, G., Manoutcharian, K., Hernández, M., Acero, G., Rosas, G., López-Casillas, F., Garfias, C.K., Vázquez, R., Terrazas, I., Sciutto, E., 1999. Towards a *Taenia solium* cysticercosis vaccine: An epitope shared by *Taenia crassiceps* and *Taenia solium* protects mice against experimental cysticercosis. Infect. Immun. 67, 2522–2530. https://doi.org/10.1128/iai.67.5.2522-2530.1999

Tsai, I.J., Zarowiecki, M., Holroyd, N., Garciarrubio, A., Sanchez-Flores, A., Brooks, K.L., Tracey, A., Bobes, R.J., Fragoso, G., Sciutto, E., Aslett, M., Beasley, H., Bennett, H.M., Cai, J., Camicia, F., Clark, R., Cucher, M., De Silva, N., Day, T.A., Deplazes, P., Estrada, K., Fernández, C., Holland, P.W.H., Hou, J., Hu, S., Huckvale, T., Hung, S.S., Kamenetzky, L., Keane, J.A., Kiss, F., Koziol, U., Lambert, O., Liu, K., Luo, X., Luo, Y., MacChiaroli, N., Nichol, S., Paps, J., Parkinson, J., Pouchkina-Stantcheva, N., Riddiford, N., Rosenzvit, M., Salinas, G., Wasmuth, J.D., Zamanian, M., Zheng, Y., Cai, X., Soberon, X., Olson, P.D., Laclette, J.P., Brehm, K., Berriman, M., Morett, E., Portillo, T., Jose, M. V., Carrero, J.C., Larralde, C., Morales-Montor, J., Limon-Lason, J., Cevallos, M.A., Gonzalez, V., Ochoa-Leyva, A., Landa, A., Jimenez, L., Valdes, V., 2013. The genomes of four tapeworm species reveal adaptations to parasitism. Nature 496, 57–63. https://doi.org/10.1038/nature12031

Valizadeh, M., Haghpanah, B., Badirzadeh, A., Roointan, E., Fallahi, S., Raeghi, S., 2017. Immunization of sheep against *Echinococcus granulosus* with protoscolex tegumental surface antigens. Vet. world 10, 854–858. https://doi.org/10.14202/vetworld.2017.854-858

Vessal, M., Bagher Tabei, S.M., 1996. Partial purification and kinetic properties of cytoplasmic malate dehydrogenase from ovine liver *Echinococcus granulosus* protoscolices. Comp. Biochem. Physiol. Part B Biochem. Mol. Biol. 113, 757–763. https://doi.org/https://doi.org/10.1016/0305-0491(95)02099-3

Virginio, V.G., Monteiro, K.M., Drumond, F., De Carvalho, M.O., Vargas, D.M., Zaha, A., Ferreira, H.B., 2012. Excretory/secretory products from in vitro-cultured *Echinococcus granulosus* protoscoleces. Mol. Biochem. Parasitol. 183, 15–22. https://doi.org/10.1016/j.molbiopara.2012.01.001

Voet, D., Voet, J., Pratt, C., 2016. Fundamentals of Biochemistry: Life at the Molecular Level 5th Editio.

Wadhwa, A., Aljabbari, A., Lokras, A., Foged, C., Thakur, A., 2020. Opportunities and

challenges in the delivery of mrna-based vaccines. Pharmaceutics 12. https://doi.org/10.3390/pharmaceutics12020102

Walsh, G., 2010. Post-translational modifications of protein biopharmaceuticals. Drug Discov. Today 15, 773–780. https://doi.org/10.1016/j.drudis.2010.06.009

Wang, B., Jiang, Y., Wang, Z., Li, F., Xing, G., Peng, X., Zhang, S., Lv, H., 2015. Arsenic trioxide negatively affects *Echinococcus granulosus*. Antimicrob. Agents Chemother. 59, 6946–6951. https://doi.org/10.1128/AAC.04340-14

Wang, S., Wei, W., Cai, X., 2015. Genome-wide analysis of excretory/secretory proteins in *Echinococcus multilocularis*: Insights into functional characteristics of the tapeworm secretome. Parasites and Vectors 8, 1–13. https://doi.org/10.1186/s13071-015-1282-7

Wang, Y., Xiao, D., Shen, Y., Han, X., Zhao, F., Li, X., Wu, W., Zhou, H., Zhang, J., Cao, J., 2015. Proteomic analysis of the excretory/secretory products and antigenic proteins of *Echinococcus granulosus* adult worms from infected dogs. BMC Vet. Res. 11, 1–7. https://doi.org/10.1186/s12917-015-0423-8

Wang, X., Zhao, Q., Dang, L., Sun, Y., Gao, J., Liu, B., Syed, S.F., Tao, H., Zhang, G., Luo, J., Zhou, E.-M., 2015. Characterization of Two Novel Linear B-Cell Epitopes in the Capsid Protein of Avian Hepatitis E Virus (HEV) That Are Common to Avian, Swine, and Human HEVs. J. Virol. 89, 5491–5501. https://doi.org/10.1128/jvi.00107-15

Wang, H., Li, Z., Gao, F., Zhao, J., Zhu, M., He, X., Niu, N., Zhao, W., 2016. Immunoprotection of recombinant Eg.P29 against *Echinococcus granulosus* in sheep. Vet. Res. Commun. 40, 73–79. https://doi.org/10.1007/s11259-016-9656-7

Wang, L., Gao, J., Lan, X., Zhao, H., Shang, X., Tian, F., Wen, H., Ding, J., Luo, L., Ma, X., 2019. Identification of combined T-cell and B-cell reactive *Echinococcus granulosus* 95 antigens for the potential development of a multi-epitope vaccine. Ann. Transl. Med. 7, 652–652. https://doi.org/10.21037/atm.2019.10.87

Wang, W., Zhou, X., Cui, F., Shi, C., Wang, Y., Men, Y., Zhao, W., Zhao, J., 2019. Proteomic Analysis on Exosomes Derived from Patients' Sera Infected with *Echinococcus granulosus*. Korean J. Parasitol. 57, 489–497. https://doi.org/10.3347/kjp.2019.57.5.489

Wilkins, M.R., Gasteiger, E., Gooley, A.A., Herbert, B.R., Molloy, M.P., Binz, P.A., Ou, K., Sanchez, J.C., Bairoch, A., Williams, K.L., Hochstrasser, D.F., 1999. High-throughput mass spectrometric discovery of protein post-translational modifications. J. Mol. Biol. 289, 645–657. https://doi.org/10.1006/jmbi.1999.2794

Wu, J., Cai, M., Yang, J., Li, Y., Ding, J., Kandil, O.M., Kutyrev, I., Ayaz, M., Zheng, Y., 2021. Comparative analysis of different extracellular vesicles secreted by *Echinococcus*

granulosus protoscoleces. Acta Trop. 213, 105756. https://doi.org/10.1016/j.actatropica.2020.105756

Wu, Zhenyu, Wang, Lingling, Li, J., Wang, Lifu, Wu, Zhongdao, Sun, X., 2019. Extracellular vesicle-mediated communication within host-parasite interactions. Front. Immunol. 10. https://doi.org/10.3389/fimmu.2018.03066

Xiang, J., Zhang, S., Leclercq, G., Nauwynck, H., 2016. Difference in replication of low-passage MCMV HaNa1 in BALB/c, C57BL/6 and NOD mice and role of different branches of immunity in susceptibility. Virus Res. 221, 38–46. https://doi.org/10.1016/j.virusres.2016.05.006

Xiao, S.H., Feng, J.J., Guo, H.F., Jiao, P.Y., Yao, M.Y., Jiao, W., 1994. Effects of mebendazole, albendazole, and praziquantel on fumarate hydratase, pyruvate kinase, and phosphoenolpyruvate carboxykinase of *Echinococcus granulosus* cyst wall harbored in mice. Zhongguo Yao Li Xue Bao 15 1, 69–72.

Xu, H., Diolintzi, A., Storch, J., 2019. Fatty acid-binding proteins: functional understanding and diagnostic implications. Curr. Opin. Clin. Nutr. Metab. Care 22, 407–412. https://doi.org/10.1097/MCO.0000000000000600

Zeghir-Bouteldja, R., Polomé, A., Bousbata, S., Touil-Boukoffa, C., 2017. Comparative proteome profiling of hydatid fluid from Algerian patients reveals cyst location-related variation in *Echinococcus granulosus*. Acta Trop. 171, 199–206. https://doi.org/10.1016/j.actatropica.2017.03.034

Zhang, W.Y., Moreau, E., Hope, J.C., Howard, C.J., Huang, W.Y., Chauvin, A., 2005. *Fasciola hepatica* and *Fasciola gigantica*: Comparison of cellular response to experimental infection in sheep. Exp. Parasitol. 111, 154–159. https://doi.org/10.1016/j.exppara.2005.06.005

Zhang, Y., Skolnick, J., 2005. TM-align: A protein structure alignment algorithm based on the TM-score. Nucleic Acids Res. 33, 2302–2309. https://doi.org/10.1093/nar/gki524

Zhang, X., Gong, W., Cao, S., Yin, J., Zhang, J., Cao, J., Shen, Y., 2020. Comprehensive Analysis of Non-coding RNA Profiles of Exosome-Like Vesicles From the Protoscoleces and Hydatid Cyst Fluid of *Echinococcus granulosus*. Front. Cell. Infect. Microbiol. 10, 1–14. https://doi.org/10.3389/fcimb.2020.00316

Zheng, H., Zhang, W., Zhang, L., Zhang, Z., Li, J., Lu, G., Zhu, Y., Wang, Y., Huang, Y., Liu, J., Kang, H., Chen, J., Wang, L., Chen, A., Yu, S., Gao, Z., Jin, L., Gu, W., Wang, Z., Zhao, L., Shi, B., Wen, H., Lin, R., Jones, M.K., Brejova, B., Vinar, T., Zhao, G., McManus, D.P., Chen, Z., Zhou, Y., Wang, S., 2013. The genome of the hydatid tapeworm *Echinococcus granulosus*. Nat. Genet. 45, 1168–1175. https://doi.org/10.1038/ng.2757

Zhou, X., Wang, W., Cui, F., Shi, C., Ma, Y., Yu, Y., Zhao, W., Zhao, J., 2019. Extracellular

vesicles derived from *Echinococcus granulosus* hydatid cyst fluid from patients: isolation, characterization and evaluation of immunomodulatory functions on T cells. Int. J. Parasitol. 49, 1029–1037. https://doi.org/10.1016/j.ijpara.2019.08.003

ARTÍCULO 1

Ultrastructural characterization of the tegument in protoscoleces of *Echinococcus ortleppi.*

Miles S, Cyrklaff M, Magnone J, García-Luna J, Ancarola ME, Cucher M, Dematteis S, Frischknecht F, Mourglia-Ettlin G.

International Journal for Parasitology

2021

doi:10.1016/j.ijpara.2021.05.004

International Journal for Parasitology 51 (2021) 989–997

Contents lists available at ScienceDirect

International Journal for Parasitology

journal homepage: www.elsevier.com/locate/ijpara

Ultrastructural characterization of the tegument in protoscoleces of *Echinococcus ortleppi*

Sebastián Miles [a,b], Javier Magnone [a], Joaquín García-Luna [a], María Eugenia Ancarola [c,d], Marcela Cucher [c,d], Sylvia Dematteis [a], Friedrich Frischknecht [b,e], Marek Cyrklaff [b,*,1], Gustavo Mourglia-Ettlin [a,*,1]

[a] *Área Inmunología, DEPBIO/IQB, Facultad de Química/Facultad de Ciencias, Universidad de la República, Montevideo, Uruguay*
[b] *Integrative Parasitology, Center for Infectious Diseases, Heidelberg University, Heidelberg, Germany*
[c] *Instituto de Investigaciones en Microbiología y Parasitología Médica (IMPaM, UBA-CONICET), Facultad de Medicina, Universidad de Buenos Aires, Buenos Aires, Argentina*
[d] *Departamento de Microbiología, Facultad de Medicina, Universidad de Buenos Aires, Buenos Aires, Argentina*
[e] *German Center for Infection Research (DZIF), partner site Heidelberg, Heidelberg, Germany*

ARTICLE INFO

Article history:
Received 9 March 2021
Received in revised form 13 May 2021
Accepted 17 May 2021
Available online 30 June 2021

Keywords:
Echinococcus granulosus
Echinococcus ortleppi
Protoscolex
Tegument
Vesicles
Electron microscopy
Electron tomography
Structural biology

ABSTRACT

Cystic echinococcosis is a globally distributed zoonosis caused by cestodes of the *Echinococcus granulosus sensu lato* (s.l.) complex, with *Echinococcus ortleppi* mainly involved in cattle infection. Protoscoleces show high developmental plasticity, being able to differentiate into either adult worms or metacestodes within definitive or intermediate hosts, respectively. Their outermost cellular layer is called the tegument, which is important in determining the infection outcome through its immunomodulating activities. Herein, we report an in-depth characterization of the tegument of *E. ortleppi* protoscoleces performed through a combination of scanning and transmission electron microscopy techniques. Using electron tomography, a three-dimensional reconstruction of the tegumental cellular territories was obtained, revealing a novel structure termed the 'tegumental vesicular body' (TVB). Vesicle-like structures, possibly involved in endocytic/exocytic routes, were found within the TVB as well as in the parasite glycocalyx, distal cytoplasm and close inner structures. Furthermore, parasite antigens (GST-1 and AgB) were unevenly localised within tegumental structures, with both being detected in vesicles found within the TBV. Finally, the presence of host (bovine) IgG was also assessed, suggesting a possible endocytic route in protoscoleces. Our data forms the basis for a better understanding of *E. ortleppi* and *E. granulosus* s.l. structural biology.

1. Introduction

Helminth infections constitute a significant proportion of neglected tropical diseases around the world. Among them, cystic echinococcosis – a zoonosis caused by cestodes from the *Echinococcus granulosus* sensu lato (s.l.) complex – has immense impacts on regional economies due to effects on livestock as well as human health (Budke et al., 2006). This parasite requires two mammalian hosts to complete its domestic life cycle, with canids (mainly dogs) being the definitive hosts harbouring the adult worm, and farm ungulates being the intermediate hosts for the metacestodes (also known as hydatids). Humans are accidental hosts for the metacestode, which develops as an ever-growing fluid-filled cyst located mainly in the host liver and lungs, bypassing and suppressing the immune response. Cysts can become fertile, producing protoscoleces by asexual reproduction, which are infective for the definitive hosts if ingested, or able to develop into new cysts if seeded within the intermediate host, i.e. after accidental cyst rupture (Heath, 1970).

The classification of *E. granulosus* has long been controversial. Considerable phenotypic, physiological and genetic variability between parasite isolates, which correlates with their intermediate hosts, has led to division of *E. granulosus* into "strains", which were further analysed by molecular techniques using the mtDNA sequences of genes for cytochrome c oxidase subunit 1 (*cox1*) and NADH dehydrogenase subunit 1 (*nad1*). In this way, *E. granulosus* s.l. was divided into nine main genotypes (G1-G8, G10) (Nakao et al., 2010) grouped into four species, *Echinococcus ortleppi* (G5) being a genotype that infects cattle as the main intermediate host but rarely affects humans.

* Corresponding authors at: Laboratorio de Inmunología, Departamento de Biociencias, Facultad de Química, Universidad de la República, Av. Alfredo Navarro 3051, C.P. 11600 Montevideo, Uruguay.
E-mail addresses: marek.cyrklaff@med.uni-heidelberg.de (M. Cyrklaff), gmourglia@higiene.edu.uy (G. Mourglia-Ettlin).
[1] Joint senior authors.

https://doi.org/10.1016/j.ijpara.2021.05.004
0020-7519/

The morphology of the protoscolex constitutes four different regions, namely (i) the rostellar region (containing the rostellar cone and hooks), (ii) the sucker region (where the suckers are found), (iii) the neck region, and (iv) the body region (Fig. 1A). The body and neck regions constitute the protoscolex soma, while the rostellar and sucker regions form the scolex. In invaginated protoscoleces, only the soma is visible (Fig. 1A). The outermost zone of the scolex and soma is known as the tegument, exhibiting differences between them (Galindo et al., 2008). A characteristic feature of cestodes is the absence of an alimentary canal, meaning that substances enter the tapeworm through the tegument, a dynamic tissue structure forming a multinucleated syncytium with no cell boundaries but connected to cellular bodies beneath the fibrous zone (Morseth, 1967). Since the tegument is the first parasite structure to interact with the host, a detailed understanding is important for the development of both anti-parasite drugs and vaccines. In this regard, the ultrastructure of the tegument in protoscoleces was studied in the second half of the 20th century (Morseth, 1967; Jha and Smyth, 1971), with little follow-up, focused mainly on their scolex (Galindo et al., 2008).

As in many other helminthiases, *E. granulosus* s.l. can inhabit immunocompetent hosts for prolonged periods, relying on intricate immunomodulating mechanisms orchestrated by the parasite. Such mechanisms involve the excretion/secretion of diverse compounds such as proteins, lipids, microRNAs and extracellular vesicles (EVs) among others (Wu et al., 2019). In particular, EVs found in hydatid fluid from fertile cysts or produced in vitro by protoscoleces were reported to induce tolerogenic profiles in immune cells and to modulate the overall host immune response (Pan et al., 2018; Nicolao et al., 2019; Zhou et al., 2019). In this regard, different '-omic' studies of EVs have shown a wide range of molecules which deserve further analysis (Siles-Lucas et al., 2017; Nicolao et al., 2019; Zhou et al., 2019; Zhang et al., 2020; Wu et al., 2021).

Here, we performed an ultrastructural characterization of the soma tegument in protoscoleces from *E. ortleppi* and explored its putative roles in parasite immunomodulation, nutrient absorption, and secretion of parasite antigens. To that end, protoscoleces were analysed by means of different electron microscopy techniques, and a three-dimensional (3D) reconstruction of the tegument

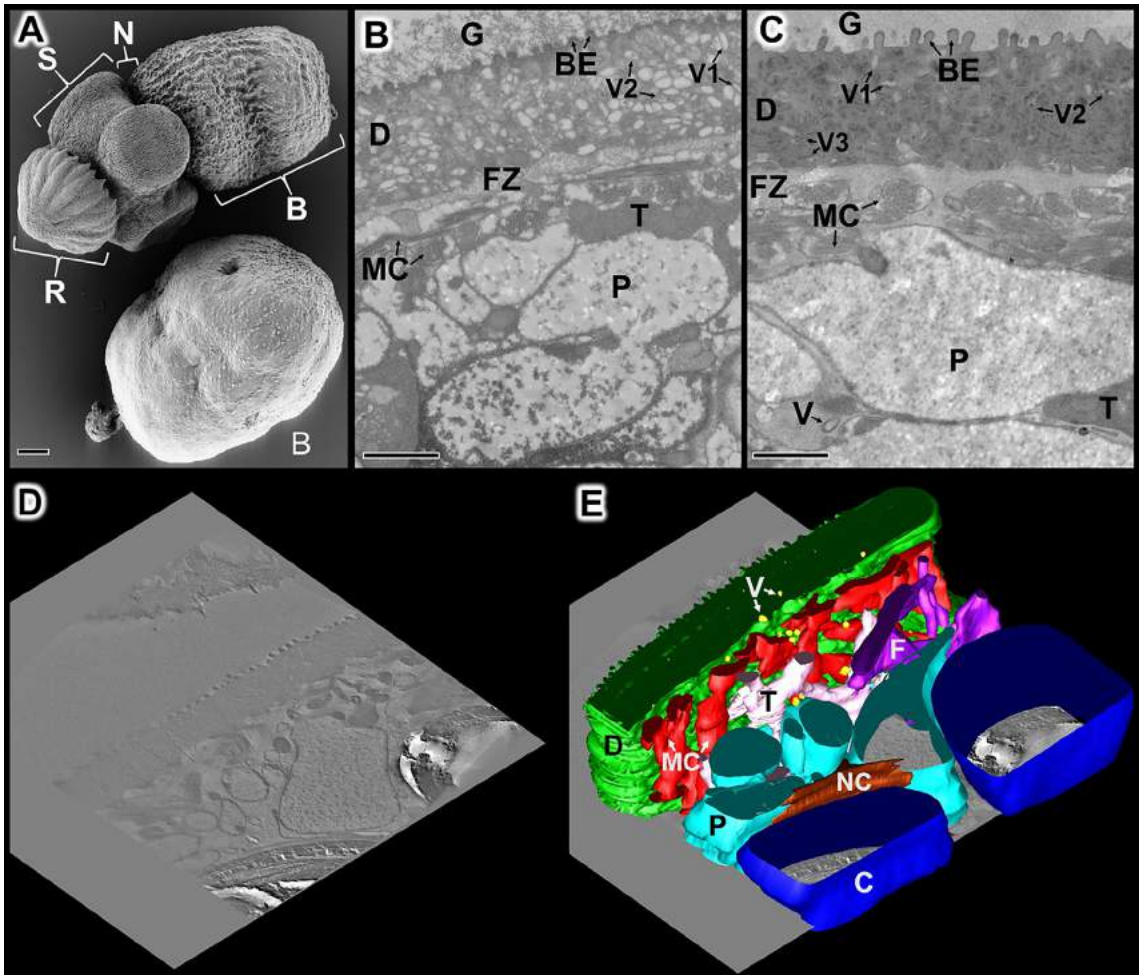

Fig. 1. Ultrastructural analysis of the soma tegument in *Echinococcus ortleppi* protoscoleces. Protoscoleces from fertile bovine hydatid cysts were obtained, washed and fixed with formaldehyde and glutaraldehyde. (A) The general protoscolex morphology was analysed by scanning electron microscopy, observing an evaginated (upper) and invaginated (bottom) protoscolex. (B, C) The soma tegument analysed by transmission electron microscopy in classical epoxy embedded (B) or in high-pressure freezing preserved protoscoleces (C). (D) Tomographic sections as obtained by cryo-electron tomography of high-pressure freezing preserved protoscoleces. (E) Three-dimensional reconstruction of soma tegumental structures as obtained from tomograms of six adjacent serial 500 nm-thick sections. R, rostellar region; S, sucker region; N, neck region; B, body region; G, glycocalyx; D, distal cytoplasm; FZ, fibrous zone; MC, muscle cell; P, parenchyma; T, tegumental cell; BE, blunt elevations; V1, V1-type vesicle; V2, V2-type vesicle; V3, V3-type vesicle; V, non-classical vesicle; F, flame cell; C, calcareous corpuscle; NC, nuclei and nuclear membrane of calcareous corpuscle. Scale bars: (A) = 10 μm; (B and C) = 500 nm.

was performed by electron tomography. Additionally, the presence of known parasite immunomodulating antigens, as well as host IgG, was studied through immuno-labelling strategies throughout the tegument and within vesicular structures. Finally, a tegumental vesicular body (TVB) was identified and characterised in 3D for the first known time.

2. Materials and methods

2.1. Parasites

Bovine hydatid cysts were obtained from Uruguayan abattoirs and maintained at 4 °C until processing (less than 36 h). Protoscoleces were rapidly collected by aseptic puncture and extensively washed with PBS, pH 7.2, containing antibiotics (60 μg/ml of penicillin, 100 μg/ml of streptomycin and 250 ng/ml of amphotericin B). Chemicals were always obtained from Sigma-Aldrich (USA) unless otherwise specified. Parasite viability was determined according to Dematteis et al. (1999) and protoscoleces with viability ≥ 90% were immediately fixed with 2.5% glutaraldehyde and 2% paraformaldehyde in PBS and stored at 4 °C until use. Aliquots of protoscoleces (without fixation) were used to determine the parasite genotype by sequencing a fragment of the gene coding for mitochondrial *cox1* as previously described (Cucher et al., 2011). Three parasite batches were obtained at different dates, belonging in all cases to *E. ortleppi* (G5 genotype).

2.2. Scanning electron microscopy (SEM)

Fixed protoscoleces were prepared for SEM following standard procedures described elsewhere (Kehrer et al., 2016) with minor modifications. Briefly, protoscoleces were allowed to adhere to 0.1% poly-L-lysine-coated class cover slips for 1 h and then were incubated for 1 h at room temperature (RT) in a solution containing 1% OsO_4 in 0.1 M cacodylate buffer. Protoscoleces were then washed, dehydrated in an ethanol series (from 15% to 100%), critical point dried in CO_2 and mounted on specimen stubs sputtered with a thin layer of gold. Analyses were performed using a Zeiss LEO 1530 scanning electron microscope (Carl Zeiss NTS Ltd., Germany).

2.3. Transmission electron microscopy (TEM)

All three batches of fixed protoscoleces were divided and embedded in resin for TEM by both classical TEM sample preparation and high-pressure freezing (HPF) as previously described in Miles et al. (2019, 2020)), respectively. Briefly, for classical sample preparation fixed protoscoleces were first transferred to cacodylate buffer (50 mM cacodylate, 50 mM KCl, 2.6 mM $CaCl_2$, 2.6 mM $MgCl_2$ and 2% sucrose) and then were incubated with 1% OsO_4 in 100 mM cacodylate buffer for 1 h at RT. After that, protoscoleces were washed and incubated overnight at 4 °C in 1% uranyl-acetate in water. Samples were then dehydrated in a graded acetone series (from 30% to 100%) at RT before being embedded in epoxy resin and polymerized for at least 48 h at 60 °C. For HPF sample preparation, fixed protoscoleces were subjected to HPF and dehydrated with acetone by freeze substitution for 24 h at slowly increasing temperatures (from −190 °C to 25 °C). Then, samples were embedded in spur resin and polymerized for at least 48 h at 60 °C. TEM analyses were performed with ultrathin sections (70 nm) obtained by sectioning using a Leica EM UC6 ultramicrotome (Leica Microsystems, Germany) with a diamond knife. Sections were collected on electron microscopy grids and examined with a Zeiss 10C transmission electron microscope (80 kV; Carl Zeiss NTS Ltd.). No counterstaining using lead citrate or uranyl-acetate was performed.

2.4. Electron tomography

For electron tomography, 500 nm-thick serial sections of HPF preserved protoscoleces were prepared. Slot electron microscopy grids were first coated with a 2.6 nm-thick carbon layer. After that, sections were collected on them and coated again with a 1.4 nm-thick carbon layer. Grids were then placed in a high-tilt holder and digital images were recorded as a single-axis tilt series over a +60° to −60° tilt range (with increments of 2°) on FEI Tecnai microscopes (FEI Company, USA): F20 on Heidelberg University campus (Germany) and F30 at EMBL, Heidelberg (Germany). Tomograms were reconstructed using etomo and IMOD software (Kremer et al., 1996) (http://bio3d.colorado.edu/imod).

2.5. Immuno-labelling

For immunoTEM analyses, 70 nm-thick sections of HPF preserved protoscoleces were obtained, blocked with PBS containing BSA 1.5% (w/v) and FSG 0.1% (w/v) for 30 min at RT, and treated with a solution of glycine 10% (w/v) in PBS for 1 h at RT. Then, grids were incubated with antibodies diluted in blocking buffer (1/10) for 2 h at RT. In-house mouse antibodies against parasite antigens were used, while *Bos taurus* IgG was detected using commercial reagents developed in rabbit (code from Sigma: B-7265). Antibodies raised against parasite GST-1 (Arbildi et al., 2017), and antigen B (AgB, 8/1 subunit) (González-Sapienza and Cachau, 2003) were kindly gifted by Dr. Verónica Fernández (Universidad de la República, Uruguay) and Dr. Andrés González-Techera (Universidad de la República, Uruguay), respectively. After five washes with blocking buffer, GST-1 and AgB samples were incubated with rabbit-anti-mouse antibodies for 1 h at RT followed by five washes with blocking buffer. Finally, all grids were incubated with goat-anti-rabbit antibodies labelled with 10 nm gold nanoparticles for 30 min at RT. Then, five washes with blocking buffer followed by five washes in PBS were performed. After that, grids were fixed in a solution of PBS containing glutaraldehyde 1% (v/v) for five min at RT, and finally washed 10 times with ultrapure H_2O. Analyses were performed using a Zeiss 10C transmission electron microscope (Carl Zeiss NTS Ltd.). No counterstaining using lead citrate or uranyl-acetate was performed.

3. Results

3.1. Ultrastructure of the tegument in protoscoleces

General protoscolex morphology was assessed by SEM, in both invaginated and evaginated protoscoleces (Fig. 1A). Evaginated protoscoleces consist of four regions: rostellar, sucker, neck and body regions (Fig. 1A, upper parasite). Rostellar and sucker regions form the parasite scolex containing the rostellar cone, hooks and suckers covered by microtriches, while the neck and body regions make up the parasite soma. In invaginated protoscoleces only the soma is observed, which is covered by a smooth layer of glycocalyx (Fig. 1A, lower parasite), known to shift to a corrugated surface still covered by glycocalyx after evagination (Fig. 1A, upper parasite).

The soma tegument was further analysed by TEM using two sample preparations corresponding to classical epoxy embedding (Fig. 1B) and HPF (Fig. 1C). Regardless of the sample preparation, previously reported cellular territories (Galindo et al., 2008) were observed: parenchyma, fibrous zone, distal cytoplasm and glycocalyx, as well as muscle and tegumental cells (Fig. 1B and C). Flame cells and their corresponding bundles of cilia were also detected

(data not shown). Blunt elevations were observed in the outer zone of the distal cytoplasm. Six distinct types of vesicles (V1-V6) have been reported to be present in the tegument of the soma and/or scolex (Bui et al., 1999). V1 vesicles (previously known as T3) are ovoid electron-lucent vesicles of unknown origin while V2 (previously known as T1) are electron-lucent comet-shaped vesicles with an electron-dense core. V3 vesicles are flattened discs or dumb-bell shaped with amorphous compact election-dense content. V4 and V5 (previously known as T2) vesicles are mostly present on the scolex tegument, exhibiting a round, double membrane with an electron-lucent and electron-dense core, respectively. Finally, V6 vesicles are similar to V1, but only observed in freeze substitution samples (Rogan and Richards, 1989; Bui et al., 1999). Only V1, V2 and V3 vesicles were observed within the soma tegument of *E. ortleppi* protoscoleces (Fig. 1B and C). Although no artifacts were detected by either sample preparation, further studies were performed with images obtained by HPF preparation due to its better performance in image sharpness.

3.2. 3D studies of tegumental structures

Tegumental structures were further characterised by means of electron tomography. To that end, tomographic tilt series were acquired from serial 500 nm-thick sections of HPF preserved protoscoleces (Fig. 1D, Supplementary Movie S1). 3D reconstructions were computed of six consecutive sections that were subsequently stitched into a 3D volume of 10 μm in X and Y directions and with a thickness of 3 μm (Fig. 1E). The reconstructions revealed calcareous corpuscles, nuclei of calcareous corpuscles, parenchyma, muscle cells, tegumental cells and distal cytoplasm (Fig. 1E). Since the fibrous zone is not a hard-limited zone and the glycocalyx is a low-density structure poorly detectable by electron tomography, their structural details could not be sufficiently revealed in reconstructions. Non-classical vesicles (i.e. not V1-V6 vesicles) were also observed within the distal cytoplasm as well as beneath the fibrous zone, in between cellular structures (Fig. 1E).

Additionally, a novel acellular electron-lucent structure located between the distal cytoplasm and the fibrous zone was observed (Fig. 2). We named this structure a 'tegumental vesicular body' (TVB) as it contained discrete vesicles ranging mostly from 75 to 250 nm in diameter (Fig. 2A, Supplementary Movie S2), although larger membrane-limited structures were also observed. The TVB was extensively found throughout the protoscolex body (Fig. 2B), even though different Z sections in the same protoscolex showed variations. 3D reconstructions showed the TVB as a single macroscopic structure (Fig. 2A), containing vesicles similar in size, morphology and electron-lucent properties to those non-classical vesicles previously observed within distal cytoplasm and beneath the fibrous zone (Fig. 1). The TVB was observed in every parasite batch by either classical epoxy-embedding (Fig. 2C) or HPF preservation (Fig. 2D). In addition, similar vesicles were also found by single section TEM analysis across the protoscolex tegument, suggesting the presence of exocytic/endocytic routes (Fig. 3).

3.3. Immuno-localization of host and parasite components

We next tested our hypothesis of exocytic/endocytic routes for vesicles across the protoscolex tegument by performing immuno-TEM analyses using antibodies against putatively absorbed (host) or secreted (parasite) components. Recent proteomic studies have

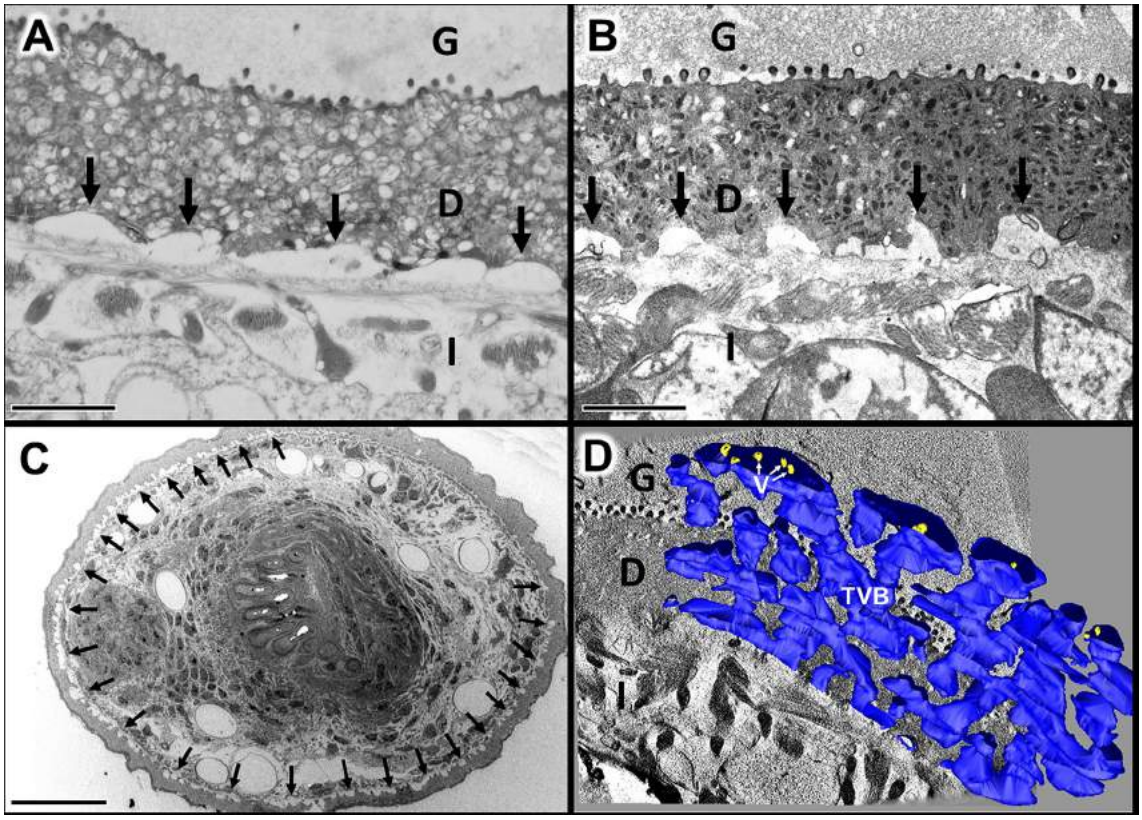

Fig. 2. Tegumental vesicular body in *Echinococcus ortleppi* protoscoleces. A novel protoscolex structure termed tegumental vesicular body (TVB) features a vesicle-containing body located between the distal cytoplasm and the fibrous zone. (A) TVB (arrows) observed by transmission electron microscopy in protoscoleces treated for classical epoxy embedding. (B) TVB (arrows) observed by transmission electron microscopy in high-pressure freezing preserved protoscoleces. (C) TVB extension (arrows) almost entirely covering the protoscolex body. (D) Three-dimensional reconstruction of a TVB, showing a content of vesicles with semi-spherical morphology. I, immediate interior; D, distal cytoplasm; G, glycocalyx; TVB, tegumental vesicular body; V, non-classical vesicles. Scale bars: (A and B) = 500 nm; (C) = 10 μm.

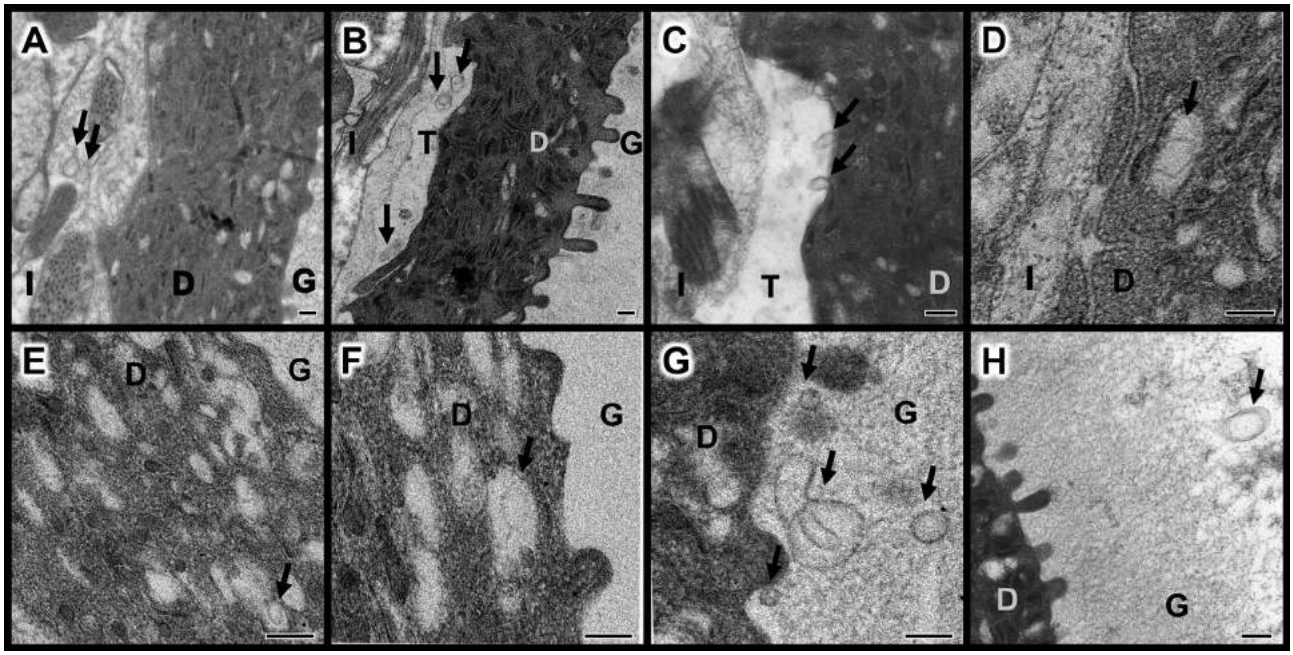

Fig. 3. Vesicles within the protoscolex tegument in *Echinococcus ortleppi*. Non-classical (not V1-V6) electron-lucent vesicles were found within the protoscolex tegument and in immediate interior structures. Identified vesicles are indicated by arrows: (A) beneath the fibrous zone, (B) within the tegumental vesicular body (TVB), (C) at the TVB-distal cytoplasm interface, (D) in the inner side of the distal cytoplasm, (E) in the middle of the distal cytoplasm, (F) in the outer side of the distal cytoplasm, (G) in the inner side of the glycocalyx, (H) in the outer side of the glycocalyx. Vesicles found within the distal cytoplasm (D, E and F) are contained within a larger electron-lucent vesicle-like structure. I, immediate interior; D, distal cytoplasm; G, glycocalyx; T, TVB. Scale bars = 200 nm.

shown the presence of *E. granulosus* s.l. GST-1 and AgB in excretion/secretion products, as well as associated with EVs (Virginio et al., 2012; Siles-Lucas et al., 2017; Nicolao et al., 2019; Zhou et al., 2019). Immuno-localization studies showed that both parasite antigens were present in the protoscolex tegument, exhibiting an even distribution but distinct representation among different tegumental structures (Fig. 4). To analyse this, in the images obtained from the parasite outermost soma, we allocated distinct areas corresponding to: (i) the glycocalyx, (ii) the distal cytoplasm, and (iii) all other parasite structures found beneath the fibrous zone, which were named as 'immediate interior'. An antigen abundance analysis was performed for each parasite component by calculating the mean density of electron-dense gold nanoparticles per μm^2 in 10 different images. Results in Fig. 4A show a high antigen abundance for GST-1 in the glycocalyx (22 ± 6 marks/μm^2), with lower values in the distal cytoplasm (3 ± 1 marks/μm^2) and immediate interior (2 ± 1 marks/μm^2). In contrast, AgB exhibited highest antigen abundance values in the distal cytoplasm (26 ± 7 marks/μm^2), followed by lower values in the glycocalyx (4 ± 2 marks/μm^2) and immediate interior (6 ± 3 marks/μm^2) (Fig. 4B). Additionally, both parasite antigens were observed associated with vesicles within the TVB (Fig. 4C and D).

Then, we used immunoTEM analyses of IgG from *B. taurus* as an example for an absorbed host molecule, observing an interesting pattern within the tegument of the soma (Fig. 5). Bovine IgG was present in every analysed protoscolex zone (glycocalyx, distal cytoplasm and immediate interior), mostly found as compact clusters of marks not associated to vesicles. Due to its non-homogeneous staining, its antigen abundance measure was not meaningful and therefore it was not determined. Additionally, no host IgG was observed in vesicles within the TVB (Fig. 5C). Interestingly, a high concentration of host IgG marks was found inside tegumental cells (Fig. 5A) and their cytoplasmic extensions (Fig. 5B) which connect to the distal cytoplasm, suggesting a possible endocytic route for host IgG.

4. Discussion

Since early studies in the 1960s and 1970s (Morseth, 1967; Jha and Smyth, 1971), all analyses regarding *E. granulosus* s.l. tegument have used classical electron microscopy techniques, although more complex methodologies have been applied to other helminths (Jabbar et al., 2010; Valverde-Islas et al., 2011; Manning and Richmond, 2015). In the present work, tegumental and inner structures in protoscoleces from *E. ortleppi* were studied, applying a combination of state-of-the-art microscopy techniques including SEM, TEM, immuno-labelling and electron tomography followed by 3D reconstruction. Such a combination has recently shed new light on the structure of pathogens, particularly on the structure–function relationship (Cyrklaff et al., 2017). Accordingly, a 3D reconstruction of the tegument cellular territories was obtained, and a novel structure, the TVB, was characterised. In addition, vesicle-like structures containing parasite antigens were found within both the TVB and the soma tegument. Finally, host IgG was detected forming concentrated cumulus throughout the soma tegument, suggesting its involvement in an active endocytic route.

The general morphology of protoscoleces observed by SEM (Fig. 1A) was in accordance with a previous report (Antoniou and Tselentis, 1993), showing differences in the soma region of evaginated (Fig. 1A, upper parasite) and invaginated (Fig. 1A, bottom parasite) parasites. The ultrastructure of the soma tegument was analysed by TEM imaging of 70 nm-thick sections, using two different embedding procedures: classical epoxy-embedding (Fig. 1B) and freeze substitution after HPF (Fig. 1C). In both cases, observed parasite structures were in accordance with a previous report (Galindo et al., 2008). Moreover, vesicle populations within the distal cytoplasm of the soma were also detected (Fig. 1B and C), corresponding only to V1, V2 and V3 vesicles (Rogan and Richards, 1989; Bui et al., 1999).

Following classical SEM and TEM analyses, 3D tomographic reconstructions of tegumental structures were obtained from the

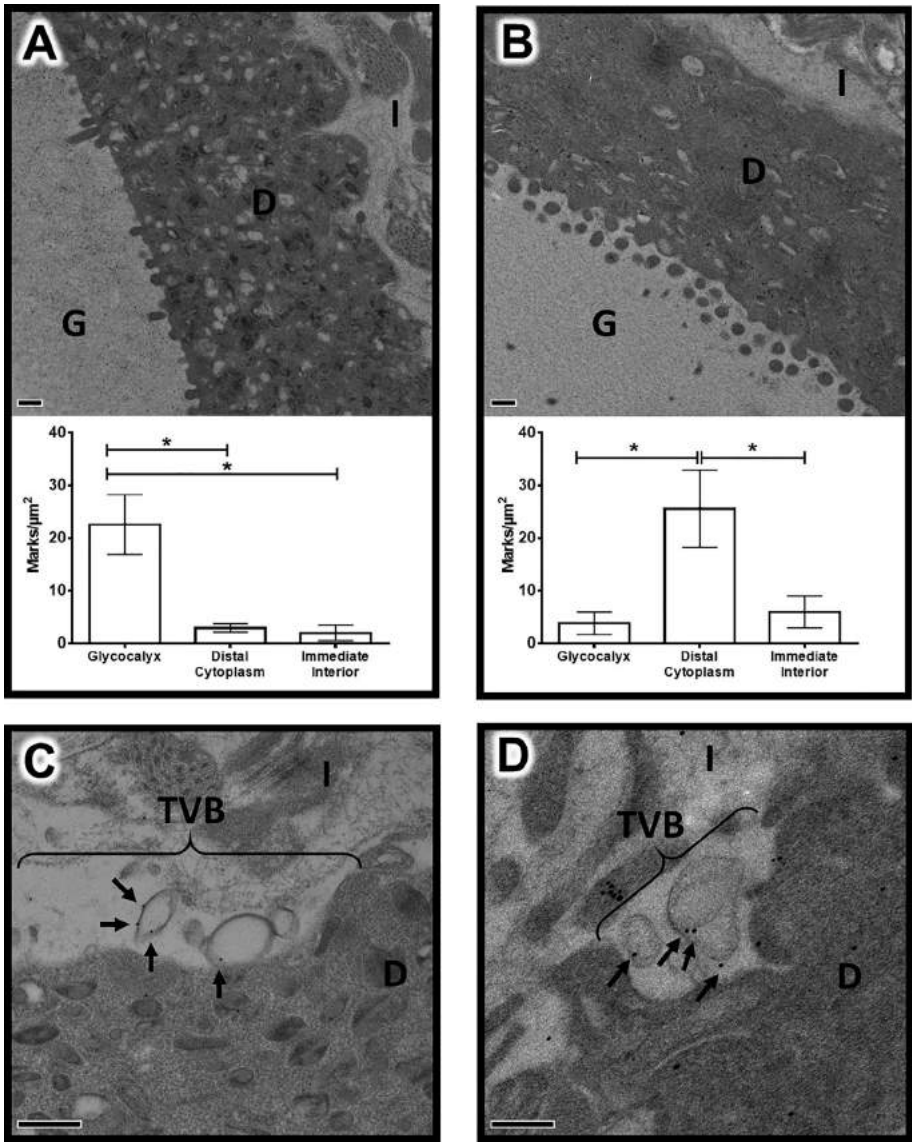

Fig. 4. Immunolocalization of *Echinococcus ortleppi* antigens. Parasitic antigens localised within the tegument by immuno-labelling with specific antibodies coupled to gold nanoparticles and analysed by transmission electron microscopy. Antigen abundance analyses were performed in 10 images for each antigen by calculating the marks density (marks per μm^2) in the glycocalyx, distal cytoplasm and immediate interior. (A, B) Representative image for GST-1 (A) and antigen B (AgB). (B) Immuno-labelling and its antigen abundance. Antigen abundance values are shown as mean ± S.D., and differences were regarded as significant (indicated by asterisks) when $P < 0.05$ (Student's *t*-test). Immunolocalization of parasite antigens (indicated by arrows) associated with vesicles (arrows) within the tegumental vesicular body was performed for GST-1 (C) and AgB (D). I, immediate interior; D, distal cytoplasm; G, glycocalyx; TVB, tegumental vesicular body. Scale bars = 200 nm.

serial 500 nm-thick sections of HPF preserved protoscoleces. That endowed us with a 3 μm-thick reconstructed volume of the tegument and close structures (Fig. 1E). Parasite structures were observed according to previous reports (Smith and Richards, 1993; Galindo et al., 2008), with muscle cells – responsible for parasite motility – forming an intricate mesh composed of longitudinal and circular muscle fibers (Coutelen et al., 1952) covering the entire protoscolex body. Among such structures, and within the distal cytoplasm, non-classical vesicles (i.e., non V1-V6) were present. These vesicles were semi-spherical and electron-lucent, and ranged from 75 to 250 nm in size (Fig. 1E).

A novel acellular electron-lucent structure containing vesicles (the TVB) was also observed between the distal cytoplasm and the fibrous zone (Fig. 2). This structure has already been observed in previous *E. granulosus* s.l. reports, but it has been completely disregarded or downplayed as vacuoles in parasite cultures (Hu et al., 2011; Wang et al., 2015), and detected with morphological changes in drug-treated protoscoleces (Lv et al., 2013; Xing et al., 2016). In the present work, the TVB was found in every batch of fresh *E. ortleppi* protoscoleces regardless of sample preparation treatment (Fig. 2C and D) and it was shown to partially cover the entire parasite soma (Fig. 2B). Moreover, the TVB was also found in fresh protoscoleces from *E. granulosus sensu stricto* (G1 genotype) (Supplementary Fig. S1). The 3D reconstruction of the TVB showed that independent structures observed in TEM images belonged to a single, large structure connected in different Z planes (Fig. 2A). In addition, vesicle-like structures found within the TVB were similar to those non-classical vesicles mentioned above, usually exhibiting a semi-spherical morphology with electron-lucent properties and ranging from 75 to 250 nm in size, although larger membrane-limited structures were also found.

The metacestode consists of a fluid-filled cyst composed of an inner germinative layer surrounded by an acellular laminated layer and an outer adventitial layer generated as a consequence of the

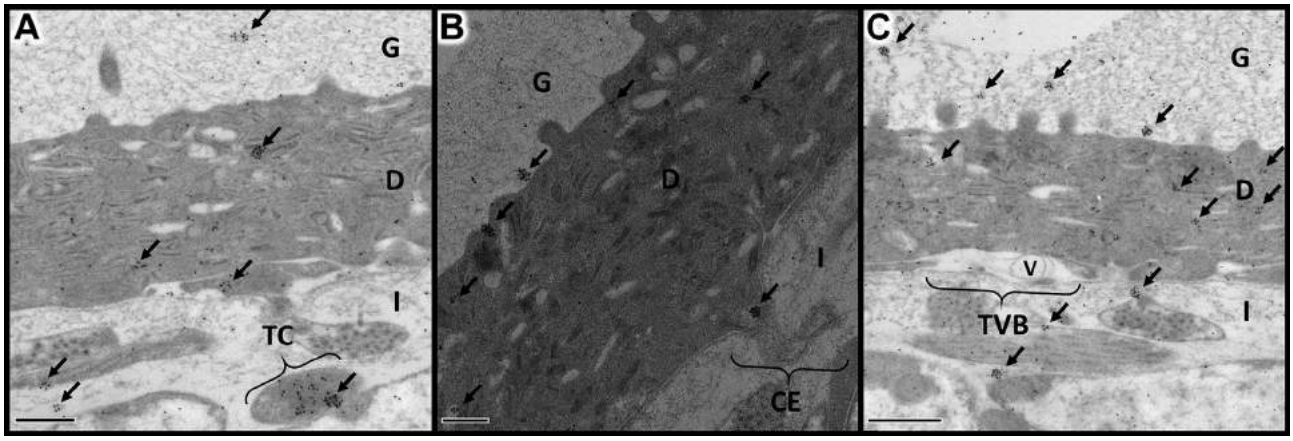

Fig. 5. Immunolocalization of host antigens. Immunolocalization of host IgG, which are abundant in the hydatid cyst fluid, as analysed by transmission electron microscopy in the protoscolex tegument using bovine IgG-specific antibodies coupled with gold nanoparticles. Clusters of marks (arrows) were found within the glycocalyx (G), distal cytoplasm (D) and immediate interior (I) of protoscoleces. The figure shows different images obtained from the same labelled section exhibiting interesting features. A high number of marks was found within tegumental cells (TC), and clusters of marks were found in their corresponding cytoplasmic extensions (CE). No marks were observed associated with vesicles (V) found within the tegumental vesicular body. Scale bars = 500 nm.

host inflammatory response. The germinative layer reproduces asexually into the cyst lumen, resulting in the formation of brood capsules containing protoscoleces. Both the germinative layer and protoscoleces excrete/secrete several parasite antigens found in the hydatid fluid (Díaz et al., 2011a, 2011b). Moreover, recent reports have shown the presence of EVs in hydatid fluid from fertile cysts (Siles-Lucas et al., 2017; Zhou et al., 2019; Zhang et al., 2020), as well as the ability – at least in vitro – of protoscoleces to produce EVs (Nicolao et al., 2019; Zhou et al., 2019; Zhang et al., 2020; Wu et al., 2021). The release of EVs in parasitic diseases acts both in parasite-parasite inter-communication as well as in parasite-host interaction, where EVs can intervene in host immune system regulation (Marcilla et al., 2014). However, the contribution of the germinative layer and protoscoleces to EVs found in fertile hydatid fluid is unclear. Since similarities in size and morphological characteristics were observed between reported *E. granulosus* s.l. EVs and the non-classical vesicles found within the tegument and TVB, we further analysed their potential exocytic/endocytic routes. TEM images and tomographic reconstructions suggested that these vesicles might be present in every step of exocytosis or endocytosis processes (Fig. 3). From an exocytic perspective, the observed vesicles could be formed by specialised cells or structures within inner parasite structures (Fig. 3A), and then loaded into the TVB (Fig. 3B) in order to enter the distal cytoplasm (Fig. 3C). Additionally, vesicles could directly enter the distal cytoplasm from inner parasite structures (Fig. 3D). Once loaded in the distal cytoplasm, vesicles could be transported outwards (Fig. 3E and F), reaching the glycocalyx (Fig. 3G) and finally being released into the hydatid fluid as EVs (Fig. 3H). The inverse process could result from endocytosis of EVs present in the hydatid fluid if putatively produced by the germinative layer or other protoscoleces (parasite-parasite interaction). From this perspective, protoscoleces would capture EVs through the glycocalyx, internalising and processing them within inner parasite structures. Interestingly, vesicles in the distal cytoplasm are contained within larger electron-lucent membrane-limited structures most likely involved in transportation processes (Fig. 3D–F).

Nutrient absorption and excretion/secretion of products are two of the most important functions of the tegument in cestodes. In *E. granulosus* s.l., excretion/secretion products and EVs produced by protoscoleces have already been shown to modulate the host immune response (Pan et al., 2018; Nicolao et al., 2019; Zhou et al., 2019), while nutrient absorption is key for parasite survival. Parasite antigens previously reported to be associated with *E. granulosus* s.l. EVs (Nicolao et al., 2019; Zhou et al., 2019), and host components present in the hydatid fluid (Aziz et al., 2011) were used to obtain further information regarding exocytic/endocytic routes of tegumental vesicles. Regarding parasite components, antigen abundance analysis for GST-1 showed it mostly within the glycocalyx (Fig. 4A). *Echinococcus granulosus* s.l. GST-1 is a well-studied enzyme involved in parasite protection against host-derived lipid peroxidation and passive detoxification of anthelmintic drugs (Arbildi et al., 2017). Thus, GST-1 abundance in the glycocalyx of protoscoleces might be in line with its parasite protection activities. Interestingly, immunoTEM analysis for AgB showed it as mostly present in the distal cytoplasm with a lower abundance in the glycocalyx and inner structures of protoscoleces (Fig. 4C). AgB is an oligomeric lipoprotein composed of 8 kDa related subunits (AgB8/1 to AgB8/5) encoded in a multigene family (Chemale et al., 2001). As the most abundant parasite protein in hydatid fluid, AgB has been involved in several host-parasite interactions promoting parasite establishment and survival within the intermediate host (Riganò et al., 2007; Monteiro et al., 2012). However, the contribution of protoscoleces and the germinative layer to its production is still unknown. Being only marginally present on the glycocalyx, protoscolex AgB – at least subunit 8/1 – might not contribute to a major degree to the parasite immunomodulating activities. However, since differences in protein expression profiles have been reported between distinct developmental stages in *E. granulosus* s.l. (Cui et al., 2013) – as well as in other relevant helminths (Sulima et al., 2018) – our hypothesis might only apply to the protoscolex stage.

Regarding host components, although the absorbing mechanisms of proteins across the hydatid cyst laminar and germinative layers are not clear, it has been proposed that *E. granulosus* s.l. would benefit from either nutrient uptake or immunomodulation by antigen disguise or inhibition of host immunity (Aziz et al., 2011). Among the host proteins found in hydatid fluid, IgG is highly abundant and its presence within the protoscolex tegument provides evidence for an endocytic process. ImmunoTEM results showed that host (*B. taurus*) IgG was present in the soma tegument, mostly as clusters of marks (Fig. 5) as opposed to the even distribution observed for parasite antigens (Fig. 4). Interestingly, a higher presence of IgG cumulus was observed in tegumental cells (Fig. 5A) and their cytoplasmic extensions (Fig. 5B), strongly suggesting that protoscoleces are able to internalise host IgG present

in the hydatid fluid. Uptake might proceed through an endocytic process that concentrates and transports host IgG in a vesicle-independent way since no cumulus were found associated with vesicles. Further evidence is needed to support this hypothesis.

Finally, and since parasite excretion/secretion products as well as host proteins were observed in the tegument of protoscoleces, we further analysed whether such components were present in the vesicles found within the TVB. Similar approaches have been previously applied to analyse protein cargo in EVs from other helminth parasites (Marcilla et al., 2012). ImmunoTEM results over vesicles within the TVB showed specific and abundant marks for both parasite antigens (Fig. 4C and D), but not for host IgG (Fig. 5C), suggesting that the TVB and its corresponding vesicles might be involved in exocytic processes. However, neither parasitic nor host antigens were observed associated with vesicles (those different from V1, V2 or V3) found within the distal cytoplasm and the glycocalyx.

In conclusion, the soma tegument of protoscoleces from *E. ortleppi* is a complex parasite structure involved in motility, nutrient absorption, secretion of parasite antigens and EVs, immunomodulation and parasite protection. Different structures and cellular territories with varied functions were characterised here for the first time by 3D reconstructions and immuno-localization of specific components. Importantly, evidence for EVs trafficking through the soma tegument of protoscoleces was obtained, and a novel single macro structure containing vesicles with immunomodulating parasite cargo was described. Further research will be required to assess the function of this structure. Additionally, evidence for an endocytic tegumental route for host components was also obtained.

Acknowledgements

The authors are grateful to the Electron Microscopy Core Facility at Heidelberg University, as well as the Electron Microscopy Facility at EMBL, Heidelberg (Germany), for the introduction and use of their microscopes. Verónica Fernández (Universidad de la República, Uruguay) and Andrés González-Techera (Universidad de la República, Uruguay) are acknowledged for their kind gift of antibodies raised against parasite antigens, while Uriel Koziol (Universidad de la República, Uruguay) is acknowledged for his valuable advice in image interpretation and general review of the manuscript. SM received a travel grant from Boehringen Ingelheim Fonds, Germany. CSIC from Universidad de la República (Uruguay), PEDECIBA-Química (Uruguay), ANII (Uruguay) and the Pérez-Guerrero Trust Fund for South-South Cooperation (PGTF) (to MC) are acknowledged for their general financial support. FF is member of the collaborative research consortium SFB 1129 of the German Research Foundation (DFG).

Appendix A. Supplementary data

Supplementary data to this article can be found online at https://doi.org/10.1016/j.ijpara.2021.05.004.

References

Antoniou, M., Tselentis, Y., 1993. Studies on *Echinococcus granulosus* using the scanning electron microscope - I. Preparations of the parasite for infection of the final host. Parasitol. Res. 79, 537–542. https://doi.org/10.1007/BF00932236.

Arbildi, P., Turell, L., López, V., Alvarez, B., Fernández, V., 2017. Mechanistic insights into EgGST1, a Mu class glutathione S-transferase from the cestode parasite *Echinococcus granulosus*. Arch. Biochem. Biophys. 633, 15–22. https://doi.org/10.1016/j.abb.2017.08.014.

Aziz, A., Zhang, W., Li, J., Loukas, A., McManus, D.P., Mulvenna, J., 2011. Proteomic characterisation of *Echinococcus granulosus* hydatid cyst fluid from sheep, cattle and humans. J. Proteomics 74, 1560–1572. https://doi.org/10.1016/j.jprot.2011.02.021.

Budke, C.M., Deplazes, P., Torgerson, P.R., 2006. Global socioeconomic impact of cystic echinococcosis. Emerg. Infect. Dis. 12, 296–303. https://doi.org/10.3201/eid1202.050499.

Bui, L.T., Stenzel, D.J., Jones, M.K., 1999. Reappraisal of vesicular types in the syncytial tegument of the *Echinococcus granulosus* protoscolex. Parasitol. Res. 85, 35–40. https://doi.org/10.1007/s004360050504.

Chemale, G., Haag, K.L., Ferreira, H.B., Zaha, A., 2001. *Echinococcus granulosus* antigen B is encoded by a gene family. Mol. Biochem. Parasitol. 116, 233–237. https://doi.org/10.1016/S0166-6851(01)00316-4.

Coutelen, F., Biquet, J., Doby, J.-M., Deblock, S.t., 1952. Le système musculaire du scolex echinococcique-Mécanismes de dévagination et d'invagination du rostre et des ventouses. Ann. Parasitol. Hum. Comparée 27, 86–94.

Cucher, M., Prada, L., Mourglia-Ettlin, G., Dematteis, S., Camicia, F., Asurmendi, S., Rosenzvit, M., 2011. Identification of *Echinococcus granulosus* microRNAs and their expression in different life cycle stages and parasite genotypes. Int. J. Parasitol. 41, 439–448. https://doi.org/10.1016/j.ijpara.2010.11.010.

Cui, S.J., Xu, L.L., Zhang, T., Xu, M., Yao, J., Fang, C.Y., Feng, Z., Yang, P.Y., Hu, W., Liu, F., 2013. Proteomic characterization of larval and adult developmental stages in *Echinococcus granulosus* reveals novel insight into host-parasite interactions. J. Proteomics 84, 158–175. https://doi.org/10.1016/j.jprot.2013.04.013.

Cyrklaff, M., Frischknecht, F., Kudryashev, M., 2017. Functional insights into pathogen biology from 3D electron microscopy. FEMS Microbiol. Rev. 41, 828–853. https://doi.org/10.1093/femsre/fux041.

Dematteis, S., Baz, A., Rottenberg, M., Fernandez, C., Örn, A., Nieto, A., 1999. Antibody and Th1/Th2-type responses in BALB/c mice inoculated with live or dead *Echinococcus granulosus* protoscoleces. Parasite Immunol. 21, 19–26. https://doi.org/10.1046/j.1365-3024.1999.00198.x.

Díaz, A., Casaravilla, C., Irigoín, F., Lin, G., Previato, J.O., Ferreira, F., 2011a. Understanding the laminated layer of larval *Echinococcus* I: Structure. Trends Parasitol. 27, 204–213. https://doi.org/10.1016/j.pt.2010.12.012.

Díaz, A., Casaravilla, C., Allen, J.E., Sim, R.B., Ferreira, A.M., 2011b. Understanding the laminated layer of larval *Echinococcus* II: Immunology. Trends Parasitol. 27, 264–273. https://doi.org/10.1016/j.pt.2011.01.008.

Galindo, M., Schadebrodt, G., Galanti, N., 2008. *Echinococcus granulosus*: cellular territories and morphological regions in mature protoscoleces. Exp. Parasitol. 119, 524–533. https://doi.org/10.1016/j.exppara.2008.04.013.

González-Sapienza, G., Cachau, R.E., 2003. Identification of critical residues of an immunodominant region of *Echinococcus granulosus* antigen B. J. Biol. Chem. 278, 20179–20184. https://doi.org/10.1074/jbc.M212724200.

Heath, D.D., 1970. The development of *Echinococcus granulosus* larvae in laboratory animals. Parasitology 60, 449–456. https://doi.org/10.1017/S0031182000078252.

Hu, H., Kang, J., Chen, R., Mamuti, W., Wu, G., Yuan, W., 2011. Drug-induced apoptosis of *Echinococcus granulosus* protoscoleces. Parasitol. Res. 109, 453–459. https://doi.org/10.1007/s00436-011-2276-9.

Jabbar, A., Swiderski, Z., Mlocicki, D., Beveridge, I., Lightowlers, M.W., 2010. The ultrastructure of taeniid cestode oncospheres and localization of host-protective antigens. Parasitology 137, 521–535. https://doi.org/10.1017/S0031182009991260.

Jha, R.K., Smyth, J.D., 1971. Ultrastructure of the rostellar tegument of *Echinococcus granulosus* with special reference to biogenesis of mitochondria. Int. J. Parasitol. 1. https://doi.org/10.1016/0020-7519(71)90012-9.

Kehrer, J., Singer, M., Lemgruber, L., Silva, P.A.G.C., Frischknecht, F., Mair, G.R., Billker, O., 2016. A putative small solute transporter is responsible for the secretion of G377 and TRAP-Containing secretory vesicles during plasmodium gamete egress and sporozoite motility. PLoS Pathog. 12, e1005734. https://doi.org/10.1371/journal.ppat.1005734.

Kremer, J.R., Mastronarde, D.N., McIntosh, J.R., 1996. Computer visualization of three-dimensional image data using IMOD. J. Struct. Biol. 116, 71–76.

Lv, H., Li, S., Zhang, J., Liang, W., Mu, X., Jiang, Y., 2013. In vitro effects of SB202190 on *Echinococcus granulosus*. Korean J. Parasitol. 51, 255–258. https://doi.org/10.3347/kjp.2013.51.2.255.

Manning, L., Richmond, J., 2015. High-pressure freeze and freeze substitution electron microscopy in *C. elegans*. Methods Mol. Biol., 121–140 https://doi.org/10.1007/978-1-4939-2842-2_10.

Marcilla, A., Martin-Jaular, L., Trelis, M., de Menezes-Neto, A., Osuna, A., Bernal, D., Fernandez-Becerra, C., Almeida, I.C., del Portillo, H.A., 2014. Extracellular vesicles in parasitic diseases. J. Extracell. Vesicles 3, 25040. https://doi.org/10.3402/jev.v3.25040.

Marcilla, A., Trelis, M., Cortés, A., Sotillo, J., Cantalapiedra, F., Minguez, M.T., Valero, M.L., Sánchez del Pino, M.M., Muñoz-Antoli, C., Toledo, R., Bernal, D., Langsley, G., 2012. Extracellular vesicles from parasitic helminths contain specific excretory/secretory proteins and are internalized in intestinal host cells. PLoS One 7, e45974. https://doi.org/10.1371/journal.pone.0045974.

Miles, S., Magnone, J., Cyrklaff, M., Arbildi, P., Frischknecht, F., Dematteis, S., Mourglia-Ettlin, G., 2020. Linking murine resistance to secondary cystic echinococcosis with antibody responses targeting *Echinococcus granulosus* tegumental antigens. Immunobiology 225, 151916. https://doi.org/10.1016/j.imbio.2020.151916.

Miles, S., Portela, M., Cyrklaff, M., Ancarola, M.E., Frischknecht, F., Durán, R., Dematteis, S., Mourglia-Ettlin, G., 2019. Combining proteomics and bioinformatics to explore novel tegumental antigens as vaccine candidates against *Echinococcus granulosus* infection. J. Cell. Biochem. 120, 15320–15336. https://doi.org/10.1002/jcb.v120.910.1002/jcb.28799.

Monteiro, K.M., Cardoso, M.B., Follmer, C., da Silveira, N.P., Vargas, D.M., Kitajima, E. W., Zaha, A., Ferreira, H.B., Ito, A., 2012. *Echinococcus granulosus* Antigen B

structure: subunit composition and oligomeric states. PLoS Negl. Trop. Dis. 6, e1551. https://doi.org/10.1371/journal.pntd.0001551.

Morseth, D.J., 1967. Fine structure of the hydatid cyst and protoscolex of *Echinococcus granulosus*. J. Parasitol. 53, 312–325. https://doi.org/10.2307/3276582.

Nakao, M., Yanagida, T., Okamoto, M., Knapp, J., Nkouawa, A., Sako, Y., Ito, A., 2010. State-of-the-art *Echinococcus* and *Taenia*: phylogenetic taxonomy of human-pathogenic tapeworms and its application to molecular diagnosis. Infect. Genet. Evol. 10, 444–452. https://doi.org/10.1016/j.meegid.2010.01.011.

Nicolao, M.C., Rodriguez Rodrigues, C., Cumino, A.C., Siles-Lucas, M., 2019. Extracellular vesicles from *Echinococcus granulosus* larval stage: Isolation, characterization and uptake by dendritic cells. PLoS Negl. Trop. Dis. 13, e0007032. https://doi.org/10.1371/journal.pntd.0007032.

Pan, W., Xu, H.W., Hao, W.T., Sun, F.F., Qin, Y.F., Hao, S.S., Liu, H., Cao, J.P., Shen, Y.J., Zheng, K.Y., 2018. The excretory-secretory products of *Echinococcus granulosus* protoscoleces stimulated IL-10 production in B cells via TLR-2 signaling. BMC Immunol. 19, 1–9. https://doi.org/10.1186/s12865-018-0267-7.

Riganò, R., Buttari, B., Profumo, E., Ortona, E., Delunardo, F., Margutti, P., Mattei, V., Teggi, A., Sorice, M., Siracusano, A., 2007. *Echinococcus granulosus* antigen B impairs human dendritic cell differentiation and polarizes immature dendritic cell maturation towards a Th2 cell response. Infect. Immun. 75, 1667–1678. https://doi.org/10.1128/IAI.01156-06.

Rogan, M.T., Richards, K.S., 1989. Development of the tegument of *Echinococcus granulosus* (Cestoda) protoscoleces during cystic differentiation in vivo. Parasitol. Res. 75, 299–306. https://doi.org/10.1007/BF00931814.

Siles-Lucas, M., Sánchez-Ovejero, C., González-Sánchez, M., González, E., Falcón-Pérez, J.M., Boufana, B., Fratini, F., Casulli, A., Manzano-Román, R., 2017. Isolation and characterization of exosomes derived from fertile sheep hydatid cysts. Vet. Parasitol. 236, 22–33. https://doi.org/10.1016/j.vetpar.2017.01.022.

Smith, S.A., Richards, K.S., 1993. Ultrastructure and microanalyses of the calcareous corpuscles of the protoscoleces of *Echinococcus granulosus*. Parasitol. Res. 79, 245–250. https://doi.org/10.1007/BF00931900.

Sulima, A., Savijoki, K., Bien, J., Näreaho, A., Salamatin, R., Conn, D.B., Mlocicki, D., 2018. Comparative proteomic analysis of *Hymenolepis diminuta* cysticercoid and adult stages. Front. Microbiol. 8, 1–14. https://doi.org/10.3389/fmicb.2017.02672.

Valverde-Islas, L.E., Arrangoiz, E., Vega, E., Robert, L., Villanueva, R., Reynoso-Ducoing, O., Willms, K., Zepeda-Rodríguez, A., Fortoul, T.I., Ambrosio, J.R., Diemert, D.J., 2011. Visualization and 3d reconstruction of flame cells of *Taenia solium* (Cestoda). PLoS One 6, e14754. https://doi.org/10.1371/journal.pone.0014754.

Virginio, V.G., Monteiro, K.M., Drumond, F., de Carvalho, M.O., Vargas, D.M., Zaha, A., Ferreira, H.B., 2012. Excretory/secretory products from in vitro-cultured *Echinococcus granulosus* protoscoleces. Mol. Biochem. Parasitol. 183, 15–22. https://doi.org/10.1016/j.molbiopara.2012.01.001.

Wang, B.o., Jiang, Y., Wang, Z., Li, F., Xing, G., Peng, X., Zhang, S., Lv, H., 2015. Arsenic trioxide negatively affects *Echinococcus granulosus*. Antimicrob. Agents Chemother. 59, 6946–6951. https://doi.org/10.1128/AAC.04340-14.

Wu, J., Cai, M., Yang, J., Li, Y., Ding, J., Kandil, O.M., Kutyrev, I., Ayaz, M., Zheng, Y., 2021. Comparative analysis of different extracellular vesicles secreted by *Echinococcus granulosus* protoscoleces. Acta Trop. 213, 105756. https://doi.org/10.1016/j.actatropica.2020.105756.

Wu, Z., Wang, L., Li, J., Wang, L., Wu, Z., Sun, X., 2019. Extracellular vesicle-mediated communication within host-parasite interactions. Front. Immunol. 9, 3066. https://doi.org/10.3389/fimmu.2018.03066.

Xing, G., Wang, B., Lei, Y., Liu, C., Wang, Z., Shi, H., Yang, R., Qin, W., Jiang, Y., Lv, H., 2016. In vitro effect of sodium arsenite on *Echinococcus granulosus* protoscoleces. Mol. Biochem. Parasitol. 207, 49–55. https://doi.org/10.1016/j.molbiopara.2016.05.011.

Zhang, X., Gong, W., Cao, S., Yin, J., Zhang, J., Cao, J., Shen, Y., 2020. Comprehensive analysis of non-coding RNA profiles of exosome-like vesicles from the protoscoleces and hydatid cyst fluid of *Echinococcus granulosus*. Front. Cell. Infect. Microbiol. 10. https://doi.org/10.3389/fcimb.2020.00316.

Zhou, X., Wang, W., Cui, F., Shi, C., Ma, Y., Yu, Y., Zhao, W., Zhao, J., 2019. Extracellular vesicles derived from *Echinococcus granulosus* hydatid cyst fluid from patients: isolation, characterization and evaluation of immunomodulatory functions on T cells. Int. J. Parasitol. 49, 1029–1037. https://doi.org/10.1016/j.ijpara.2019.08.003.

ARTÍCULO 2

Combining proteomics and bioinformatics to explore novel tegumental antigens as vaccine candidates against *Echinococcus granulosus* infection.

Miles S, Portela M, Cyrklaff M, Ancarola ME, Frischknecht F, Durán R, Dematteis S, Mourglia-Ettlin G.

Journal of cellular biochemistry

2019

doi: 10.1002/jcb.28799

Received: 13 December 2018 | Revised: 30 January 2019 | Accepted: 4 February 2019

DOI: 10.1002/jcb.28799

RESEARCH ARTICLE

WILEY Journal of Cellular Biochemistry

Combining proteomics and bioinformatics to explore novel tegumental antigens as vaccine candidates against *Echinococcus granulosus* infection

Sebastián Miles[1] | Madelón Portela[2] | Marek Cyrklaff[3] | María Eugenia Ancarola[4] | Friedrich Frischknecht[3] | Rosario Durán[2] | Sylvia Dematteis[1] | Gustavo Mourglia-Ettlin[1]

[1]Área Inmunología, DEPBIO/IQB, Facultad de Química/Facultad de Ciencias, Universidad de la República, Montevideo, Uruguay

[2]Unidad de Bioquímica y Proteómica Analíticas, Institut Pasteur de Montevideo and IIBCE, Montevideo, Uruguay

[3]Integrative Parasitology, Center for Infectious Diseases, Heidelberg University, Heidelberg, Germany

[4]Instituto de Investigaciones en Microbiología y Parasitología Médica (IMPaM, UBA-CONICET), Facultad de Medicina, Universidad de Buenos Aires, Buenos Aires, Argentina

Correspondence
Gustavo Mourglia-Ettlin, PhD, Área Inmunología, DEPBIO/IQB, Facultad de Química/Facultad de Ciencias, Universidad de la República, Montevideo 11600, Uruguay.
Email: gmourglia@higiene.edu.uy

Abstract

Echinococcus granulosus is the parasite responsible for cystic echinococcosis (CE), an important worldwide-distributed zoonosis. New effective vaccines against CE could potentially have great economic and health benefits. Here, we describe an innovative vaccine design scheme starting from an antigenic fraction enriched in tegumental antigens from the protoscolex stage (termed PSEx) already known to induce protection against CE. We first used mass spectrometry to characterize the protein composition of PSEx followed by Gene Ontology analysis to study the potential Biological Processes, Molecular Functions, and Cellular Localizations of the identified proteins. Following, antigenicity predictions and determination of conservancy degree against other organisms were determined. Thus, nine novel proteins were identified as potential vaccine candidates. Furthermore, linear B cell epitopes free of posttranslational modifications were predicted in the whole PSEx proteome through colocalization of in silico predicted epitopes within peptide fragments identified by matrix-assisted laser desorption/ionization-TOF/TOF. Resulting peptides were termed "clean linear B cell epitopes," and through BLASTp scanning against all nonhelminth proteins, those with 100% identity against any other protein were discarded. Then, the secondary structure was predicted for peptides and their corresponding proteins. Peptides with highly similar secondary structure respect to their parental protein were selected, and those potentially toxic and/or allergenic were discarded. Finally, the selected clean linear B cell epitopes were mapped within their corresponding 3D-modeled protein to analyze their possible antibody accessibilities, resulting in 14 putative peptide vaccine candidates. We propose nine novel proteins and 14 peptides to be further tested as vaccine candidates against CE.

KEYWORDS

Echinococcus granulosus, immunoinformatics, linear B cell epitopes, MALDI-TOF/TOF, tegument, vaccine

1 | INTRODUCTION

Cystic echinococcosis (CE) is an important zoonotic disease, currently listed as a Neglected Tropical Disease by the World Health Organisation (WHO). *Echinococcus granulosus*—the parasite responsible for CE—is a cestode that requires two mammalian hosts for completing its life cycle: canids (mainly dogs) act as definitive hosts, whereas farm or wild ungulates are usually the intermediate hosts. Humans are considered accidental intermediate hosts, and the WHO estimates that more than 1 million people worldwide are infected at any one time.[1] Intermediate hosts become infected by ingesting infective eggs containing oncospheres, which migrate to various visceral organs, such as liver and lungs, and develop into the metacestode stage (hydatid cyst). When hydatid cysts are fertile, they asexually produce protoscoleces (PSC) turning into the infective stage for definitive hosts.[2] Interestingly, if a fertile cyst accidentally ruptures within an intermediate host, spilled PSC have the developmental plasticity to develop into new cysts in a process called secondary infection.[3]

Efforts to mitigate CE worldwide have focused on controlling the parasite life cycle by using antithelmintic drugs, by promoting hygienic slaughter and by improving health education in rural communities. Reported costs for controlling CE is over U$S 3 billion annually, and despite those efforts, the number of human cases is substantially increasing worldwide every year.[4] In the last decades, efforts in designing effective vaccines against *E. granulosus* infection have increased, focusing on both intermediate and definitive hosts, but showing different and inconsistent success. Up to date, only one vaccine against CE (named EG95) has reached the market. EG95 contains a recombinant 17 kDa protein derived from *E. granulosus* oncospheres, and induces over 95% protection in sheep.[5,6] However, the EG95 vaccine antigen —originally developed for the G1 parasite genotype—has been shown to be polymorphic and immunologically different in other parasite genotypes and/or isolates, raising the question whether the current EG95 vaccine would be effective against every *E. granulosus* genotype.[7,8]

Currently, there are two main approaches for designing vaccines. Originally, most vaccines were created by immunization with the whole pathogen, and—when possible—using some purified antigens responsible for the overall protection. More recently, after the concept of reverse vaccinology was proposed, new vaccine candidates are selected from the whole pathogen genome/proteome by in silico tools.[9] Both approaches have pros and cons, and currently approved vaccines have been designed following both strategies. Additionally, strategies for peptide-based (or epitope-based) vaccines can complement both abovementioned approaches through finding the smallest part of an antigen retaining protective activity. The primary advantage of this approach is that peptides can be produced in nonbiological synthetic ways, reducing production costs enormously. Peptide mapping (or epitope mapping) can be performed in vitro or in silico, being the second option less accurate although virtually costless.[10] In this regard, peptide-based vaccines for helminth-derived infections have also been reported.[11-15] In the case of CE, two studies using different approaches to obtain peptide-based vaccines derived from the EG95 antigen have been reported. In the case of Woollard et al,[16] they studied four different EG95-derived peptides, which all successfully induce anti-EG95 antibodies in immunized sheep, although no oncospheres-killing activity was observed in vitro. In the other study, Read et al[17] worked with an EG95-derived mimotope (a linear peptide that mimics a conformational B cell epitope) named E-100, which showed high efficiency in inducing antibodies able to kill oncospheres in vitro.

In the present work, we identified novel protein candidates to be further tested as vaccine antigens, and we also proposed a new strategy for designing peptide-based candidates through the integration of proteomics, systems vaccinology, and bioinformatics. To that end, we first performed a proteomic characterization of a PSC-derived fraction composed of tegumental antigens, and then applied a systematic bioinformatic and immunoinformatic pipeline. After that, novel proteins were proposed as vaccine candidates against *E. granulosus*. Additionally, through an innovative bio-informatic workflow, we identified peptides for being further tested in peptide-based vaccines, which represent linear B cell epitopes most likely to be accessible to antibodies and free of posttranslational modifications within the native protein. Their sequences were studied in depth and peptides were selected for their specificity, for not being neither toxic nor allergenic, and for retaining a secondary structure similar to the native peptide within their parental protein, thus improving the likelihood of inducing protective cross-reacting responses after immunization.

2 | MATERIALS AND METHODS

2.1 | Parasites and antigens

E. granulosus PSC were collected by opening fertile hydatid cysts from natural bovine infections with a scalpel and they were washed several times with phosphate-buffered saline (PBS) pH 7.2 containing antibiotics (penicillin 60 μg/mL, streptomycin 100 μg/mL, and amphotericin-B 250 ng/mL). Tegumental proteins were extracted from highly viable PSC (viability ≥ 80%) using

an extracting solution consisting of the detergent MEGA-10 (1% w/v), EDTA (5 mM) and phenylmethylsulfonyl fluoride (2 mM) in PBS according to Hernández and Nieto.[18] Briefly, 125.000 viable PSC/mL of extracting solution were incubated for 2 hours at room temperature with soft constant shaking. Then, PSC were allowed to settle down and the supernatant was removed and extensively dialyzed at room temperature against PBS through a dialysis tube cellulose membrane (MW cut-off: 12 000 Da). Obtained antigens (termed PSEx) were characterized in terms of lipid, protein, and carbohydrate content according to,[19] and stored at −20°C until used. Treated PSC were washed three times with PBS, and their integrity was assessed by observation under a light microscope staining with eosin to improve contrast.

2.2 | Transmission electron microscopy

Aliquots of PSC pre- and post-extraction were fixed with 2.5% glutaraldehyde and 2% paraformaldehyde in PBS and stored at 4°C until use. After changing fixing buffer to cacodylate buffer (50 mM cacodylate, 50 mM KCl, 2.6 mM $CaCl_2$, 2.6 mM $MgCl_2$, and 2% sucrose), PSC samples were incubated with 1% osmium tetroxide in 100 mM cacodylate buffer for 60 minutes at room temperature, washed two times with 100 mM cacodylate buffer and two times with EM-grade water and incubated overnight at 4°C in 1% uranyl acetate in water. Samples were rinsed two times with water, dehydrated in a graded acetone series (from 30% to 100%) at room temperature before being embedded in epoxy resin, and polymerized for at least 48 hours at 60°C. Ultrathin sections of 70 nm were obtained by sectioning PSC with a Leica EM UC6 ultramicrotome (Leica Microsystems, Wetzlar, Germany) and a diamond knife. Sections were collected on EM grids, counterstained using lead citrate and uranyl acetate, and examined with a Zeiss 10C transmission electron microscope (80 kV; Carl Zeiss, Goettinger, Germany).

2.3 | 2D sample preparation and electrophoresis

PSEx antigens were resolved by 2D electrophoresis as described elsewhere.[20] Briefly, 300 μg of proteins were incubated overnight at −20°C in 300 μL of ice-cold acetone containing 20% of trichloracetic acid and 0.07% dithiothreitol (DTT). After centrifugation for 15 minutes at 10 000*g* and 4°C, the supernatant was discarded and 300 μl of ice-cold acetone containing 20% dimethylsulfoxide and 0.07% DTT was added and incubated for 60 minutes at −20°C. Then, the sample was centrifuged for 15 minutes at 10.000 g and 4°C, the supernatant was discarded and 300 μl of ice-cold acetone containing 0.07% DTT was added. This step was repeated twice. Finally, the pellet was lyophilized, resuspended in IPG buffer and frozen at −80°C for 24 hours to improve solubilization. For the first dimension, 7 cm linear pH gradient (pH 3-10) Immobiline DryStrips (GE Healthcare, Darmstadt, Germany) were rehydrated with the sample and run on an IPGphore isoelectric focusing system (9.5 hours run and a total of 35.500 Vh), and stored at −80°C until use. Strips were then equilibrated in equilibration buffer (50 mM, Tris-Cl pH 8.8; urea, 6 M; glycerol, 30%; sodium dodecyl sulfate (SDS), 2%; and traces of bromphenol blue) containing DTT (10 mg/mL) for 15 minutes, further equilibrated in equilibration buffer containing iodoacetamide (25 mg/mL) for 15 minutes, and sealed to 10% acrylamide gels using 0.5% agarose in standard Tris-glycine electrophoresis buffer. Second dimension SDS-PAGE was run at 50 V for the first 15 minutes and then raised to 150 V until ending. Finally, replicates of 2D gels were stained with either Coomassie blue dye or mass-spectrometry compatible silver nitrate staining.

2.4 | Mass spectrometry

Spots obtained from both Coomassie blue and silver nitrate-stained 2D gels were analyzed by matrix-assisted laser desorption/ionization (MALDI)-TOF/TOF mass spectrometry. First, spots were excised, faded and tryptic digestions were performed using sequencing-grade modified trypsin (Promega, Madison, WI). After gel extraction into 60% acetonitrile containing 0.1% TFA, the excess of acetonitrile was removed by speed vacuum. Peptide samples were then combined with an equal volume of matrix and spotted onto a MALDI sample plate and allowed to dry at room temperature. Mass spectra were acquired on a MALDI-TOF/TOF mass spectrometer (4800 MALDI TOF/TOF Mass Analyzer, Abi Sciex, Warrington, UK) operating in the positive ion reflector mode. Protein identifications were performed using an in-house Mascot v.2.3 search engine by searching a custom database that includes the full proteome of *E. granulosus* and *Echinococcus multilocularis,* composed of 20 787 sequences (10 310 548 residues) obtained from the Sanger Helminth Database (http://www.sanger.ac.uk/resources/downloads/helminths/). Additionally, every mass spectrum was also analyzed using NCBI database to discard possible host related proteins. The search criteria used were cystein carbamidomethylation and methionine oxidation as variable modification, and mass deviation < 200 ppm with peptide fragment tolerance of 0.45 Da. Scores > 56 were considered significant ($P < 0.05$).

2.5 | Gene ontology analysis

A global comprehension of PSEx was obtained by analyzing the relationship between all protein-related Gene Ontology (GO). In the first place, GO terms were collected from UniProtKB database for each protein. Since protein annotation was incomplete in terms of GO codes, further terms were assigned to each protein using the software FFPred3, which predicts the functions based on the amino acid sequence and the relationship between biophysical attributes (secondary structure, transmembrane helices, intrinsically disordered regions, and signal peptides among other motifs) and protein functions.[21] Only terms with high storage virtual machine (SVM) reliability and $P > 0.8$ for Biological Process and Molecular Function, and $P > 0.7$ for Cellular Component were included. If no terms reached the abovementioned thresholds, the highest probability term was included. Due to software limitations, only proteins less than 1500 amino acids in length were analyzed. Finally, the proteome GO analysis was performed by REVIGO[22] and visualized as pie charts showing the top represented "superclusters" of loosely related terms. For this, all the GO terms were submitted to REVIGO and set to use SimRel as the semantic similarity measure and allowing similarities of 0.9.

2.6 | In silico proteome characterization

An extensive in silico characterization of MALDI-TOF/TOF identified proteins was performed. First, each protein cellular sublocalization was predicted by DeepLoc software.[23] Then, individual and global antigenicity was assessed by predictions with ANTIGENpro software,[24] and abundance of antigenic regions (AAR) was predicted using the web server Secret-AAR.[25] Proteins with ANTIGENpro scores ≥ 0.5 were considered as highly antigenic.[26] Finally, we obtained a "uniqueness score" (US) of each protein by BlastP, where we defined the US as the product between query coverage and identity percentages of the highest max score match against all the proteins on the nonredundant NCBI database (excluding Cestoda, Trematoda, and Nematoda taxonomy). US values of 0.5 to 0.8 identified "highly divergent" proteins, while US values ≤ 0.5 corresponded to "unique" proteins.

2.7 | Clean linear B cell epitopes

Linear B cell epitopes were predicted in each protein using the algorithm Bepipred (version 2.0).[27] Continuous antigenic segments more than or equal to six amino acids in length were considered as linear B cell epitopes. Epitopes were further colocalized on the matching peptides used to identify the corresponding protein by MALDI-TOF/TOF, assuming those regions are free of posttranslational modifications (PTMs). Linear B cell epitopes that completely overlapped with those regions or included the N-terminal Lys/Arg of the trypsin-cut peptides, were termed "clean linear B cell epitopes."

2.8 | Peptide quality control

Sequences identified as clean linear B cell epitopes were evaluated in terms of safety before proposing them as peptide-based vaccine candidates. A pipeline was designed to avoid unwanted-cross reactivity, toxicity, and/or allergenicity. In addition, a study of secondary structure similarity (SSS) was performed to compare the possible secondary structure of synthetic peptides with the corresponding sequence on the native protein. For this, we first discarded every peptide exhibiting a 100% similarity (BlastP) with any protein on the nonredundant NCBI database (excluding Cestoda, Trematoda, and Nematoda taxonomy). Then, secondary structures of clean linear B cell epitopes and their corresponding proteins were predicted using SOPMA software,[28] and the percentage of amino acids in the same conformation (SSS) was calculated. Only peptides with SSS $\geq 80\%$ were selected. Finally, peptides predicted to be toxic and/or—if longer than 11 amino acids—allergenic were excluded from further analyses. Such predictions were performed using Toxinpred[29] and AlgPred[30] softwares, respectively.

2.9 | 3D modeling and epitope mapping

Clean linear B cells epitopes that successfully passed the above-mention pipeline were mapped within the 3D structure of their corresponding protein to analyze the antibody accessibility according to.[26] Briefly, we first performed a 3D structure modeling by low-homology protein threading using RaptorX software[31] to every protein that exhibited at least one peptide that successfully passed the previous pipeline. Only 3D models with uGDT (unnormalize Global Distance Test) higher than 50 were taken into account, and for proteins with more than one predicted 3D model, the structure with the highest uGDT was chosen. Then, clean linear B cell epitopes were mapped within each selected structure using SWISS-PdbViewer,[32] and their antibody accessibility was evaluated.

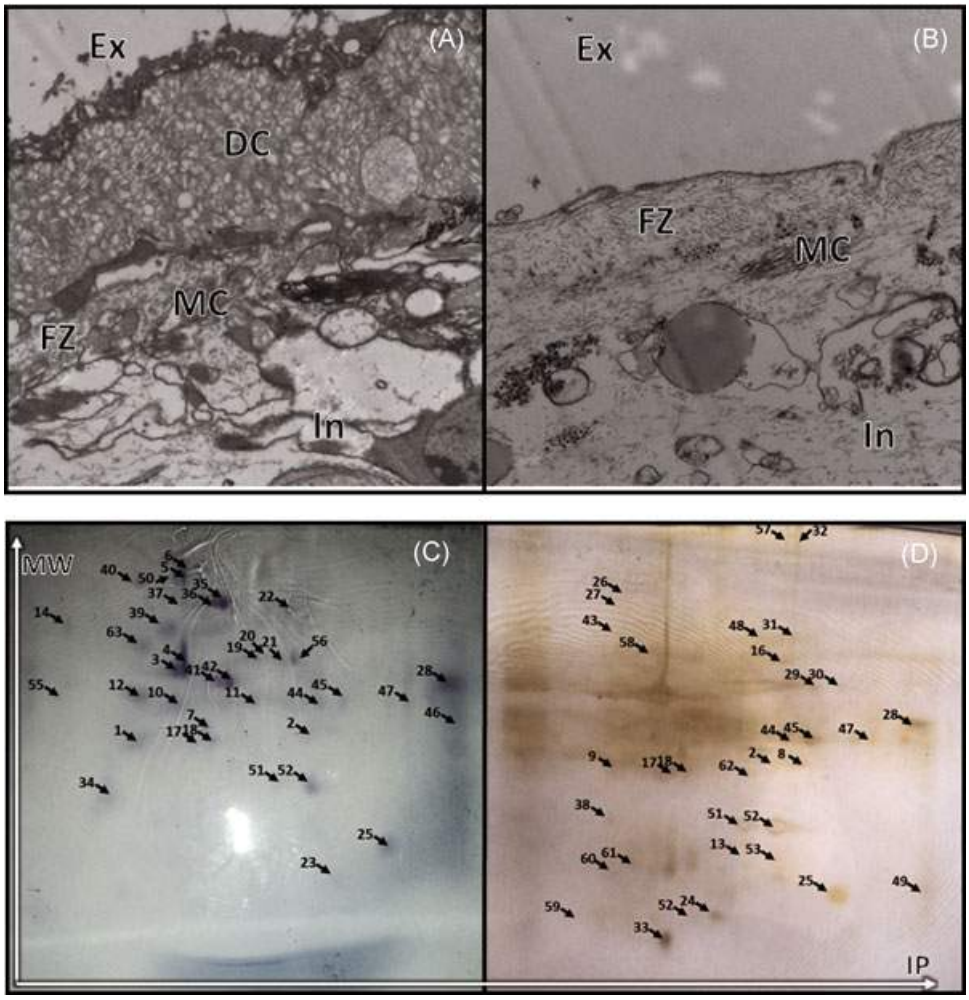

FIGURE 1 Tegumental ultrastructure and 2D-electrophoresis. Micrographs (top row) depict TEM images of pre-PSEx-extracted (A) and post-PSEx-extracted (B) PSC at ×6000. The Ex, FZ, MC, and In of the parasite are shown in (A) and (B), as well as the DC in (A). 2D-PAGE (bottom row) show 2DE of PSEx stained with Coomassie blue (C) or silver nitrate (D). Gels show proteins typically less than 120 kDa with IP values in the linear range 3 to 10 (from left to right). Arrows in gels indicate localization of proteins identified by mass spectrometry, and numbering correspond to the description in Table 1. DC, distal cytoplasm; Ex, exterior; FZ, fibrous zone; In, interior; MC, muscle cell; PAGE, polyacrylamide gel; PSE, protoscolex; TEM, transmission electron microscopy

3 | RESULTS

3.1 | Structural morphology of PSC

Tegument morphology in PSC pre-extraction (Figure 1A) and post-extraction (Figure 1B) was analyzed in 70 nm thick sections by transmission electron microscopy (TEM). A comparative study between them showed that after protein extraction, the general parasite structure remained mostly intact, while a complete disruption of tegumental distal cytoplasm was observed (Figure 1B). In fact, while distal cytoplasm and tegumental spines almost completely disappeared, the fibrous zone, muscle cells and inner structures were still observed with little or no changes. This suggests that the PSEx fraction was composed mostly of proteins present in classical tegumental structures, with few internal parasite proteins as contaminants.

3.2 | PSEx proteome

Biochemical composition of PSEx showed protein-to-carbohydrates and protein-to-lipids mass ratios of 7.2 and 1.3, respectively; suggesting that PSEx is an antigenic fraction enriched in proteins and lipids. Therefore, an extensive proteomic analysis of PSEx was performed by 2D gel electrophoresis followed by mass spectrometry (MALDI-TOF/TOF). To that end, after removal of lipids and highly hydrophobic proteins from PSEx, 2D SDS-PAGE (linear pH 3%-10% and 10% acrylamide) were run and stained with either Coomassie blue (Figure 1C) or silver nitrate (Figure 1D). After that, 96 spots were

TABLE 1 Proteomic characterization of PSEx

Number	Spot	Protein name	Accession number	MW (Da)	IP	Length (aa)	MASCOT score	Fragmented peptides	Consensus coverage, %	Previously identified
1	1	14-3-3 Protein	Q56J98	27 928	4.91	247	155	3	72	
2	2	3-Oxoacyl acyl carrier protein reductase	A0A068WAT3	34 833	5.63	326	145	2	42	[37]
3	3/4/5/6/7	Actin	W6UMH9	41 718	5.30	393	105	2	64	–
4	3/4/5/6	Actin cytoplasmic A3	U6JLF5	41 789	5.31	375	138	2	64	[37]
5	3/4/5/6/7	Actin, cytoplasmic 2	W6UFA4	40 189	5.66	377	105	2	64	–
6	3/4/5/6/7	Actin-2	Q03341	41 856	5.37	376	104	2	37	–
7	8	Aldo keto reductase family 1 member B4	A0A068WU90	42 259	8.58	375	185	2	22	–
8	9	Ankyrin	A0A068WVL6	89 159	8.11	823	66	1	20	–
9	10	Annexin	A0A068WJF9	36 659	5.17	323	329	4	54	[36,37]
10	10	Annexin	A0A068WRH5	34 805	5.38	310	77	3	59	[37]
11	11	Annexin	A0A068WUR8	38 733	4.82	348	315	3	58	[37]
12	12	Annexin	U6JIM9	37 280	5.89	331	75	1	11	–
13	13	Basement membrane specific heparan sulfate	A0A068X0X0	859 349	5.01	7809	69	1	24	[35]
14	14	Calreticulin	A5YTY7	45 339	4.48	395	95	1	39	[36]
15	15	Cathepsin d lysosomal aspartyl protease	A0A068WAA1	47 109	5.59	423	57	1	13	–
16	16	Citrate synthase	U6J0K5	51 378	8.26	465	231	3	56	[35,36]
17	17/18	Endophilin B1	A0A068WMU2	28 782	5.83	252	245	3	67	[20,34,35,37]
18	19/20/21/22	Enolase	D0VLV3	46 532	6.48	433	126	2	59	[33]
19	23	Expressed protein	A0A068WLY9	22 367	9.55	192	96	2	32	[37,39]
20	24	Fatty acid binding protein FABP2	A0A068WLT8	23 901	8.41	213	64	1	62	[34,37]
21	25	Fatty acid binding protein FABP2	U6JF28	15 361	5.64	133	86	1	23	–
22	26/27	Filamin	A0A068WYB5	276 623	5.37	2558	62	1	16	–
23	28	Fructose-bisphosphate aldolase	U6IXV3	39 641	8.31	363	210	3	77	
24	29/30	Gelsolin	U6IX85	41 998	7.63	364	101	2	47	[36]
25	31/32	Glucose-6-phosphate isomerase	A0A068WLH0	61 566	6.48	547	61	1	20	[35]
26	33	Glyceraldehyde-3-phosphate dehydrogenase	A0A068WKQ2	37 739	8.55	352	108	2	46	[34,35,37]

(Continues)

TABLE 1 (Continued)

Number	Spot	Protein name	Accession number	MW (Da)	IP	Length (aa)	MASCOT score	Fragmented peptides	Consensus coverage, %	Previously identified
27	34	Heat shock 70 kDa protein	A0A068X4W2	28 849	5.80	252	61	1	23	–
28	35/36/37/38	Heat shock 70 kDa protein 4	A0A068WHV0	72 510	5.59	664	208	3	62	–
29	35/36	Heat shock 70 kDa protein 4	U6JIC8	71 039	5.65	651	60	1	75	34,36,38
30	39	Heat shock protein 60	A0A068WSG0	60 575	5.37	568	261	3	59	37
31	35/36	Heat shock protein 71 kDa protein	A0A068X560	72 526	5.52	665	204	3	63	–
32	40	Heat shock protein HSP 90α	W6UM50	73 829	5.03	738	180	2	40	36
33	41/42	Major egg antigen p40	U6JBW8	35 825	5.81	314	99	1	71	34,36,37
34	5/43	Major vault protein	A0A068WUZ9	97 000	5.33	869	64	1	27	37
35	44/45/46	Malate dehydrogenase	A0A068WYB8	35 519	8.82	338	63	1	17	35,37
36	44/47	Malate dehydrogenase	A0A068X1L3	36 547	7.62	332	74	1	24	34,35,37
37	48	Mechanosensory protein 2	A0A068WM93	53 528	8.21	484	59	1	32	–
38	49	Nucleoside diphosphate kinase	A0A068WL30	16 676	10.16	149	101	2	21	40
39	5/6/50	Paramyosin	A0A068WA67	98 882	5.29	863	69	1	60	34,37
40	51/52/53	Peptidyl-prolyl cis-trans isomerase	P14088	17 343	6.41	162	232	3	35	20,33,37,38
41	54	Peptidylprolyl isomerase	A0A068X276	7885	9.98	65	64	1	33	–
42	55	Phosphatase 2a inhibitor i2pp2a	A0A068WLN2	34 168	4.35	300	86	1	19	–
43	56/57	Phosphoenolpyruvate carboxykinase	A0A068X1L0	71 188	6.93	635	57	1	58	34,35,37
44	58	Protein disulfide-isomerase	A0A068WIL3	81 413	7.86	716	64	1	41	39
45	59	SPRY domain containing protein	A0A068WNG3	136 955	5.92	1223	154	2	14	–
46	48	Structural maintenance of chromosomes protein	A0A068WEW7	149 088	6.21	1347	71	1	9	36
47	54	Superoxide dismutase [Cu-Zn]	W6V988	40 189	5.66	177	100	2	33	34,35,37
48	60/61	Thioredoxin peroxidase	Q8T6C4	21 392	5.78	193	79	1	55	19,31-34,41
49	2/62	Triosephosphate isomerase	U6JN02	27 122	6.60	250	54	1	78	32-34,41
50	63	Tubulin β chain	A0A068WEL5	49 630	4.79	443	93	1	33	–
51	63	Tubulin β chain	A0A068WLA0	52 862	4.88	472	68	1	37	–
52	63	Tubulin β chain	A0A068WQC9	57 714	5.36	509	71	1	41	–
53	63	Tubulin β chain	U6JJN6	49 802	4.79	445	100	2	49	–
54	63	Tubulin β chain	U6JM68	49 584	4.79	444	104	2	41	–

(Continues)

TABLE 1 (Continued)

Number	Spot	Protein name	Accession number	MW (Da)	IP	Length (aa)	MASCOT score	Fragmented peptides	Consensus coverage, %	Previously identified
55	63	Tubulin β/β2 chain	A0A068WML9	49 841	4.75	445	293	4	67	[36,37]
56	60	Uncharacterized protein	U6JRE4	50 538	9.32	444	71	1	33	–
57	48	UTP--glucose-1-phosphate uridylyltransferase	W6UT22	57 047	6.31	533	123	2	27	[38]
58	59	Vesicular amine transporter	A0A068X307	49 068	4.99	443	124	2	36	[35,39]

Abbreviations: aa, amino acid; IP, isoelectric point.; MW, molecular weight; IP, isoelectric point.
The full PSEx proteome was obtained through MALDI-TOF/TOF. "Spot" column shows the corresponding spot from 2DE gels (Figure 1C and 1D). "Accession number" refers to the UniProtKB IDs. "MASCOT score" corresponds to the lowest score for proteins identified in several spots. "Fragmented peptides" corresponds to the lowest number of matched MS/MS peptides. "Consensus coverage" is the percentage of the sum of all peptides used to identify the same protein in several spots.

excised from gels (50 spots from Coomassie blue stained gels and 46 spots from silver stained gels), and then they were faded and trypsin-digested for mass spectrometry analysis. Finally, 58 different proteins were successfully identified within 63 spots (Table 1). Among these, 27 proteins were identified only in Coomassie blue-stained gels, 20 proteins only in silver-stained gels, and 11 proteins were found in spots excised from both gels. In some spots, more than one protein—exhibiting similar molecular weights and isoelectric points—were identified. Since, in that case, it is virtually impossible to differentiate such proteins in a 2D gel, all of them were included in the final proteome. At the end, 22 new proteins were described for the first time in this study, while the remaining 36 have been already reported in previous *E. granulosus* proteomic analyses (Table 1). Interestingly, no host-derived proteins (ie *Bos taurus*) were identified.

3.3 | PSEx Gene Ontology

For each identified protein, GO terms were first obtained from their corresponding annotation in UniProtKB database. Then, the prediction of complementary terms was performed for each protein using FFPred3 software. Due to software limitations, only proteins less than 1500 amino acids long were analyzed. From annotated proteins in UniProtKB database, 197 GO terms were obtained, which did not cover the three categories (Biological Process, Molecular Function, and Cellular Component) for most proteins. After GO prediction using FFPred3 software, 544 additional terms were obtained. Finally, by combining both GO terms sources—and removing duplicates between annotated and predicted terms—711 terms corresponding to 56 proteins were obtained. Among them, 184 unique GO terms were found, which were reduced into a two-level hierarchy of GO terms resulting in 67, 79, and 33 unique Biological Processes, Molecular Functions, and Cellular Components, respectively. Pie charts show top represented loosely related terms joined into "superclusters."[22] From this analysis, PSEx components could globally be described as mostly vesicle-related proteins involved in microtubule-based processes with diverse metabolic functions (Figure 2).

3.4 | In silico PSEx characterization

To obtain a protein-by-protein characterization of PSEx, an extensive in silico study of its identified proteome was performed (Table 2). Prediction of cellular localization showed a predominance (73%) of cytoplasmic proteins (42 in 57), followed by 11% characterized as mitochondrial

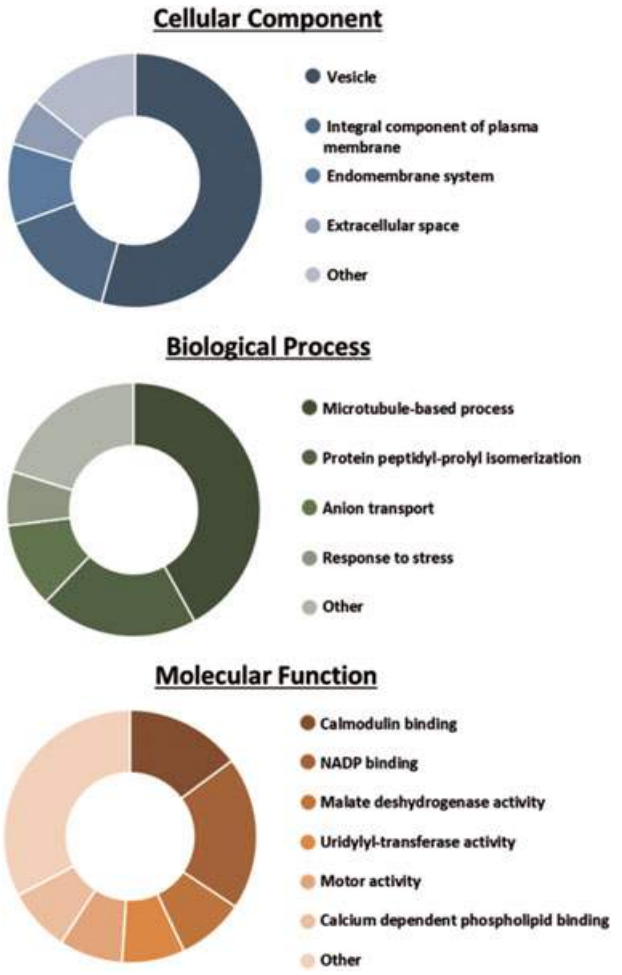

FIGURE 2 Gene Ontology study of PSEx proteome. GO analysis of PSEx proteins is shown for Cellular Component, Biological Process, and Molecular functions. For each category, the unique terms were reduced into a two-level hierarchy of GO terms, and visualized as pie-charts showing top represented loosely related terms joined into "superclusters." GO, Gene Ontology; PSEx, protoscolex

proteins (6 in 57), and the remaining 16% classified as belonging to other cellular or extracellular compartments (9 in 57). Additionally, the overall antigenicity of PSEx proteome was determined. In this sense, ANTIGENpro obtained a mean antigenicity score of 0.67, while a mean AAR value of 41.0 was calculated through Secret-AAR. Proteins with ANTIGENpro scores > 0.50 are usually considered highly antigenic,[26] and according to this threshold, 74% of proteins within PSEx proteome (43 in 58) belonged to that category (Table 2). Finally, a US was calculated for each protein, resulting in 40% of "highly divergent" proteins (23 in 58), and 34% of "unique" proteins (20 in 58) within PSEx proteome (Table 2). Interestingly, similar values were obtained when considering only first time-identified proteins: 0.68 and 40.0 mean values for antigenicity score and AAR, respectively. Furthermore, 27% of such proteins (5 in 22) were categorized as "highly divergent", while 36% (8 in 22) were "unique" (Table 2).

3.5 | Identification of clean linear B cell epitopes

Proteins within PSEx proteome were scanned for linear sequences potentially recognizable by antibodies (eg, linear B cell epitopes). Due to software limitations, only proteins less than 2500 amino acids in length (56 out of 58) were analyzed. Results showed 578 lineal B cell epitopes within the PSEx proteome (Figure 3), with a mean value of 10 epitopes per protein. Every protein showed at least two linear B cell epitopes, and two proteins (#37 and #46) exhibited 33 epitopes, the largest number observed. Then, in the interest of identifying clean linear B cell epitopes, for example those PTMs-free, we evaluated the colocalization of every obtained epitope over the sequence fragments used to identify proteins by mass spectrometry. Since the mass of those fragments is practically equal to the overall sum of their constituent amino acids, we can assume that such regions are free of PTMs. After colocalization, 146 clean linear B cell epitopes were predicted in 46 proteins within PSEx proteome (Figure 3). Those epitopes ranged from six to 46 amino acids in length, with a mean value of 12 amino acids per epitope. Then, aiming to avoid unwanted cross-reactivity, the 146 sequences were scanned against all nonhelminth proteins by BlastP, and those peptides matching with 100% identity to any protein were discarded (Figure 3). Interestingly, only peptides ranging from 9 to 46 amino acids in length were identified among the 50 epitopes selected, which belonged to 29 different proteins (Figure 3). After that, and in pursuance of maximizing the likelihood of selecting peptides able to induce cross-reacting antibodies against their parental native proteins, SSS values were calculated for those 50 selected epitopes. Results showed that 17 peptides—belonging to 15 different proteins—exhibited SSS scores $\geq 80\%$ (Figure 3), being 16 and 1 of them mostly random coil and α-helix in secondary structure, respectively. Finally, those sequences were further analyzed for safety considerations, removing peptides predicted to be toxic and/or allergenic. Only one peptide was discarded in this step, leaving 16 peptide candidates from 15 different proteins present in PSEx (Figure 3). Summing up, from the initially 578 peptides identified (derived from an input of 56 proteins), only 16 of them (roughly 3%) belonging to 15 different proteins successfully passed through our rationally designed pipeline. Interestingly, four of these proteins were identified for the first time in this study (#3, #8, #45, and #53),

TABLE 2 Immunobioinformatic characterization of PSEx

Number	Protein name	Accession number	Localization	Antigenicity	AAR	US
1	14-3-3 Protein	Q56J98	Cytoplasm	0.76	41.3	0.62
2	3-Oxoacyl acyl carrier protein reductase	A0A068WAT3	Peroxisome	0.10	65.4	0.40
3	Actin	W6UMH9	Cytoplasm	0.43	32.8	0.93
4	Actin cytoplasmic A3	U6JLF5	Cytoplasm	0.39	47.0	0.91
5	Actin, cytoplasmic 2	W6UFA4	Cytoplasm	0.35	34.4	0.97
6	Actin-2	Q03341	Cytoplasm	0.35	47.1	0.90
7	Aldo keto reductase family 1 member B4	A0A068WU90	Cytoplasm	0.63	62.7	0.40
8	Ankyrin	A0A068WVL6	Cytoplasm	0.76	37.5	0.28
9	Annexin	A0A068WJF9	Cytoplasm	0.50	46.3	0.43
10	Annexin	A0A068WRH5	Cytoplasm	0.85	31.1	0.46
11	Annexin	A0A068WUR8	Cytoplasm	0.72	24.9	0.42
12	Annexin	U6JIM9	Cytoplasm	0.30	47.4	0.34
13	Basement membrane specific heparan sulfate	A0A068X0X0	NP	NP	27.9	0.05
14	Calreticulin	A5YTY7	ER	0.90	49.5	0.51
15	Cathepsin d lysosomal aspartyl protease	A0A068WAA1	Vesicle	0.26	42.4	0.50
16	Citrate synthase	U6J0K5	Mitochondrion	0.43	35.8	0.65
17	Endophilin B1	A0A068WMU2	Mitochondrion	0.94	42.2	0.24
18	Enolase	D0VLV3	Cytoplasm	0.53	31.0	0.88
19	Expressed protein	A0A068WLY9	Extracellular	0.74	21.4	0.12
20	Fatty acid binding protein FABP2	A0A068WLT8	Cytoplasm	0.52	42.8	0.61
21	Fatty acid binding protein FABP2	U6JF28	Cytoplasm	0.67	33.5	0.74
22	Filamin	A0A068WYB5	Cytoplasm	NP	25.8	0.52
23	Fructose-bisphosphate aldolase	U6IXV3	Cytoplasm	0.75	33.1	0.73
24	Gelsolin	U6IX85	Cytoplasm	0.82	33.2	0.32
25	Glucose-6-phosphate isomerase	A0A068WLH0	Cytoplasm	0.80	49.8	0.67
26	Glyceraldehyde-3-phosphate dehydrogenase	A0A068WKQ2	Cytoplasm	0.80	29.4	0.71
27	Heat shock 70 kDa protein	A0A068X4W2	Cytoplasm	0.96	36.1	0.67
28	Heat shock 70 kDa protein 4	A0A068WHV0	Cytoplasm	0.92	35.0	0.82
29	Heat shock 70 kDa protein 4	U6JIC8	Cytoplasm	0.90	34.3	0.84
30	Heat shock protein 60	A0A068WSG0	Mitochondrion	0.66	33.5	0.79
31	Heat shock protein 71 kDa protein	A0A068X560	Cytoplasm	0.93	35.1	0.82
32	Heat shock protein HSP 90α	W6UM50	Cytoplasm	0.73	38.9	0.74
33	Major egg antigen p40	U6JBW8	Mitochondrion	0.74	31.5	0.28
34	Major vault protein	A0A068WUZ9	Cytoplasm	0.42	39.5	0.56
35	Malate dehydrogenase	A0A068WYB8	Mitochondrion	0.43	37.7	0.63
36	Malate dehydrogenase	A0A068X1L3	Cytoplasm	0.45	41.6	0.63
37	Mechanosensory protein 2	A0A068WM93	Cell membrane	0.58	69.3	0.40
38	Nucleoside diphosphate kinase	A0A068WL30	Cytoplasm	0.24	150	0.43
39	Paramyosin	A0A068WA67	Cytoplasm	0.87	34.6	0.73
40	Peptidyl-prolyl cis-trans isomerase	P14088	Cytoplasm	0.92	32.6	0.77
41	Peptidylprolyl isomerase	A0A068X276	Cytoplasm	0.89	22.0	0.58
42	Phosphatase 2a inhibitor i2pp2a	A0A068WLN2	Nucleus	0.85	50.2	0.38
43	Phosphoenolpyruvate carboxykinase	A0A068X1L0	Cytoplasm	0.60	35.3	0.61
44	Protein disulfide-isomerase	A0A068WIL3	Cytoplasm	0.80	37.7	0.27
45	SPRY domain containing protein	A0A068WNG3	Cytoplasm	0.94	35.0	0.11

(Continues)

TABLE 2 (Continued)

Number	Protein name	Accession number	Localization	Antigenicity	AAR	US
46	Structural maintenance of chromosomes protein	A0A068WEW7	Nucleus	0.66	42.1	0.41
47	Superoxide dismutase [Cu-Zn]	W6V988	Cytoplasm	0.86	35.6	0.58
48	Thioredoxin peroxidase	Q8T6C4	Cytoplasm	0.67	64.7	0.65
49	Triosephosphate isomerase	U6JN02	Cytoplasm	0.62	35.9	0.81
50	Tubulin β chain	A0A068WEL5	Cytoplasm	0.83	37.0	0.97
51	Tubulin β chain	A0A068WLA0	Plastid	0.84	43.0	0.86
52	Tubulin β chain	A0A068WQC9	Cytoplasm	0.73	42.5	0.78
53	Tubulin β chain	U6JJN6	Cytoplasm	0.84	37.2	0.97
54	Tubulin β chain	U6JM68	Cytoplasm	0.78	37.1	0.96
55	Tubulin β/β2 chain	A0A068WML9	Cytoplasm	0.76	37.2	0.96
56	Uncharacterized protein	U6JRE4	Mitochondrion	0.46	37.1	NH
57	UTP-glucose-1-phosphate uridylyltransferase	W6UT22	Cytoplasm	0.69	59.3	0.58
58	Vesicular amine transporter	A0A068X307	Cell membrane	0.72	24.7	0.17

Abbreviations: AAR, abundance of antigenic region; ER, endoplasmic reticulum; NH, no hit protein obtained by BLASTp; NP, not performed due to software limitations; US, uniqueness score.

The full PSEx proteome was characterized through several immunobioinformatic tools. "Localization" column shows the predicted subcellular localization of each protein. "Antigenicity" and "AAR" columns show the predicted values for antigenicity and abundance of antigenic regions, respectively. "US" column shows the uniqueness score calculated for each protein. NH, no hit protein obtained by BLASTp (indicating query coverage and identity percentage smaller than 25%), thus a US value of 0.00 was assigned. Details of software settings are described in Section 2.

7 corresponded to "unique" proteins (#8, #11, #17, #33, #44, #45, and #58), and four were "highly divergent" proteins (#1, #14, #16, and #23). Moreover, two of them (#8 and #45) were "unique" as well as highly antigenic, and were identified for the first time in this study (Tables 1 and 2).

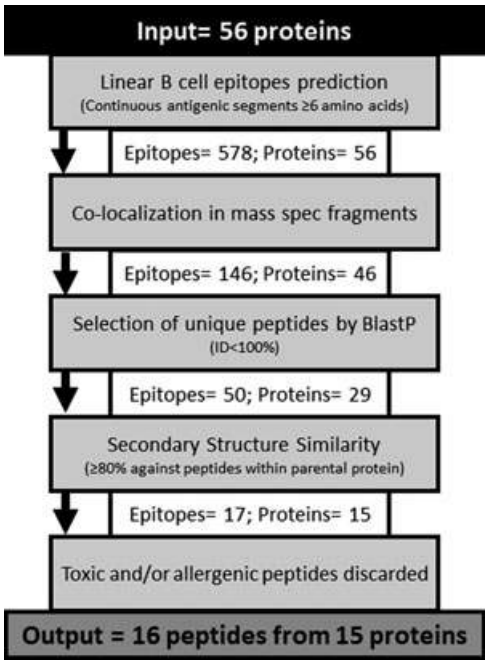

FIGURE 3 In silico prediction of peptide-based vaccine candidates. Bioinformatic workflow designed and used for predicting antigenic peptides derived from experimentally identified proteins within PSEx. Details on software settings are described in Section 2

3.6 | 3D modeling and epitope mapping

3D models of those 15 proteins exhibiting at least one clean linear B cell epitope that overcame our previous analysis, were obtained using RaptorX software. In this regard, among the 15 obtained models not a clear predominant tertiary structure was observed (Figure 4). Then, to analyze epitope surface accessibility, selected petides etides were mapped in their 3D-modeled parental protein as described elsewhere.[26] Only models with uGDT ≥ 50 were selected, resulting in 14 good models (Figure 4). Regarding "SPRY domain containing protein" (#45 in our set), its 3D model did not reach the uGDT threshold and it was discarded from accessibility analysis (Figure 4P). Then, by means of SWISS-PdbViewer, we assessed the surface accessibility to antibodies, obtaining 14 accessible epitopes. One of them, corresponding to "Heat shock 70 kDa protein 4" (#29 in our set), although mapped on a good 3D model (uGDT = 470), it located on a highly disordered portion of the predicted model, and therefore it was discarded (Figure 4O). Finally, we rationally identified 14 accessible clean linear B cell epitopes—belonging to 13 different proteins present in PSEx—which deserve further testing as vaccine candidates against *E. granulosus* infection (Table 3). Interestingly, among the parental proteins of such epitopes, 3 of them belonged to the set of 22 proteins identified for the

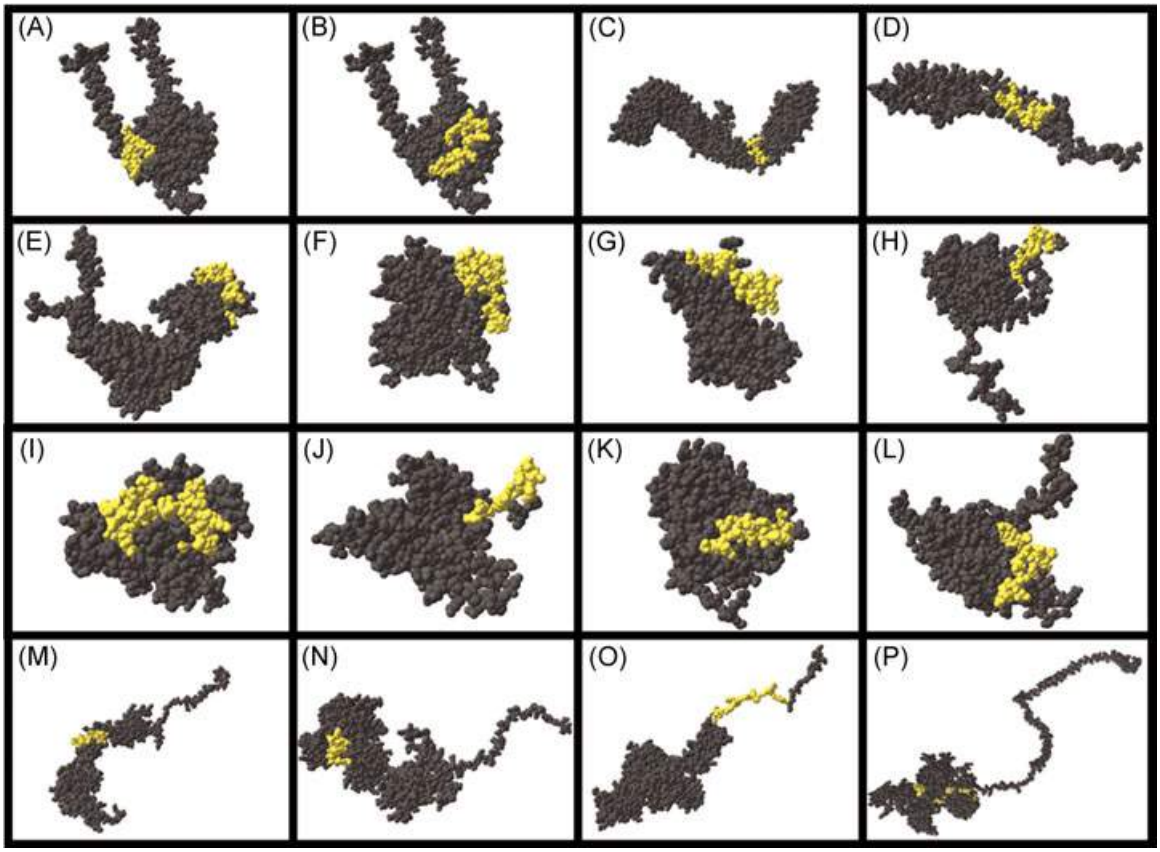

FIGURE 4 Mapping of clean linear B cell epitopes in 3D-modeled protein structures. For every protein that exhibited at least one selected peptide, a 3D-modeled structure was predicted by means of RaptorX software, and the clean linear B cell epitopes were visualized in the 3D models using DeepView. For visualization purposes, 3D overall structure are represented in gray, while mapped epitopes are depicted in yellow. The corresponding proteins are: A,B, calreticulin (#14); C, ankyrin (#8); D, endophilin B1 (#17); E, heat shock protein 60 (#30); F, actin (#3); G, annexin (#11) H, citrate synthase (#16); I, tubulin β chain (#53); J, 14-3-3 protein (#1); K, fructose-bisphosphate aldolase (#23); L, major egg antigen p40 (#33); M, vesicular amine transporter (#58); N, protein disulfide-isomerase (#44); O, heat shock 70 kDa protein 4 (#29); P, SPRY domain containing protein (#45)

first time in this study (#3, #8, and #53). Additionally, 4 (#1, #14, #16, and #23) and 6 (#8, #11, #17, #33, #44, and #58) proteins were classified as "highly divergent" or "unique", respectively (Table 2).

4 | DISCUSSION

Due to the increasingly high economic and health costs of CE, new effective vaccines are needed for primary and/or secondary infections. The only currently marketed vaccine was designed for primary infection of sheep against parasite G1 genotype, but its performance against different *E. granulosus sensu lato* genotypes has to be analyzed.[7,8,42] Several studies have shown promising results for new vaccines against CE, although a robust alternative has not been proposed so far.[4] In this sense, an antigenic fraction composed of tegumental antigens from *E. granulosus* PSC (termed PSEx) has been previously shown to induce specific antibodies in dogs[43] as well as in sheep[44]; and to induce protection against secondary infection in CD1 immunized mice.[18] Although PSEx is assumed to contain only tegumental antigens, no extensive characterization has been performed so far. Additionally, since tegumental components would be the first ones to interact with the host immune system, identifying putative protective antigens within this fraction is a logical approach for designing new vaccines against *E. granulosus*. In the present study, we aimed at identifying—and designing—novel vaccine candidates against *E. granulosus* based on PSEx characterization through a multidisciplinary approach that combined TEM, proteomics, and bio-immuno-informatics.

First, we characterized some biochemical properties of PSEx. In this sense, we initially measured its protein, carbohydrate and lipid content, showing that PSEx is an antigenic fraction mainly enriched in proteins and lipids. Then, to test whether PSEx is primarily composed of tegumental antigens, we performed TEM studies on pre-PSEx-extracted and post-PSEx-extracted PSC. In this

TABLE 3 Epitope-based vaccine candidates

Peptide candidate	Sequence	Length (aa)	Theoretical mass (Da)	Theoretical IP	Parental protein	Parental position	SSS (%)
#1	TEGNIDKWQKSKYDESKLGLC	21	2442.73	5.88	A5YTY7	27-47	90
#2	HAKPKGDFDDRED	13	1529.59	4.75	A5YTY7	49-61	92
#3	ADFNIRNWR	9	1191.31	9.64	A0A068WVL6	190-198	100
#4	GELVNKNEKTSYPTRTSD	18	2039.19	6.18	A0A068WMU2	32-49	88
#5	EADMYKLEDAQLQDLGR	17	1995.19	4.11	A0A068WSG0	324-340	82
#6	CYVLDFEQEMATAASSSSLEKSYELPDG	28	3071.33	3.77	W6UMH9	218-245	92
#7	RHEPTEQQLKDIANRGIDSIIDKKAAEADAQK	32	3589.97	5.61	A0A068WUR8	175-207	90
#8	LPIERPKSLSTDGLRT	16	1783.06	8.75	U6J0K5	445-461	82
#9	PGTMDSVRAGPFGQIFRPDNFVFGQSGAGNNWAKGHYTEGAELVDS	46	4886.31	4.83	U6JJN6	70-115	80
#10	LWNSDAGDTDAAEP	14	1461.46	3.37	Q56J98	230-243	85
#11	DLGVVPLGGTADECTTQGLDNL	22	2188.39	3.37	U6IXV3	110-131	81
#12	APNYKAIKLTPEKGLAIQPTEAQERQLAVTNKEGLEIVTADDGS	44	4709.29	4.77	U6JBW8	189-232	97
#13	MDLSGARELEALPDEKP	17	1871.09	4.18	A0A068X307	213-229	94
#14	RSGPPATEILDESRYKELF	19	2208.46	4.87	A0A068WIL3	358-376	94

Abbreviations: aa, amino acid; IP, isoelectric point; SSS, secondary structure similarity.

The table shows each identified peptide sequence, as well as their length (in amino acids), theoretical mass, and theoretical IP. "Parental protein" and "parental position" columns show protein accession number from which the peptide derives, as well as the position within that protein (from N-terminal amino acid), respectively. Finally, SSS score for each peptide is shown in the last column.

regard, we observed that PSEx extraction completely disrupted the external tegumental layer of PSC, without any remarkable morphological changes in inner parasite structures. In fact, while distal cytoplasm and tegumental spikes disappeared almost completely after PSEx extraction, the fibrous zone, muscle cells, and inner PSC structures showed little, if any, modifications (Figure 1A and 1B). Therefore, we concluded that PSEx mostly contains antigens derived from PSC distal cytoplasm and tegumental spikes, which might include cytoplasmic, vesicular, and/or mitochondrial proteins.

Second, 2D electrophoresis was applied to PSEx to the extent of performing proteomic analyses by mass spectrometry. A complete list of the 58 identified proteins in PSEx is shown in Table 1. It is worth mentioning that some proteins were found in multiple spots—either in both gels or multiple times within the same gel—and, therefore, their MASCOT scores correspond to the lowest one and the sequence coverage correspond to a reconstruction made with the peptides obtained from every matching spot (maximum combined sequence coverage).

Several proteomic analyses of different *E. granulosus* stages or antigenic fractions have been reported up to date, including PSC excretion/secretion products,[33] somatic antigens of PSC[20,34,37,40] somatic antigens of adult worms,[34] hydatid fluid from fertile, and infertile cysts,[35,38,39] as well as extracellular vesicles obtained from fertile hydatid fluid.[36] Among the 58 proteins we reported for PSEx, 36 of them were previously identified in at least one of the abovementioned studies, while 22 proteins were described for the first time in the present work (Table 1). Furthermore, several of the here-identified proteins have been proposed as vaccine candidates against *E. granulosus*.[4,45,46] Among them, Eg.P29—also known as endophilin B1 (#17 in our set)—revealed significant protective activity against secondary infection in mice,[47] as well as against primary infection in sheep,[48] inducing in both cases roughly 95% protection levels. According to our classification, this protein is "unique" (US: 0.24) and highly antigenic (ANTIGENpro score: 0.94), showing an AAR value (42.2) similar to the one obtained for the whole PSEx proteome.

Third, we performed an extensive immunobioinformatic characterization of PSEx proteome, including global as well as a protein-by-protein analyses. Regarding PSEx global analysis, we performed a GO terms study. It is worth mentioning that since PSEx proteome was identified via 2DE followed by MALDI-TOF/TOF, it is impossible to know which protein(s) is more abundant. Thus, unlike GO enrichment analysis—where the frequency a term is found is taken into consideration—our GO analysis only included unique terms describing the whole fraction characteristics. Therefore, our results show that proteins within PSEx are mostly involved in microtubules-associated processes related to vesicles structures, and exhibit diverse metabolic functions (Figure 2). These results are in accordance with the already known functions of PSC tegument.[49] As seen in Figure 1A, PSC tegument (particularly its distal cytoplasm) is heavily composed of vesicular structures, which can be arranged in tegumental spikes (probably through microtubule rearrangement). Additionally, PSC tegument is extremely important in several aspects of parasite metabolism, like nutrient absorption and waste disposal.[49] Our GO analysis also suggested that PSC tegument might act as a defensive barrier against the host attack, as it is involved in stress response processes (eg, removal of superoxide radicals). Also, our results showed a predominance of cytoplasmic and, to a lesser extent, mitochondrial proteins within PSEx (Table 1), and although such results might seem contradictory with GO results, it is important to bear in mind that PSC tegument is a cellular syncytium whose outer layer is the distal cytoplasm, where mitochondria are usually found.[49]

Although the information provided by our GO and subcellular analyses is valuable, it does not allow to identify novel putative protective antigens. Therefore, we further studied other characteristics of PSEx proteome, such as protein-by-protein intrinsic antigenicity and conservancy values. Regarding antigenicity, most proteins within PSEx (74%) were predicted to be highly antigenic and displaying relatively low AAR values (mean of PSEx proteome = 41.0). AAR value is an inverse measure of antigenicity, mostly used to measure the antigenicity of a set of proteins. Interestingly, the mean AAR value of PSEx proteome is slightly higher than the value predicted for a set of secreted proteins from parasitic cestodes (mean AAR = 24.5) proposed as highly antigenic candidates useful for serodiagnosis.[26] Then, when analyzing proteins' "uniqueness score"—a measure of protein divergence obtained by BLASTp against nonhelminth organisms—we observed that over 40% of PSEx proteins can be assessed as "highly divergent" (US values in the 0.5-0.8 range) and 34% as "unique" proteins (US < 0.5). On the basis of these results, and bearing in mind that PSEx is able to induce protection after immunization,[18]we propose nine new proteins to be further tested as vaccine candidates against *E. granulosus* infection. Those proteins were selected from the set of 22 proteins identified for the first time in the present study since they are: (i) either "highly divergent" or "unique", and (ii) highly antigenic. According to our protein set, candidate proteins are: (#7) aldo keto reductase family 1 member B4, (#8) ankyrin, (#21) fatty acid binding protein FABP2, (#27) heat shock 70 kDa protein,

(#37) mechanosensory protein 2, (#41) peptidylprolyl isomerase, (#42) phosphatase 2a inhibitor i2pp2a, (#45) SPRY domain containing protein, and (#52) tubulin β chain. Unfortunately, since no additional information is available on possible polymorphisms in such proteins, their potential as universal vaccine candidates needs to be further studied.

Additionally, we also predicted and selected PSEx-derived peptides to be further tested as epitope-based vaccines. To that end, we designed and applied a novel working pipeline following a step-by-step reduction to select linear B cell epitopes free of PTMs on the native protein, which are not present in any other non-helminth organism, exhibiting similar secondary structure to the native peptide within the parental protein and displaying neither toxicity nor allergenicity potential (Figure 3). Additionally, surface antibody accessibility to the peptides within the native protein was also assessed (Figure 4). Here, it is worth mentioning that when deciding to use peptides as vaccines antigens in a carrier-conjugated format, some considerations must be taken into account. In this sense, although peptide synthesis can be performed in a nonbiological way, greatly reducing manufacturing costs, only a half of them, when conjugated to a carrier protein, have shown the ability to induce cross-reactive antibodies against the native protein.[41] In this sense, our workflow aimed at maximizing this cross-reactivity potential by performing SSS analyses in early developmental stages. In addition, predicting their surface accessibility to antibodies would probably increase their success.[26] Another key-step in our pipeline is selecting peptides only found in helminth species. This step, in combination with the "uniqueness" analysis would be useful for two main reasons. On the one hand, if peptide sequences are present in host proteins, no antibody induction would probably occur because of tolerance processes or, if produced, self-reacting antibodies could display autoimmunity-inducing potential. On the other hand, if peptide sequences are present in other pathogens, then induced antibodies could interfere in diagnostic tests deriving in false-positive results in clinical settings. An additional consideration that must be taken into account when designing peptide-based vaccines is the need for protein carriers, which possess T cell epitopes useful for T-dependent antibody production. Although this seems to be a drawback for peptide-based vaccines, it may actually be an opportunity for success since "unique" epitopes could be used even when the whole protein shows low US. For example, by attaching unique epitopes like those described for actin (#3, US: 0.93) or tubulin β chain (#50, US: 0.97) to a carrier protein, specific antibodies against the peptide could be obtained, with cross-reactive binding to the native protein, bypassing possible host tolerance mechanisms. However, this hypothesis has still to be experimentally confirmed.

Finally, it is important to highlight that as far as our knowledge extends, the present study is the first one to perform linear B cell epitope predictions within mass spectrometry identified protein fragments to identify clean linear B cell epitopes, that is, free of PTMs. Such a strategy, in combination with additional bioinformatic tools, constitutes a novel rational approach for identification of potential peptide-based vaccine candidates. In this regard, we finally suggested 14 novel peptides derived from 13 different proteins—ranging from 9 to 46 amino acids in length—to be further tested as vaccine candidates against *E. granulosus* infection (Table 3). Interestingly, one of those peptides (#3 in Table 3) belonged to one of the proteins also proposed as new vaccine candidates (#8 in Table 1). We are currently designing the effectiveness testing of the suggested vaccine candidates. To that end, in vivo immunogenicity will be firstly assessed in mice, and those effectively immunogenic will be further studied for their ability to induce antibodies with in vitro parasite-killing activity. Finally, promising candidates will be tested in the murine model of secondary CE,[50] and protective antigens might be later assayed in experimental infections using relevant livestock species.

ACKNOWLEDGEMENTS

Authors are grateful to the Electron Microscopy Center Facility of Heidelberg University for the introduction and use of their microscopes. MSc Paula Arbildi is acknowledged for valuable suggestions on figures' esthetics. MEA was recipient of a short-term grant funded by United Nations University-Biotechnology for Latin America and the Caribbean (UNU-BIOLAC). CSIC-Universidad de la República (Uruguay), PEDECIBA-Química (Uruguay) and ANII (Uruguay) are acknowledged for their general financial support.

CONFLICT OF INTERESTS

The authors declare that there are no conflict of interests.

AUTHOR CONTRIBUTIONS

Conceptualization: SM and GM-E. Funding acquisition: SM, SD, RD, FF, and GM-E. Investigation: SM, MP, MC, MEA, and GM-E. Writing manuscript: SM and GM-E.

ORCID

Gustavo Mourglia-Ettlin http://orcid.org/0000-0002-2418-2908

REFERENCES

1. World Health Organization, 2018. Neglected Tropical Diseases. Echinococcosis. www.who.int/en/news-room/fact-sheets/detail/echinococcosis
2. Thompson RCA, Lymbery AJ. Echinococcus and hydatid disease. . Wallingford: CAB International; 1995.
3. Heath DD. The development of *Echinococcus granulosus* larvae in laboratory animals. *Parasitology*. 1970;60(3):449-456.
4. Pourseif MM, Moghaddam G, Saeedi N, Barzegari A, Dehghani J, Omidi Y. Current status and future prospective of vaccine development against *Echinococcus granulosus*. *Biologicals*. 2018;51:1-11.
5. Heath DD, Jensen O, Lightowlers MW. Progress in control of hydatidosis using vaccination: a review of formulation and delivery of the vaccine and recommendations for practical use in control programs. *Acta Trop*. 2003;85(2):133-143.
6. Lightowlers MW, Jensen O, Fernandez E, et al. Vaccination trials in Australia and Argentina confirm the effectiveness of the EG95 hydatid vaccine in sheep. *Int J Parasitol*. 1999;29(4):531-534.
7. Pan W, Chen DS, Lu YJ, et al. Genetic diversity and phylogenetic analysis of EG95 sequences of *Echinococcus granulosus*: Implications for EG95 vaccine application. *Asian Pac J Trop Med*. 2017;10(5):524-527.
8. Álvarez-Rojas CA, Romig T, Lightowlers MW. *Echinococcus granulosus sensu lato* genotypes infecting humans--review of current knowledge.. *Int J Parasitol*. 2014;44(1):9-18.
9. Mahmoud A. New vaccines: challenges of discovery. *Microb Biotechnol*. 2016;9(5):549-552.
10. Larsen JE, Lund O, Nielsen M. Improved method for predicting linear B-cell epitopes. *Immunome Res*. 2006;2:2.
11. de Aluja AS, Villalobos NM, Nava G, et al. Therapeutic capacity of the synthetic peptide-based vaccine against *Taenia solium* cysticercosis in pigs. *Vaccine*. 2005;23(31):4062-4069.
12. Jezek J, El Ridi R, Salah M, et al. *Fasciola gigantica* cathepsin L proteinase-based synthetic peptide for immunodiagnosis and prevention of sheep fasciolosis.. *Biopolymers*. 2008;90(3):349-357.
13. Robinson K, Bellaby T, Chan WC, Wakelin D. High levels of protection induced by a 40-mer synthetic peptide vaccine against the intestinal nematode parasite *Trichinella spiralis*. *Immunology*. 1995;86(4):495-498.
14. Rojas-Caraballo J, López-Abán J, Pérez del Villar L, et al. In vitro and in vivo studies for assessing the immune response and protection-inducing ability conferred by *Fasciola hepatica*-derived synthetic peptides containing B- and T-cell epitopes. *PLoS One*. 2014;9(8):e105323.
15. Arnon R, Tarrab-Hazdai R, Steward M. A mimotope peptide-based vaccine against *Schistosoma mansoni*: synthesis and characterization. *Immunology*. 2000;101(4):555-62..
16. Woollard DJ, Gauci CG, Lightowlers MW. Synthetic peptides induce antibody against a host-protective antigen of *Echinococcus granulosus*. *Vaccine*. 1999;18(9-10):785-794.
17. Read AJ, Casey JL, Coley AM, et al. Isolation of antibodies specific to a single conformation-dependant antigenic determinant on the EG95 hydatid vaccine. *Vaccine*. 2009;27(7):1024-1031.
18. Hernández A, Nieto A. Induction of protective immunity against murine secondary hydatidosis. *Parasite Immunol*. 1994;16(10):537-544.
19. Míguez M, Baz A, Nieto A. Carbohydrates on the surface of *Echinococcus granulosus* protoscoleces are immunodominant in mice. *Parasite Immunol*. 1996;18(11):559-569.
20. Mourglia-Ettlin G, Miles S, Velasco-De-Andrés M, et al. The ectodomains of the lymphocyte scavenger receptors CD5 and CD6 interact with tegumental antigens from *Echinococcus granulosus sensu lato* and protect mice against secondary cystic echinococcosis. *PLoS Negl Trop Dis*. 2018;12(11):e0006891.
21. Cozzetto D, Minneci F, Currant H, Jonesa DT. FFPred 3: feature-based function prediction for all Gene Ontology domains. *Sci Rep*. 2016;6:31865.
22. Supek F, Bošnjak M, Škunca N, Šmuc T. REVIGO summarizes and visualizes long lists of gene ontology terms. *PLoS One*. 2011;6(7):e21800.
23. Almagro Armentero JJ, Sønderby CK, Sønderby SK, Nielsen H, Winther O. DeepLoc: prediction of protein subcellular localization using deep learning. *Bioinformatics*. 2017;33(21):3387-3395.
24. Magnan CN, Zeller M, Kayala MA, et al. High-throughput prediction of protein antigenicity using protein microarray data. *Bioinformatics*. 2010;26(23):2936-2943.
25. Cornejo-Granados F, Hurtado-Ramírez JM, Hernández-Pando R, Ochoa-Leyva A. Secret-AAR: a web server to assess the antigenic density of proteins and homology search against bacterial and parasite secretome proteins. *Genomics*. 2018.
26. Miles S, Navatta M, Dematteis S, Mourglia-Ettlin G. Identification of universal diagnostic peptide candidates for neglected tropical diseases caused by cestodes through the integration of multi-genome-wide analyses and immunoinformatic predictions. *Infect Gent Evol*. 2017;54:338-346.
27. Jespersen MC, Peters B, Nielsen M, Marcatili P. BepiPred-2.0: improving sequence-based B-cell epitope prediction using conformational epitopes. *Nucleic Acids Res*. 2017;45:W24-W29. https://doi.org/10.1093/nar/gkx352
28. Geourjon C, Deléage G. SOPMA: significant improvements in protein secondary structure prediction by consensus prediction from multiple alignments. *Comput Appl Biosci*. 1995;11(6):681-684.
29. Gupta S, Kapoor P, Chaudhary K, et al. In silico approach for predicting toxicity of peptides and proteins. *PLoS One*. 2013;8(9):e73957.
30. Saha S, Raghava GP. AlgPred: prediction of allergenic proteins and mapping of IgE epitopes. *Nucleic Acids Res*. 2006;34(web server issue):202-209.
31. Källberg M, Wang H, Wang S, et al. Template-based protein structure modeling using the RaptorX web server. *Nat Protoc*. 2012;7(8):1511-1522.
32. Guex N, Peitsch MC. SWISS-MODEL and the Swiss-PdbViewer: an environment for comparative protein modeling. *Electrophoresis*. 1997;18(15):2714-23..
33. Virginio VG, Monteiro KM, Drumond F, et al. Excretory/secretory products from in vitro-cultured *Echinococcus granulosus* protoscoleces. *Mol Biochem Parasitol*. 2012;183(1):15-22.

34. Cui SJ, Xu LL, Zhang T, et al. Proteomic characterization of larval and adult developmental stages in *Echinococcus granulosus* reveals novel insight into host-parasite interactions.. *J Proteomics*. 2013;84:158-175.
35. Ahn CS, Kim JG, Han X, Kang I, Kong Y. Comparison of *Echinococcus multilocularis* and *Echinococcus granulosus* hydatid fluid proteome provides molecular strategies for specialized host-parasite interactions. *Oncotarget*. 2017;8(57): 97009-97024..
36. Siles-Lucas M, Sánchez-Ovejero C, González-Sánchez M, et al. Isolation and characterization of exosomes derived from fertile sheep hydatid cysts. *Vet Parasitol*. 2017;236:22-33.
37. Lorenzatto KR, Kim K, Ntai I, et al. Top Down proteomics reveals mature proteoforms expressed in subcellular fractions of the *Echinococcus granulosus* preadult stage. *J Proteome Res*. 2015;14(11):4805-4814.
38. Zeghir-Bouteldja R, Polomé A, Bousbata S, Touil-Boukoffa C. Comparative proteome profiling of hydatid fluid from Algerian patients reveals cyst location-related variation in *Echinococcus granulosus*. *Acta Trop*. 2017;171:199-206.
39. dos Santos GB, Monteiro KM, da Silva ED, Battistella ME, Ferreira HB, Zaha A. Excretory/secretory products in the *Echinococcus granulosus* metacestode: is the intermediate host complacent with infection caused by the larval form of the parasite? *Int J Parasitol*. 2016;46(13-14):843-856.
40. Hidalgo C, García MP, Stoore C, et al. Proteomics analysis of *Echinococcus granulosus* protoscolex stage. *Vet Parasitol*. 2016;218:43-45.
41. Hancock DC, O'Reilly NJ. Synthetic peptides as antigens for antibody production. *Methods Mol Biol*. 2005;295:13-26.
42. Álvarez-Rojas CA, Gauci CG, Lightowlers MW. Antigenic differences between the EG95-related proteins from *Echinococcus granulosus* G1 and G6 genotypes: implications for vaccination. *Parasite Immunol*. 2013;35(2):99-102.
43. Carol H, Nieto A. A mucosal IgA response, but no systemic antibody response, is evoked by intranasal immunisation of dogs with Echinococcus granulosus surface antigens iscoms. *Vet Immunol Immunopathol*. 1998;65(1):29-41.
44. Valizadeh M, Haghpanah B, Badirzadeh A, Roointan E, Fallahi S, Raeghi S. Immunization of sheep against *Echinococcus granulosus* with protoscolex tegumental surface antigens. *Vet World*. 2017;10(8):854-858.
45. Li ZJ, Zhao W. Analysis of protoscoleces-specific antigens from *Echinococcus granulosus* with proteomics combined with Western blot.. *Biomed Environ Sci*. 2012;25(6):718-723.
46. Wang F, Ye B. In silico cloning and B/T cell epitope prediction of triosephosphate isomerase from *Echinococcus granulosus*. *Parasitol Res*. 2016;115(10):3991-3998.
47. Shi Z, Wang Y, Li Z, et al. Cloning, expression, and protective immunity in mice of a gene encoding the diagnostic antigen P-29 of *Echinococcus granulosus*. *Acta Biochim Biophys Sin*. 2009;41(1):79-85.
48. Wang H, Li Z, Gao F, et al. Immunoprotection of recombinant Eg.P29 against *Echinococcus granulosus* in sheep. *Vet Res Commun*. 2016;40:73-79.
49. Morseth DJ. Fine structure of the hydatid cyst and protoscolex of *Echinococcus granulosus*. *J Parasitol*. 1967;53(2):312-325.
50. Mourglia-Ettlin G, Cucher M, Arbildi P, Rosenzvit M, Dematteis S. Natural and induced antibodies contribute to differential susceptibility to secondary cystic echinococcosis of Balb/c and C57Bl/6 mice. *Immunobiology*. 2016;221(1):103-115.

How to cite this article: Miles S, Portela M, Cyrklaff M, et al. Combining proteomics and bioinformatics to explore novel tegumental antigens as vaccine candidates against *Echinococcus granulosus* infection. *J Cell Biochem*. 2019;1-17. https://doi.org/10.1002/jcb.28799

ARTÍCULO 3

Unraveling post-translational modifications in *Echinococcus granulosus sensu lato*.

Miles S, Magnone J, García-Luna J, Dematteis S, Mourglia-Ettlin G.

Acta Tropica

2022

doi: 10.1016/j.actatropica.2022.106410

Acta Tropica 230 (2022) 106410

Contents lists available at ScienceDirect

Acta Tropica

journal homepage: www.elsevier.com/locate/actatropica

Unraveling post-translational modifications in *Echinococcus granulosus sensu lato*

Sebastián Miles [a,b], Javier Magnone [a,b], Joaquín García-Luna [a,b], Sylvia Dematteis [a], Gustavo Mourglia-Ettlin [a,*]

[a] Área Inmunología, DEPBIO/IQB, Facultad de Química/Facultad de Ciencias, Universidad de la República, Montevideo, Uruguay
[b] Graduate Program in Chemistry, Facultad de Química, Universidad de la República, Uruguay

ARTICLE INFO

Keywords:
Post-translational modifications
Proteomics
Echinococcus granulosus
Mass spectrometry
PTMs
Platyhelminthes

ABSTRACT

Echinococcus granulosus sensu lato (s.l.) is the helminth parasite responsible for cystic echinococcosis, a neglected tropical disease currently affecting millions of people worldwide. Incomplete knowledge on the parasite biochemistry contributes, at least partially, to the limited development of useful biotechnological advances for the infection control. In this sense, little information is available regarding post-translational modifications (PTMs) occurring in *E. granulosus* s.l. proteins, which ultimately may affect the performance of biotechnological products to be developed. Therefore, we report here a proteomic analysis of the parasite PTMs identified through FindMod software applied to a set of tegumental proteins previously characterized by mass spectrometry (MALDI-TOF/TOF) analysis of protein spots from a 2D electrophoresis gel. Manual searches for already annotated proteins exhibiting such PTMs were also performed within proteome databases of *E. granulosus* s.l. and other platyhelminthes. In addition, key enzymes involved in PTMs modifications were searched for within *E. granulosus* s.l. proteome. Finally, the presence of selected PTMs was further confirmed by a high-resolution proteomic approach (nanoLC-MS/MS). A set of 22 different PTMs most likely to be present in the parasite was suggested, 9 of them with high confidence as they were identified in the same *m/z* fragment by both proteomic techniques (acetylation, deamidation, deamidation followed by methylation, mono- and di-hydroxylation, mono- and di-methylation, *S*-nitrosylation and phosphorylation). Interestingly, 5 PTMs were herein identified for the first time in *E. granulosus* s.l. proteins. Our results expand the scarcely studied topic of PTMs in platyhelminthes.

1. Introduction

Echinococcus granulosus sensu lato (s.l.) is a helminth parasite affecting both the human and livestock health, resulting in major impacts in public sanitary systems as well as in regional economies. Human incidence of this cosmopolitan infection, known as cystic echinococcosis, is estimated to be as high as one million people worldwide, accompanied by annual livestock production losses reaching USD 2 billion (Budke et al., 2006). Different control programs against *E. granulosus* s.l. infection have been applied, focusing on health education, anthelmintic drugs administration, and control/elimination of home slaughters. However, a deeper knowledge on *E. granulosus* s.l. biology is required for an optimal control of the infection (Craig et al., 2007). The complex life cycle of this parasite makes the study even more difficult, since it requires two different mammalian hosts with several parasite stages adapted to each one: while the adult worms infect the intestines of definitive hosts (canids), the metacestodes -or hydatid cysts- are found within intermediate hosts (domestic and wild ungulates, accidentally humans). Fertile hydatid cysts are filled with infective protoscoleces which can developed either into adult worms if ingested by definitive hosts, or into new hydatid cysts within intermediate hosts in case of cyst rupture (Thompson and Lymbery, 1995).

Development of novel or improved diagnostic tools and vaccination strategies against *E. granulosus* s.l. infection is not an easy task, and several important features of parasite proteins must be considered. For example, the natural presence of post-translational modifications (PTMs) is of outstanding importance for designing recombinant antigens. Since PTMs normally affect the biochemical properties of proteins through influencing their structure and/or function, the selection of expression systems with different abilities to generate PTMs is a highly

* Corresponding author.
E-mail address: gmourglia@higiene.edu.uy (G. Mourglia-Ettlin).

https://doi.org/10.1016/j.actatropica.2022.106410
Received 15 June 2021; Received in revised form 8 November 2021; Accepted 13 March 2022
Available online 15 March 2022

relevant bottleneck. Hundreds of PTMs have been characterized up-to-date in different organisms, which are mostly introduced into target proteins through specific enzymatic steps and/or pathways (Walsh, 2010). However, systematic analyses on PTMs within *E. granulosus* s.l. proteins are lacking, and only few works reporting glycosylation (Alvarez Errico et al., 2001; Khoo et al., 1997), acetylation (Virginio et al., 2012) and amidation (McVeigh et al., 2005) are available.

Herein we report novel proteomic evidence regarding PTMs present in tegumental proteins from *E. granulosus* s.l. protoscoleces. Additionally, deep literature revisions and database searches on PTMs-related key enzymes were also performed. Finally, we propose a list of different PTMs most likely to be present in tegumental proteins from *E. granulosus* s.l. protoscoleces.

2. Materials and methods

2.1. MALDI-TOF/TOF identification of PTMs

Putative PTMs present in *E. granulosus* s.l. tegumental proteins were analyzed by means of the free online software FindMod (Wilkins et al., 1999) using data from 63 MALDI-TOF/TOF spectra corresponding to 58 proteins previously obtained by our group after 2D-PAGE spots analysis (Miles et al., 2019). The same criteria as in MASCOT searches were applied: cysteine carbamidomethylation and methionine oxidation were set as variable modifications, mass deviation < 200 ppm, and allowance up to one trypsin miss-cut. Accordingly, a list of putative PTMs exhibiting suitable masses likely to be present in at least one non-matching *m/z* value was obtained. FindMod analyses considered a set of additional rules for each PTM, accessible through the software website (https://web.expasy.org/findmod/findmod_masses.html), such as the presence of specific amino acid(s) within the resulting peptide.

2.2. Database searches for PTMs and related enzymes

An exhaustive literature revision regarding PTMs present in *E. granulosus* s.l. proteins was performed, focusing on PTMs identifiable through FindMod software. UniProtKB database (last access on August 2020) was also manually searched for annotated proteins showing PTMs within *E. granulosus* s.l. and/or other platyhelminthes proteomes. A list of key enzymes usually involved in each analyzed PTM was obtained, and their presence was searched for within the *E. granulosus* s.l. proteome. Key enzymes as well as their generic terms are listed in Supplementary 1.

2.3. Confirmation of PTMs by nanoLC-MS/MS

A tegumental proteome obtained by nanoLC-MS/MS was further used for confirmation of the PTMs identified through FindMod software applied to MALDI-TOF/TOF spectra, as well as supported by previous annotations and/or identification of their corresponding key enzymes. Mass spectra previously acquired in an Orbitrap analyzer (CEQUIBIEM, CONICET, Buenos Aires, Argentina) (Miles et al., 2020) were analyzed by means of the software PatternLab for Proteomics 4 (Carvalho et al., 2016). The presence of empirically identified PTMs was analyzed over a custom database composed of the 58 proteins previously identified by MALDI-TOF/TOF (Miles et al., 2019). For each PTM, a search was performed including cysteine carbamidomethylation and methionine oxidation, as well as the corresponding PTMs, as variable modifications. In addition, up to one trypsin miss-cut was allowed.

3. Results

3.1. Identification of PTMs through MALDI-TOF/TOF

Mass spectra previously used to identify *E. granulosus* s.l. tegumental proteins were analyzed through FindMod software (Wilkins et al., 1999). Firstly, we obtained a list of PTMs derived from the subtraction of their masses in original non-matching *m/z* values resulting in new matching peptides within each protein. Then, non-enzymatic PTMs and cofactors were excluded from the list, as well as PTMs limited to phylogenetic kingdoms or taxonomies not including Platyhelminthes (e.g. bacteria, archaea, plants or chordata). Additionally, since no elongation factor was identified among the 58 proteins, PTMs associated with such proteins were not considered in further analyses. Results in Table 1 show the resulting 27 PTMs identified through FindMod software.

3.2. Analyses of potential PTMs in protein databases

Annotated proteins showing any of the FindMod-identified PTMs were searched for within UniProtKB database under *E. granulosus* s.l. species or Platyhelminthes phylum. Accordingly, 13 FindMod-identified PTMs were successfully identified: 5 of them within *E. granulosus* s.l. annotated proteins and 8 additional PTMs in other platyhelminthes (Table 1). In parallel, a list of key enzymes required to perform each of the identified PTMs (Supplementary 1) were searched for within *E. granulosus* s.l. protein database. In this regard, 22 key enzymes were directly identified within *E. granulosus* s.l. proteome, corresponding to all of the 13 PTMs found annotated within *E. granulosus* s.l. and/or platyhelminthes proteomes, as well as 9 additional FindMod-identified PTMs (Table 1).

3.3. Confirmation of PTMs through nanoLC-MS/MS

FindMod-identified PTMs that were additionally supported by either database annotations and/or identification of their corresponding key enzymes (22 PTMs in total), were further studied using mass spectra previously acquired by nanoLC-MS/MS (Orbitrap). Most PTMs (19 in total) found within the MALDI-TOF/TOF proteome were also observed by Orbitrap. Only ADP-ribosylation, amidation and glutathionylation were not identified in the nanoLC-MS/MS proteome (Fig. 1).

3.4. High confidence PTMs

PTMs identified in the same protein by both MALDI-TOF/TOF and nanoLC-MS/MS were further searched for within *m/z* peptide fragments. In this way, 9 PTMs (acetylation, deamidation, deamidation followed by methylation, mono- and di-hydroxylation, mono- and di-methylation, *S*-nitrosylation and phosphorylation) were identified in the same *m/z* values granting them a high presence confidence.

4. Discussion

Post-translational modifications (PTMs) in proteins from eukaryotic organisms are of outstanding relevance not only for studying basic aspects of their biology, but also for the development of potential biotechnological applications. In most helminth parasites, including *E. granulosus* s.l., such information is an almost unexplored topic. Available reports have shown only a small number of PTMs to be present in *E. granulosus* s.l. proteins, like amidation (McVeigh et al., 2005), N-terminal acetylation (Virginio et al., 2012) and *N*- and *O*-glycosylation (Alvarez Errico et al., 2001; Liu et al., 2002), mostly within the protoscolex stage. In addition, geranyl-geranylation (Spiliotis and Brehm, 2004) and *S*-farnesylation (Spiliotis et al., 2005) have been reported in the closely related cestode parasite *E. multilocularis*, while mannosylation was reported within *Taenia solium* proteins (Plancarte et al., 1999).

Identification of PTMs within a protein is a hard task, which turns really complex when trying to do it for a complex mixture of proteins. The present study aimed at obtaining empiric evidence regarding potential PTMs present in tegumental proteins of *E. granulosus* s.l. by means of mass spectrometry analysis. Spectra previously obtained for protein

Table 1
FindMod-identified PTMs. For each identified PTM, proteins annotated exhibiting them were searched for in the UniProtKB database of *E. granulosus* s.l. species and Platyhelminthes phylum. *"Abbreviation"* corresponds to the code used to identify each PTM by the software. Check mark (P) indicates that at least one protein was found exhibiting any identified PTMs, or a related key enzyme for that PTM in UniProtKB database.

Abbreviation	Post-translational Modification	Monoisotopic mass (Da)	Found in		Key enzyme in *E. granulosus* s.l.
			E. granulosus s.l.	Other Platyhelminthes	
ACET	Acetylation	42.0106	✓	✓	✓
ADP	ADP-ribosylation	541.0610	–	–	✓
AMID	Amidation	−0.9847	–	✓	✓
BROM	Bromination	77.9105	–	–	–
CSEA	Cysteine sulfenic acid (-SOH)	15.9949	✓	✓	✓
CSIA	Cysteine sulfinic acid (-SO_2H)	31.9898	–	–	–
CYSP	Cysteine persulfide	31.9721	–	✓	✓
DEAM	Deamidation	0.9840	–	–	✓
DEAME	Deamidation followed by a methylation	14.9997	–	–	✓
DIHYDR	Dihydroxylation	31.9898	–	–	✓
DIMETH	Dimethylation	28.0314	–	–	✓
FARN	*S*-farnesyl cysteine	204.1878	–	✓	✓
FORM	Formylation	27.9949	–	–	–
GERA	Geranyl-geranylation	272.2504	–	✓	✓
GGLU	Gamma-carboxyglutamic acid	43.9898	–	–	–
GLCN	*O*-GlcNac	203.0794	✓	✓	✓
GLUT	Glutathionylation	305.0681	–	–	✓
HYDR	Hydroxylation	15.9949	–	✓	✓
METH	Methylation	14.0157	–	✓	✓
MYRI	Myristoylation	210.1984	–	✓	✓
NTRY	*S*-Nitrosylation	28.9902	–	–	✓
OCTA	n-Octanoate	126.1044	–	–	✓
PALM	Palmitoylation	238.2297	–	✓	✓
PHOS	Phosphorylation	79.9663	✓	✓	✓
SULF	Sulfation	79.9568	✓	✓	✓
TRIMETH	Trimethylation	42.0470	–	–	✓
TRIMETK	N6,N6,N6-Trimethyl-5-hydroxylysine	59.0497	–	–	–

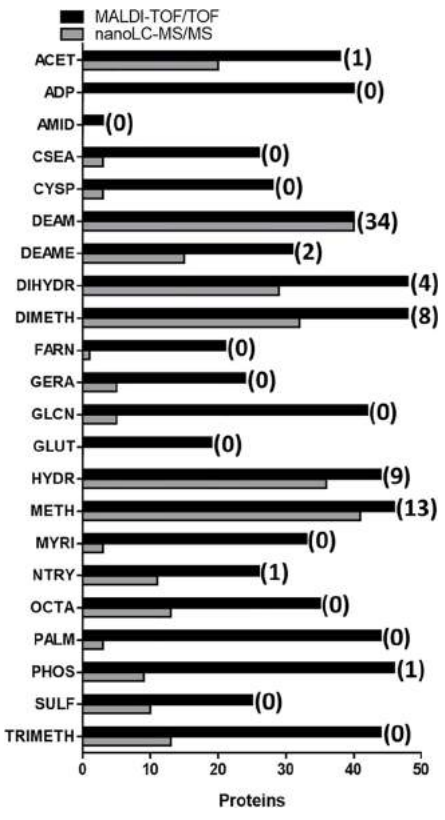

Fig. 1. Relative presence of PTMs according to the proteomic techinque. The number of proteins each PTM was identified in either by MALDI-TOF/TOF (black) or nanoLC-MS/MS (gray) is shown. The number of *m/z* fragments showing the same PTMs identified by both proteomic techniques is shown in brackets.

identification by MALDI-TOF/TOF (Miles et al., 2019) were firstly analyzed through FindMod software (Wilkins et al., 1999), resulting in a list of 27 putative mass-adequate PTMs (Table 1). Then, in deep searches within UniProtKB database were performed looking for annotated proteins with any of the 27 suggested PTMs. Interestingly, and since database entries are independent of published reports, some *E. granulosus* s.l. proteins were found to be annotated with PTMs not previously found in our literature revision. In fact, although 5 different PTMs were found within *E. granulosus* s.l. annotated proteins (Table 1), only 2 of them (acetylation and glycosylation) belonged to published reports (Alvarez Errico et al., 2001; Khoo et al., 1997; Virginio et al., 2012). UniProtKB database regarding *E. granulosus* s.l. is largely incomplete, and thus we further complemented the analysis by expanding the searches for PTMs-containing proteins in other members of the Platyhelminthes phylum. This strategy allowed us to identify 8 additional PTMs within annotated proteins: 3 of them (methylation, geranyl-geranylation and cysteine persulfide) in the closely related cestode *E. multilocularis*, and 5 in other more distant Platyhelminthes. Thus, 13 out of the 27 FindMod-identified PTMs received additional supporting data within annotated proteins in UniProtKB database (Table 1).

Since only PTMs introduced through specific enzymatic steps and/or pathways were analyzed, key enzymes involved in the list of 27 FindMod-identified PTMs were looked for within the *E. granulosus* s.l. proteome. Searches retrieved 22 key enzymes, including those required for the 13 PTMs previously identified in annotated proteins from *E. granulosus* s.l. and/or other platyhelminthes (Table 1). The key enzymes required for the 9 additional FindMod-identified PTMs were also found, even though no annotated protein carrying such PTMs was present within the phylum Platyhelminthes in the UniProtKB database. However, it is worth mentioning that 3 of them (di-hydroxylation, di-methylation and tri-methylation) can be considered as multiples of single modifications, which were successfully found within annotated proteins (Table 1). Taking into account both the proteomic evidence obtained through FindMod software as well as the supporting evidence found in the UniProtKB database, we proposed 22 PTMs to be most likely

present within *E. granulosus* s.l. tegumental proteins, even though additional PTMs might also occur. Furthermore, 19 of those PTMs were also identified within tegumental proteins by proteomic analysis with a higher-resolution mass spectrometry technique, as well as 9 PTMs were observed in the same protein-derived *m/z* fragment by both techniques, greatly increasing their likelihood to be present in that protein.

Both utilized proteomic techniques have intrinsic limitations, but the in-tandem combination of MALDI-TOF/TOF followed by nanoLC-MS/MS for PTMs identification complements each other. FindMod and PatternLab software use the monoisotopic mass of the PTM, and a set of rules (i.e. the presence of an amino acid the PTM can be bound to), to identify potential PTMs within a single *m/z* value. Unfortunately, some PTMs share such criteria. For example, molecular masses for phosphorylation (79.9663 Da) and sulfation (79.9568 Da) are not only similar, but also both can be bound to the same amino acid (tyrosine). This turns their discrimination into a hard task for the softwares, as both PTMs are predicted within the output of a single *m/z* value. For MALDI-TOF/TOF spectra, this limitation is even worse due to its lower resolution. However, the number of matching *m/z* values used to identify proteins through MALDI-TOF/TOF is higher than in nanoLC-MS/MS since only one 2D-PAGE spot is analyzed at a time, corresponding most likely to only one protein (Miles et al., 2019). On the other hand, in nanoLC-MS/MS the whole proteome is analyzed all together, and thus a lower number of matching *m/z* values are required to identify a single protein (Miles et al., 2020). Therefore, identification of PTMs firstly by MALDI-TOF/TOF usually results in a high number of *m/z* fragments potentially containing PTMs -and a greater number of possible PTMs- that can be validated in a second step by a higher resolution technique (nanoLC-MS/MS). Nevertheless, this is an exploratory analysis that might require further studies to corroborate the existence of the suggested PTMs.

Nine PTMs -mostly simple modifications- were identified in tegumental proteins with an extremely high confidence, as they were identified in the same *m/z* fragment by both techniques. Protein deamidation has been recently linked to apoptosis and other regulatory functions (Yang and Zubarev, 2010), which involves the removal of the amine functional group in the side chain of asparagine or glutamine. This modification can occur either spontaneously or in an enzyme driven way, affecting the reliability of its identification in proteomic studies, as in our cases (Miles et al., 2020, 2019). Protein (mono- and di-) hydroxylation and (mono- and di-) methylations are known to be common eukaryotic modifications involved in protein regulation and protein/-protein interaction (Biggar and Li, 2015; Zurlo et al., 2016), similar to phosphorylations, which were found to a lesser extend. Protein deamidation followed by methylation is a combination of those two previously mentioned modifications. Non-histone protein acetylation was also indentified which has been recently asociated with gene transcription and signal transduction functions (Xia et al., 2020), while the covalent attachment of a nitric oxide group to cysteine thiol (*S*-nitrosylation), has been assigned regulatory and signaling roles (Hess et al., 2005). In accordance to previous reports (Virginio et al., 2012), proteins exhibiting acetylation in the same *m/z* peptide were also observed by both techniques. Interestingly, 5 of these high confidence PTMs (deamidation, deamidation followed by methylation, *S*-nitrosylation, di-hydroxylation and di-methylation) have not been previously reported neither in *E. granulosus* s.l. nor in other platyhelminthes. Ten additional PTMs were identified by both techniques, 9 of which were previously reported in *E. granulosus* s.l. or other platyhelminthes, with key enzymes observed in *E. granulosus* s.l. proteome for all 10 of them.

Although the results reported here are sustained by bioinformatic as well as empiric evidence, relevant considerations must be taken into account. Firstly, taxonomic classification of *E. granulosus* is still a controversial issue which led to the division of *E. granulosus* into nine main genotypes (G1-G8, G10) (Nakao et al., 2010), being *E. granulosus* s.l. the name that includes them all. Secondly, UniProtKB data regarding *E. granulosus* s.l. is mostly composed of annotations from two G1-strain genome analyses (Tsai et al., 2013; Zheng et al., 2013), which exhibit important differences among them. Thirdly, *E. granulosus* s.l. exhibits a complex life cycle with several parasite stages, and here analyses were performed only over tegumental proteins from protoscoleces. Although these proteins could also be expressed in other stages, additional PTMs could be present throughout the parasite life cycle.

5. Conclusions

The present study provides proteomic evidence for potential PTMs present in tegumental proteins of *E. granulosus* s.l. protoscoleces. Supporting data on their occurrence was searched for within annotated proteins in UniProtKB database, as well as through identification of key enzymes involved in their generation within the *E. granulosus* s.l. proteome. We suggest 22 different PTMs most likely to be found within tegumental proteins, 9 of them identified with an extremely high confidence: acetylation, hydroxylation, methylation, phosphorylation, deamidation, deamidation followed by methylation, *S*-nitrosylation, di-hydroxylation and di-methylation. In addition, the last 5 PTMs were here identified for the first time in *E. granulosus* s.l. and in other platyhelminthes. Our results expand the scarcely studied topic of PTMs within members of the phylum Platyhelminthes, whether parasites or free-living.

Supplementary material

Supplementary 1. List of key enzymes required to perform each of the identified PTMs. Enzymes found within *E. granulosus* s.l. database are shown in bold letters. *"Abbreviation"* corresponds to the code used to identify each PTM by the software. Asterisks (*) indicate that not a single enzyme is known to perform the corresponding PTM or that an involved enzyme has not been described yet.

CRediT authorship contribution statement

Sebastián Miles: Conceptualization, Methodology, Investigation, Formal analysis, Writing – original draft. **Javier Magnone:** Investigation. **Joaquín García-Luna:** Investigation, Writing – review & editing. **Sylvia Dematteis:** Funding acquisition, Writing – review & editing. **Gustavo Mourglia-Ettlin:** Conceptualization, Funding acquisition, Writing – review & editing.

Declaration of Competing Interest

The authors declare that they have no known competing financial interests or personal relationship that could have appeared to influence the work reported in this paper.

Acknowledgments

Authors are grateful to Madelon Portela and Rosario Durán for the introduction to mass spectrometry data analysis and to the Unidad de Bioquímica y Proteómica Analíticas, Institut Pasteur de Montevideo (Uruguay) for the use of their MALDI-TOF/TOF. CSIC-Universidad de la República (Uruguay), PEDECIBA-Química (Uruguay) and ANII (Uruguay) are acknowledged for their general financial support.

Supplementary materials

Supplementary material associated with this article can be found, in the online version, at doi: 10.1016/j.actatropica.2022.106410.

References

Alvarez Errico, D., Medeiros, A., Míguez, M., Casaravilla, C., Malgor, R., Carmona, C., Nieto, A., Osinaga, E., 2001. O-glycosylation in Echinococcus granulosus:

identification and characterization of the carcinoma-associated Tn antigen. Exp. Parasitol. 98, 100–109. https://doi.org/10.1006/expr.2001.4620.
Biggar, K.K., Li, S.S.C., 2015. Non-histone protein methylation as a regulator of cellular signalling and function. Nat. Rev. Mol. Cell Biol. 16, 5–17. https://doi.org/10.1038/nrm3915.
Budke, C.M., Deplazes, P., Torgerson, P.R., 2006. Global socioeconomic impact of cystic echinococcosis. Emerg. Infect. Dis. 12, 296–303. https://doi.org/10.3201/eid1202.050499.
Carvalho, P.C., Lima, D.B., Leprevost, F.V., Santos, M.D.M., Fischer, J.S.G., Aquino, P.F., Moresco, J.J., Yates, J.R., Barbosa, V.C., 2016. Integrated analysis of shotgun proteomic data with PatternLab for proteomics 4.0. Nat. Protoc. 11, 102–117. https://doi.org/10.1038/nprot.2015.133.
Craig, P.S., McManus, D.P., Lightowlers, M.W., Chabalgoity, J.A., Garcia, H.H., Gavidia, C.M., Gilman, R.H., Gonzalez, A.E., Lorca, M., Naquira, C., Nieto, A., Schantz, P.M., 2007. Prevention and control of cystic echinococcosis. Lancet Infect. Dis. 7, 385–394. https://doi.org/10.1016/S1473-3099(07)70134-2.
Hess, D.T., Matsumoto, A., Kim, S.O., Marshall, H.E., Stamler, J.S., 2005. Protein S-nitrosylation: purview and parameters. Nat. Rev. Mol. Cell Biol. 6, 150–166. https://doi.org/10.1038/nrm1569.
Khoo, K.H., Nieto, A., Morris, H.R., Dell, A., 1997. Structural characterization of the N-glycans from Echinococcus granulosus hydatid cyst membrane and protoscoleces. Mol. Biochem. Parasitol. 86, 237–248. https://doi.org/10.1016/S0166-6851(97)00036-4.
Liu, B., Koo, G.C., Yap, E.H., Chua, K.L., Gan, Y.H., 2002. Model of differential susceptibility to mucosal Burkholderia pseudomallei infection. Infect. Immun. 70, 504–511. https://doi.org/10.1128/IAI.70.2.504-511.2002.
McVeigh, P., Kimber, M.J., Novozhilova, E., Day, T.A., 2005. Neuropeptide signalling systems in flatworms. Parasitology 131. https://doi.org/10.1017/S0031182005008851.
Miles, S., Portela, M., Cyrklaff, M., Ancarola, M.E., Frischknecht, F., Durán, R., Dematteis, S., Mourglia-Ettlin, G., 2019. Combining proteomics and bioinformatics to explore novel tegumental antigens as vaccine candidates against Echinococcus granulosus infection. J. Cell. Biochem. 120, 15320–15336. https://doi.org/10.1002/jcb.28799.
Miles, S., Velasco-de-Andrés, M., Lozano, F., Mourglia-Ettlin, G., 2020. Interactome analysis of CD5 and CD6 ectodomains with tegumental antigens from the helminth parasite Echinococcus granulosus sensu lato. Int. J. Biol. Macromol. 164, 3718–3728. https://doi.org/10.1016/j.ijbiomac.2020.08.219.
Nakao, M., Yanagida, T., Okamoto, M., Knapp, J., Nkouawa, A., Sako, Y., Ito, A., 2010. State-of-the-art Echinococcus and Taenia: phylogenetic taxonomy of human-pathogenic tapeworms and its application to molecular diagnosis. Infect. Genet. Evol. 10, 444–452. https://doi.org/10.1016/j.meegid.2010.01.011.
Plancarte, A., Hirota, C., Martínez-Ocaña, J., Mendoza-Hernández, G., Zenteno, E., Flisser, A., 1999. Characterization of GP39-42 and GP24 antigens from Taena solium cysticerci and of their antigenic GP10 subunit. Parasitol. Res. 85, 680–684. https://doi.org/10.1007/s004360050615.
Spiliotis, M., Brehm, K., 2004. Echinococcus multilocularis: identification and molecular characterization of a Ral-like small GTP-binding protein. Exp. Parasitol. 107, 163–172. https://doi.org/10.1016/j.exppara.2004.05.006.
Spiliotis, M., Tappe, D., Brückner, S., Mösch, H.-.U., Brehm, K., 2005. Molecular cloning and characterization of Ras- and Raf-homologues from the fox-tapeworm Echinococcus multilocularis. Mol. Biochem. Parasitol. 139, 225–237. https://doi.org/10.1016/j.molbiopara.2004.11.013.
Thompson, R., Lymbery, A., 1995. Echinococcus and Hydatid Disease. CAB International, Wallingford.
Tsai, I.J., Zarowiecki, M., Holroyd, N., Garciarrubio, A., Sanchez-Flores, A., Brooks, K.L., Tracey, A., Bobes, R.J., Fragoso, G., Sciutto, E., Aslett, M., Beasley, H., Bennett, H.M., Cai, J., Camicia, F., Clark, R., Cucher, M., De Silva, N., Day, T.A., Deplazes, P., Estrada, K., Fernández, C., Holland, P.W.H., Hou, J., Hu, S., Huckvale, T., Hung, S.S., Kamenetzky, L., Keane, J.A., Kiss, F., Koziol, U., Lambert, O., Liu, K., Luo, X., Luo, Y., MacChiaroli, N., Nichol, S., Paps, J., Parkinson, J., Pouchkina-Stantcheva, N., Riddiford, N., Rosenzvit, M., Salinas, G., Wasmuth, J.D., Zamanian, M., Zheng, Y., Cai, X., Soberon, X., Olson, P.D., Laclette, J.P., Brehm, K., Berriman, M., Morett, E., Portillo, T., Jose, M.V., Carrero, J.C., Larralde, C., Morales-Montor, J., Limon-Lason, J., Cevallos, M.A., Gonzalez, V., Ochoa-Leyva, A., Landa, A., Jimenez, L., Valdes, V., 2013. The genomes of four tapeworm species reveal adaptations to parasitism. Nature 496, 57–63. https://doi.org/10.1038/nature12031.
Virginio, V.G., Monteiro, K.M., Drumond, F., De Carvalho, M.O., Vargas, D.M., Zaha, A., Ferreira, H.B., 2012. Excretory/secretory products from in vitro-cultured Echinococcus granulosus protoscoleces. Mol. Biochem. Parasitol. 183, 15–22. https://doi.org/10.1016/j.molbiopara.2012.01.001.
Walsh, G., 2010. Post-translational modifications of protein biopharmaceuticals. Drug Discov. Today 15, 773–780. https://doi.org/10.1016/j.drudis.2010.06.009.
Wilkins, M.R., Gasteiger, E., Gooley, A.A., Herbert, B.R., Molloy, M.P., Binz, P.A., Ou, K., Sanchez, J.C., Bairoch, A., Williams, K.L., Hochstrasser, D.F., 1999. High-throughput mass spectrometric discovery of protein post-translational modifications. J. Mol. Biol. 289, 645–657. https://doi.org/10.1006/jmbi.1999.2794.
Xia, C., Tao, Y., Li, M., Che, T., Qu, J., 2020. Protein acetylation and deacetylation: an important regulatory modification in gene transcription (Review). Exp. Ther. Med. 2923–2940. https://doi.org/10.3892/etm.2020.9073.
Yang, H., Zubarev, R.A., 2010. Mass spectrometric analysis of asparagine deamidation and aspartate isomerization in polypeptides. Electrophoresis 31, 1764–1772. https://doi.org/10.1002/elps.201000027.
Zheng, H., Zhang, W., Zhang, L., Zhang, Z., Li, J., Lu, G., Zhu, Y., Wang, Y., Huang, Y., Liu, J., Kang, H., Chen, J., Wang, L., Chen, A., Yu, S., Gao, Z., Jin, L., Gu, W., Wang, Z., Zhao, L., Shi, B., Wen, H., Lin, R., Jones, M.K., Brejova, B., Vinar, T., Zhao, G., McManus, D.P., Chen, Z., Zhou, Y., Wang, S., 2013. The genome of the hydatid tapeworm Echinococcus granulosus. Nat. Genet. 45, 1168–1175. https://doi.org/10.1038/ng.2757.
Zurlo, G., Guo, J., Takada, M., Wei, W., Zhang, Q., 2016. New insights into protein hydroxylation and its important role in human diseases. Biochim. Biophys. Acta - Rev. Cancer 1866, 208–220. https://doi.org/10.1016/j.bbcan.2016.09.004.

ARTÍCULO 4

Linking murine resistance to secondary cystic echinococcosis with antibody responses targeting *Echinococcus granulosus* tegumental antigens.

Miles S, Magnone J, Cyrklaff M, Arbildi P, Frischknecht F, Dematteis S, Mourglia-Ettlin G.

Immunobiology

2020

doi: 10.1016/j.imbio.2020.151916

Immunobiology 225 (2020) 151916

Contents lists available at ScienceDirect

Immunobiology

journal homepage: www.elsevier.com/locate/imbio

Linking murine resistance to secondary cystic echinococcosis with antibody responses targeting *Echinococcus granulosus* tegumental antigens

Sebastián Miles[a], Javier Magnone[a], Marek Cyrklaff[b], Paula Arbildi[a], Friedrich Frischknecht[b], Sylvia Dematteis[a], Gustavo Mourglia-Ettlin[a,*]

[a] Área Inmunología, DEPBIO/IQB - Facultad de Química/Facultad de Ciencias, Universidad de la República, Montevideo, Uruguay
[b] Integrative Parasitology, Center for Infectious Diseases, Heidelberg University, Heidelberg, Germany

ARTICLE INFO

Keywords:
Echinococcus granulosus
Antibodies
Susceptibility
Tegument
immunoTEM
Proteomics
Immunoinformatics

ABSTRACT

Successful establishment of a parasite infection depends partially on the host intrinsic susceptibility to the pathogen. In cystic echinococcosis (CE), a zoonotic disease caused by the cestode parasite *Echinococcus granulosus*, the infection outcome in the murine model of secondary CE varies according to the mouse strain used. In this regard, intrinsic differences in susceptibility to the infection were previously reported for Balb/c and C57Bl/6 mice, being C57Bl/6 animals less permissive to secondary CE. Induction of parasite-specific antibodies has been suggested to play relevant roles in such susceptibility/resistance phenomena. Here, we report an in deep comparison of antibody responses induced in both mouse strains. Firstly, only C57Bl/6 mice were shown to induce specific-antibodies with efficient anti-parasite activities during early secondary CE. Then, through ImmunoTEM and Serological Proteome Analysis (SERPA), an evaluation of specific antibody responses targeting parasite tegumental antigens was performed. Both strategies showed that infected C57Bl/6 mice -unlike Balb/c animals- narrowed their IgG recognition repertoire against tegumental antigens, targeting fewer but potentially more relevant parasite components. In this sense, tegumental antigens recognition between Balb/c and C57Bl/6 mice, either by natural and/or induced antibodies, was analyzed through SERPA and MALDI-TOF/TOF studies. A total of 13 differentially recognized proteins (DRPs) uniquely targeted by antibodies from C57Bl/6 mice were successfully identified, wherein a subset of 7 DRPs were only recognized by infection-induced antibodies, suggesting their potential as natural protective antigens. In this regard, immunoinformatic analyses showed that such DRPs exhibited higher numbers of possible T cell epitopes towards the H-2-IA^b haplotype, which is present in C57Bl/6 mice but absent in Balb/c animals. In summary, our results showed that the genetic predisposition to generate better T-dependent antibody responses against particular tegumental antigens might be a key factor influencing host susceptibility in the murine model of secondary CE.

1. Introduction

Animal models are essential for infectious disease research, and murine models are the most used due to their advantages in small size, ease of handling, relative low cost and availability of outbred stocks and inbred strains which can be genetically modified with relative ease. In addition, the immune system of mice is well characterized and similar to the human immune system. Also, mice are experimentally susceptible to many infections by human pathogens (Colby et al., 2017). However, differences in susceptibility to numerous diseases among mouse strains have been extensively reported. For example, between the most used mouse strains Balb/c and C57Bl/6, several differences have been reported in autoimmunity (Matsuo et al., 2019; Qiao et al., 2010) and cancer models (Díaz-Zaragoza et al., 2017; Maronpot, 2009; Ponnaiya et al., 2006), as well as in the outcome of viral (Henderson et al., 2015; Kulcsar et al., 2015; Xiang et al., 2016), bacterial (Cheers et al., 1978; Chiodini and Buergelt, 1993; Fornefett et al., 2018; Liu et al., 2002), protozoan (Ferreira et al., 2018; Mols-Vorstermans et al., 2013), and helminth infections (Anthony et al., 2007; Mourglia-ettlin et al., 2016a; Pereira et al., 2016; Zhang et al., 2005). Among the known differences in immune responses between Balb/c and C57Bl/6 strains, cellular, cytokine and humoral responses are well characterized for some diseases. In this sense, the recruitment of immune-cells after infection differs greatly between strains depending on the pathogen species and the site of infection (Canivet et al., 2019; Jiang et al., 2010; Zeng et al., 2016), and differences in cytokine responses have also been

* Corresponding author.
E-mail address: gmourglia@higiene.edu.uy (G. Mourglia-Ettlin).

https://doi.org/10.1016/j.imbio.2020.151916
Received 18 November 2019; Received in revised form 4 February 2020; Accepted 18 February 2020
Available online 19 February 2020

observed (Jovicic et al., 2015; Schulte et al., 2008; Watanabe et al., 2004). In addition, differences in antibody production have also been reported between Balb/c and C57Bl/6 mice, not only in intensities and isotype profiles, but also in their specificities and production kinetics (Fornefett et al., 2018; Mourglia-ettlin et al., 2016a; Vlkova et al., 2012). Furthermore, MHC-II haplotypes in each mouse strain are different (Sofron et al., 2016) influencing antigen presentation and ultimately the effector responses derived by that process.

Helminthiases are among the most common infections worldwide, affecting the poorest and most deprived communities, mostly distributed in tropical and sub-tropical areas. According to the WHO report on Neglected Tropical Diseases (WHO, 2017), more than 1.5 billion people -roughly 24 % of the world population- are infected with at least one helminth species. Although canonical responses to parasitic worms have always been associated with a Th2-mediated immunity -characterized by high IL-4, IL-5 and IL-13 production by $CD4^+$ T cells and induction of IgE antibodies (Anthony et al., 2007)- such responses are not necessarily the best to limit infection establishment by any helminth parasite. For example, in the case of the hookworm model *Heligmosomoides polygyrus*, a highly polarized Th2-type response mediates stress resulting in worm expulsion, and for *Schistosoma mansoni* Th2 responses down-regulate otherwise pathological Th1 responses (Anthony et al., 2007). However, in *Fasciola hepatica* infection, early Th1 responses are involved in host protection (Zhang et al., 2005).

Among the Neglected Tropical Diseases listed by the WHO, cystic echinococcosis (CE) is a zoonotic disease caused by the parasite *Echinococcus granulosus*, a cestode with a complex life cycle. Definitive hosts are mainly dogs which harbor the adult parasite in their intestines and through feces release eggs containing oncospheres. Once ingested by potential intermediate hosts (*e.g.* farm mammals and wild ungulates), oncospheres develop into fluid-filled cysts known as hydatid cysts -mainly located in liver and lungs- able to produce protoscoleces (PSC). Humans act as accidental intermediate hosts carrying chronic infections for many years with varied symptoms depending on cyst location and the pressure it exerts on surrounding tissues and organs. Due to biosafety and easy-to-use issues, most studies on *E. granulosus* are based on the murine model of secondary infection, which induce CE in a non-natural intermediate host through intraperitoneal inoculation of PSC (Heath, 1970). This model has been widely used to study the biology of *E. granulosus* infection (Barrios et al., 2019; Baz et al., 2006; Cucher et al., 2013; Dematteis et al., 2003, 1999; Mourglia-Ettlin et al., 2011), as well as to test new chemotherapeutics or therapeutical protocols (Breijo et al., 2011; Ceballos et al., 2010; Cumino et al., 2012), vaccine candidates (Burgu et al., 2007; Hashemitabar et al., 2005; Hernández and Nieto, 1994), and diagnostic or follow-up tools (Denegri et al., 1995; Ferragut et al., 1998; Mamuti et al., 2002). However, several mouse strains have been indistinctly used for the study of experimental secondary CE. In this regard, we previously reported intrinsic differences in susceptibility to the infection between Balb/c and C57Bl/6 mice, with Balb/c animals being more permissive than C57Bl/6. Furthermore, we reported relevant differences in the role of natural antibodies in the differential susceptibility to secondary CE (Mourglia-ettlin et al., 2016a). Our present work constitutes an in-deep analysis of the antibody specificity profile in each mouse strain followed by the identification of natural potentially protective antigens against CE.

2. Materials and methods

2.1. Ethics statement

Animal experiments were performed in compliance with *Comisión Honoraria de Experimentación Animal* (CHEA) from *Universidad de la República*, according to the Canadian Guidelines on Animal Care and the National Uruguayan Legislation Nº 18.611. Experimental protocols were approved by the Ethics Committee of *Facultad de Química* (*Universidad de la República*) and were given the approval number 101900-000884-17.

2.2. Parasites and antigens

E. granulosus PSC obtained by aseptic puncture of fertile bovine hydatid cysts from Uruguayan abattoirs were extensively washed with phosphate buffered saline (PBS) pH 7.2 containing gentamicin (40 μg/mL), and parasites viability was determined according to Dematteis et al. (1999). Only those batches with a viability ≥90 % were used for experimental infections. Protoscoleces somatic antigens (PSA) were obtained by ultrasonic disruption of PSC according to Miguez et al. (1996), and Protoscoleces tegumental antigens (PSEx) were extracted from viable PSC (viability ≥80 %) using a solution of MEGA-10 (1% w/v), EDTA (5 mM) and PMSF (2 mM) in PBS according to Hernández and Nieto (1994). Both antigenic fractions (PSA and PSEx) were characterized in terms of their lipid, protein and carbohydrate contents according to Miguez et al. (1996), and stored at −20 °C until used.

2.3. Mice, infections and immunizations

Female Balb/c and C57Bl/6 mice were obtained from DILAVE-MGAP (Uruguay) and housed at the animal facility of *Instituto de Higiene* (Montevideo, Uruguay). Experimental infections and immunization protocols were performed with 6–8 weeks old mice. For infections, mice (n = 5–8) from both strains were inoculated by the intraperitoneal ip route with 200 μL of a PBS suspension containing 2000 viable PSC. At day 21 post-infection (pi), all mice were bled and euthanized. Sera were obtained by regular means and store at −80 °C until use. For immunizations, mice (n = 5–8) from both strains were inoculated ip with 200 μL of PBS containing 100 μg of PSEx proteins twice: day 0 and 10. No adjuvants were used. At day 17 post-priming, all mice were bled and euthanized. Sera were obtained by regular means and store at −80 °C until use. Either for "infection" or "immunization" protocols, groups of mice (n = 5–8) from both strains were ip inoculated with 200 μL of sterile PBS, and used as control mice ("naïve"). For *in vitro* assays of PSC killing, naïve mice (n = 3–5) from both strains were bled and euthanized, and sera were stored at −80 °C (for a maximum of 3 days) until their use as a source of fresh naïve sera.

2.4. Antibody titrations and avidity studies

Titers of natural and induced antibodies in individualized serum samples, or pools when indicated, were measured by ELISA. Briefly, 96-wells microtiter plates were coated with 100 μL/well of PBS containing 1 μg of either PSA or PSEx and incubated ON at 4 °C. After blocking with PBS-BSA (1% w/v) during 1 h at RT, samples were dispensed at non-saturating dilutions, incubated ON at 4 °C, and specific IgM, IgA, IgG, IgE, IgG1, IgG2a/c, IgG2b and/or IgG3 were determined using appropriate goat anti-mouse antibodies labeled with peroxidase. TMB (3,3′,5,5′-tetramethylbenzidine) was used as the chromogenic substrate, and absorbance values were recorded at 450 nm after adding H_2SO_4. Then, when possible, the avidity index of PSEx-specific antibodies was determined according to Pullen et al. (1986) with some modifications. Briefly, samples were dispensed in duplicates at non-saturating dilutions on PSEx-coated and BSA-blocked ELISA plates, and incubated as described above. Then, 100 μL/well of PBS or a 3.0 M solution of KSCN in PBS were added to one of the duplicates, followed by an incubation during 30 min at RT. After washing both solutions, the ELISA protocol was performed as previously described. Avidity indexes were calculated as the percentage of absorbance in the KSCN-treated well *vs.* the PBS control.

2.5. PSC killing activity

Firstly, γ-globulins from pooled sera obtained either from naïve, infected or PSEx-immunized Balb/c or C57Bl/6 mice (n = 5–8) were

purified by precipitation with NH_4SO_4 at 50 % (Hebert, 1974). Then, their PSC killing activities were assessed *in vitro* according to (Mourglia-ettlin et al., 2016a) with some modifications. Briefly, viable PSC were incubated during 4 h at 37 °C with constant shaking in a 100 µL total volume containing fresh serum from naïve Balb/c or C57Bl/6 mice supplemented -or not- with purified strain-matched γ-globulins. Roughly 50 viable PSC suspended in gentamicin-containing PBS (40 µg/mL) were dispensed in every well of a 96-wells microtiter plate, and fresh serum was immediately added (final dilution 1:3). Then, purified γ-globulins were added (final dilution 1:10 respect to the starting concentration in the original serum), or an equal volume of PBS. After incubation, viability of PSC was determined according to Dematteis et al. (1999), and PSC killing activity was expressed as the fold increase of non-viable PSC percentage respect to control PSC incubated in fresh naïve serum plus PBS.

2.6. Transmission Electron microscopy and immuno-labelling

Freshly obtained PSC were washed and fixed with a solution of glutaraldehyde 2.5 % (v/v) and paraformaldehyde 2% (v/v) in PBS, and stored at 4 °C until use. PSC samples were high pressure frozen and dehydrated with acetone by freeze substitution for 24 h at slowly increasing temperatures (from −190 °C to 25 °C). Then, samples were embedded in spur resin and polymerized for at least 48 h at 60 °C. Ultrathin sections of 70 nm were obtained by sectioning PSC with a Leica EM UC6 ultra-microtome using a diamond knife. Sections were collected on electron microscopy grids, blocked with PBS containing BSA 1.5 % (w/v) and FSG 0.1 % (w/v) for 30 min at RT, and treated with a solution of glycine 10 % (w/v) in PBS for 1 h at RT. Then, grids were incubated with appropriate pools of sera diluted in blocking buffer (1:10) for 2 h at RT. After 5 washes with blocking buffer, grids were incubated with goat-anti-mouse antibodies labeled with gold nanoparticles (mix of 5, 10 and 15 nm) for 1 h at RT. Then, 5 washes with blocking buffer followed by 5 washes in PBS were performed, and the grids were fixed in a solution of PBS containing glutaraldehyde 1% (v/v) for 5 min. Finally, the grids were washed 10 times in ultrapure H_2O and examined with a Zeiss 10C transmission electron microscope. No counterstained using led citrate and uranyl acetate was performed.

2.7. Two-dimension SDS-PAGE

PSEx was resolved through 2D SDS-PAGE according to Mourglia-Ettlin et al. (2018b). Briefly, 300 µg of PSEx was precipitated ON at −20 °C in 300 µL ice-cold acetone containing trichloracetic acid 20 % (v/v) and dithiothreitol (DTT) 0.07 % (w/v). After centrifugation, the supernatant was discarded and 300 µL of ice-cold acetone containing dimethyl-sulfoxide 20 % (v/v) and DTT 0.07 % (w/v) was added and incubated for 1 h at −20 °C. Then, samples were centrifuged, the supernatants discarded, and 300 µL ice-cold acetone containing DTT 0.07 % (w/v) was added. This step was repeated twice. Finally, the pellet was lyophilized, rehydrated in immobilized pH gradient (IPG) buffer and frozen at −80 °C for 24 h. For the first dimension, 7 cm linear pH gradient (pH 3–10) Immobilie DryStrips were re-hydrated with the sample in IPG buffer and run on an IPGphore isoelectric focusing system (9.5 h run and a total of 35.5 KV/h) and stored at −80 °C until use. Strips were then soaked for 15 min in equilibration buffer (Tris−HCl 50 mM pH 8.8, urea 6 M, glycerol 30 % (v/v), SDS 2% (w/v), and traces of bromphenol blue) containing DTT 10 mg/mL, further soaked for 15 min in equilibration buffer containing iodoacetamide 25 mg/mL, and finally sealed to acrylamide gel 10 % (w/v) using agarose 0.5 % (w/v) in standard Tris-glycine electrophoresis buffer. Second dimension was run at 50 V for the first 15 min and then raised to 150 V until ending. Finally, replicates of 2D SDS-PAGE gels were subjected either to mass-spec compatible silver nitrate staining or to electro-transference to PVDF membranes for Western blotting.

2.8. Serological proteome analysis

A strategy of Serological Proteome Analysis (SERPA) was followed to identify PSEx antigens uniquely recognized by antibodies from C57Bl/6 mice (henceforth Differentially Recognized Proteins, DRP). SERPA was performed on Western blots over 2D SDS-PAGE followed by mass spectrometry protein identification. To that end, electro-transferred PVDF membranes from 2D SDS-PAGE were blocked with PBS containing BSA 1% (w/v) for 2 h at RT. Then, membranes were incubated with appropriately diluted pooled sera (1:100 and 1:500 for sera from naïve and infected mice, respectively) ON at 4 °C. Membranes were then incubated for 1 h at 37 °C in a PBS solution containing BSA 0.1 % (w/v) and Tween-20 0.05 % (v/v) with specific goat-anti-mouse antibodies labeled with peroxidase (sera from naïve mice were analyzed only for IgM, IgA, IgG and IgE; meanwhile sera from infected mice was additionally studied for every IgG subclass). Finally, membranes were extensively washed with PBS containing Tween-20 0.05 % (v/v), and blots were developed by chemo-luminescence SuperSignal West Pico Substrate (ThermoScientific) in a G-Box equipment (Syngene). Then, DRPs were identified by mass spectrometry. To that end, DRPs -either from naïve or infected samples- were manually back-mapped on gels, spots were collected, and mass spectrometry identification through MALDI-TOF/TOF was applied at the Proteomic Facility of Pasteur Institut of Montevideo (Uruguay). Briefly, spots were excised, faded and tryptic digestions were performed using sequencing-grade modified trypsin. After gel extraction into acetonitrile 60 % (v/v) containing trifluoro-acetic acid 0.1 % (v/v), acetonitrile was removed by speed vacuum. Peptide samples were then combined with an equal volume of matrix, spotted onto a MALDI sample plate, and allowed to dry at RT. Mass spectra were acquired on a 4800 MALDI-TOF/TOF Mass Analyzer operating in the positive ion reflector mode. Protein identifications were performed using an in-house Mascot v.2.3 search engine by searching a custom database that includes the full proteome of *E. granulosus sensu lato* and *E. multilocularis*, composed of 20,787 sequences (10,310,548 residues) obtained from the Sanger Helminth Database. Applied searching criteria were cysteine carbamidomethylation and methionine oxidation as variable modification, and mass deviation < 200 ppm with a peptide fragment tolerance of 0.45 Da. Scores > 56 were considered significant ($P < 0.05$).

2.9. Bioinformatics

Each DRP from the "Only induced" set was analyzed through several bio- and immuno-informatic algorithms according to Miles et al. (2019). To that end, antigenicity was assessed by predictions with ANTIGENpro software (Magnan et al., 2010), considering proteins with scores ≥0.5 as antigenic (Miles et al., 2017). Also, the Abundance of Antigenic Regions (AAR) was predicted using the webserver Secret-AAR (Cornejo-Granados et al., 2018). Then, we obtained a "Uniqueness Score" (US) of each protein by BlastP, which is defined as the product between "Query coverage" and "Identity percentages" of the highest Max score match against all non-helminth proteins on the non-redundant NCBI database (excluding Cestoda, Trematoda and Nematoda taxonomy). US values of 0.5-0.8 correspond to "highly divergent proteins", while US values ≤0.5 identified "unique proteins" (Miles et al., 2019). Finally, each DRP was searched for the presence of T-cell epitopes potentially presented by specific haplotypes of MHC-II molecules only present in Balb/c (H-2-IA^d) or C57Bl/6 (H-2-IA^b) mice. For each DRP, the binding affinity of every possible 15-mer peptide was predicted against both haplotypes using the algorithm NetMHCII (version 2.2) (Nielsen and Lund, 2009). Every 15-mer was categorized according to its binding affinity into 3 categories: "Strong Binding" (SB, $IC_{50} \leq 50$ nM), "Weak Binding" (WB, $IC_{50} \leq 500$ nM), and "No Binding" (NB, $IC_{50} > 500$ nM).

2.10. Statistics

Comparisons when only one parameter was analyzed at a time were assessed either by non-parametric Mann-Whitney-Wilcoxon *U* test or Student t-test; meanwhile when more than one parameter was analyzed at a time a 2-way ANOVA test was applied. In all cases, differences were regarded as significant with $p < 0.05$.

3. Results

3.1. Infected C57Bl/6 mice - unlike Balb/c - induce antibodies with efficient anti-parasite activities

Differences in the outcome of secondary CE in Balb/c and C57Bl/6 mice have already been observed by our group (Mourglia-Ettlin et al., 2016a). Additionally, we reported differences in the anti-parasite activity of their natural cross-reacting antibodies (Mourglia-Ettlin et al., 2016a), as well as in their cytokine production profiles and local recruitment of immune-related cells (Mourglia-Ettlin et al., 2016b). Further studies were performed in the present work, mainly exploring the protective roles of the early-induced antibodies in infected Balb/c and C57Bl/6 mice. Firstly, we analyzed the anti-parasite activity of serum γ-globulins purified from both mouse strains, either from naïve or infected animals. Results in Fig. 1.A. show the assessment of their *in vitro* PSC killing activities expressed as the fold-change of non-viable PSC percentage incubated with fresh sera from naïve mice supplemented with purified γ-globulins. No differences in PSC killing enhancement was observed between purified γ-globulins from naïve or infected Balb/c mice. However, γ-globulins from infected C57Bl/6 animals significantly increased the PSC killing activity compared to their homologous naïve controls by about 2.5 fold (Fig. 1.A.). Then, we characterized the global anti-parasite IgG response in both mouse strains by their titration using PSA-coated ELISA plates. Interestingly, significant differences between mouse strains were already observed in naïve mice, yet no differences in PSA-specific IgG titers were observed in the serum of infected animals (Fig. 1.B.). Therefore, subtler differences in antibody responses developed by infected C57Bl/6 mice, unlike by Balb/c, might explain the PSC killing enhancement uniquely observed by γ-globulins from infected C57Bl/6 animals.

3.2. Antibody responses targeting parasite tegumental antigens differ in Balb/c and C57Bl/6 mice

In order to understand the subtle differences in antibody responses developed by infected Balb/c and C57Bl/6 mice, we further analyzed whether parasite structures are differentially recognized by antibodies from each mouse strain. To that end, a strategy of transmission electron microscopy and gold-nanoparticles specific immuno-labelling (immunoTEM) was followed. Ultrathin sections of fixed PSC were incubated with pooled sera from either naïve or infected Balb/c and C57Bl/6 mice, and stained with gold nanoparticle-linked goat-anti-mouse-IgG antibodies. Several ImmunoTEM images from different PSC structures were obtained, gold marks were counted, and mark densities (marks/μm^2) were calculated. Marks mostly occurred near the PSC surface, and therefore, analyses were divided into three parasite zones: *(i)* Gx (Glycocalyx, the outermost layer mainly composed of carbohydrates), *(ii)* Tg (Tegument, the external cellular syncytial layer), and *(iii)* In (Inner structures, any other PSC structures than glycocalyx and tegument). For each serum and mouse strain condition, six immunoTEM images were counted, and representative images comparing them are shown in Fig. 2A. This showed, firstly, that mark densities were highest in Tg, followed by In and weakest in Gx (Fig. 2.A. and B.). Secondly, Balb/c sera exhibited generally higher mark densities than C57Bl/6 sera, either from naïve or infected mice. Thirdly, mark densities in Tg or In increased for Balb/c sera when comparing infected *vs.* naïve animals, while the opposite situation was observed for C57Bl/6 samples (Fig. 2.B.).

After showing that antibody responses targeting Tg antigens might associate with differential susceptibility to secondary CE in Balb/c and C57Bl/6 mice, we further obtained an antigenic fraction of PSC -termed PSEx- mainly composed of such antigens (Miles et al., 2019), and analyzed the Tg-specific antibody profiles in naïve and infected Balb/c and C57Bl/6 mice. To that end, ELISA plates were coated with PSEx and specific antibodies (classes and subclasses) were characterized in terms of titers and avidities using individualized serum samples, observing several relevant differences between mouse strains (Fig. 2.C.). Firstly, PSEx-specific natural antibodies showed usually higher titers in Balb/c mice than in C57Bl/6 counterparts, which is in accordance with anti-PSA IgG titers (Fig. 1.B.) and immunoTEM results (Fig. 2.B.). Secondly, infected Balb/c mice showed a mixed anti-PSEx antibody response -with significant IgE titers-, yet infected C57Bl/6 animals exhibited a prominent IgG2b/IgG2c-bias, both in terms of titer and avidity indexes (Fig. 2.C.).

Taken together, our immunoTEM and ELISA results (Fig. 2) showed that C57Bl/6 mice, the less susceptible mouse strain to secondary CE, narrowed their IgG recognition repertoire of parasite antigens after infection, suggesting a possible targeting against fewer but more relevant PSC components present in the parasite tegument.

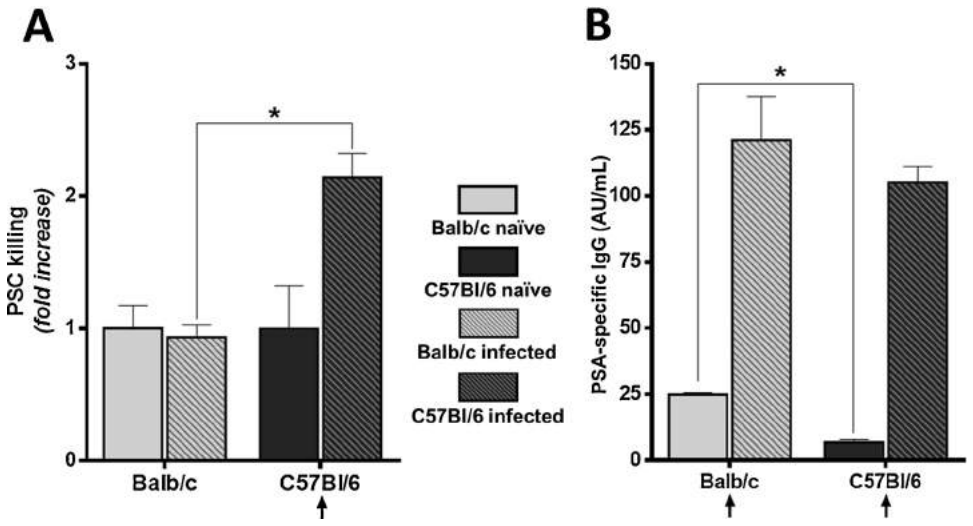

Fig. 1. C57Bl/6 mice generate more efficient anti-parasite antibodies than Balb/c littermates. **(A)** Fold-increase in PSC killing activity of control serum supplemented with γ-globulins from homologous naïve or infected mice. Stats: 2-way ANOVA. **(B)** PSA-specific IgG titers were determined through ELISA. Titers were calculated as the absorbance values times the inverse of the highest non-saturating dilution detected. Stats: Mann-Whitney-Wilcoxon *U* test. In any case, results are shown as mean ± SEM. Differences were regarded as significant with $p < 0.05$, and are depicted as arrows (comparisons within mouse strains) or asterisks (comparisons between conditions).

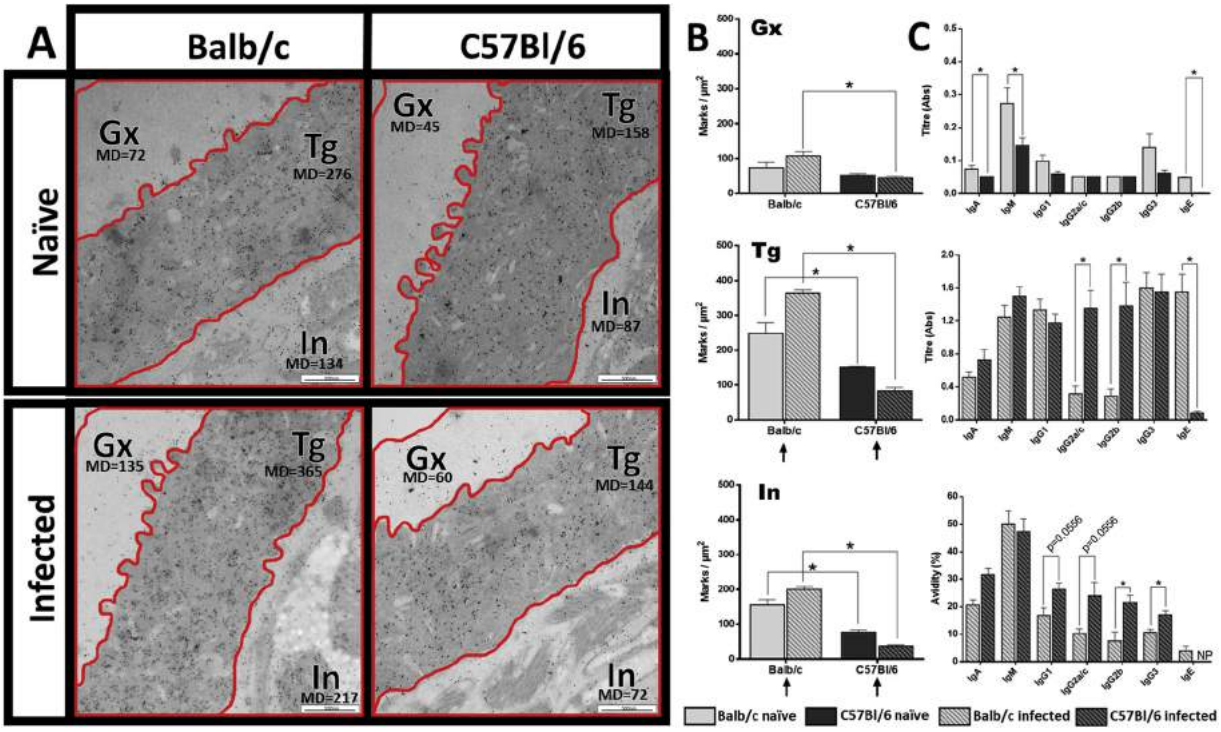

Fig. 2. Antibody responses against tegumental antigens. **(A)** Representative images of immunoTEM analyzed conditions are shown (scale bars in white boxes represent 500nm). Within representative images, borders for each parasite structure are highlighted in red, and mark densities (MD) are shown. Ultrathin sections of PSC were incubated with pooled sera from naïve or infected Balb/c and C57Bl/6 mice. Murine IgG were revealed with goat-anti-mouse-IgG antibodies labeled with gold nanoparticles. **(B)** IgG recognition was expressed as mark densities (marks/µm) for glycocalyx (Gx), tegument (Tg) and inner structures (In) of PSC, and were calculated for six replicates in each condition. Stats: Student's t-test. **(C)** PSEx-specific antibody titers were characterized through ELISA in serum samples from naïve (top) and infected (middle) Balb/c and C57Bl/6 mice. Titers were expressed as the absorbance values detected at the highest non-saturating dilution analyzed. Avidity indexes (bottom) of PSEx-specific antibodies were determined through ELISA with chaotropic elution only for serum samples from infected mice. Stats: Mann-Whitney-Wilcoxon *U* test. In any case, results are shown as mean ± SEM. Differences were regarded as significant with $p < 0.05$, and are depicted as arrows (comparisons within mouse strains) or asterisks (comparisons between conditions). Gx (glycocalyx), Tg (tegument), In (inner structures), NP (not performed) (For interpretation of the references to colour in this figure legend, the reader is referred to the web version of this article).

3.3. Immunization with PSC tegumental antigens resembles early-induced antibody responses in murine secondary CE

PSEx has been described as an antigenic fraction able to induce specific antibodies in mice (Hernández and Nieto, 1994), dogs (Carol and Nieto, 1998) and sheep (Valizadeh et al., 2017). However, characterization of the antibodies induced through PSEx-immunization is scarce. Therefore, we further analyzed PSEx-specific antibodies in immunized Balb/c and C57Bl/6 mice following a similar set of experiments to those described above.

Firstly, we performed immunoTEM studies with pooled sera from PSEx-immunized Balb/c and C57Bl/6 mice, resulting in similar observations to those obtained for infected animals (Fig. 2): (*i*) Tg was the main PSC structure recognized by IgG antibodies regardless the condition analyzed, (*ii*) Balb/c sera showed higher mark densities than C57Bl/6 counterparts, and (*iii*) mark densities for Balb/c samples increased post-immunization, while the opposite was observed for C57Bl/6 animals (Fig. 3.A.). Therefore, C57Bl/6 mice -unlike Balb/c- would seem to narrow their IgG recognition repertoire of parasite antigens either after infection (Fig. 2.B.) or following PSEx-immunization (Fig. 3.A.).

We next characterized the PSEx-specific antibody response post-immunization in both mouse strains. To that end, ELISA plates were coated with PSEx and specific antibodies (classes and subclasses) were characterized in terms of titers and avidities using individualized serum samples. Again, similarities were observed with results obtained from infected animals (Fig. 2.C.). Thus, both strains showed a mixed PSEx-specific antibody response after immunization, yet Balb/c mice exhibited significant higher IgE titers, while C57Bl/6 animals displayed an IgG2c-biased response, even though revealing lower global avidity indexes (Fig. 3.B.).

Finally, we also assessed the *in vitro* PSC killing activity of γ-globulins induced after PSEx-immunization and results were expressed as the fold-increase in the percentage of non-viable PSC post-incubation with fresh homologous sera from naïve mice supplemented with purified γ-globulins. In this sense, and in accordance with results obtained with sera from infected mice (Fig. 1.A.), no significant differences in PSC killing were observed between purified γ-globulins from naïve or immunized Balb/c mice (Fig. 3.C.). However, γ-globulins from PSEx-immunized C57Bl/6 mice significantly increased PSC killing activity with respect to their homologous naïve controls by a roughly 3 fold-increase (Fig. 3.C.). It is worth mentioning that immunizations with PSEx were performed without any adjuvant, suggesting that components within PSEx are intrinsically immunogenic, and could be further used for modelling antibody responses induced during early murine secondary CE.

3.4. Identification of potentially protective antigens against secondary CE through SERPA

Effective and efficient humoral responses against pathogens not only depend on the quality and intensity of the induced antibodies, but also -and of outstanding importance- on the antigens targeted by such antibodies. Those antigens are usually termed protective antigens, and their identification is not an easy task. In this regard, we further applied a SERPA strategy (Fulton et al., 2013) in order to identify potentially protective antigens within PSEx by their unique early-induced antibodies recognition in infected C57Bl/6 mice, but not in infected Balb/c.

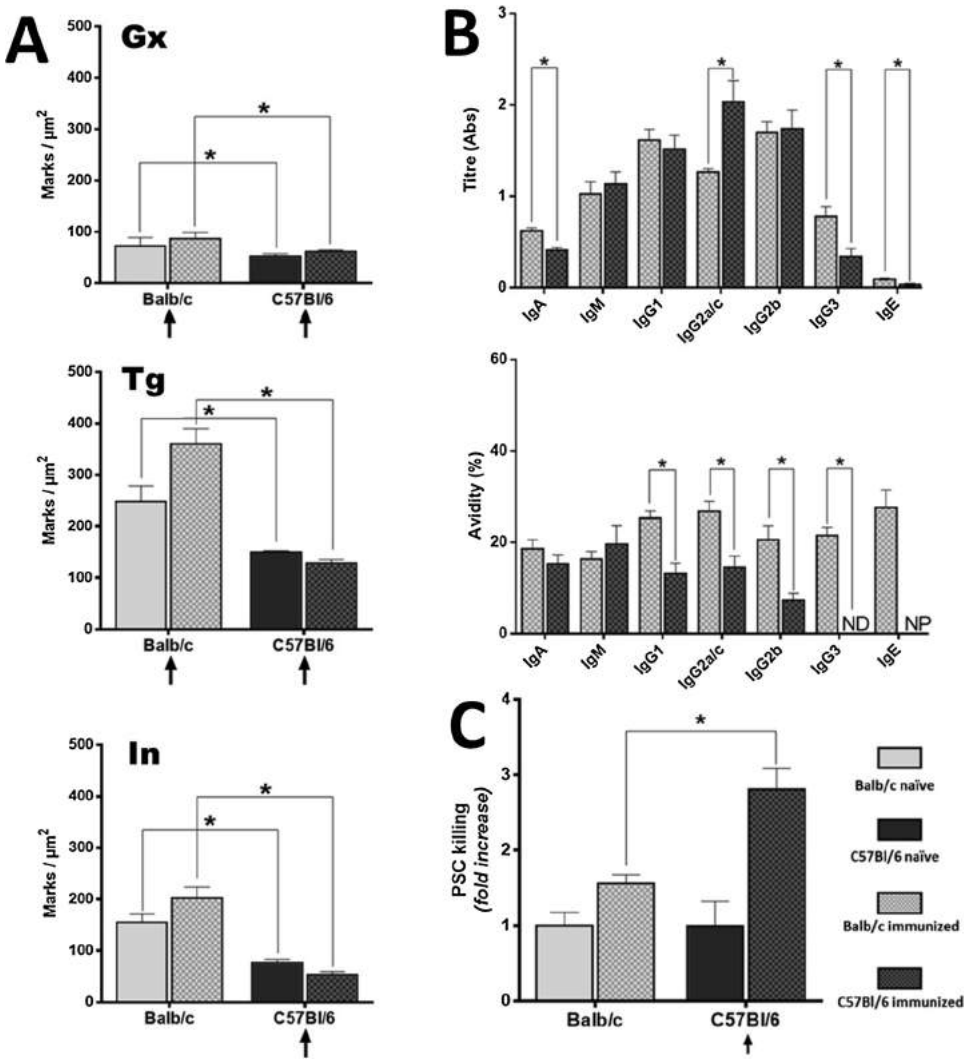

Fig. 3. PSEx-immunization resembles early-induced antibody responses in secondary CE. **(A)** ImmunoTEM analyses were analogous to those shown in Fig. 2, but ultrathin sections of PSC were incubated with pooled sera from naïve or PSEx-immunized Balb/c and C57Bl/6 mice. Murine IgG were revealed with goat-anti-mouse-IgG antibodies labeled with gold nanoparticles. IgG recognition was expressed as mark densities (marks/µm^2) for glycocalyx (Gx), tegument (Tg) and inner structures (In) of PSC, and were calculated for six replicates in each condition. Stats: Student's t-test. **(B)** PSEx-specific antibody titers (top left) were characterized through ELISA in serum samples from naïve and PSEx-immunized Balb/c and C57Bl/6 mice. Titers were expressed as the absorbance values detected at the highest non-saturating dilution analyzed. Avidity indexes (middle left) of PSEx-specific antibodies were determined through ELISA with chaotropic elution only for serum samples from PSEx-immunized mice. Stats: Mann-Whitney-Wilcoxon *U* test. **(C)** Fold-increase in PSC killing activity of control serum supplemented with γ-globulins from homologous naïve or PSEx-immunized mice. Stats: 2-way ANOVA. In any case, results are shown as mean ± SEM. Differences were regarded as significant with $p < 0.05$, and are depicted as arrows (comparisons within mouse strains) or asterisks (comparisons between conditions). Gx (glycocalyx), Tg (tegument), In (inner structures), NP (not performed), ND (not detected).

To that end, our SERPA study was performed on 2D SDS-PAGE resolved PSEx followed by electro-transference to Western blot membranes, which were developed to detect antigen recognition profiles by every antibody class/subclass. SERPAs were performed with pooled sera from either naïve or infected Balb/c and C57Bl/6 mice, spots were counted and their patterns were compared (Fig. 4). Firstly, for sera from naïve animals, only classes of antibodies (IgM, IgA, IgG and IgE) were analyzed. C57Bl/6 sera showed a higher number of IgM-recognized spots with lower counts in IgG- or IgA-recognized spots. Secondly, for sera from infected animals, every class and subclass of antibodies were tested. In this case, Balb/c sera showed a higher number of IgA-, IgG1-, IgG2a- and IgG2b-recognized spots with lower counts in IgM-recognized spots. Neither IgE- nor IgG3-recognized spots were detected (Fig. 4).

Then, spots only observed in Western blots incubated with sera from C57Bl/6 mice, but not observed in those incubated with sera from Balb/c (DRPs), were manually back-mapped into silver-stained 2D SDS-PAGE resolved PSEx gels, and were submitted to MALDI-TOF/TOF analyses. Finally, our SERPA identified 3 DRPs only recognized by natural antibodies, 3 DRPs recognized either by natural and/or infection-induced antibodies, and 7 DRPs only recognized by infection-induced antibodies (Table 1). Since the most resistant mouse strain -C57Bl/6- is the only one able to generate specific antibodies targeting the last mentioned set of DRPs, they could be suggested as being potentially protective antigens.

3.5. Strain-specific genetics may account for C57Bl/6 ability to induce antibodies against DRPs

The ability of generating antibodies against specific antigens, *e.g.* protective antigens, during an infection depends on several factors. From the antigen side, its availability, intrinsic antigenicity/immunogenicity and B- and T-cell epitope content are among the most important. From the host side, one of the main factors influencing antibody responses rely on its ability to process and present T-cell epitopes to specific B-cells in order to favor the development of T-dependent antibody response. In this sense, Balb/c and C57Bl/6 mice -due to their endogamic characteristics- do differ in the process of T-cell epitopes presentation, since both mouse strains harbor different MHC-II molecules: Balb/c and C57Bl/6 have been shown to exclusively carry the H-2-IA^d and H-2-IA^b haplotypes, respectively (Sofron et al., 2016). Therefore, we further analyzed the list of 7 DRPs -suggested to be potentially protective antigens- through several bio- and immuno-informatic approaches according to Miles et al. (2019).

We first studied several intrinsic characteristics of the selected set of 7 DRPs, like intrinsic antigenicity, AAR values and US scores (Table 2). Results showed an unclear classification of the proteins since they exhibit (*i*) highly variable degrees of antigenicity (scores ranging from 0.24 to 0.92), (*ii*) disperse AAR values (from 24.7–150.0), and (*iii*) varied divergence levels (US scores ranging from 0.09 to 0.92).

On the other hand, when analyzing the possible interactions

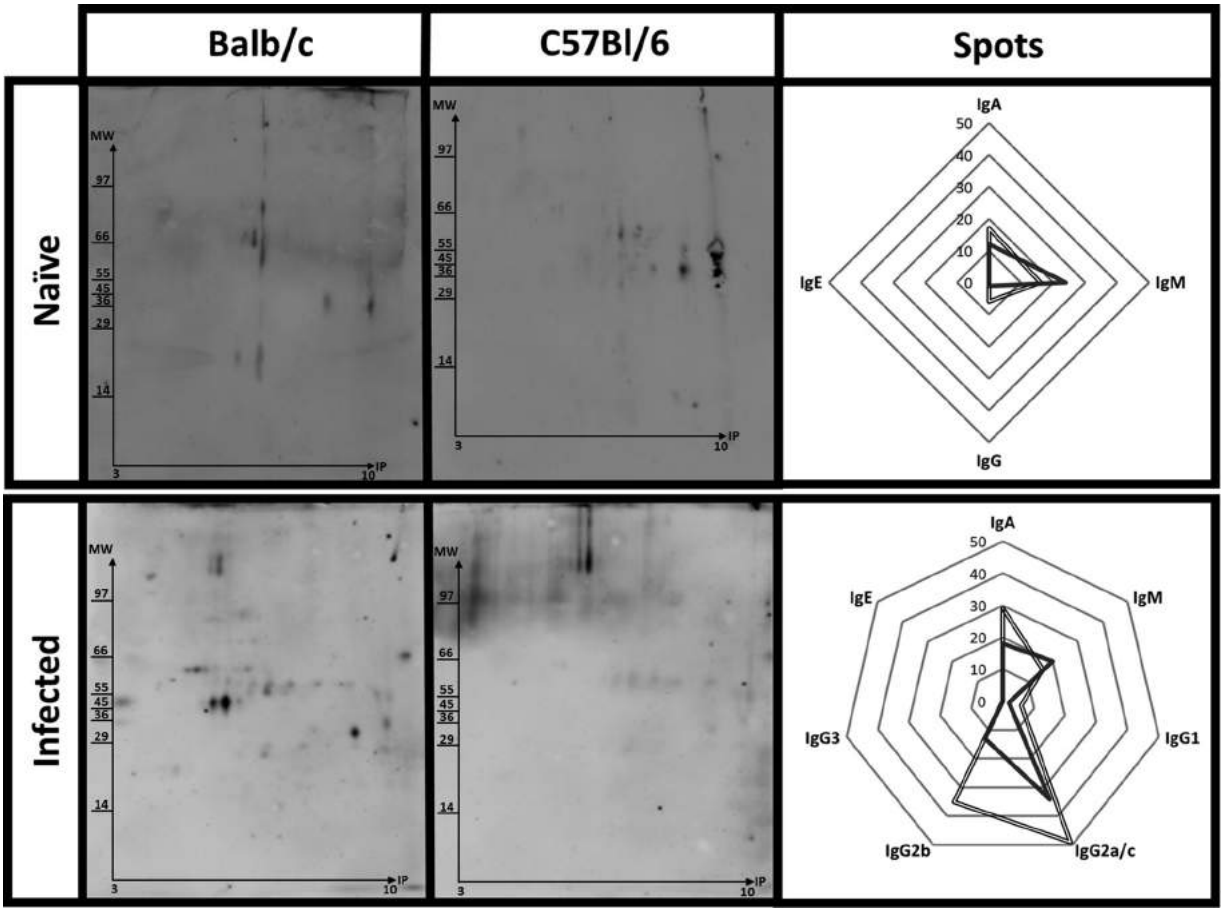

Fig. 4. Diversity of lineal B cell epitope recognition. SERPA studies were performed on 2D SDS-PAGE resolved PSEx followed by electro-transference to Western blot membranes, which were developed to detect antigen recognition profiles by every class/subclass of antibody. SERPAs were performed with pooled sera from either naïve or infected Balb/c and C57Bl/6 mice, and their spots were counted. Representative blots for naïve and infected Balb/c and C57Bl/6 samples are shown. Number of different spots detected, related to each antibody class/subclass, is depicted in schematic diagrams. Each concentric line represents a value of 10 spots. The hollow and solid black lines represent Balb/c and C57Bl/6 results, respectively. MW (molecular weight in KDa), IP (isoelectric point).

between the host and the selected set of proteins, relevant information was obtained. Results in Fig. 5 show -for the set of 7 DRPs- the number of every possible T-cell epitopes and its predicted affinity for the MHC-II haplotypes H-2-IA^d (Balb/c mice) and H-2-IA^b (C57Bl/6 mice). For the 7 DRPs, C57Bl/6 mice showed always greater numbers of possible T-cell epitopes than Balb/c mice, and the mean affinities were higher (lower IC_{50}) for the C57Bl/6 haplotype as well. Moreover, strong binding T-cell epitopes ($IC_{50} \leq 50$ nM) were only observed for the C57Bl/6 MHC-II haplotype (in 4 out of the 7 DRPs). Finally, the number of different T-cell epitope cores was also greater for the C57Bl/6 MHC-II haplotype, except for one DRP exhibiting the same number of different cores for both MHC-II haplotypes (Table 2).

Taken together, our results suggest that C57Bl/6 mice are more efficient than Balb/c in presenting T-cell epitopes from selected parasite

Table 1
Differentially Recognized Proteins identified through SERPA. PSEx antigens uniquely recognized by pooled sera from naïve and/or infected C57Bl/6 mice were identified through SERPA followed by MALDI-TOF/TOF. "Antibody type" refers to the origin of the sera which allowed the identification, while "Recognized by" refers to the antibody class/subclass that recognized the corresponding antigen in the SERPA. "Accession number" refers to the UniProtKB IDs. "MASCOT score" correspond to the score obtained in protein identification (scores > 56 were considered significant, $p < 0.05$). "Coverage" is the percentage of the protein identified. Abbreviations: aa (amino acid), MW (theoretical molecular weight), IP (theoretical isoelectric point).

Antibody type	Recognized by	Protein Name	Accession number	Lenght (aa)	MW (kDa)	IP	MASCOT Score	Coverage %
Only natural	IgG	Hydatid disease diagnostic antigen P-29	W6V2P2	238	27.1	5.63	143	32
	IgG	1,5-anhydro-D-fructose reductase	W6UTJ3	343	39.0	7.23	159	29
	IgG	Glyceraldehyde 3 phosphate dehydrogenase	W6V1T8	336	36.1	8.44	106	22
Natural and Induced	IgG/IgG1	thioredoxin peroxidase	Q8T6C4	193	21.4	5.79	385	56
	IgG/IgG2c	Fatty acid binding protein FABP2	A0A068WLT8	213	23.9	8.41	167	41
	IgM/IgG/IgG2c	Fructose-bisphosphate aldolase	U6IXV3	363	39.6	8.31	424	66
Only induced	IgM	Malate dehydrogenase mitochondrial	A0A068 × 1L3	332	35.5	8.80	148	33
	IgG1	Nucleoside diphosphate kinase A 2	A0A068WL30	149	16.7	10.20	104	21
	IgG1/IgG2b	Actin	U6JMK8	376	41.7	5.30	178	23
	IgM	Severin/Gelosin	U6IX85	364	42.0	7.60	283	21
	IgG2c	Malate dehydrogenase cytoplasmatic	A0A068WYB8	338	36.5	7.60	438	42
	IgG2c	Vesicular amine transporter	A0A068 × 307	443	49.0	5.00	126	32
	IgG1	Peptidyl-prolyl cis-trans isomerase	U6JRP2	162	17.3	6.40	231	75

Table 2
Immunoinformatic characterization of selected DRPs. DRPs only recognized by infection-induced antibodies were characterized through several immuno-bio-informatic tools. "Antigenicity" and "AAR" (Abundance of Antigenic Regions) columns show predicted values obtained through the use of ANTIGENpro software and Secret-AAR webserver, respectively. US column refers to calculated "Uniqueness score". "Different MHC-II binding cores" columns show the number of every possible and different T cell epitope cores able to bind to MHC-II haplotypes H-2-IA^d and H-2-IA^b.

DRP	Protein Name	Antigenicity	AAR	US	Different MHC-II binding cores	
					Balb/c (H-2-IAd)	C57Bl/6 (H-2-IAb)
1	Malate dehydrogenase mitochondrial	0.45	41.6	0.57	4	12
2	Nucleoside diphosphate kinase A 2	0.24	150	0.39	2	8
3	Actin	0.43	32.8	0.92	3	12
4	Severin/Gelosin	0.82	33.2	0.24	1	7
5	Malate dehydrogenase cytoplasmatic	0.43	37.7	0.57	3	11
6	Vesicular amine transporter	0.72	24.7	0.09	0	9
7	Peptidyl-prolyl cis-trans isomerase	0.92	32.6	0.70	1	1

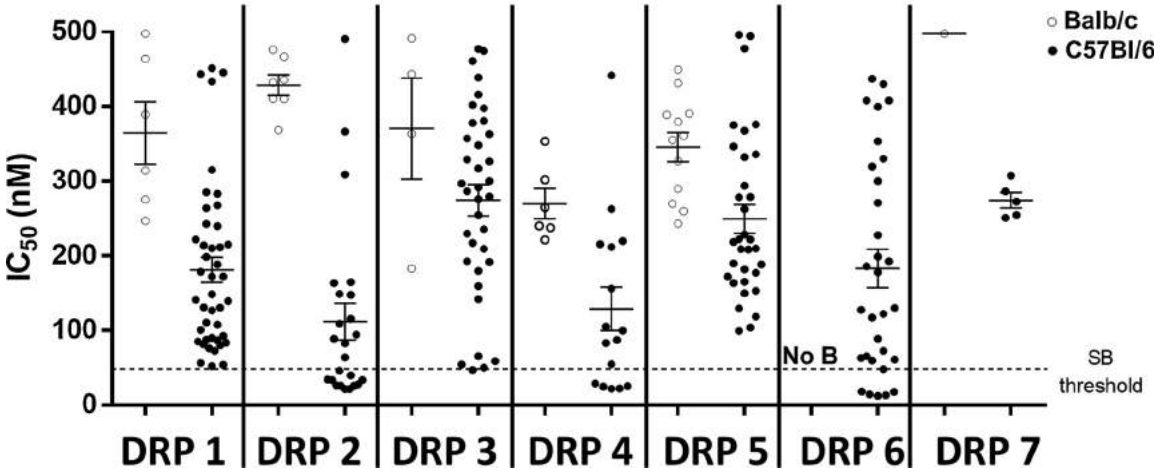

Fig. 5. Immunoinformatic characterization of potential T cell epitopes. For the set of 7 DRPs uniquely recognized by pooled sera from infected C57Bl/6 mice, every theoretically possible T cell epitope with binding affinity (IC_{50}) ≤ 500 nM is shown as a dot. Predictions were performed using NetMHCII software against the MHC-II haplotypes H-2-IA^d (Balb/c mice, hollow dots) and H-2-IA^b (C57Bl/6 mice, solid dots). Dotted line represents the threshold defining Strong Binding peptides (IC_{50} ≤ 50 nM). No B (no predicted binding peptide with IC_{50} ≤ 500 nM). Vertical lines represent mean ± SEM values.

antigens, *e.g.* potentially protective antigens, in order to favor T-dependent antibody responses, and therefore, inducing antibodies with more effective anti-parasite activities.

4. Discussion

Differences in hosts' genetic background are known to influence the outcome of various diseases. This is especially true for endogamic mice, such as Balb/c and C57Bl/6 strains, which have been reported to exhibit important differences in susceptibility to numerous diseases, including every major pathogen families (Anthony et al., 2007; Cheers et al., 1978; Chiodini and Buergelt, 1993; Ferreira et al., 2018; Fornefett et al., 2018; Henderson et al., 2015; Kulcsar et al., 2015; Liu et al., 2002; Mols-Vorstermans et al., 2013; Mourglia-Ettlin et al., 2016a; Pereira et al., 2016; Xiang et al., 2016; Zhang et al., 2005). Among the known key differences between Balb/c and C57Bl/6 mouse strains, immune-related factors are of outstanding importance, including variations in cellular, cytokine and antibody responses as well as -and interconnected with- distinct patterns of specific molecule allotypes/haplotypes (Canivet et al., 2019; Fornefett et al., 2018; Jiang et al., 2010; Jovicic et al., 2015; Mourglia-Ettlin et al., 2016a; Schulte et al., 2008; Sofron et al., 2016; Vlkova et al., 2012; Watanabe et al., 2004; Zeng et al., 2016).

The present study represents a follow up to previous reports from our group showing differences in local immune-cell recruitment, cytokine production and antibody responses associated with Balb/c and C57Bl/6 mice differential susceptibility to secondary CE (Mourglia-Ettlin et al., 2016a, 2016b). Here, we further analyzed the role of *E. granulosus*-induced antibodies in the murine model of secondary CE, and its relationship with the host susceptibility to the infection. Firstly, differences in PSC killing activity of induced antibodies generated by both mouse strains were assessed, observing that only γ-globulins from infected C57Bl/6 mice enhanced the natural serum anti-PSC activity (Fig. 1.A). Then, we concluded that subtler differences in the antibody response developed by infected C57Bl/6 mice, other than intensity (Fig. 1.B), might explain the observed PSC killing enhancement.

In this sense, quality characteristics of antibodies in an immune response are influenced by their specificity profile, avidity and isotypes generated. In order to uncover the quality characteristics in our model of differential susceptibility to secondary CE, we studied each of these factors independently. Firstly, the recognition profile of naïve *vs.* infection-induced antibodies was studied for both mouse strains against different PSC structures by immunoTEM. Results showed that the tegument was the main PSC structure recognized by murine IgG antibodies, and that while mark densities increased for Balb/c sera following infection, the opposite situation was observed for C57Bl/6 samples (Fig. 2.B.). In this regard, assuming that parasite antigens are equally represented alongside the tegument, mark densities would be proportional -not necessarily in a linear way- with the diversity/profile of antigen recognition by infection-induced antibodies. Therefore, higher mark densities would correlate with a more diverse antibody recognition spectrum, while lower mark densities would correlate with the inverse situation. Taking this into account, our results suggest that only C57Bl/6 mice -the less susceptible strain to secondary CE- narrow

their IgG recognition repertoire of parasite antigens during infection, suggesting a possible targeting against fewer but more relevant PSC components present in the parasite tegument. Similar results have been reported for both mouse strains in other parasite infection model (Bryan et al., 2010). This results might explain the better PSC killing activity observed for the γ-globulins from infected C57Bl/6 mice.

Tegumental antigens are accessible to immune components since they are present on the surface of the parasite. Therefore, immunization with tegumental antigens could potentially be useful to model the early antibody response during secondary CE; and fortunately there is currently a tegumental antigenic fraction -termed PSEx- which has been previously described (Hernández and Nieto, 1994; Miles et al., 2019). Additionally, we recently reported an approximation to PSEx proteome, through 2D SDS-PAGE followed by MALDI-TOF/TOF, which showed that it is composed of at least 58 different parasite proteins (Miles et al., 2019). Specific antibody production against PSEx antigens have been observed in PSEx-immunized dogs (Carol and Nieto, 1998) and sheep (Valizadeh et al., 2017), as well as protection against secondary CE in CD1 immunized mice (Hernández and Nieto, 1994). In order to assess the usefulness of PSEx as a model for antibody responses early-induced during secondary CE, comparative studies on antibody production following adjuvant-free PSEx-immunization of Balb/c and C57Bl/6 mice were performed. An analogous set of experiments to those performed for infected mice (Fig. 1 and Fig. 2), were applied to immunized mice (Fig. 3), showing similar results for both settings: (*i*) immunoTEM studies showed that C57Bl/6 mice -unlike Balb/c- narrowed their IgG recognition repertoire of tegumental parasite antigens either after infection (Fig. 2.B.) or following PSEx-immunization (Fig. 3 A.); (*ii*) ELISA analyses showed similarities in the PSEx-specific antibody response either during early infection (Fig. 2.C.) or following PSEx-immunization in both mouse strains (Fig. 3.B.); and (*iii*) only γ-globulins from infected (Fig. 1.A.) or PSEx-immunized (Fig. 3.C.) C57Bl/6 mice significantly increased the PSC killing activity of homologous naïve serum. Therefore, the similarities observed between infected and PSEx-immunized mice, independently of the strain analyzed, suggest that PSEx could be further used for modelling antibody responses induced during early murine secondary CE. Additional key advantages for its use include their partially-known composition (previously characterized at the proteomic level by Miles et al. (2019)), its intrinsic antigenicity/immunogenicity (no adjuvant need for immunizations), and its relative production easiness.

Once we observed that infection-induced antibodies do play a role in host resistance/susceptibility to secondary CE, we further characterized their profile of tegumental recognition using PSEx as a model source of parasite antigens. In this regard, recognition diversity was performed following a SERPA strategy, showing differences between mouse strains with pooled sera either obtained from naïve or infected mice. Again, as observed through immunoTEM studies (Fig. 2.B.), SERPA analyses revealed that infected Balb/c mice generated a broader antibody repertoire targeting components present in PSEx than C57Bl/6 counterparts (Fig. 4). It is worth mentioning that, since our SERPA strategy was based on 2D SDS-PAGE resolved PSEx under denaturalizing conditions, it allowed us to quantify only “lineal B cell epitopes” recognized by antibodies because “conformational B cell epitopes” were lost. In this regard, although antibodies targeting “linear B cell epitopes” during an immune response are estimated to be only the 10 % of all induced antibodies (Sanchez-Trincado et al., 2017), our SERPA results were in accordance with immunoTEM studies and PSC killing activity assays: infected C57Bl/6 mice -the more resistant strain to secondary CE- developed more efficient antibodies towards a smaller number of tegumental antigens/epitopes than Balb/c counterparts.

In addition, SERPA studies allowed us to identified tegumental antigens/epitopes differentially recognized between antibodies from naïve/infected C57Bl/6 but not Balb/c mice. Such antigens were then termed DRPs, and since PSEx was reported to induce protection in the murine model of secondary CE (Hernández and Nieto, 1994), these DRPs could be suggested as potentially protective antigens. Therefore, we further focused on the molecular identification of DRPs through MALDI-TOF/TOF, resulting in a total of 13 different DRPs successfully identified: 3 DRPs only recognized by natural antibodies, 3 DRPs recognized either by natural and/or infection-induced antibodies, and 7 DRPs only recognized by infection-induced antibodies (Table 1). Interestingly, among the 13 DRPs identified, several of them have been previously reported as potential protective molecules against *E. granulosus* and/or other helminth parasites, either as vaccine candidates or as pharmacological targets. In order to simplify the description of the 13 DRPs, we categorized them into three different groups: (*i*) DRPs previously suggested and/or tested as targets against helminth parasites belonging to the genus *Echinococcus*, (*ii*) DRPs previously suggested and/or tested as targets against helminth parasites except *Echinococcus* spp., and (*iii*) DRPs not previously tested against helminth parasites.

Out of the 13 DRPs, 7 have been previously suggested and/or tested as targets against *Echinococcus* spp. parasites. Among them, hydatid disease diagnostic antigen P-29 has been successfully tested as a vaccine candidate, revealing significant protective activity against secondary CE in mice (Shi et al., 2009), as well as against primary infection in sheep (Wang et al., 2016). Thioredoxin peroxidase has been reported as a key enzyme for reactive oxygen species detoxification in *E. granulosus* and suggested that its blockade could be an interesting target for prevention/treatment of CE (Salinas et al., 1998; Li et al., 2004). Peptidyl-prolyl cis-trans isomerases belong to the cyclophilins family with isomerase activity catalyzing the *cis*-to-*trans* conversion of peptide substrates which has also been suggested as an interesting target for *E. granulosus*. Cyclophilins display the ability to bind cyclosporine A (CsA), an immunosuppressive drug with well-known anti-parasite effects (Bell et al., 1996), and *E. granulosus* was shown to be adversely affected by CsA, since its administration in the murine model of secondary CE reduced both the number and weight of developed hydatid cysts (Hurd et al., 1993), being peptidyl-prolyl cis-trans isomerase associated with such sensitivity to CsA (Colebrook et al., 2002). Additionally, our group have recently identified these three proteins as potential *E. granulosus* ligands for either the CD5 or CD6 scavenger-like receptors, and reported that infusing mice with recombinant CD5 or CD6 induces significant and mild protection against secondary CE, respectively (Mourglia-Ettlin et al., 2018a). Thus, blocking either hydatid disease diagnostic antigen P-29, thioredoxin peroxidase and/or peptidyl-prolyl cis-trans isomerase may contribute to a better parasite control. Regarding fatty acid-binding protein, it has also been suggested as an interesting vaccine candidate against *E. granulosus* (Chabalgoity et al., 1997; Paulino et al., 1998; Chabalgoity et al., 2000). Parasitic platyhelminthes have a limited capacity to synthesize lipids *de novo*, being therefore highly dependent on their uptake from the host, and fatty acid-binding proteins are believed to be involved in such processes. Within the group of DRPs being described, malate dehydrogenases are enzymes occurring in eukaryotic cells in two isoforms, one mitochondrial, which participates in the tricarboxylic acid cycle, and one cytosolic, which is usually involved in shuttle systems for the transfer of reducing equivalents from the cytosol into the mitochondrion. In *E. granulosus* and other parasitic helminths with an extremely active glycolytic pathway these enzyme are very important (McManus and Smyth, 1982). In this regard, *E. granulosus* malate dehydrogenases have been largely known to be competitively inhibited by different anthelmintic drugs like benzimidazoles (Xiao et al., 1993; Vessal and Tabei, 1996), and thus, blocking *E. granulosus* malate dehydrogenases seems a beneficial strategy from the host point of view. Finally, immunization of mice with *E. multilocularis* glyceraldehyde-3-phosphate dehydrogenase resulted in significant protection, reducing the number of developed metacestodes (Muller-Schollenberger et al., 2001). Taken together, these results reinforce our hypothesis that DRPs listed in Table 1 could be considered natural protective antigens. In this sense, we previously reported that natural antibodies from C57Bl/6 mice -unlike Balb/c- were able to induce protection after heterologous

transference into Balb/c animals (Mourglia-ettlin et al., 2016a); and therefore the DRPs recognized by natural antibodies, at least, would deserve further studies to determine their potential as protective antigens.

Additionally, 4 out of the 13 DRPs were previously suggested and/or tested as targets against other helminth parasites than *Echinococcus spp*. Among them, nucleoside diphosphate kinases are key enzymes in the purine-salvage pathway, a biosynthetic process on which helminth parasites are largely dependent for supplying purine precursors for its energy and DNA synthesis needs. Nucleoside diphosphate kinases are one of the most active enzymes in that pathway, being therefore interesting targets for rational drug discovery and design. In this sense, although no information is available for *E. granulosus*, there are some reports suggesting its potential as a pharmacological target in other helminth infections, like *Brugia malayi* (Ghosh et al., 1995), *Schistosoma mansoni* (Marques et al., 2012), and *Trichuris suis* (Leroux et al., 2018). The remaining DRPs within this category (*e.g.* actin, gelsolin and fructose-bisphosphate aldolase) are directly or indirectly involved in cytoskeleton dynamics. In this sense, helminth parasites exhibit high plasticity of their cytoskeletons, probably as an acquired strategy to allow them to enter, settle and develop into their hosts. Therefore, cytoskeleton components have been proposed as interesting targets for therapeutic drugs. In *S. mansoni* it has been reported that interference of actin dynamics using cytochalasins indirectly affects other functions than movement, like glucose uptake from the host (Skelly et al., 1994) or tegumental shedding needed for optimal immune evasion (Kemp et al., 1980). Additionally, it is well-known that the assembly and disassembly of actin filaments are regulated by a variety of actin-binding proteins; including gelsolin superfamily whose members control actin organization by severing filaments, capping filament ends, and nucleating actin assembly (Nag et al., 2013). Also in *S. mansoni*, gelsolin was shown to be involved in the process of tegumental disruption induced by praziquantel (Linder and Thors, 1992). Regarding *E. granulosus*, although gelsolin and related proteins have scarcely been studied (Cortez-Herrera et al., 2001; Grimm et al., 2006), potential relevant roles could be easily assigned due to the highly organized F-actin cytoskeleton recently described in the parasite (La-Rocca et al., 2019). Finally, the glycolytic enzyme fructose-bisphosphate aldolase has been described as a complex multifunctional protein that may perform non-glycolytic moonlighting functions. Although *E. granulosus* fructose-bisphosphate aldolase functions have been poorly studied, it has been shown to bind F-actin filaments suggesting it has alternative multifunctional properties (Lorenzatto et al., 2012). Therefore, blocking parasite fructose-bisphosphate aldolase might also influence actin dynamics, as above suggested for gelsolin and actin itself. In this sense, parasite fructose-bisphosphate aldolase has been tested as a promising vaccine candidate against the infection by *Onchocerca volvulus* (McCarthy et al., 2002), *S. mansoni* (Saber et al., 2013), and *Trichinella spiralis* (Yang et al., 2019).

Only 2 of the 13 DRPs have not been tested against any helminth parasite to our knowledge. One of them is a vesicular amine transporter probably involved in the parasite neurobiology. In this regard, neurotransmitters biology in helminth parasites have been quite recently suggested as interesting targets for the development of new drugs (McVeigh et al., 2012). Among different components, neurotransmitters transporters play fundamental roles in controlling signaling and homeostasis, remarking vesicular transporters which sequester the neurotransmitter into synaptic vesicles for subsequent release. Although neurotransmitter transporters have been widely studied in mammals, they have been barely characterized among parasite helminths (Ribeiro and Patocka, 2013). Regarding the genus *Echinococcus*, recent studies have been published on its neurotransmitters biology, and some vesicular amine transporters were described (Camicia et al., 2013; Koziol et al., 2016; Preza et al., 2018). However, the vesicular amine transporter we identified here as a DRP is still uncharacterized. Finally, 1,5-anhydro-D-fructose reductase is the least studied of the 13 DRPs. The enzyme is involved in the anhydro-fructose pathway, an alternative glycogen catabolic pathway described in the last decade occurring in certain bacteria, fungi, algae and mammals. It is a pathway consisting in more than 10 enzymatic steps showing an array of secondary metabolites from glycogen *via* the central intermediate 1,5-anhydro-D-fructose (Yu and Fiskesund, 2006; Yu, 2008). Unfortunately, there are no reports regarding its occurrence in parasites to our knowledge; and besides its metabolic roles, 1,5-anhydro-D-fructose has shown to exert interesting immunosuppressive functions (Meng et al., 2009a,2009b). Therefore, the anhydro-fructose pathway might be worthy to be studied in helminth parasites, since 1,5-anhydro-D-fructose reductase druggability would probably deserve further attention.

Taken together, the above described data reinforce our hypothesis that DRPs listed in Table 1 could be considered natural protective antigens. In this regard, it is worth noting to mention that murine secondary CE can be divided into two stages: an early one-month pre-encystment stage with PSC developing into hydatid cysts, followed by a chronic post-encystment stage with already differentiated cysts growing and eventually becoming fertile cysts, *e.g.* producing PSC (Richards et al., 1983; Rogan et al., 2015; Tamarozzi et al., 2016). It is generally accepted that during the pre-encystment stage *E. granulosus* is more susceptible to host immune attack; thus, antibodies induced during that stage would be relevant in the overall anti-parasite response. In the present work, assays were performed with infection-induced antibodies obtained 3 weeks after PSC inoculation, and therefore the set of 7 DRPs identified only with those antibodies (Table 1) deserved a more detailed analysis. Among them malate dehydrogenases and peptidyl-prolyl cis-trans isomerase have been already suggested as interesting targets against CE. On the other hand, nucleoside diphosphate kinases, actin and gelsolin were reported as relevant molecules against other helminth parasite; while vesicular amine transporter has not been tested against any helminth parasite yet. The set of such 7 DRPs greatly varied in terms of intrinsic antigenicity and sequence divergence, according to our bioinformatic characterization (Table 2). However, when immunoinformatic studies were performed interesting results were obtained. In order to generate optimal T-dependent antibody responses, antigens should be correctly presented by antigen presenting cells to T cells, and such a process greatly depend on the ability of MHC-II molecules to bind T cell epitopes derived from the antigen. In this regard, Balb/c and C57Bl/6 mice are known to carry different MHC-II haplotypes (Sofron et al., 2016), leading to potential differences in T cell epitope binding profiles and affinities. Through analyzing the binding affinity of every theoretically possible T cell epitope derived from the set of 7 DRPs previously mentioned against Balb/c (H-2-IA^{d}) and C57Bl/6 (H-2-IA^{b}) MHC-II haplotypes, we found that every DRP in the set showed higher numbers of possible T cell epitopes, higher numbers of different MHC-II-binding-cores, and higher global affinities (lower IC_{50} values) towards the MCH-II haplotype exclusively present in C57Bl/6 mice. Moreover, 4 out of the 7 DRPs showed at least one T cell epitope for that haplotype categorized as “Strong Binding” ($IC_{50} < 50$ nM), while none was predicted towards the MHC-II haplotype present in Balb/c mice (Table 2) suggesting that the 7 DRPs in the set are more likely to be successfully presented by antigen presenting cells from C57Bl/6 mice to T cells. Therefore, if any of those 7 DRPs were effectively a natural protective antigen, C57Bl/6 mice would be more likely to generate specific antibodies targeting those tegumental antigens, which could explain -at least partially- the more efficient anti-PSC response developed by C57Bl/6 mice. Further studies on the possible use of DRPs as vaccine candidates against *E. granulosus* will be carried out soon.

5. Conclusion

Summing up, we showed here that differential susceptibility to secondary CE observed for Balb/c and C57Bl/6 mice is influenced by the early-induced antibody response. Moreover, we suggested that subtle differences in antibody responses against parasite tegumental

antigens might be linked to a genetic predisposition of C57Bl/6 mice to successfully induce T-dependent antibody responses targeting natural protective antigens. In this regard, antibodies produced by infected C57Bl/6 mice were more efficient in inducing PSC death, probably through the targeting of a selected number of relevant antigens, as well as through polarizing their isotype profiles towards potent anti-parasite IgG subclasses. Also, the present work showed the usefulness of PSEx antigens to model early-induced antibody responses during murine secondary CE. Finally, several novel parasite proteins were suggested for their further testing as novel vaccine candidates against *E. granulosus* infection. Indeed, one of them -vesicular amine transporter- was recently suggested by us as an interesting vaccine candidate following a very different research approach (Miles et al., 2019).

CRediT authorship contribution statement

Sebastián Miles: Conceptualization, Data curation, Formal analysis, Funding acquisition, Investigation, Methodology, Project administration, Writing - original draft, Writing - review & editing. **Javier Magnone:** Data curation, Investigation. **Marek Cyrklaff:** Investigation, Methodology, Resources, Supervision. **Paula Arbildi:** Investigation. **Friedrich Frischknecht:** Methodology, Resources, Supervision, Funding acquisition, Writing - original draft. **Sylvia Dematteis:** Funding acquisition, Resources, Supervision, Writing - original draft. **Gustavo Mourglia-Ettlin:** Conceptualization, Data curation, Formal analysis, Funding acquisition, Methodology, Resources, Supervision, Project administration, Writing - original draft, Writing - review & editing.

Declaration of Competing Interest

The authors declare that there are no conflict of interests.

Acknowledgements

Authors are grateful to the Electron Microscopy Core Facility at Heidelberg University (Germany) for the introduction and use of their microscopes. SM received a travel grant from Boehringen Ingelheim Fonds. CSIC-Universidad de la República (Uruguay), PEDECIBA-Química (Uruguay), and ANII (Uruguay) are acknowledged for their general financial support.

References

Anthony, R.M., Rutitzky, L.I., Urban, J.F., Stadecker, M.J., Gause, W.C., 2007. Protective immune mechanisms in helminth infection. Nat. Rev. Immunol. 7, 975–987. https://doi.org/10.1038/nri2199.

Barrios, A.A., Grezzi, L., Miles, S., Mariconti, M., Mourglia-Ettlin, G., Seoane, P.I., Díaz, A., 2019. Inefficient and abortive classical complement pathway activation by the calcium inositol hexakisphosphate component of the Echinococcus granulosus laminated layer. Immunobiology. https://doi.org/10.1016/J.IMBIO.2019.05.009.

Baz, A., Ettlin, G.M., Dematteis, S., 2006. Complexity and function of cytokine responses in experimental infection by Echinococcus granulosus. Immunobiology 211, 3–9. https://doi.org/10.1016/j.imbio.2005.09.001.

Bell, A., Roberts, H.C., Chappell, L.H., 1996. The antiparasite effects of cyclosporin A: possible drug targets and clinical applications. Gen. Pharmacol. 27, 963–971. https://doi.org/10.1016/0306-3623(95)02148-5.

Breijo, M., Isnardi, F., Brauer, M., Schenker, R., Ferrari, M., Ferreira, A.M., 2011. An insect growth inhibitor - lufenuron - enhances albendazole activity against hydatid cyst. Vet. Parasitol. 181, 341–344. https://doi.org/10.1016/j.vetpar.2011.04.011.

Bryan, M.A., Guyach, S.E., Norris, K.A., 2010. Specific humoral immunity versus polyclonal B cell activation in Trypanosoma cruzi infection of susceptible and resistant mice. PLoS Negl. Trop. Dis. 4, e733. https://doi.org/10.1371/journal.pntd.0000733.

Burgu, A., Sarimehmetoglu, O., Gonenc, B., Oge, H., Sahin, G., Aypak, S., 2007. Effects of immunization with purified specific proteins on the formation of secondary hydatid cysts in mice. Tierarztl. Wochenschr. 114, 349–353.

Camicia, F., Herz, M., Prada, L.C., Kamenetzky, L., Simonetta, S.H., Cucher, M.A., Bianchi, J.I., Fernandez, C., Brehm, K., Rosenzvit, M.C., 2013. The nervous and prenervous roles of serotonin in Echinococcus spp. Int. J. Parasitol. 43, 647–659. https://doi.org/10.1016/j.ijpara.2013.03.006.

Canivet, C., Uyar, O., Rheaume, C., Piret, J., Boivin, G., 2019. The recruitment of peripheral blood leukocytes to the brain is delayed in susceptible BALB/c compared to resistant C57BL/6 mice during herpes simplex virus encephalitis. J. Neurovirol. https://doi.org/10.1007/s13365-019-00730-5.

Carol, H., Nieto, A., 1998. A mucosal IgA response, but no systemic antibody response, is evoked by intranasal immunisation of dogs with Echinococcus granulosus surface antigens iscoms. Vet. Immunol. Immunopathol. 65, 29–41.

Ceballos, L., Elissondo, C., Sánchez Bruni, S., Confalonieri, A., Denegri, G., Alvarez, L., Lanusse, C., 2010. Chemoprophylactic activity of flubendazole in cystic echinococcosis. Chemotherapy 56, 386–392. https://doi.org/10.1159/000316827.

Chabalgoity, J.A., Harrison, J.A., Esteves, A., Demarco de Hormaeche, R., Ehrlich, R., Khan, C.M., Hormaeche, C.E., 1997. Expression and immunogenicity of an Echinococcus granulosus fatty acid-binding protein in live attenuated Salmonella vaccine strains. Infect. Immun. 65, 2402–2412.

Chabalgoity, J.A., Moreno, M., Carol, H., Dougan, G., Hormaeche, C.E., 2000. Salmonella typhimurium as a basis for a live oral Echinococcus granulosus vaccine. Vaccine 19, 460–469. https://doi.org/10.1016/s0264-410x(00)00197-3.

Cheers, C., McKenzie, I.F., Pavlov, H., Waid, C., York, J., 1978. Resistance and susceptibility of mice to bacterial infection: course of listeriosis in resistant or susceptible mice. Infect. Immun. 19, 763–770.

Chiodini, R.J., Buergelt, C.D., 1993. Susceptibility of Balb/c, C57/B6 and C57/B10 mice to infection with Mycobacterium paratuberculosis. J. Comp. Pathol. 109, 309–319. https://doi.org/10.1016/S0021-9975(08)80295-2.

Colby, L.A., Quenee, L.E., Zitzow, L.A., 2017. Considerations for infectious disease research studies using animals. Comp. Med. 67, 222–231.

Colebrook, A.L., Jenkins, D.D., Lightowlers, M.W., 2002. Anti-parasitic effect of cyclosporin A on Echinococcus granulosus and characterization of the associated cyclophilin protein. Parasitology 125, 485–493. https://doi.org/10.1017/s0031182002002330.

Cornejo-Granados, F., Hurtado-Ramirez, J.M., Hernandez-Pando, R., Ochoa-Leyva, A., 2018. Secret-AAR: a web server to assess the antigenic density of proteins and homology search against bacterial and parasite secretome proteins. Genomics. https://doi.org/10.1016/j.ygeno.2018.10.007.

Cortez-Herrera, E., Yamamoto, R.R., Rodrigues, J.J., Farias, S.E., Ferreira, H.B., Zaha, A., 2001. Echinococcus granulosus: cloning and functional in vitro characterization of an actin filament fragmenting protein. Exp. Parasitol. 97, 215–225. https://doi.org/10.1006/expr.2001.4605.

Cucher, M., Mourglia-Ettlin, G., Prada, L., Costa, H., Kamenetzky, L., Poncini, C., Dematteis, S., Rosenzvit, M.C., 2013. Echinococcus granulosus pig strain (G7 genotype) protoscoleces did not develop secondary hydatid cysts in mice. Vet. Parasitol. 193, 185–192. https://doi.org/10.1016/j.vetpar.2012.11.027.

Cumino, A.C., Nicolao, M.C., Loos, J.A., Denegri, G., Elissondo, M.C., 2012. Echinococcus granulosus tegumental enzymes as in vitro markers of pharmacological damage: A biochemical and molecular approach. Parasitol. Int. 61, 579–585. https://doi.org/10.1016/j.parint.2012.05.007.

Dematteis, S., Baz, A., Rottenberg, M., Fernández, C., Örn, A., Nieto, A., 1999. Antibody and Th1/Th2-type responses in BALB/c mice inoculated with live or dead Echinococcus granulosus protoscoleces. Parasite Immunol. 21, 19–26. https://doi.org/10.1046/j.1365-3024.1999.00198.x.

Dematteis, S., Rottenberg, M., Baz, A., 2003. Cytokine response and outcome of infection depends on the infective dose of parasites in experimental infection by Echinococcus granulosus. Parasite Immunol. 25, 189–197. https://doi.org/10.1046/j.1365-3024.2003.00620.x.

Denegri, G., Perez-Serrano, J., Casado, N., Rodriguez-Caabeiro, F., 1995. [13C]-nuclear magnetic resonance spectral profiles of serum from normal and Echinococcus granulosus-infected mice: a kinetic study. Parasitol. Res. 81, 170–172.

Díaz-Zaragoza, M., Hernández-Ávila, R., Ostoa-Saloma, P., 2017. Recognition of tumor antigens in 4T1 cells by natural IgM from three strains of mice with different susceptibilities to spontaneous breast cancer. Oncol. Lett. 13, 271–274. https://doi.org/10.3892/ol.2016.5427.

Ferragut, G., Ljungstrom, I., Nieto, A., 1998. Relevance of circulating antigen detection to follow-up experimental and human cystic hydatid infections. Parasite Immunol. 20, 541–549.

Ferreira, B.L., Ferreira, É.R., de Brito, M.V., Salu, B.R., Oliva, M.L.V., Mortara, R.A., Orikaza, C.M., 2018. BALB/c and C57BL/6 mice cytokine responses to Trypanosoma cruzi infection are independent of parasite strain infectivity. Front. Microbiol. 9, 1–12. https://doi.org/10.3389/fmicb.2018.00553.

Fornefett, J., Krause, J., Klose, K., Fingas, F., Hassert, R., Benga, L., Grunwald, T., Müller, U., Schrödl, W., Baums, C.G., 2018. Comparative analysis of humoral immune responses and pathologies of BALB/c and C57BL/6 wildtype mice experimentally infected with a highly virulent Rodentibacter pneumotropicus (Pasteurella pneumotropica) strain. BMC Microbiol. 18, 1–11. https://doi.org/10.1186/s12866-018-1186-8.

Fulton, K.M., Martin, S.S., Wolfraim, L., Twine, S.M., 2013. Methods and applications of serological proteome analysis. Methods Mol. Biol. 1061, 97–112. https://doi.org/10.1007/978-1-62703-589-7_5.

Ghosh, I., Raghavan, N., FitzGerald, P.C., Scott, A.L., 1995. Nucleoside diphosphate kinase from the parasitic nematode Brugia malayi. Gene 164, 261–266. https://doi.org/10.1016/0378-1119(95)00500-6.

Grimm, E.D., Portugal, R.V., de Oliveira Neto, M., Martins, N.H., Polikarpov, I., Zaha, A., Ferreira, H.B., 2006. Structural analysis of an Echinococcus granulosus actin-fragmenting protein by small-angle x-ray scattering studies and molecular modeling. Biophys. J. 90, 3216–3223. https://doi.org/10.1529/biophysj.105.067801.

Hashemitabar, G.R., Razmi, G.R., Naghibi, A., 2005. Trials to induce protective immunity in mice and sheep by application of protoscolex and hydatid fluid antigen or whole body antigen of Echinococcus granulosus. J. Vet. Med. Ser. B Infect. Dis. Vet. Public Heal. 52, 243–245. https://doi.org/10.1111/j.1439-0450.2005.00847.x.

Heath, D.D., 1970. The development of Echinococcus granulosus larvae in laboratory

animals. Parasitology 60, 449–456. https://doi.org/10.1017/s0031182000078252.
Hebert, G.A., 1974. Ammonium sulfate fractionation of sera: mouse, hamster, guinea pig, monkey, chimpanzee, swine, chicken, and cattle. Appl. Microbiol. 27, 389–393.
Henderson, K.S., Pritchett-Corning, K.R., Perkins, C.L., Banu, L.A., Jennings, S.M., Francis, B.C., Shek, W.R., 2015. A comparison of mouse parvovirus 1 infection in BALB/c and C57BL/6 mice: susceptibility, replication, shedding, and seroconversion. Comp. Med. 65, 5–14.
Hernández, A., Nieto, A., 1994. Induction of protective immunity against murine secondary hydatidosis. Parasite Immunol. 16, 537–544. https://doi.org/10.1111/j.1365-3024.1994.tb00308.x.
Hurd, H., Mackenzie, K.S., Chappell, L.H., 1993. Anthelmintic effects of cyclosporin A on protoscoleces and secondary hydatid cysts of Echinococcus granulosus in the mouse. Int. J. Parasitol. 23, 315–320. https://doi.org/10.1016/0020-7519(93)90005-j.
Jiang, X., Shen, C., Yu, H., Karunakaran, K.P., Brunham, R.C., 2010. Differences in innate immune responses correlate with differences in murine susceptibility to Chlamydia muridarum pulmonary infection. Immunology 129, 556–566. https://doi.org/10.1111/j.1365-2567.2009.03157.x.
Jovicic, N., Jeftic, I., Jovanovic, I., Radosavljevic, G., Arsenijevic, N., Lukic, M.L., Pejnovic, N., 2015. Differential immunometabolic phenotype in Th1 and Th2 dominant mouse strains in response to high-fat feeding. PLoS One 10, 1–21. https://doi.org/10.1371/journal.pone.0134089.
Kemp, W.M., Brown, P.R., Merritt, S.C., Miller, R.E., 1980. Tegument-associated antigen modulation by adult male Schistosoma mansoni. J. Immunol. 124, 806–811.
Koziol, U., Koziol, M., Preza, M., Costabile, A., Brehm, K., Castillo, E., 2016. De novo discovery of neuropeptides in the genomes of parasitic flatworms using a novel comparative approach. Int. J. Parasitol. 46, 709–721. https://doi.org/10.1016/j.ijpara.2016.05.007.
Kulcsar, K.A., Baxter, V.K., Abraham, R., Nelson, A., Griffin, D.E., 2015. Distinct immune responses in resistant and susceptible strains of mice during neurovirulent alphavirus encephalomyelitis. J. Virol. 89, 8280–8291. https://doi.org/10.1128/jvi.00173-15.
La-Rocca, S., Farias, J., Chalar, C., Kun, A.E., Fernandez, V., 2019. Echinococcus granulosus: insights into the protoscolex F-actin cytoskeleton. Acta Trop. 199, 105122. https://doi.org/10.1016/j.actatropica.2019.105122.
Leroux, L.-P., Nasr, M., Valanparambil, R., Tam, M., Rosa, B.A., Siciliani, E., Hill, D.E., Zarlenga, D.S., Jaramillo, M., Weinstock, J.V., Geary, T.G., Stevenson, M.M., Urban, J.F.J., Mitreva, M., Jardim, A., 2018. Analysis of the Trichuris suis excretory/secretory proteins as a function of life cycle stage and their immunomodulatory properties. Sci. Rep. 8, 15921. https://doi.org/10.1038/s41598-018-34174-4.
Li, J., Zhang, W.-B., Loukas, A., Lin, R.-Y., Ito, A., Zhang, L.-H., Jones, M., McManus, D.P., 2004. Functional expression and characterization of Echinococcus granulosus thioredoxin peroxidase suggests a role in protection against oxidative damage. Gene 326, 157–165. https://doi.org/10.1016/j.gene.2003.10.027.
Linder, E., Thors, C., 1992. Schistosoma mansoni: praziquantel-induced tegumental lesion exposes actin of surface spines and allows binding of actin depolymerizing factor, gelsolin. Parasitology 105 (Pt 1), 71–79. https://doi.org/10.1017/s0031182000073704.
Liu, B., Koo, G.C., Yap, E.H., Chua, K.L., Gan, Y.H., 2002. Model of differential susceptibility to mucosal Burkholderia pseudomallei infection. Infect. Immun. 70, 504–511. https://doi.org/10.1128/IAI.70.2.504-511.2002.
Lorenzatto, K.R., Monteiro, K.M., Paredes, R., Paludo, G.P., da Fonseca, M.M., Galanti, N., Zaha, A., Ferreira, H.B., 2012. Fructose-bisphosphate aldolase and enolase from Echinococcus granulosus: genes, expression patterns and protein interactions of two potential moonlighting proteins. Gene 506, 76–84. https://doi.org/10.1016/j.gene.2012.06.046.
Magnan, C.N., Zeller, M., Kayala, M.A., Vigil, A., Randall, A., Felgner, P.L., Baldi, P., 2010. High-throughput prediction of protein antigenicity using protein microarray data. Bioinformatics 26, 2936–2943. https://doi.org/10.1093/bioinformatics/btq551.
Mamuti, W., Yamasaki, H., Sako, Y., Nakaya, K., Nakao, M., Lightowlers, M.W., Ito, A., 2002. Usefulness of Hydatid Cyst Fluid of Echinococcus granulosus Developed in Mice with Secondary Infection for Serodiagnosis of Cystic Echinococcosis in Humans. Clin. Diagn. Lab. Immunol. 9, 573–576. https://doi.org/10.1128/CDLI.9.3.573.
Maronpot, R.R., 2009. Biological basis of differential susceptibility to hepatocarcinogenesis among mouse strains. J. Toxicol. Pathol. 22, 11–33. https://doi.org/10.1293/tox.22.1.
Marques, I., de, A., Romanello, L., DeMarco, R., Pereira, H.D., 2012. Structural and kinetic studies of Schistosoma mansoni adenylate kinases. Mol. Biochem. Parasitol. 185, 157–160. https://doi.org/10.1016/j.molbiopara.2012.07.003.
Matsuo, T., Hashimoto, M., Sakaguchi, S., Sakaguchi, N., Ito, Y., Hikida, M., Tsuruyama, T., Sakai, K., Yokoi, H., Shirakashi, M., Tanaka, M., Ito, H., Yoshifuji, H., Ohmura, K., Fujii, T., Mimori, T., 2019. Strain-specific manifestation of lupus-like systemic autoimmunity caused by Zap70 mutation. J. Immunol. https://doi.org/10.4049/jimmunol.1801159.
McCarthy, J.S., Wieseman, M., Tropea, J., Kaslow, D., Abraham, D., Lustigman, S., Tuan, R., Guderian, R.H., Nutman, T.B., 2002. Onchocerca volvulus glycolytic enzyme fructose-1,6-bisphosphate aldolase as a target for a protective immune response in humans. Infect. Immun. 70, 851–858. https://doi.org/10.1128/iai.70.2.851-858.2002.
McManus, D.P., Smyth, J.D., 1982. Intermediary carbohydrate metabolism in protoscoleces of Echinococcus granulosus (horse and sheep strains) and E. multilocularis. Parasitology 84, 351–366. https://doi.org/10.1017/s0031182000044899.
McVeigh, P., Atkinson, L., Marks, N.J., Mousley, A., Dalzell, J.J., Sluder, A., Hammerland, L., Maule, A.G., 2012. Parasite neuropeptide biology: seeding rational drug target selection? Int. J. Parasitol. Drugs drug Resist. 2, 76–91. https://doi.org/10.1016/j.ijpddr.2011.10.004.
Meng, X., Kawahara, K., Matsushita, K., Nawa, Y., Shrestha, B., Kikuchi, K., Sameshima, H., Hashiguchi, T., Maruyama, I., 2009a. Attenuation of LPS-induced iNOS expression by 1,5-anhydro-d-fructose. Biochem. Biophys. Res. Commun. 387, 42–46. https://doi.org/10.1016/j.bbrc.2009.06.108.
Meng, X., Kawahara, K., Nawa, Y., Miura, N., Shrestha, B., Tancharoen, S., Sameshima, H., Hashiguchi, T., Maruyama, I., 2009b. 1,5-Anhydro-D-fructose attenuates lipopolysaccharide-induced cytokine release via suppression of NF-kappaB p65 phosphorylation. Biochem. Biophys. Res. Commun. 380, 343–348. https://doi.org/10.1016/j.bbrc.2009.01.084.
Miguez, M., Baz, A., Nieto, A., 1996. Carbohydrates on the Surface of Echinococcus granulosus Protoscoleces Are Immunodominant in Mice. pp. 559–569.
Miles, S., Navatta, M., Dematteis, S., Mourglia-Ettlin, G., 2017. Identification of universal diagnostic peptide candidates for neglected tropical diseases caused by cestodes through the integration of multi-genome-wide analyses and immunoinformatic predictions. Infect. Genet. Evol. 54. https://doi.org/10.1016/j.meegid.2017.07.020.
Miles, S., Portela, M., Cyrklaff, M., Ancarola, M.E., Frischknecht, F., Durán, R., Dematteis, S., Mourglia-Ettlin, G., 2019. Combining proteomics and bioinformatics to explore novel tegumental antigens as vaccine candidates against Echinococcus granulosus infection. J. Cell. Biochem. https://doi.org/10.1002/jcb.28799.
Mols-Vorstermans, T., Hemphill, A., Monney, T., Schaap, D., Boerhout, E., 2013. Differential effects on survival, humoral immune responses and brain lesions in inbred BALB/C, CBA/CA, and C57BL/6 mice experimentally infected with neospora caninum tachyzoites. ISRN Parasitol. 2013, 1–11. https://doi.org/10.5402/2013/830980.
Mourglia-ettlin, G., Cucher, M., Arbildi, P., Rosenzvit, M., Dematteis, S., 2016a. Natural and induced antibodies contribute to differential susceptibility to secondary cystic echinococcosis of Balb/c and C57Bl/6 mice. Immunobiology. https://doi.org/10.1016/j.imbio.2015.07.016.
Mourglia-ettlin, G., Merlino, A., Capurro, R., Dematteis, S., 2016b. Associations between mouse strains and early peritoneal immune responses. Immunobiology. https://doi.org/10.1016/j.imbio.2015.11.012.
Mourglia-Ettlin, G., Marqués, J.M., Chabalgoity, J.A., Dematteis, S., 2011. Early peritoneal immune response during echinococcus granulosus establishment displays a biphasic behavior. PLoS Negl. Trop. Dis. 5, 1–11. https://doi.org/10.1371/journal.pntd.0001293.
Mourglia-Ettlin, G., Miles, S., Hernández, A., Dematteis, S., 2018a. Antibody profiling in ultrasound normal individuals with positive serology for cystic echinococcosis. Parasite Immunol. 38. https://doi.org/10.1111/pim.12302.
Mourglia-Ettlin, G., Miles, S., Velasco-de-Andres, M., Armiger-borr, N., Cucher, M., Dematteis, S., Lozano, F., 2018b. The Ectodomains of the Lymphocyte Scavenger Receptors CD5 and CD6 Interact With Tegumental Antigens From Echinococcus granulosus Sensu Lato and Protect Mice Against Secondary Cystic Echinococcosis. pp. 1–24.
Muller-Schollenberger, V., Beyer, W., Schnitzler, P., Merckelbach, A., Roth, S., Kalinna, B.H., Lucius, R., 2001. Immunisation with Salmonella typhimurium-delivered glyceraldehyde-3-phosphate dehydrogenase protects mice against challenge infection with Echinococcus multilocularis eggs. Int. J. Parasitol. 31, 1441–1449. https://doi.org/10.1016/s0020-7519(01)00244-2.
Nag, S., Larsson, M., Robinson, R.C., Burtnick, L.D., 2013. Gelsolin: the tail of a molecular gymnast. Cytoskeleton Hoboken (Hoboken) 70, 360–384. https://doi.org/10.1002/cm.21117.
Nielsen, M., Lund, O., 2009. NN-align. An artificial neural network-based alignment algorithm for MHC class II peptide binding prediction. BMC Bioinformatics 10, 296. https://doi.org/10.1186/1471-2105-10-296.
Paulino, M., Esteves, A., Vega, M., Tabares, G., Ehrlich, R., Tapia, O., 1998. Modelling a 3D structure for EgDf1 from Echinococcus granulosus: putative epitopes, phosphorylation motifs and ligand. J. Comput. Aided Mol. Des. 12, 351–360. https://doi.org/10.1023/a:1007938710249.
Pereira, Í.M., Lima, S.B., Freitas, A., de, A., Vinaud, M.C., Lino Junior, R., de, S., 2016. Experimental subcutaneous cysticercosis by Taenia crassiceps in BALB/c and C57BL/6 mice. Rev. Inst. Med. Trop. Sao Paulo 58. https://doi.org/10.1590/S1678-9946201658055.
Ponnaiya, B., Cornforth, M.N., Ullrich, R.L., 2006. Radiation-induced chromosomal instability in BALB/c and C57BL/6 mice: the difference is as clear as black and white. Radiat. Res. 147, 121. https://doi.org/10.2307/3579411.
Preza, M., Montagne, J., Costabile, A., Iriarte, A., Castillo, E., Koziol, U., 2018. Analysis of classical neurotransmitter markers in tapeworms: evidence for extensive loss of neurotransmitter pathways. Int. J. Parasitol. 48, 979–992. https://doi.org/10.1016/j.ijpara.2018.06.004.
Pullen, G.R., Fitzgerald, M.G., Hosking, C.S., 1986. Antibody avidity determination by ELISA using thiocyanate elution. J. Immunol. Methods 86, 83–87. https://doi.org/10.1016/0022-1759(86)90268-1.
Qiao, G., Li, Z., Minto, A.W., Shia, J., Yang, L., Bao, L., Tschopp, J., Gao, J., Wang, J., Quigg, R.J., Zhang, J., Cytokines, B., Corporation, I., 2010. Inhibitory Protein in T Cells Causes Lupus-Like Syndrome in 17. pp. 522–533. https://doi.org/10.1038/cdd.2009.143.Altered.
Ribeiro, P., Patocka, N., 2013. Neurotransmitter transporters in schistosomes: structure, function and prospects for drug discovery. Parasitol. Int. 62, 629–638. https://doi.org/10.1016/j.parint.2013.06.003.
Richards, K.S., Arme, C., Bridges, J., 1983. Echinococcus granulosus equinus: an ultrastructural study of murine tissue response to hydatid cysts. Parasitology 86, 407–417. https://doi.org/10.1017/S0031182000050605.
Rogan, M.T., Bodell, A.J., Craig, P.S., 2015. Post-encystment/established immunity in cystic echinococcosis: is it really that simple? Parasite Immunol. 37, 1–9. https://doi.org/10.1111/pim.12149.
Saber, M., Diab, T., Hammam, O., Karim, A., Medhat, A., Khela, M., El-Dabaa, E., 2013. Protective and anti-pathology effects of Sm fructose-1,6-bisphosphate aldolase-based

DNA vaccine against schistosoma mansoni by changing route of injection. Korean J. Parasitol. 51, 155–163. https://doi.org/10.3347/kjp.2013.51.2.155.
Salinas, G., Fernandez, V., Fernandez, C., Selkirk, M.E., 1998. Echinococcus granulosus: cloning of a thioredoxin peroxidase. Exp. Parasitol. 90, 298–301. https://doi.org/10.1006/expr.1998.4339.
Sanchez-Trincado, J.L., Gomez-Perosanz, M., Reche, P.A., 2017. Fundamentals and methods for t- and B-Cell epitope prediction. J. Immunol. Res. 2017, 1–14. https://doi.org/10.1155/2017/2680160.
Schulte, S., Sukhova, G.K., Libby, P., 2008. Genetically programmed biases in Th1 and Th2 immune responses modulate atherogenesis. Am. J. Pathol. 172, 1500–1508. https://doi.org/10.2353/ajpath.2008.070776.
Shi, Z., Wang, Y., Li, Zongji, Li, Zhaoyu, Bo, Y., Ma, R., Zhao, W., 2009. Cloning, expression, and protective immunity in mice of a gene encoding the diagnostic antigen P-29 of Echinococcus granulosus. Acta Biochim. Biophys. Sin. (Shanghai). 41, 79–85. https://doi.org/10.1093/abbs/gmn009.
Skelly, P.J., Kim, J.W., Cunningham, J., Shoemaker, C.B., 1994. Cloning, characterization, and functional expression of cDNAs encoding glucose transporter proteins from the human parasite Schistosoma mansoni. J. Biol. Chem. 269, 4247–4253.
Sofron, A., Ritz, D., Neri, D., Fugmann, T., 2016. High-resolution analysis of the murine MHC class II immunopeptidome. Eur. J. Immunol. 46, 319–328. https://doi.org/10.1002/eji.201545930.
Tamarozzi, F., Mariconti, M., Neumayr, A., Brunetti, E., 2016. The intermediate host immune response in cystic echinococcosis. Parasite Immunol. 38, 170–181. https://doi.org/10.1111/pim.12301.
Valizadeh, M., Haghpanah, B., Badirzadeh, A., Roointan, E., Fallahi, S., Raeghi, S., 2017. Immunization of sheep against Echinococcus granulosus with protoscolex tegumental surface antigens. Vet. World 10, 854–858. https://doi.org/10.14202/vetworld.2017.854-858.
Vessal, M., Tabei, S.M., 1996. Partial purification and kinetic properties of cytoplasmic malate dehydrogenase from ovine liver Echinococcus granulosus protoscolices. Comp. Biochem. Physiol. B, Biochem. Mol. Biol. 113, 757–763. https://doi.org/10.1016/0305-0491(95)02099-3.
Vlkova, M., Rohousova, I., Hostomska, J., Pohankova, L., Zidkova, L., Drahota, J., Valenzuela, J.G., Volf, P., 2012. Kinetics of antibody response in BALB/c and C57BL/6 mice bitten by phlebotomus papatasi. PLoS Negl. Trop. Dis. 6, 1–9. https://doi.org/10.1371/journal.pntd.0001719.
Wang, H., Li, Z., Gao, F., Zhao, J., Zhu, M., He, X., Niu, N., Zhao, W., 2016. Immunoprotection of recombinant Eg.P29 against Echinococcus granulosus in sheep. Vet. Res. Commun. 40, 73–79. https://doi.org/10.1007/s11259-016-9656-7.
Watanabe, H., Numata, K., Ito, T., Takagi, K., Matsukawa, A., 2004. Innate immune response in Th1- and Th2-dominant mouse strains. Shock 22, 460–466. https://doi.org/10.1097/01.shk.0000142249.08135.e9.
WHO, 2017. Integrating Neglected Tropical Diseases Into Global Health and Development: Fourth WHO Report on Neglected Tropical Diseases. World Health Organization.
Xiang, J., Zhang, S., Leclercq, G., Nauwynck, H., 2016. Difference in replication of low-passage MCMV HaNa1 in BALB/c, C57BL/6 and NOD mice and role of different branches of immunity in susceptibility. Virus Res. 221, 38–46. https://doi.org/10.1016/j.virusres.2016.05.006.
Xiao, S.H., Feng, J.J., Guo, H.F., Jiao, P.Y., Yao, M.Y., Jiao, W., 1993. Effects of mebendazole, albendazole, and praziquantel on succinate dehydrogenase, fumarate reductase, and malate dehydrogenase in Echinococcus granulosus cysts harbored in mice. Zhongguo Yao Li Xue Bao 14, 151–154.
Yang, Y., Bai, X., Li, C., Tong, M., Zhang, P., Cai, W., Liu, X., Liu, M., 2019. Molecular characterization of Fructose-1,6-bisphosphate aldolase from Trichinella spiralis and its potential in inducing immune protection. Front. Cell. Infect. Microbiol. 9, 122. https://doi.org/10.3389/fcimb.2019.00122.
Yu, S., 2008. The anhydrofructose pathway of glycogen catabolism. IUBMB Life 60, 798–809. https://doi.org/10.1002/iub.125.
Yu, S., Fiskesund, R., 2006. The anhydrofructose pathway and its possible role in stress response and signaling. Biochim. Biophys. Acta 1760, 1314–1322. https://doi.org/10.1016/j.bbagen.2006.05.007.
Zeng, M., Nourishirazi, E., Guinet, E., Nouri-Shirazi, M., 2016. The genetic background influences the cellular and humoral immune responses to vaccines. Clin. Exp. Immunol. 186, 190–204. https://doi.org/10.1111/cei.12841.
Zhang, W.Y., Moreau, E., Hope, J.C., Howard, C.J., Huang, W.Y., Chauvin, A., 2005. Fasciola hepatica and Fasciola gigantica: comparison of cellular response to experimental infection in sheep. Exp. Parasitol. 111, 154–159. https://doi.org/10.1016/j.exppara.2005.06.005.

ARTÍCULO 5

Identification of universal diagnostic peptide candidates for neglected tropical diseases caused by cestodes through the integration of multi-genome-wide analyses and immunoinformatic predictions.

Miles S, Navatta M, Dematteis S, Mourglia-Ettlin G.

Infection, Genetics and Evolution

2017

doi: 10.1016/j.meegid.2017.07.020

Infection, Genetics and Evolution 54 (2017) 338–346

Contents lists available at ScienceDirect

Infection, Genetics and Evolution

journal homepage: www.elsevier.com/locate/meegid

Research paper

Identification of universal diagnostic peptide candidates for neglected tropical diseases caused by cestodes through the integration of multi-genome-wide analyses and immunoinformatic predictions☆,☆☆

Sebastián Miles, Marco Navatta, Sylvia Dematteis, Gustavo Mourglia-Ettlin *

Cátedra de Inmunología, DEPBIO/IQB. Facultad de Química/Facultad de Ciencias, Universidad de la República, Montevideo, Uruguay

ARTICLE INFO

Article history:
Received 3 March 2017
Received in revised form 16 June 2017
Accepted 15 July 2017
Available online 17 July 2017

Keywords:
Neglected tropical diseases
Secretome
Linear B cell epitopes
Immunoinformatics
Serodiagnosis

ABSTRACT

Neglected tropical diseases caused by helminth infections currently affect millions of people worldwide. Among them, there are three tapeworm species of outstanding importance: *Echinococcus granulosus*, *E. multilocularis*, and *Taenia solium*, which are responsible for cystic echinococcosis, alveolar echinococcosis, and cysticercosis, respectively. Despite several attempts, there is still a need for an effective and low-cost serological diagnostic test that can be used in endemic countries. In the present work, we described an innovative bioinformatic workflow for a rational prediction of putative peptide candidates for one-step serological diagnosis of any of these infections. First, we predicted the theoretical secretome shared by the three tapeworms starting from their full reported proteomes. Then, through immunoinformatics, we identified proteins within the shared secretome displaying high antigenicity scores and bearing T cell epitopes able to bind most human MHC-II alleles. Secondly, in such proteins, we identified linear B cell epitopes without post-translational modifications, and mapped them on 3D modelled structures to visualize their antibody accessibilities. As a result, we finally suggested two antigenic peptides shared between the secretomes of the three parasite species, which could be further tested for their immunodiagnostic potential.

1. Introduction

On the list of neglected tropical diseases determined by the WHO, three of them are infections caused by tapeworms: cysticercosis (*Taenia solium*), cystic echinococcosis (*Echinococcus granulosus*), and alveolar echinococcosis (*E. multilocularis*) (WHO, 2016). The three parasite species undergo complex life cycles, involving two different mammalian hosts (*e.g.* definitive and intermediate hosts). In *T. solium* infection, humans are the only known definitive host for the adult tapeworm, whereas both pigs and humans may act as intermediate hosts. Adult *T. solium* inhabits the small intestine of humans releasing fertile eggs into the environment through host feces. Eggs can later develop into cysticerci if ingested by pigs. Human feeding with poorly cooked meat from infected pork closes the parasite life cycle. However, humans can also act as intermediate hosts for *T. solium* after ingesting eggs, developing human cysticercosis (Del Brutto, 2012). It is worth mentioning that when the infection establishes in the central nervous system (neurocysticercosis), it is considered the most important neurological parasitic disease, being responsible for almost one third of the acquired epilepsy cases in *T. solium* endemic areas (Coral-Almeida et al., 2015). On the other hand, for cystic echinococcosis, dogs and other canids act as definitive hosts for the intestinal tapeworms, releasing eggs through host feces. Domestic and wild ungulates become intermediate host when the tissue-invading metacestode stage develops, mainly in their livers and lungs. Metacestodes are fluid-filled, spherical, unilocular cysts, which can produce protoscoleces by asexual reproduction (Moro and Schantz, 2009). Humans may act as accidental intermediate hosts after the ingestion of eggs. Finally, alveolar echinococcosis is transmitted from definitive hosts (mainly foxes bearing adult *E. multilocularis* worms in their intestines) to natural intermediate hosts (*e.g.* rodents) through eggs expelled along with definitive host feces. The clinical manifestation of alveolar echinococcosis in humans (accidental intermediate hosts) resembles an alveolar-like pattern of microvesicles that proliferates indefinitely and primarily in the liver. Alveolar echinococcosis can cause liver failure and spread into nearby tissues or even into the brain (Moro and Schantz, 2009).

Medical diagnosis for any of the three infections relies on imaging techniques and/or immunodiagnostic tests (Giri and Parija, 2012;

☆ **Disclosure**: All authors declare that there are NONE potential conflicts of interest relevant to this article to declare.

☆☆ **Contributions**: SM and GM-E conceptualized the work. SM and MN performed the research. SM, MN, SD and GM-E discussed results. SM and GM-E wrote the paper.

* Corresponding author at: Instituto de Higiene, Av. Alfredo Navarro 3051, C.P. 11600 Montevideo, Uruguay.
E-mail address: gmourglia@higiene.edu.uy (G. Mourglia-Ettlin).

http://dx.doi.org/10.1016/j.meegid.2017.07.020
1567-1348/

Mihmanli et al., 2016). Among imaging techniques ultrasonography, computed tomography and magnetic resonance are the most useful tools, but their accuracy/sensitivity levels are highly dependent on cyst localization and/or infection stages. Moreover, such mid-high technology facilities and infrastructures are not always available in endemic areas (Giri and Parija, 2012). On the other hand, immunodiagnostic tests such as enzyme-linked immunosorbent assays (ELISA) are the preferred option in developing countries because of their simplicity and low costs. In this sense, different ELISA using crude cyst fluid have been developed for each infection, exhibiting quite good sensitivities but not optimal specificities. Other immunodiagnostic techniques have also been tested, but they are rarely used in clinical settings (Giri and Parija, 2012).

A major shortcoming in the development of new serodiagnostic tests is the identification/choice of proper antigens. Although different antigenic components from *E. granulosus*, *E. multilocularis* and *T. solium* have been evaluated, no better diagnostic performances were achieved. The main disadvantage in using crude antigens is the cross-reactivity seen with sera from patients infected with other parasites (Giri and Parija, 2012). To overcome this low-specificity issue, many purified antigens have been evaluated, such as Ag5 for both cystic and alveolar echinococcosis (Giri and Parija, 2012) and AgB for each of the three parasites (Giri and Parija, 2012; Rodriguez et al., 2012). Unfortunately, limitations in parasite material availability turned that strategy into a great drawback. To avoid this problem, recombinant antigens have also been evaluated in the past decades, with reports of varying performance degrees (Giri and Parija, 2012). However, some recombinant antigens showed less immunoreactivity than their native counterparts did, most probably due to altered post-translational modifications and/or because of misfolded structures. In addition, high quality and quantity production of recombinant proteins is not easy and rather expensive (Gómara and Haro, 2007).

More recently, the use of synthetic peptides as antigens for immunodiagnostic tests has risen in popularity as a way to overcome most of the problems already mentioned. These peptides mimic linear or conformational B cell epitopes from antigenic proteins, lowering the overall cost of the test, and therefore making them more suitable for low-income countries. The use of synthetic peptides for immunodiagnosis have been widely evaluated, leading to the development of several high sensitivity and specificity tests in recent years against infections caused by viruses (Gauna et al., 2015; Ma et al., 2016; X. Wang et al., 2015), bacteria (Aguiar et al., 2016; Yin et al., 2016) and parasites (Guimarães-Peixoto et al., 2016; Wang et al., 2016). In the present post-genomic era, the availability of complete genome sequences and advanced analysis algorithms have contributed to the possibility of predicting antigens *in silico*, which could be useful for designing new immunodiagnostic tests (Carvalho et al., 2011; Seib et al., 2012). Bioinformatic tools reduce time and costs through *in silico* prediction of known biological and physical interactions, and although such predictions are not perfect yet, continuous improvements of algorithms are made on a daily basis, due to their machine learning properties (Backert and Kohlbacher, 2015). In this sense, although prediction accuracy varies greatly depending on the complexity of available data, it can be improved by combining multiple tools to achieve a common goal. For example, although the prediction of secreted proteins in animals by using a single software show low-medium confidence for any available tool (63–82% of accuracy), the prediction can be significantly improved by a combined-software approach (up to 92.1% in sensitivity and 98.9% in specificity) (Lum and Min, 2011; Meinken and Min, 2012; Min, 2010). Therefore, it is extremely important to design and develop new and creative rational bioinformatics workflows for immunoinformatic studies.

In this work, we performed for the first time an unbiased multi-genome-wide screening of the three tapeworm species that cause neglected tropical diseases (*E. granulosus*, *E. multilocularis* and *T. solium*) in order to identify common potential diagnostic peptides derived from their shared predicted secretomes. Similar secretome predictions have already been performed for *E. multilocularis* (S. Wang et al., 2015; X. Wang et al., 2015) and *T. solium* (Gomez et al., 2015); however, this is the first study to predict not only the potential secretome of *E. granulosus* from its full proteome, but also to apply a systematic bio- and immuno-informatic pipeline for the three cestodes. Secreted proteins are assumed to easily interact with the host immune system, leading to the production of specific antibodies against some, if not all of them. Thus, we first predicted the secretomes for each parasite using a complete bioinformatic approach, and then a common secretome shared by the three species was selected based on homology analyses. After that, proteins showing no significant homologous within the human proteome were further studied for their antigenicity and potential for being presented by most human MHC class II alleles. Finally, in selected proteins, we identified and mapped some shared antigenic amino acid sequences potentially able to be recognized by antibodies. As a result, putative diagnostic peptides for neglected tropical diseases caused by cestodes were suggested.

2. Materials and methods

2.1. Prediction of secretomes

Full proteomes from *E. granulosus*, *E. multilocularis* and *T. solium* reported by Tsai et al. (2013) were downloaded on January 2016, from the helminth genome database of Sanger Institute (http://www.sanger.ac.uk/resources/downloads/helminths/). The workflow described in the present work for prediction of secretomes uses a strategy for integration of several tools similar to the one described by S. Wang et al. (2015) and X. Wang et al. (2015) but with some modifications (Fig. 1A). Only proteins between 40 and 4000 amino acids long were analyzed due to software limitations. Briefly, proteins containing no predicted transmembrane (TM) regions were selected using the algorithm TMHMM (version 2.0) (Krogh et al., 2001). TM prediction was additionally performed on 1-TM containing proteins by Phobius algorithm to discriminate between TM and signal peptides (Käll et al., 2004). Then, remaining proteins were screened for the presence of signal peptides corresponding either to classical or non-classical secretion mechanisms. SignalP (version 4.1) was used for classical secreted proteins (choosing eukaryote organism categories and other default options) (Petersen et al., 2011), while SecretomeP (version 2.0) was used for the prediction of non-classical secreted proteins (using NN-scores ≥ 0.9 and other default options for mammalian organisms) (Bendtsen et al., 2004). Predicted secreted proteins – classical and non-classical – were scanned for subcellular localization to eliminate mitochondrial proteins from the analysis using TargetP algorithm (version 1.1), with a specificity ≥ 0.90 and non-plant options (Emanuelsson et al., 2000). Then, signals for ER and GPI-anchored proteins were scanned on the remaining predicted proteins using PS-Scan (Prosite pattern: PS00014) (de Castro et al., 2006) and PredGPI (default options) (Pierleoni et al., 2008), respectively. Proteins that successfully got through our workflow were assumed to belong to each parasite secretome.

2.2. Homology analyses

In order to identify secreted proteins highly conserved between the studied cestodes, amino acid identity search was performed between them by BLAST using the software ViroBLAST (BLASTp program and default options) (Deng et al., 2007). Sequences with identities ≥ 90% were considered as orthologous proteins and were denominated tapeworms shared secretome (Fig. 1B and Table 1). Then, in order to identify which proteins from the tapeworms shared secretome show low levels of homology with human proteins, we performed homology searches against the full *Homo sapiens* proteome by BLASTp algorithm using the software e!Ensembl (http://www.ensembl.org/Multi/Tools/Blast?db=core). Proteins in the three parasite species showing ≤40% of identity with

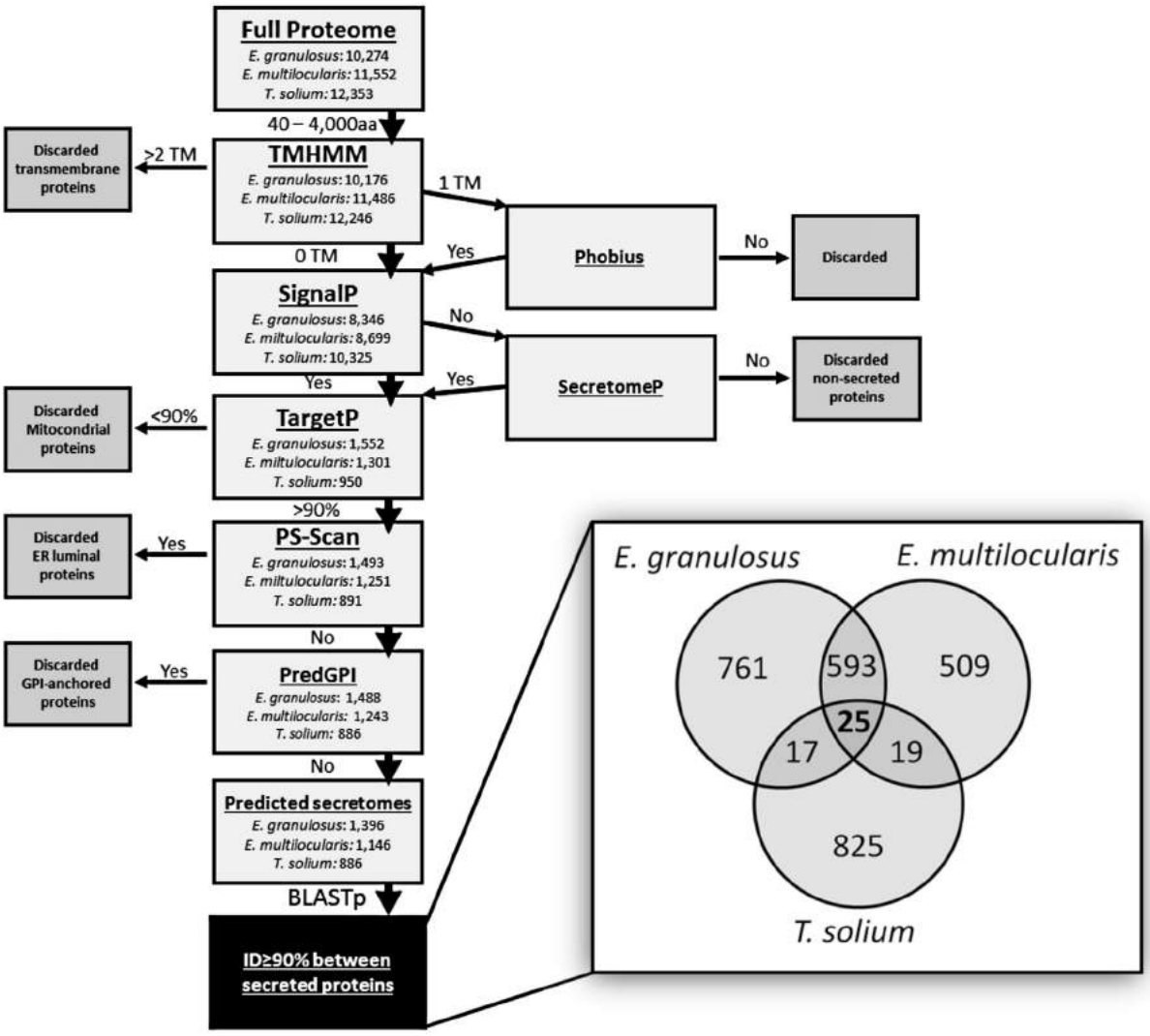

Fig. 1. *In silico* prediction of secretomes. (A) Bioinformatics workflow used for the prediction of secretomes starting from full reported proteomes. Details on software settings are described in Materials and methods (Section 2). (B) Venn diagrams showing the number of proteins shared by the predicted secretomes of the three cestodes.

human proteins were considered as non-orthologous proteins and further analyses were performed with them (Fig. 2A).

2.3. Antigenicity and T cell epitopes predictions

Non-human orthologous proteins from the tapeworms shared secretome were scanned for their antigenicity using the sequence-based, alignment-free and pathogen-independent predictor ANTIGENpro (http://scratch.proteomics.ics.uci.edu/). Proteins with antigenicity scores ≥ 0.5 were selected as probably antigenic (Magnan et al., 2010), and only proteins over this threshold in the three parasite species were chosen (Fig. 2B). Abundance of Antigenic Regions (AAR) is a value used to normalize the number of antigenic regions by the sequence length, and this value was calculated as the ratio between the protein sequence length and the number of predicted antigenic regions by Bepipred software according to Gomez et al. (2015). Then, MHC-II epitopes were predicted using the algorithm NetMHCII (version 2.2) (Nielsen and Lund, 2009). For every antigenic protein, the binding affinity of every possible 15-mer peptides was predicted against 26 human MHC-II molecules belonging to HLA-DR, HLA-DP and HLA-DQ alleles. Proteins bearing at least one strong binding peptide ($IC_{50} < 50$ nM) in >20 alleles were considered as promiscuous MHC-II binding proteins (Fig. 2C).

2.4. Prediction of post-translational modifications

Further analyses were performed on the sets of promiscuous MHC-II binding proteins to predict possible sites for post-translational modifications (PTMs). Predictions were performed using the servers GPS (http://ibs.biocuckoo.org/) and CBS (http://www.cbs.dtu.dk/services/). Analyzed PTMs included: (i) protein glycation (NetGlycate) (Johansen et al., 2006); (ii) tyrosine nitration (GPS-YNO2) (Liu et al., 2011); (iii) *S*-nitrosylation (GPS-SNO) (Xue et al., 2010); (iv) *N*-terminal acetylation (NetAcet) (Kiemer et al., 2005); (v) tyrosine sulfation (GPS-TSP) (Z. Pan et al., 2014); (vi) *N*-linked glycosylation (NetNGlyc) (Gupta et al., 2004); (vii) *O*-GalNAc glycosylation (NetOGlyc) (Steentoft et al., 2013); (viii) *S*-farnesylation (GPS-Lipid); (ix) *N*-myristoylation (GPS-Lipid); (x) other lipid modifications (GPS-Lipid) (Xie et al., 2016); (xi) palmitoylation (CSS-Palm) (Ren et al., 2008); (xii) sumoylation (GPS-SUMO) (Zhao et al., 2014); (xiii) protein methylation (GPS-MSP) (Chen et al., 2006), and (xiv) *C*-mannosylation (NetCGly) (Julenius, 2007). Predicted PTMs and their location within protein sequences are depicted in Fig. 3.

2.5. Prediction of linear B cell epitopes

Linear B cell epitopes in each set of promiscuous MHC-II binding proteins were predicted using the algorithm Bepipred (version 1.0) (Larsen

Table 1
Cestodes common shared secretome. List of the 25 sets of proteins from *E. granulosus*, *E. multilocularis* and *T. solium* showing ≥90% identity between them. Protein names and accession numbers for each parasite are shown.

Set no	Protein name	Accession number		
		E. granulosus	*E. multilocularis*	*T. solium*
1	Calcium binding protein	EgrG_000504600	EmuJ_000504600	TsM_000553800
2	Expressed conserved protein	EgrG_000632300	EmuJ_000632300	TsM_000705700
3	Expressed conserved protein	EgrG_000806200	EmuJ_000806200	TsM_000862900
4	Intraflagellar transport protein 20	EgrG_000553100	EmuJ_000553100	TsM_001182700
5	cAMP dependent protein kinase regulatory subunit type I II alpha beta	EgrG_000395400	EmuJ_000395400	TsM_000218300
6	Eukaryotic translation initiation factor 4E	EgrG_000809800	EmuJ_000809800	TsM_000763200
7	Hypothetical protein	EgrG_000932700	EmuJ_000932700	TsM_000219200
8	Complement C1q tumor necrosis factor	EgrG_001189200	EmuJ_001189200	TsM_000038900
9	TonB box	EgrG_000554900	EmuJ_000554900	TsM_000051800
10	Ankyrin repeat domain containing protein 10	EgrG_000245900	EmuJ_000245900	TsM_000225900
11	Programmed cell death protein	EgrG_000925800	EmuJ_000925800	TsM_000414300
12	Expressed protein	EgrG_001072800	EmuJ_001072800	TsM_001271600
13	Protein Wnt-04//Wingless type MMTV integration site family	EgrG_000804000	EmuJ_000804000	TsM_000297700
14	Mitochondrial import inner membrane translocase	EgrG_001050000	EmuJ_001050000	TsM_000927900
15	Small subunit ribosomal protein S30e	EgrG_000855200	EmuJ_000855200	TsM_000629600
16	PRKR interacting protein 1	EgrG_001012600	EmuJ_001012600	TsM_001062400
17	Ubiquitin conjugating enzyme	EgrG_000616800	EmuJ_000616800	TsM_000558000
18	PolyU binding splicing factor PUF60	EgrG_001087600	EmuJ_001087600	TsM_001209200
19	DNA directed RNA polymerases I II and III	EgrG_000230200	EmuJ_000230200	TsM_000656900
20	Sorting nexin	EgrG_000922200	EmuJ_000922200	TsM_000174000
21	dUTP pyrophosphatase	EgrG_000119100	EmuJ_000119100	TsM_000610800
22	Transcription factor IIb	EgrG_000056800	EmuJ_000056800	TsM_000752000
23	N alpha acetyltransferase 11	EgrG_000792500	EmuJ_000792500	TsM_000644500
24	Ubiquitin conjugating enzyme rad6	EgrG_000834100	EmuJ_000834100	TsM_000046400
25	Calmodulin family member cmd 1	EgrG_000491400	EmuJ_000491400	TsM_001257700

et al., 2006). Continuous antigenic segments ≥ 7 amino acids in length were considered as linear B cell epitopes, and those showing 100% identity between the three parasite species were selected. Predicted PTMs were mapped on protein sequences and those linear B cell epitopes without sites for PTMs were denominated clean linear B cell epitopes. Similarity analyses were performed between predicted clean linear B cell epitopes and all known linear B cell epitopes present in the Immune Epitope Database (http://www.IEDB.org). Additionally, clean linear B cell epitopes were scanned over the whole human proteome by BLASTp using the NIH server (http://blast.ncbi.nlm.nih.gov/Blast.cgi?PAGE=Proteins).

2.6. 3D modelling and mapping of clean linear B cell epitopes

3D structures for promiscuous MHC-II binding proteins were modelled by homology using RaptorX software, which performs well at aligning hard targets with <30% sequence identity respect to solved structures in Protein Data Bank. For each protein, the predicted structure with the highest uGDT (unnormalized Global Distance Test) was selected. uGDT measures the absolute model quality, being uGDT ≥ 50 a good indicator for proteins >100 amino acids long (Källberg et al., 2012). The following 3D models were used as templates. *E. granulosus* protein N°9 used 2qyu:A (27.3% identity) and protein N°10 used 4rlv:A, 1n11:A, 5et0:A, 4nik:A and 3b7b:A (identities range: 27.1–36.1%). *E. multilocularis* protein N°9 used 5is5:A and 4ph4:B (24.3% and 37.5% identity, respectively) and protein N°10 used 4rlv:A, 1n11:A, 5et1:A, 4nik:A and 3b7b:A (identities range: 27.6–36.1%). *T. solium* protein N°9 used 1ea0:A (36.1% identity) and protein N°10 used 4rlv:A, 1n11:A, 4g8k:A, 4o1o:A and 1wdy:A (identities range: 26.5–32.1%). Then, in order to visualize antibody accessibility, clean linear B cell epitopes were mapped onto each selected structure using DeepView software (Swiss-PdbViewer) (Guex and Peitsch, 1997). Clean linear B cell epitopes mapped on selected 3D models are depicted in Fig. 4.

3. Results

3.1. Prediction of secretomes

Tapeworm proteomes obtained from the helminth genome database of Sanger Institute were composed of 10,247, 11,552 and 12,353 hypothetical proteins for *E. granulosus*, *E. multilocularis* and *T. solium*, respectively. Our bioinformatic workflow for secretome prediction is shown in Fig. 1A. After eliminating hypothetical proteins out of the 40–4000 amino acids range (due to software limitations), and predicting no TM domains by TMHMM and Phobius, 8346, 8699 and 10,325 sequences were identified as TM-free for *E. granulosus*, *E. multilocularis* and *T. solium*, respectively. Further analyses on TM-free proteins were performed in order to predict secreted proteins, both by classical peptide signaling (SignalP) and non-classical protein secretion (SecretomeP). Combining results from both predictors, we found a total of 1552, 1301 and 950 secreted proteins - either classical or non-classical - for *E. granulosus*, *E. multilocularis* and *T. solium*, respectively. Proteins identified as mitochondrial by TargetP software were discarded, and remaining proteins were analyzed for extra subcellular localization (ER signal peptides and GPI anchor sequences), by PS-Scan and PredGPI softwares. Finally, 1396 (*E. granulosus*), 1146 (*E. multilocularis*) and 886 (*T. solium*) sequences were identified as the probable secretome for each tapeworm representing a 13.6%, 9.9% and 7.1% of their respective full proteomes (Fig. 1A).

3.2. Identification of the common shared proteome

Homology analyses of secreted proteins between the three tapeworm species showed different levels of conservation, from highly diverse and unique to almost identical proteins based on their amino acidic sequences. Shared secretome results obtained by BLASTp (identity ≥ 90%) are shown in Fig. 1B. We found 593 proteins exclusively shared by *E. granulosus* and *E. multilocularis*, while 17 and 19 proteins were solely shared by *T. solium* and *E. granulosus* or *E. multilocularis*,

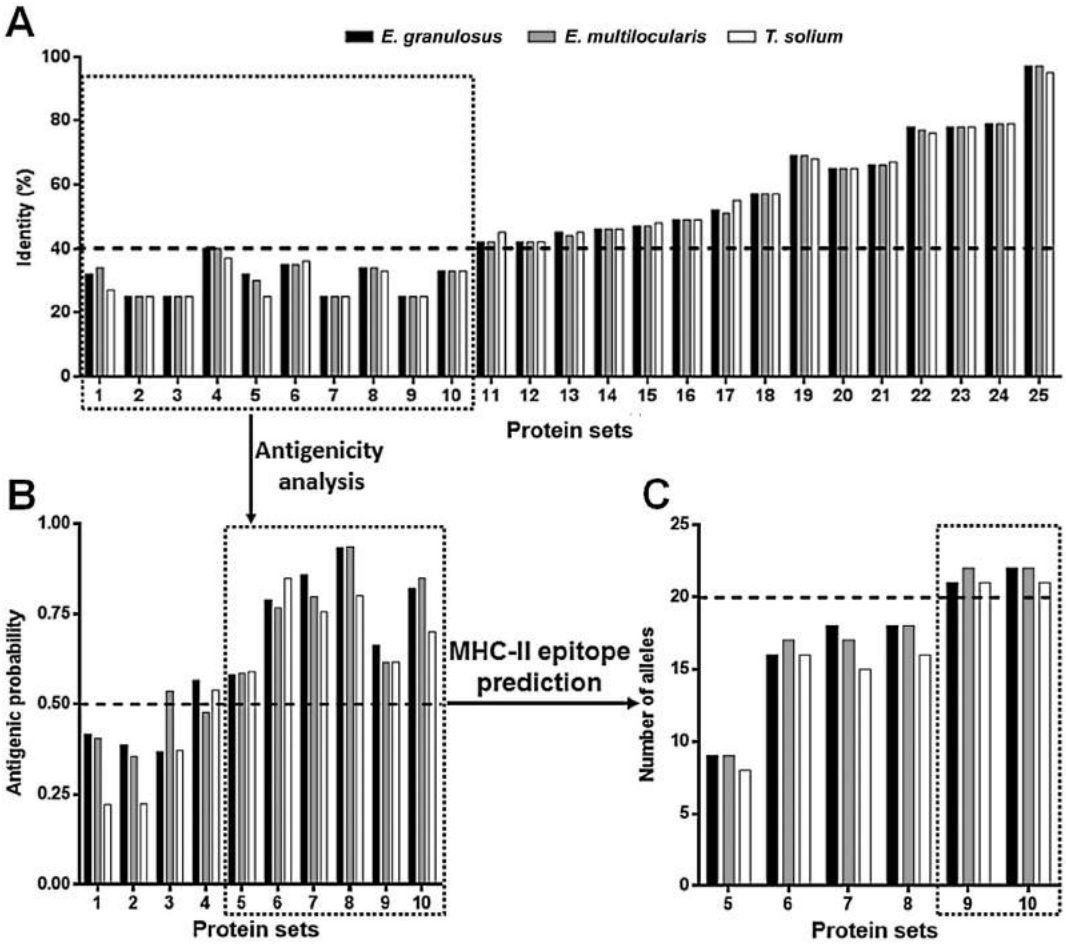

Fig. 2. Immunoinformatic identification of diagnostic candidates. Protein sets within the common shared secretome were searched for candidates with diagnostic potential. (A) Homology analysis between proteins in the cestodes common shared secretome and *Homo sapiens* full proteome were performed by BLASTp, and the highest identity score (%) is shown for each protein within the 25 sets. (B) Antigenicity probability scores for proteins showing identities ≤ 40% against *Homo sapiens* were obtained by ANTIGENpro software. (C) Within antigenic proteins, those exhibiting at least one 15-mer strong binding peptide (IC_{50} < 50 nM) in >20 MHC-II alleles were considered promiscuous MHC-II binding proteins. Epitopes and affinity predictions were performed with NetMHCII software.

respectively (Fig. 1B). Finally, only 25 proteins showed high levels of homology between the three tapeworms, representing a 1.8% (*E. granulosus*), 2.2% (*E. multilocularis*) and 2.8% (*T. solium*) of their respective secretomes (Fig. 1B). A detailed list of such 25 proteins is shown in Table 1, which were grouped into sets for further analyses.

3.3. Analyses of human homologies and antigenicity probabilities

Sequence homology analyses were performed for the 25 sets of proteins against the whole *Homo sapiens* proteome, and top score identities after BLASTp are shown in Fig. 2A. Proteins exhibiting a % ID ≤ 40 were considered non-orthologous to humans and were selected for additional studies. From the 25 shared proteins, 10 (40%) were classified as non-orthologous, and their probabilities of being antigenic were predicted by ANTIGENpro software. Antigenicity scores are shown in Fig. 2B. Proteins with scores ≥ 0.5 for the three tapeworm species were considered as highly antigenic. Six proteins out of 25 shared by the three parasite species were non-homologous to humans as well as highly antigenic (Fig. 2B). Additionally, we calculated the Abundance of Antigenic Regions (AAR) in the 10 sets of proteins that displayed low human homology, and we observed average AAR values of 24.5, 23.7 and 24.2 for *E. granulosus*, *E. multilocularis* and *T. solium*, respectively. Interestingly, average AAR values reported for *T. solium* and *E. multilocularis* secretomes were roughly 4-fold higher than our values (Gomez et al., 2015), suggesting that our selected set represents a subgroup of secreted proteins with more antigenic density.

3.4. Identification of promiscuous MHC-II binding proteins

For the six sets of proteins shared by the predicted secretomes of *E. granulosus*, *E. multilocularis* and *T. solium* showing low homologies to humans and high antigenicity probabilities, the binding affinity of every possible 15-mer peptides to different human MHC-II molecules was predicted by NetMHCII software. Analyses were performed over 26 MHC-II molecules belonging to HLA-DR, HLA-DP and HLA-DQ alleles. Proteins displaying at least one strong binding peptide (IC_{50} < 50 nM) in >20 alleles were considered promiscuous MHC-II binding proteins. Results depicted in Fig. 2C show that only protein sets termed N°9 and N°10 could be considered promiscuous MHC-II binding proteins. Regarding proteins in set N°9, they showed strong binding to 21 (*E. granulosus*), 22 (*E. multilocularis*), and 21 (*T. solium*) MHC-II alleles. On the other hand, proteins in set N°10 showed strong binding to 22 (*E. granulosus*), 22 (*E. multilocularis*), and 21 (*T. solium*) MHC-II alleles.

3.5. Prediction of PTMs and analyses of linear B cell epitopes

Both sets of promiscuous MHC-II binding proteins were analyzed for their potential sites of PTMs and for the identification of putative linear B cell epitopes. Firstly, PTMs prediction softwares showed - with some differences among tapeworms - the existence of putative sites for protein glycation, palmitoylation, tyrosine nitration, *S*-nitrosylation, tyrosine sulfation, *N*-glycosylation, *O*-GalNAc glycosylation and *N*-

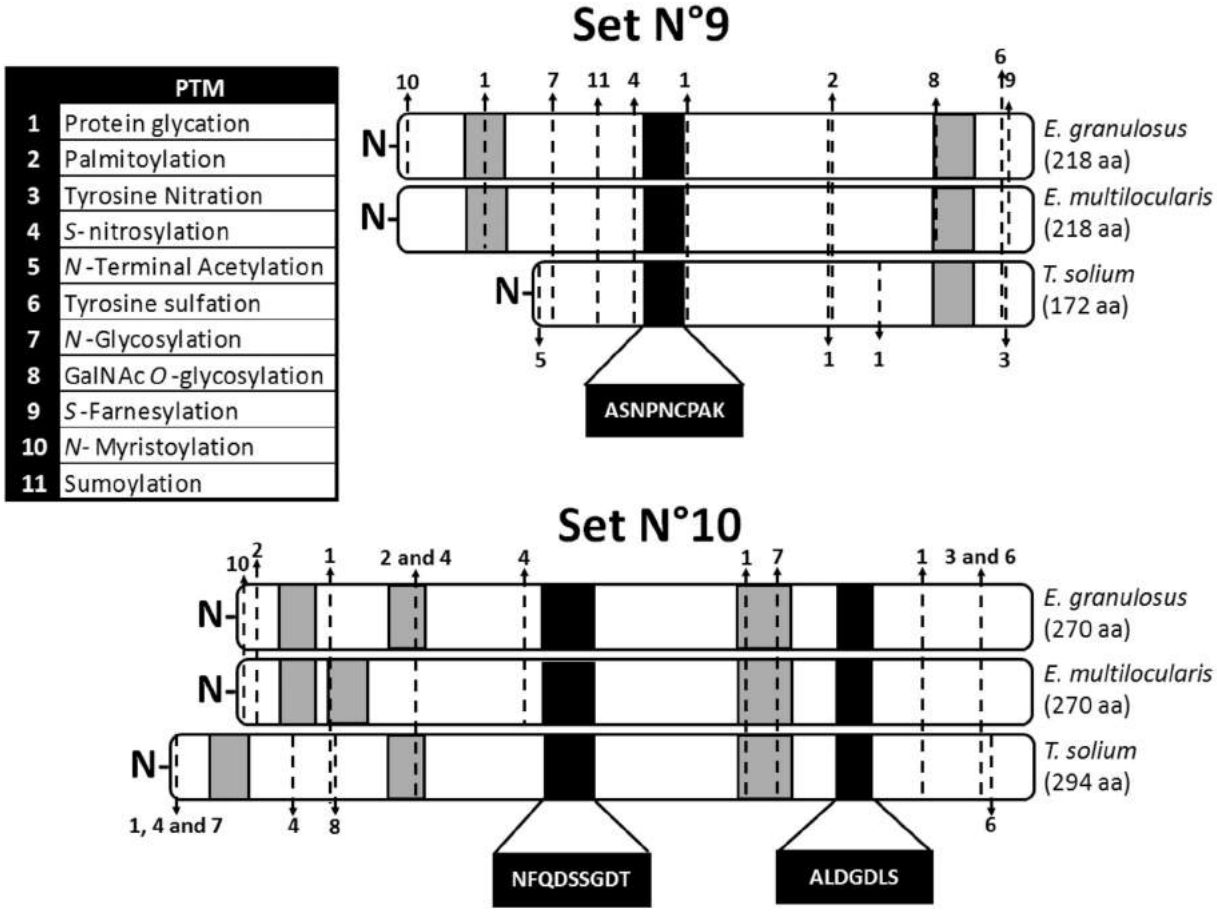

Fig. 3. Identification of clean linear B cell epitopes. Promiscuous MHC-II binding proteins (sets N°9 and N°10) were analyzed for their PTMs sites (using GPS and CBS servers) and linear B cell epitopes (predicted by means of Bepipred 1.0 software). PTMs sites for any of the eleven possible modifications studied are shown as dashed lines. Predicted linear B cell epitopes in each protein are shown as grey boxes, while those in black boxes represent clean linear B cell epitopes shared by the three protein within each set.

myristoylation (Fig. 3). Additionally, sites for *N*-terminal acetylation, *S*-farnesylation and sumoylation were also predicted but only for proteins in set N°9 (Fig. 3). Secondly, both sets of promiscuous MHC-II binding proteins were also scanned for sequences able to be recognized by antibodies (*e.g.* linear B cell epitopes). Results showed that proteins in set N°9 exhibit 2 (*T. solium*) and 3 (*E. granulosus* and *E. multilocularis*) putative linear B cell epitopes, while those in set N°10 displayed 5 putative linear B cell epitopes independently of the parasite species (Fig. 3). Finally, in order to identify clean linear B cell epitopes (*e.g.* those without possible sites for PTMs), mapping studies for co-localization of predicted PTMs and putative linear B cell epitopes were performed for every protein present in both sets. Results in Fig. 3 show that in set N°9 there is only one clean linear B cell epitope shared by the three proteins (ASNPNCPAK), while in set N°10 two sequences were identified as clean linear B cell epitopes shared by the three proteins (NFQDSSGDT and ALDGDLS). Homology studies for these linear B cell epitopes against every known linear B cell epitope in the Immune Epitope Database showed no exact matches, nor >90% similar epitopes (data not shown). This is important from a diagnostic point of view because the probability of false positive results due to cross-reaction with other antigens should be as low as possible. However, the exact sequence ALDGDLS (set N°10) is present in a large number of proteins from bacteria, fungi and plants, as revealed by comparisons against all known proteins present on the non-redundant protein sequences database (data not shown). Interestingly, none of the three sequences showed an exact match (100% identity and coverage) against the full human proteome (data not shown). This would increase the probability of generating specific antibodies against the clean linear B cell epitopes, because B cells should be able to overcome immune tolerance mechanisms.

3.6. Mapping of clean linear B cell epitopes in 3D-modelled protein structures

Linear B cell epitopes need to locate on protein surfaces to be easily recognized by antibodies within the native structure. Therefore, it is of outstanding relevance to map putative linear B cell epitopes in 3D protein structures. Due to low levels of homology between our protein sets and all 3D-elucidated protein structures available (by either crystallography or NMR); an exact mapping of epitopes is not feasible. However, partial models could give valuable information. In this sense, by means of RaptorX software, we achieved quite acceptable models for proteins in set N°9 (45, 46 and 36 uGDT for *E. granulosus*, *E. multilocularis* and *T. solium*, respectively), although showing some differences between them (Fig. 4). Regarding proteins in set N°10, our results revealed much higher confidence models (159, 163 and 173 uGDT for *E. granulosus*, *E. multilocularis* and *T. solium*, respectively), and 3D structures for the three proteins within the set were very similar (Fig. 4). Further mapping analysis on 3D structure models showed that predicted clean linear B cell epitopes in each set exhibited mostly mid-high surface accessibility (Fig. 4).

4. Discussion

Infections caused by tapeworms affect millions of people worldwide. Among them, the WHO classifies cystic echinococcosis, alveolar

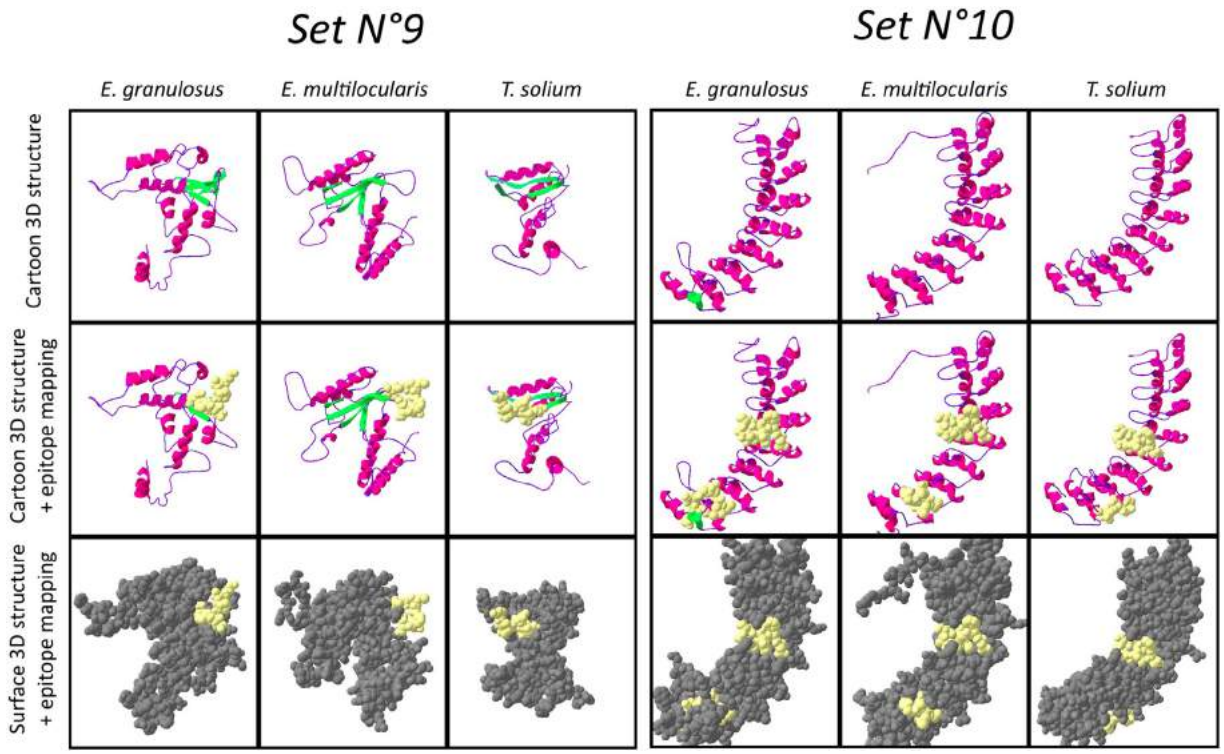

Fig. 4. Mapping of clean linear B cell epitopes in 3D-modelled protein structures. For every protein within sets N°9 and N°10, a 3D-modelled structure was predicted by means of RaptorX software, and clean linear B cell epitopes were visualized in 3D models using DeepView. For visualization purposes, secondary structures are shown in pink (α-helixes) and green (β-sheets), while 3D overall structures are represented in grey. Mapped epitopes are depicted in yellow. (For interpretation of the references to color in this figure legend, the reader is referred to the web version of this article.)

echinococcosis and cysticercosis as zoonotic neglected tropical diseases. Despite numerous attempts, high-sensitivity and high-specificity serological diagnostic tests against these infections are still needed, since no tested antigens have shown outstanding diagnostic performance thus far (List et al., 2010; Manzano-Román et al., 2015; Rodriguez et al., 2012; Zhang et al., 2012). In this study, we propose a rational *in silico* analysis, *via* application of different bioinformatic and immunoinformatic approaches to identify new diagnostic candidates. To the best of our knowledge, the present study is the first multi-genome-wide analysis and *in silico* prediction of universal diagnostic peptides that could aid in determining human infections by any relevant tapeworm species causing neglected tropical diseases (*e.g. E. granulosus*, *E. multilocularis* and *T. solium*). Endemic areas for any of the three cestodes are largely overlapped and localized mostly in low/middle-income countries. Thus, it is very important to have a simple and cheap serodiagnostic tool that allows for identification of any of these diseases in one-step. Once a sample turns into a positive result, further species-specific analyses should be perform to identify the cestode responsible for the disease in order to choose the most appropriate treatment. Having a single serodiagnostic tool would provide relevant results in primary screening studies or in epidemiological surveys at geographical places with limited resources for serological analyses. To that end, we predicted *in silico* a subset of secreted proteins shared by the three tapeworms. Since secreted proteins are in constant contact with the host immune system, identifying immunodiagnostic candidates from secretomes is a logical approach (S. Wang et al., 2015; X. Wang et al., 2015). Similar secretome predictions have already been performed for *E. multilocularis* (S. Wang et al., 2015; X. Wang et al., 2015) and *T. solium* (Gomez et al., 2015), as well as the prediction of secreted proteins from transcriptome profiles of *E. granulosus* protoscoleces (W. Pan et al., 2014; Z. Pan et al., 2014). However, this is the first study to predict secreted proteins from the full proteome of *E. granulosus*. Our results showed that secretomes correspond to 13.6, 9.9 and 7.1% of all hypothetical proteins in the full proteomes of *E. granulosus*, *E. multilocularis* and *T. solium*, respectively. In contrast with the reported results similarly obtained for *E. multilocularis* (6.4%) (S. Wang et al., 2015; X. Wang et al., 2015) and *T. solium* (6.5%) (Gomez et al., 2015), our results showed a higher number of secreted proteins for both cestodes. This may be due to the constant update of the genomes, since the number of hypothetical proteins in the full proteomes we downloaded from the Sanger helminth genome database is quite different to those used in the above-mentioned works. For example, while Gomez et al. (2015) used a full proteome for *T. solium* of 12,902 hypothetical proteins, and S. Wang et al. (2015) and X. Wang et al. (2015) reported a full proteome for *E. multilocularis* of 10,552 hypothetical proteins; our work started with proteomes made of 12,353 and 11,552 hypothetical proteins, respectively. Additionally, differences in the bioinformatic pipelines used might also affect the results; *e.g.* no PS-Scan nor PredGPI softwares were applied in Gomez et al. (2015). Therefore, in order to obtain *E. granulosus*, *E. multilocularis* and *T. solium* predicted secretomes we applied the same conditions in a systematic way to the three available full proteomes.

Our prediction of a common shared secretome between *E. granulosus*, *E. multilocularis* and *T. solium* showed 25 sets of proteins exhibiting >90% of identities between them (Fig. 1B and Table 1). These proteins seemed to be conserved among cestodes, since at least 21 sets displayed >65% ID with other cestode proteins (BLASTp against non-redundant protein sequences database, data not shown). Moreover, 10 sets showed low levels of homology with human proteins (Fig. 2A), which is very important from a serodiagnostic point of view since immune tolerance mechanisms must be overcome in order to develop an antibody response in the infected host. Additionally, for any protein within such 10 sets, the second best cestode hit belonged to *Hymenolepis microstoma* (median sequence identity: 69%, range: 49–86%). Interestingly, like *E. granulosus*, *E. multilocularis* and *T. solium*; *H. microstoma* is also a member of the Cyclophyllidea order of cestodes, although it has been very rarely reported to infect humans (Macnish et al., 2003; Tsai et al., 2013). Once human non-homologous proteins were

identified, they were analyzed with a probability of antigenicity software, and 6 out of 10 studied sets were classified as highly antigenic for the three proteins within each set (Fig. 2). Although being antigenic is necessary for antibody production, successful antibody responses also require T cell-B cell collaboration through peptides loaded in MHC class II molecules. In order to select protein candidates with the best chance for an efficient T cell-B cell collaboration in the vast majority of the population, we identified sets of promiscuous MHC-II binding proteins. Such proteins were defined as containing at least one 15-mer peptide able to be bound with strong affinity by most (>20 out of 26 studied) human MHC-II molecules. Only two sets of proteins belonged to such a category: sets N°9 and N°10. However, it is worth mentioning that although selected promiscuous MHC-II binding proteins are able to be presents by at least 77% of MHC-II analyzed molecules, this does not directly reflect the percentage of the population able to present them. The issue of population coverage in relation to MHC polymorphism is further complicated by the fact that different MHC molecules are expressed at dramatically different frequencies in different ethnicities (Sidney et al., 2010).

Proteins within set N°9 are characterized by presenting an N-terminal TonB box domain. This domain is a conserved pentapeptide sequence found in TonB-dependent colicins and receptors in bacteria, and is involved in the uptake of specific substrates into the periplasmic space (Tuckman and Osburne, 1992). Little information is available about the role of TonB box domain in Eukarya, though it is found in fungi, plants, and animals. TonB box region in proteins belonging to set N°9 is found in their N-terminal region, with no other identifiable domains (data not shown). Thus, most sequences in such proteins have an uncharacterized structure and function. No other proteins bearing a TonB box domain where present in the three predicted secretomes, although 3, 4 and 5 TonB box-containing proteins were found in the full proteomes of *T. solium*, *E. granulosus* and *E. multilocularis*, respectively (data not shown). On the other hand, proteins within set N°10 contain one of the most common protein motifs in nature: the Ankyrin repeat domain. Proteins bearing such motif are usually implicated in specific protein-protein interactions involved in many cellular processes. Additionally, they can interact with a highly diverse and unrelated number of molecules (Parra et al., 2015). Proteins within set N°10 present two N-terminal motifs of Ankyrin repeats (data not shown). In the analyzed proteomes, there were 68 (*E. granulosus*), 71 (*E. multilocularis*) and 70 (*T. solium*) proteins with Ankyrin repeats, while in the predicted secretomes 2, 3 and 5 of such proteins were found for *E. granulosus*, *E. multilocularis* and *T. solium*, respectively (data not shown).

Further analyses of sets N°9 and N°10 were performed in order to identify common antigenic regions. First, potential sites for several PTMs were predicted, followed by identification of linear B cell epitopes within each protein. Little information is available on PTMs in tapeworms. Thus, to overcome this issue we analyzed a high number of PTMs present in mammals, independently of whether tapeworms exhibit similar modifications or not. This strategy was used since we did not want to characterize possible PTMs *per se*, but to search for regions that most likely do not contain any potential sites for PTMs. Co-localization of PTMs-free sites and linear B cell epitopes allowed us to identify clean linear B cell epitopes, which were further compared between the three proteins within each set. Our results showed that proteins in set N°9 share one clean linear B cell epitope (ASNPNCPAK), whereas proteins within set N°10 share two (NFQDSSGDT and ALDGDLS). Further analyses were performed on these sequences in order to suggest their potential use as diagnostic peptides. Any of these sequences were found in the human proteome (100% identity and coverage), reinforcing their possibility of being targeted by specific antibodies in the human host through overcoming B cell tolerance mechanisms. In addition, these sequences showed no similarity with any known linear B cell epitope reported in the Immune Epitope Data Base, reducing potential interferences by other pathogens which could produce false-positive results. Moreover, when the three sequences were compared against all known proteins present on the non-redundant protein sequences database by BLASTp, no exact match (100% identity and coverage) was found for the sequences ASNPNCPAK (set N°9) and NFQDSSGDT (set N°10). However, large numbers of proteins from bacteria, fungi and plants exhibited the ALDGDLS sequence, reducing its confidence as a specific peptide for potential use in serodiagnosis.

Finally, 3D structure modelling and mapping of clean linear B cell epitopes was performed to evaluate the accessibility of antibodies to them. Due to the low level of homology between proteins in set N°9 and N°10 with any available 3D protein structures (by either crystallography or NMR); an exact mapping of epitopes was not possible. However, to overcome this problem, we built partial 3D protein models by using RaptorX software. For proteins within set N°9 - which possess mostly uncharacterized structures with an N-terminal TonB box domain - we achieved acceptable models. Relevant structural differences were observed between the three proteins in this set. Clean linear B cell epitopes mapping in any of the three proteins showed mid-high surface accessibilities, although the 3D location of the epitopes was highly variable between the three proteins (Fig. 4). Certainly, higher confidence models for proteins in set N°9 are needed for more reliable analyses. On the other hand, the 3D models for proteins in set N°10 showed high confidence levels and were very similar for the three proteins. Moreover, the 3D location of the clean linear B cell epitopes showed to be quite similar in the three cases (Fig. 4). Clean linear B cell epitopes showed relatively good accessibilities (except for the ALDGDLS sequence in the model for *E. granulosus*). Taking all these results together, we suggest the peptide sequences ASNPNCPAK (from proteins in set N°9) and NFQDSSGDT (from proteins in set N°10) as potentially useful in designing new serodiagnostic tools able to detect antibodies raised by humans against *E. granulosus*, *E. multilocularis* and/or *T. solium*.

5. Conclusion

In summary, we reported here a novel bio- and immuno-informatic workflow for predicting antigenic candidates with potential diagnostic value against the three neglected tropical diseases caused by tapeworms. In this sense, our results not only suggested two new proteins common to the shared secretome of *E. granulosus*, *E. multilocularis* and *T. solium* as immunodiagnostic candidates, but also proposed two potentially antigenic peptides derived from them that could lower research and development costs. In this sense, their putative diagnostic potential needs to be further tested and our overall results validated in an experimental setting. Therefore, experimental validation will be assessed soon.

Acknowledgements

Authors are grateful to Dra. Cecilia Fernández for her valuable help with databases selection. CSIC-Universidad de la República (Uruguay), PEDECIBA-Química (Uruguay) and ANII (Uruguay) are acknowledged for their general financial support.

Funding

This research did not receive any specific grant from funding agencies in the public, commercial, or not-for-profit sectors.

References

Aguiar, D.M., Zhang, X., Braga, I.A., Taques, I.I.G.G., McBride, J.W., 2016. Detection of genotype-specific *Ehrlichia canis* exposure in Brazilian dogs by TRP36 peptide ELISA. Ticks Tick Borne Dis. 7, 142–145.

Backert, L., Kohlbacher, O., 2015. Immunoinformatics and epitope prediction in the age of genomic medicine. Genome Med. 7, 119.

Bendtsen, J.D., Jensen, L.J., Blom, N., Von Heijne, G., Brunak, S., 2004. Feature-based prediction of non-classical and leaderless protein secretion. Protein Eng. Des. Sel. 17, 349–356.

Carvalho, G.B.F., da Silva-Pereira, R.A., Pacífico, L.G.G., Fonseca, C.T., 2011. Identification of *Schistosoma mansoni* candidate antigens for diagnosis of schistosomiasis. Mem. Inst. Oswaldo Cruz 106, 837–843.
Chen, H., Xue, Y., Huang, N., Yao, X., Sun, Z., 2006. MeMo: a web tool for prediction of protein methylation modifications. Nucleic Acids Res. 34, 249–253.
Coral-Almeida, M., et al., 2015. *Taenia solium* human cysticercosis: a systematic review of sero-epidemiological data from endemic zones around the world. PLoS Negl. Trop. Dis. 9, e0003919.
de Castro, E., et al., 2006. ScanProsite: detection of PROSITE signature matches and ProRule-associated functional and structural residues in proteins. Nucleic Acids Res. 34, 362–365.
Del Brutto, O.H., 2012. Neurocysticercosis: a review. Sci. World J. 2012, 1–8.
Deng, W., Nickle, D.C., Learn, G.H., Maust, B., Mullins, J.I., 2007. ViroBLAST: a stand-alone BLAST web server for flexible queries of multiple databases and user's datasets. Bioinformatics 23, 2334–2336.
Emanuelsson, O., Nielsen, H., Brunak, S., von Heijne, G., 2000. Predicting subcellular localization of proteins based on their N-terminal amino acid sequence. J. Mol. Biol. 300, 1005–1016.
Gauna, A., et al., 2015. Synthetic peptides for the immunodiagnosis of hepatitis A virus infection. J. Immunol. Methods 427, 1–5.
Giri, S., Parija, S.C., 2012. A review on diagnostic and preventive aspects of cystic echinococcosis and human cysticercosis. Trop. Parasitol. 2, 99–108.
Gómara, M.J., Haro, I., 2007. Synthetic peptides for the immunodiagnosis of human diseases. Curr. Med. Chem. 14, 531–546.
Gomez, S., et al., 2015. Genome analysis of excretory/secretory proteins in *Taenia solium* reveals their abundance of antigenic regions (AAR). Sci Rep 5, 9683.
Guex, N., Peitsch, M.C., 1997. SWISS-MODEL and the Swiss-PdbViewer: an environment for comparative protein modeling. Electrophoresis 18, 2714–2723.
Guimarães-Peixoto, R.P.M., et al., 2016. Evaluation of a synthetic peptide from the *Taenia saginata* 18kDa surface/secreted oncospheral adhesion protein for serological diagnosis of bovine cysticercosis. Acta Trop. 164, 463–468.
Gupta, R., Jung, E., Brunak, S., 2004. In: Gupta, R., Jung, E., Brunak, S. (Eds.), Prediction of N-Glycosylation Sites in Human Proteins http://www.cbs.dtu.dk/services/NetNGlyc/.
Johansen, M.B., Kiemer, L., Brunak, S., 2006. Analysis and prediction of mammalian protein glycation. Glycobiology 16, 844–853.
Julenius, K., 2007. NetCGlyc 1.0: prediction of mammalian C-mannosylation sites. Glycobiology 17, 868–876.
Käll, L., Krogh, A., Sonnhammer, E.L.L., 2004. A combined transmembrane topology and signal peptide prediction method. J. Mol. Biol. 338, 1027–1036.
Källberg, M., et al., 2012. Template-based protein structure modeling using the RaptorX web server. Nat. Protoc. 7, 1511–1522.
Kiemer, L., Bendtsen, J.D., Blom, N., 2005. NetAcet: prediction of N-terminal acetylation sites. Bioinformatics 21, 1269–1270.
Krogh, A., Larsson, B., von Heijne, G., Sonnhammer, E., 2001. Predicting transmembrane protein topology with a hidden Markov model: application to complete genomes. J. Mol. Biol. 305, 567–580.
Larsen, J.E.P., Lund, O., Nielsen, M., 2006. Improved method for predicting linear B-cell epitopes. Immunome Res. 2, 2.
List, C., et al., 2010. Serodiagnosis of *Echinococcus* spp. infection: explorative selection of diagnostic antigens by peptide microarray. PLoS Negl. Trop. Dis. 4 (e771).
Liu, Z., et al., 2011. GPS-YNO2: computational prediction of tyrosine nitration sites in proteins. Mol. BioSyst. 7, 1197–1204.
Lum, G., Min, X.J., 2011. FunSecKB: The Fungal Secretome KnowledgeBase. Database 2011. pp. 1–10.
Ma, F., et al., 2016. Development of a peptide ELISA for the diagnosis of Aleutian Mink Disease. PLoS One 11, e0165793.
Macnish, M.G., Ryan, U.M., Behnke, J.M., Thompson, R.C., 2003. Detection of the rodent tapeworm *Rodentolepis* (=*Hymenolepis*) *microstoma* in humans. A new zoonosis? Int. J. Parasitol. 33, 1079–1085.
Magnan, C.N., et al., 2010. High-throughput prediction of protein antigenicity using protein microarray data. Bioinformatics 26, 2936–2943.
Manzano-Román, R., Sánchez-Ovejero, C., Hernández-González, A., Casulli, A., Siles-Lucas, M., 2015. Serological diagnosis and follow-up of human cystic echinococcosis: a new hope for the future? Biomed. Res. Int. 2015, 428205.
Meinken, J., Min, X.J., 2012. Computational prediction of protein subcellular locations in eukaryotes: an experience report. Comput. Mol. Biol. 2, 1–7.
Mihmanli, M., et al., 2016. Current status of diagnosis and treatment of hepatic echinococcosis. World J. Hepatol. 8, 1169–1181.
Min, X., 2010. Evaluation of computational methods for secreted protein prediction in different eukaryotes. J. Proteomics Bioinform. 3, 143–147.
Moro, P., Schantz, P.M., 2009. Echinococcosis: a review. Int. J. Infect. Dis. 13, 125–133.
Nielsen, M., Lund, O., 2009. NN-align. An artificial neural network-based alignment algorithm for MHC class II peptide binding prediction. BMC Bioinf. 10 (296).
Pan, W., et al., 2014a. Transcriptome profiles of the protoscoleces of *Echinococcus granulosus* reveal that excretory-secretory products are essential to metabolic adaptation. PLoS Negl. Trop. Dis. 8, 1–15.
Pan, Z., et al., 2014b. Systematic analysis of the in situ crosstalk of tyrosine modifications reveals no additional natural selection on multiply modified residues. Sci Rep 4, 7331.
Parra, R.G., Espada, R., Verstraete, N., Ferreiro, D.U., 2015. Structural and energetic characterization of the ankyrin repeat protein family. PLoS Comput. Biol. 11, 1–20.
Petersen, T.N., Brunak, S., von Heijne, G., Nielsen, H., 2011. SignalP 4.0: discriminating signal peptides from transmembrane regions. Nat. Methods 8, 785–786.
Pierleoni, A., Martelli, P., Casadio, R., 2008. PredGPI: a GPI-anchor predictor. BMC Bioinf. 9, 392–403.
Ren, J., et al., 2008. CSS-Palm 2.0: an updated software for palmitoylation sites prediction. Protein Eng. Des. Sel. 21, 639–644.
Rodriguez, S., Wilkins, P., Dorny, P., 2012. Immunological and molecular diagnosis of cysticercosis. Pathog. Glob. Health 106, 286–298.
Seib, K.L., et al., 2012. Developing vaccines in the era of genomics: a decade of reverse vaccinology. Clin. Microbiol. Infect. 18 (Suppl. 5), 109–116.
Sidney, J., et al., 2010. Five HLA-DP molecules frequently expressed in the worldwide human population share a common HLA supertypic binding specificity. J. Immunol. 184, 2492–2503.
Steentoft, C., et al., 2013. Precision mapping of the human O-GalNAc glycoproteome through SimpleCell technology. EMBO J. 32, 1478–1488.
Tsai, I., Zarowiecki, M., Holroyd, N., 2013. The genomes of four tapeworm species reveal adaptations to parasitism. Nature 496, 57–63.
Tuckman, M., Osburne, M.S., 1992. In vivo inhibition of TonB-dependent processes by a TonB box consensus pentapeptide. J. Bacteriol. 174, 320–323.
Wang, S., Wei, W., Cai, X., 2015a. Genome-wide analysis of excretory/secretory proteins in *Echinococcus multilocularis*: insights into functional characteristics of the tapeworm secretome. Parasit. Vectors 8, 1–13.
Wang, X., et al., 2015b. Characterization of two novel linear B-cell epitopes in the capsid protein of avian hepatitis E virus (HEV) that are common to avian, swine, and human HEVs. J. Virol. 89, 5491–5501.
Wang, Y.H., Wang, G.X., Cai, J.P., 2016. Identifying novel B cell epitopes within *Toxoplasma gondii* GRA6. Korean J. Parasitol. 54, 431–437.
World Health Organization, 2016. Neglected Tropical Diseases. http://www.who.int/neglected_diseases/diseases/en/ - accessed 02.09.2017.
Xie, Y., et al., 2016. GPS-Lipid: a robust tool for the prediction of multiple lipid modification sites. Sci Rep 6, 28249.
Xue, Y., et al., 2010. GPS-SNO: computational prediction of protein S-nitrosylation sites with a modified GPS algorithm. PLoS One 5, 1–7.
Yin, D., et al., 2016. A novel multi-epitope recombined protein for diagnosis of human brucellosis. BMC Infect. Dis. 16, 219.
Zhang, W., Wen, H., Li, J., Lin, R., McManus, D.P., 2012. Immunology and immunodiagnosis of cystic echinococcosis: an update. Clin. Dev. Immunol. 2012, 101895.
Zhao, Q., et al., 2014. GPS-SUMO: a tool for the prediction of sumoylation sites and SUMO-interaction motifs. Nucleic Acids Res. 42, 325–330.

ARTÍCULO 6

In silico design and experimental evaluation of peptide-based vaccines against secondary cystic echinococcosis.

Miles S, Dematteis S, Mourglia-Ettlin G.

Biologicals

2022, *submitted*

TITLE

In silico design and experimental evaluation of peptide-based vaccines against secondary cystic echinococcosis.

AUTHORS

Sebastian Miles[1,2]; Sylvia Dematteis[1]; Gustavo Mourglia-Ettlin[1]

AFFILIATIONS

[1]Area Inmunología, DEPBIO/IQB, Facultad de Química/Facultad de Ciencias, Universidad de la Republica, Montevideo, Uruguay.

[2]Graduate Program in Chemistry, Facultad de Química, Universidad de la Republica, Uruguay.

ABSTRACT

Vaccines are among the most important advances in medicine throughout the human history. However, conventional vaccines exhibit several drawbacks in terms of design and production costs. Peptide-based vaccines are attractive alternatives, since they can be designed mainly *in silico*, can be produced cheaply and safely, and are able to induce immune responses exclusively towards protective epitopes. Yet, a proper peptide design is needed, not only to generate peptide-specific immune responses, but also for them to recognize the native protein in the occurrence of a natural infection. Herein, we propose a design workflow for peptide-based vaccines including novel steps assuring the cross-recognition of native proteins. In this regard, we increased the probability of generating efficient antibodies through the selection of linear B-cell epitopes free of post-translational modifications followed by analyzing the 3D-structure similarity between the peptide in-solution vs. within its parental native protein. This workflow was applied to a set of seven previously suggested potential protective antigens against the infection by *Echinococcus granulosus sensu lato*. Finally, two peptides were obtained showing the capacity to induce specific antibodies able to exert anti-parasite activities in different *in vitro* settings, as well as to provide significant protection in the murine model of secondary echinococcosis.

KEYWORDS

Peptide-based vaccine; Vaccine design; Reverse vaccinology; Bioinformatics; *Echinococcus granulosus*, epitope

1. INTRODUCCTION

Next generation vaccines are current important technologies that include the ability of rapid design at usually low-cost production. Within such technologies, peptide-based vaccines are among the least explored alternatives (Azmi et al., 2014). Contrary to subunit or DNA/mRNA vaccines, where the (final) antigen is an entire protein and the immune response is generated against multiple portions of the antigen, peptide-based vaccines are composed of small peptides derived from an antigenic protein. Such peptides are able to induce specific B- and/or T-cell responses exhibiting cross-reactivity with the native parental protein. Depending on the vaccine candidate, peptides may act either as B- and/or T-cell epitopes, although in-tandem constructions with multiple epitopes are often used to achieve immune responses that are more robust (Zhang, 2018).

The simplest and fastest peptide-based vaccines to design are B-cell vaccines for infections that can be resolved and/or prevented mainly by antibody dependent mechanisms. Contrary to T-cell epitopes, which depend on the host genetics (i.e. MHC molecules), B-cell epitopes are mostly genetic background independent (Sanchez-Trincado et al., 2017). Thus, B-cell vaccines can be designed either by selecting antigenic linear peptides or by "creating" lineal peptides that mimic conformational epitopes (known as mimotopes) (Larsen et al., 2006). Then, designed peptides can be non-biologically synthetized, bound to a carrier protein (to overcome the lack of intrinsic T-cell epitopes) and formulated with an adequate adjuvant (Li et al., 2014). Importantly, in the peptide selection stage several considerations must be taken into account to assure the cross-reactivity of peptide-specific antibodies with the native parental protein. In this regard, designed peptides have to be superficially exposed in the parental protein to enable antibody recognition (Li et al., 2014). Additionally, post-translational modifications along the peptide sequence in the native parental protein should be avoided because they might affect antibody recognition by steric impairment. Lastly, for a successful antibody cross-reactivity between the peptide and the parental protein, the 3D conformation of the synthetic peptide should resemble its conformation within the native parental protein (Li et al., 2014). This last consideration is hard to overcome for short peptides since their conformations can be modified through the antibody interaction.

Vaccines against neglected tropical diseases are scarce, and although several breakthroughs have been made in pre-clinical stages in the last decade (Bethony et al., 2011; Hotez, 2018; Hotez et al., 2016), the manufacturing and distribution costs are still one of their major disadvantages. In zoonotic helminth infections, vaccine developments have focused on animal hosts in an attempt to interrupt the parasite life cycle, leading to several commercial veterinary vaccines (Monath, 2013). Vaccines against *Echinococcus granulosus sensu lato* (s.l.) are hard to achieve, as the taxonomical

classification of *E. granulosus* s.l. is still controversial, since considerable phenotypic, physiological and genetic variability have been reported among parasite isolates, mostly correlating with differences in intermediate host preferences. Nowadays, the *E. granulosus* s.l. complex has been divided into nine genotypes (G1-G8, G10) grouped in four species (Nakao et al., 2010). Despite this, one recombinant vaccine (named EG95) has reached the market exhibiting almost complete protection in sheep against the G1 parasite genotype (Heath et al., 2003; Lightowlers et al., 1999, 1996).

In the present work, we propose a novel *in silico* rational approach to design B-cell epitope vaccines from potentially protective antigens. Our group has recently identified seven *E. granulosus* s.l. vaccine candidates, which have been linked to effective parasite-specific antibodies induced either after infection and/or immunization (Miles et al., 2020a). From them, six lineal and superficial B-cell epitopes -free of post-translational modifications- were selected. Peptide sequences were not found in any mammalian protein and their 3D structures resembled their native structure within their parental proteins. Specific antibodies against each peptide were produced, showing *in vitro* anti-parasite activity and *in vivo* protective capacity using the murine model of secondary cystic echinococcosis. At the end, a promising peptide-based vaccine composed of two peptides was obtained, thus validating our vaccine design strategy.

2. MATHERIALS AND METHODS

B-cell epitope selection. Peptide-based vaccines against *E. granulosus* s.l. were designed from a list of seven novel vaccine candidates recently suggested by our group (Miles et al., 2020a). Firstly, lineal B cell epitopes present on the seven potentially protective antigens were predicted using the algorithm Bepipred (version 2.0) (Jespersen et al., 2017), considering only continuous antigenic segments ≥ 7 amino acids in length. (Table 1). Then, we analyzed the presence of post-translational modifications (PTMs) within the peptide sequences by two complementary criteria, by selecting only those that did not exhibited any possible PTMs and referring to them as “clean epitopes”. In the first place, since vaccine candidates were identified by mass spectrometry techniques (Miles et al., 2020a), epitopes that co-localized with(in) the matching peptides used in the identification of the corresponding protein by MALDI-TOF/TOF were selected (as peptides exhibiting PTMs would not be used in the identification process). Then, by using PTMomics data recently reported by our group for *E. granulosus* s.l. tegumental proteins (Miles et al., 2022), we analyzed the possible amino acidic localization of 22 different enzymatic PTMs within the seven antigens. Through this strategy, we discarded epitopes that co-localized with any of these possible PTMs. The sequences of the selected

clean epitopes were then searched for against all mammalian proteins trough BLASTp, discarding any exact match. Remaining peptides were considered "unique epitopes" and were further analyzed (Table 1).

3D model prediction. Identified "unique epitopes" were mapped within the 3D structure of their corresponding parental protein to analyze their antibody accessibilities according to Miles et al., (2017). Modeling of 3D structures by low-homology protein threading was performed on each antigen by means of RaptorX software (Källberg et al., 2012). Only 3D models with uGDT (unnormalized Global Distance Test) higher than 50 were selected, and for proteins with more than one predicted 3D model, the structure with the highest uGDT was chosen. "Unique epitopes" were mapped within each selected structure using SWISS-PdbViewer (Guex and Peitsch, 1997), and their antibody accessibilities were manually evaluated, discarding non-accessible epitopes (Table 1). The 3D structure of accessible "unique epitopes" was manually extracted from the PDB files of their parental proteins by deleting all non-selected peptide amino acids. These peptides were referred as "native peptides". The 3D structure adopted by accessible "unique epitopes" in-solution was predicted by means of the software PEPFold3 (Lamiable et al., 2016), selecting the five highest confidence models for each peptide. These peptides were referred as "in-solution peptides".

Comparison of peptide 3D models. Tertiary structure similarity (TSS) analyses were performed using the TM-Align software (Zhang and Skolnick, 2005) by comparing the 3D structure of "native peptides" to each one of the five models obtained for "in-solution peptides". Only peptides that showed a TM-Aling score greater than 0.5 in at least one comparison were selected (Table 1). For peptides longer than 13 amino acids that showed a TM-Align score lower that 0.5, but exhibited at least 7 amino acids with an apparent high structure similarity, a manual selection of those amino acids was performed by deleting non-selected amino acids. Then, new 3D structure predictions and TSS analyses were performed as above, selecting the ones that exhibited a TM-Align score greater than 0.5, considering them "modified epitopes".

Peptide synthesis. High TSS "unique epitopes" (n=4) and "modified epitopes" (n=2) were commercially synthesized by SbsBio either as single peptides (for further ELISA assays) and covalently conjugated to KLH as a carrier protein (for further immunization protocols). In any case, the peptides were synthesized with a purity greater than 90%, and the KLH conjugation was done at the N-terminus, adding a cysteine as a linker. Lyophilized conjugates were reconstituted in sterile phosphate-buffered saline (PBS) pH 7.2, filtered by 0.22 μm and stored at -80°C until use.

Parasites and antigens. Protoscoleces (PSC) from *E. granulosus* s.l. were obtained by aseptic puncture of fertile bovine hydatid cysts from Uruguayan abattoirs, washed several times with PBS containing antibiotics (penicillin 60 µg/mL, streptomycin 100 µg/mL, and amphotericin-B 250 ng/mL), and their viability was assessed according to Dematteis et al. (1999). For experimental infections, only parasite batches with viabilities ≥ 95% were used. Tegumental proteins were extracted from highly viable PSC (viability ≥ 80%) using an extracting solution consisting of detergent MEGA-10 (1% w/v), EDTA (5 mM) and phenylmethyl-sulfonyl fluoride (2 mM) in PBS according to Hernández and Nieto (1994). Briefly, 125,000 viable PSC/mL of extracting solution were incubated for 2 hours at room temperature with soft constant rotation. Then, PSC were allowed to settle down and the supernatant was removed and extensively dialyzed against PBS at room temperature using a cellulose membrane (MW cut-off: 12,000 Da). Obtained antigens (termed PSEx) were characterized in terms of protein content according to Miguez et al. (1996), and stored at -20°C until use. Treated PSC were washed three times with PBS, stained with eosin and their integrity was confirmed by observation under a light microscope.

Ethic statements. Animal experiments were performed in compliance with *Comisión Honoraria de Experimentación Animal* (CHEA) from *Universidad de la República*, according to the Canadian Guidelines on Animal Care and the National Uruguayan Legislation N°18.611. Experimental protocols were approved by the Ethics Committee of *Facultad de Química (Universidad de la República)* and were given the approval number 101900-00185-16.

Mice and immunizations. Female CD1 mice (6-8 weeks old) were obtained from -and were housed at- the animal facility of *Instituto de Higiene* (Montevideo, Uruguay). Anti-peptide sera were obtained through the s.c. immunization of nine groups of mice inoculated with 100 µL/dose/mouse of the formulations under study, applying a priming/booster/booster scheme (days 0/15/30). Six groups (n= 7 per group) were inoculated with 100 µg of each synthetic peptide conjugated with KLH, using QuillA® in PBS (1:1 volume ratio) as adjuvant. Mice inoculated only with PBS (n=7), QuillA® in PBS (n=5) or PBS containing 100 µg of unconjugated KLH plus QuillA® as adjuvant (n=5) were used as controls. At day 45 post-priming, all mice from every experimental group were bled and euthanized. Sera were obtained by regular means and store at -80°C until use.

Evaluation of specific antibodies. Firstly, KLH-specific antibodies were analyzed to corroborate the immunization success. For this, 96-wells microtiter plates were coated with 100 µL/well of PBS containing 1 µg of commercial KLH (Thermo-Pierce) and incubated ON at 4°C. After blocking with PBS-BSA (1% w/v) during 1 h at RT, sera were dispended at 1:1,000 dilutions, incubated ON at 4°C, and KLH-specific IgG were determined using peroxidase-labeled goat anti-mouse antibodies. TMB

(3,3′, 5,5;-TetraMethylBenzidine) was used as the chromogenic substrate, and absorbance values were recorded at 450 nm after stopping the reaction through H_2SO_4 addition. Only sera exhibiting high levels of KLH-specific IgG were used for further analyses. To evaluate the production of peptide-specific IgG we followed a similar procedure but coating the microtiter plates with 100 µL/well of PBS containing 1 µg of each peptide, and dispended the sera at serial dilutions starting at 1:50. The cross-reactivity of peptide-specific IgG against native proteins was analyzed similarly but coating microtiter plates with 100 µL/well of PBS containing 1 µg of PSEx, and dispensing sera at serial dilutions starting at 1:50 dilution. In both cases, specific antibodies were determined as previously described by selecting a single non-saturating sample dilution, recording absorbance values, and defining IgG titres in all cases as the absorbance value times the chosen dilution factor.

Purification of γ-globulins. Further *in vitro* analyses were performed using purified γ-globulins. For this, the same serum volume from each mouse within a group (n=5-7) were pooled, and γ-globulins were purified by precipitation with NH_4SO_4 at 50% (Hebert, 1974). Purified γ-globulins were finally reconstituted in the same volume of the starting pool, filtered through 0.22 µm, and stored at -20°C until use.

Parasite killing activity. Anti-parasite (anti-PSC) activities of purified γ-globulins were assessed *in vitro* using three different strategies set-up by our group. Firstly, the intrinsic killing activity through direct interaction between γ-globulins and PSC was assessed in a culture system where parasites were incubated in the presence of purified γ-globulins. Briefly, using a 96-well non-adherent flat-bottom culture plate, 100 viable PSC were dispensed per well in 100 µL of sterile PBS containing antibiotics (60 µg/ml of penicillin, 100 µg/ml of streptomycin and 250 ng/ml of amphotericin B). Purified γ-globulins at 1:50 (final dilution respect to the starting concentration in the original pool) or equal volumes of PBS were immediately added. Then, PSC were incubated during 48hs at 37°C and 5% CO_2, and their viability was determined as previously described. Secondly, the killing of PSC by impairment of nutrient absorption through antibody-mediated interference was assessed using a similar culture design but using RPMI culture medium -instead of PBS- containing antibiotics, and by incubating the parasites during 120hs (5 days) at 37°C and 5% CO_2. Thirdly, parasite killing through classical activation of the complement system by the purified γ-globulins was assessed according to Miles et al., (2020) with some modifications. Briefly, using a 96-well non-adherent flat-bottom culture plate, 100 viable PSC were dispensed per well in 100 µL of sterile Veronal buffer saline (VBS) containing antibiotics. Freshly obtained sera from CD1 mice was added at 1:60 dilution, thus limiting the potential activation of the alternative pathway while still being able to activate the classical pathway (Palarasah et al., 2011). Immediately, purified γ-globulins at 1:50 (final dilution

respect to the starting concentration in the original pool) -or equal volumes of VBS as controls- were also added to the wells. Then, PSC were incubated during 48hs at 37°C and 5% CO_2. In any of the three *in vitro* strategies, each condition was assayed in eight replicates and the PSC viability after incubation was determined according to Dematteis et al., (1999). Finally, anti-parasite activities were expressed as the fold increase in the percentage of non-viable PSC respect to the corresponding mock control (P1A).

Evaluation of vaccine efficacy. The potential *in vivo* protection achievable by the vaccine candidates was assessed by immunizations followed by experimental infections in the murine model of secondary echinococcosis. To that end, three vaccine preparations were formulated mixing the following KLH-peptide conjugates (1:1 mass ratio) and QuilA® as the adjuvant: "Vaccine 1" (P1A-KLH + P1B-KLH); "Vaccine 2" (P2A-KLH + P2B-KLH); and "Vaccine 3" (P3A-KLH + P3B-KLH). Four groups of CD1 female mice (n=8-9 per group) were used (one of them acting as an unvaccinated control group), and the immunization scheme was the same as previously described. Briefly, mice were s.c. immunized with 100 µg of each vaccine preparation (1:1 mass ratio of each peptide-KLH conjugate) in a priming-booster-booster scheme at days 0, 15 and 30. Control group received equal volumes of sterile PBS. Then, experimental infections were performed at day 45 post-priming by the i.p. inoculation of each mouse with 200 µL of a PBS suspension containing 2,000 viable PSC. Mice were euthanized 6 months post-challenge and peritoneal cysts were recovered. Groups were compared in terms of the proportion of mice harboring at least one hydatid cyst, and regarding the number of developed hydatid cysts within each mouse.

Statistics. Comparisons between experimental and control groups were assessed by either non-parametric Kruskal-Walis test, Mann-Whitney-Wilcoxon U test or parametric Student's t-test, depending on the situation. Infection frequencies were evaluated through the Fisher's exact test. *Statistical significance was confirmed when p-value <0.05.

3. RESULTS

3.1. In silico design of peptide-based vaccine candidates.

Peptides derived from potentially protective proteins present in the tegument of PSC from *E. granulosus* s.l. were designed following a novel scheme herein proposed by our group. To that end, we started from 7 parasitic proteins recently reported as novel vaccine candidates (Miles et al., 2020a), which are listed in Table 1. Firstly, we predicted all possible linear B-cell epitopes with a length

greater than 7 amino acids, resulting in 48 linear B-cell epitopes. Among them, only those free of any PTM in the native parental protein were selected by applying two successive and complementary approaches: *(i)* based on mass spectrometry matching peptides used to identify the parental proteins (Miles et al., 2020a), and *(ii)* based on PTMomics analyses (Miles et al., 2022). In this sense, 16 and 14 "clean epitopes" were identified by each criterion, respectively, yielding 30 different "clean epitopes". Then, the exact sequence of each "clean epitope" was searched for against every mammalian protein present in the UniProtKB database, discarding those with 100% identity to maximize antigenicity and to reduce potential auto-reactive drawbacks. Interestingly, we obtained 21 "unique epitopes" derived from only 5 proteins (Table 1).

Next, and since linear B-cell epitopes must be accessible to antibody recognition, only those potentially exposed epitopes were selected for further analyses. For this selection, we predicted the 3D structure of the 5 parental proteins exhibiting at least one "unique epitope" and then we manually mapped each epitope, where all 21 epitopes were found to be superficial (Table 1). After that, we performed a TSS analysis by comparing the conformational structure of peptides "in-solution" vs. within their parental proteins. The peptides "in-solution" structures were predicted *de novo*, while the native peptide conformation was manually obtained from the parental protein PDB file. TSS analyses resulted in 4 peptides with highly similar native and "in-solution" conformation belonging to 3 proteins. Long peptides (≥13 amino acids) which unmet such criterion, but exhibited at least 7 amino acids with an apparent high structure similarity, were manually modified keeping only those amino acids. Then, their 3D structures were obtained and TSS analyses were performed again, selecting 2 additional peptides. At the end, 6 peptide candidates were selected, belonging only to 3 out of the 7 initial proteins (Figure 1). To simplify further studies we named them as P1A and P1B (derived from protein P1); P2A and P2B (derived from protein P2); P3A and P3B (derived from protein P3).

3.2. Assessment of peptides' immunogenicity.

The 6 designed and selected peptides were commercially synthesized as covalent conjugates to KLH, which acted as a carrier protein to provide T-cell epitopes. Then, and in order to assess peptides' immunogenicity, groups of CD1 mice were immunized with each peptide-KLH conjugate -or with their corresponding controls- using QuillA® as an adjuvant, and following a priming-booster-booster scheme. After 45 days post-priming, all mice were bled and euthanized, and the antibody production was analyzed through ELISA. Firstly, and in order to confirm the immunization success, KLH-specific IgG antibodies were determined (Figure 2.A.). Then, we proceeded to analyze peptide-

specific IgG through ELISA by directly coating of the plates with unconjugated synthetic peptides. Accordingly, we observed high levels of P2A- and P2B-specific IgG, as well as low but significant levels of P3A- and P3B-specific antibodies, in comparison to mice immunized with unconjugated KLH (Figure 2.B.).

Finally, and in order to analyze the cross-reactivity of the peptide-specific IgG against their native parental proteins, we firstly calculated each protein abundance within the PSEx fraction. To that end, and using own previously published proteomic data (Miles et al., 2020b), we applied the exponentially modified protein abundance index (emPAI) method (Ishihama et al., 2005) to each one of the 3 parental proteins. Briefly, for every protein within PSEx (roughly 1250 proteins), their emPAI values were determined and the relative abundance of every single protein was defined as the percentage of each protein's emPAI value relative to the overall sum of every proteins' emPAI values. This analysis showed a relative abundance of 2.58%, 1.79% and 0.51% for proteins P1, P2 and P3, respectively; meaning that the 3 proteins are highly abundant within the PSEx fraction. Once we confirmed their high abundance, we determined the cross-reactivity of peptide-specific IgG against the components present within the PSEx extract. Accordingly, peptide-specific IgG showed mostly significant cross-reactivity against their native parental proteins present within PSEx (Figure 2.C.). Interestingly, sera obtained from mice immunized with P1A-KLH showed neither significant levels of peptide-specific IgG (Figure 2.B.), nor evident cross-reactivity against PSEx components (Figure 2.C.), in comparison to mice immunized with unconjugated KLH (control group). These results suggest that the induced IgG antibodies in the group of mice immunized with P1A-KLH may have no potential for an efficient vaccine formulation. Therefore, and since P1A-KLH is a highly similar preparation to any of the other 5 peptide-KLH conjugates in terms of the adjuvant and carrier content, we utilized it as mock control in the further studies.

3.3. Anti-parasite activity of peptide-specific antibodies.

The potential efficiency of the designed peptide-based vaccines was firstly explored *in vitro* using three complementary assays, each one aimed to dissect potential anti-parasite mechanisms induced by specific antibodies. Firstly, we analyzed whether the direct interaction of peptide-specific antibodies with viable PSC was able to induce the parasite death (Figure 3.A.). Then, we evaluated if peptide-specific antibodies could interfere with metabolic processes in PSC (e.g. nutrient absorption) (Figure 3.B.). Finally, we assessed the effects of the activation of the complement system through peptide-specific antibodies (classical activation) on the viability of PSC (Figure 3.C.). In the three

strategies, results were expressed as the fold-increase in the percentage of dead PSC respect to the results obtained with P1A-specific antibodies.

In the first place, P1B-specific antibodies showed similar results to P1A-specific antibodies (mock control) regardless the experimental setting used (Figure 3). On the other hand, and among P2-derived peptides, P2A-specific antibodies increased the parasite death induced by classical activation of the complement system (Figure 3.C.), while P2B-specific antibodies interfered with metabolic processes in PSC (Figure 3.B.). Interestingly, the antibodies raised against the two peptides derived from the P3 protein exhibited the best anti-parasite activities in our *in vitro* settings. Accordingly, while P3A-specific antibodies showed the highest intrinsic anti-PSC activity compared to P1A-specific antibodies (Figure 3.A.), and additionally increased the parasite death by classical activation of the complement system (Figure 3.C.); P3B-specific antibodies induced significant increments in PSC death regardless the *in vitro* setting analyzed (Figure 3).

3.4. Efficacy evaluation of the peptide candidates in the murine model of infection.

The protection induced by our peptide-based vaccines was assessed in the murine model of secondary cystic echinococcosis. To that end, three groups of CD1 mice were s.c. immunized each one with a vaccine formulated with QuilA® (*"Vaccine 1"*: P1A-KLH + P1B-KLH; *"Vaccine 2"*: P2A-KLH + P2B-KLH; *"Vaccine 3"*: P3A-KLH + P3B-KLH). The vaccine selection was made based on the previous *in vitro* results (Figure 3). Thus, peptide-KLH conjugates were mixed in pairs according to the following criteria: *(i)* pairs displaying no *in vitro* anti-parasite activity (*"Vaccine 1"*), *(ii)* pairs showing only one *in vitro* anti-parasite activity each (*"Vaccine 2"*), and *(iii)* pairs exhibiting at least two *in vitro* anti-parasite activities (*"Vaccine 3"*). Working with mixtures of peptide-KLH conjugates allowed us to reduce the number of mice used in this exploratory assay, since further experiments will be require to optimize potentially better formulations and/or immunization schemes. The immunization protocol used corresponded to a priming-booster-booster scheme (days 0, 15 and 30), followed by an i.p. parasite challenge at day 45 post-priming. An additional group of unvaccinated, but challenged, mice was used as a control. After 6 months of infection, all mice in every group were euthanized and their peritoneal cavities were inspected for developed hydatid cysts.

Results in Figure 4 show the percentage of infected mice (Figure 4.A.), as well as the number of developed hydatid cysts within each mouse (Figure 4.B.) according to the experimental group. Again, based on our *in vitro* results, *"Vaccine 1"* was used as a mock vaccine that included potentially

unspecific effects induced by the anti-KLH immune response. Accordingly, the *"Vaccine 1"* group did not show any significant difference with the unvaccinated group, neither in the proportion of infected mice (Figure 4.A.), nor in the number of peritoneal hydatid cysts per mouse (Figure 4.B.). On the other hand, although in the *"Vaccine 2"* group a 33% protection against *E. granulosus* s.l. infection was observed, results were not statistically significant respect to neither the unvaccinated nor the *"Vaccine 1"* groups (Figure 4.A.). However, in the *"Vaccine 3"* group a statistically significant protection of 50% was observed in comparison to either the unvaccinated or the *"Vaccine 1"* (mock vaccine) group (Figure 4.A.). In addition, tmice in the *"Vaccine 3"* group harbored a significant lower number of hydatid cysts in their peritoneal cavities, respect either to the unvaccinated or to the *"Vaccine 1"* group (Figure 4.B.).

4. DISCUSSION

Although no peptide-based vaccine has reached the market yet, there is a significant interest in developing this type of vaccines against both infectious and non-infectious diseases (Malonis et al., 2020). Currently, several peptide-based vaccines for cancer are in phase II and III clinical trials, as well as a few peptide-based vaccines against infectious diseases are in phase I trials (Di Natale et al., 2020). Pre-clinical studies of such vaccines against helminth infections have shown promising results, including *Trinchinella spialis* (McGuire et al., 2002), *Taenia solium* (Huerta et al., 2001; Toledo et al., 1999), *Fasciola gigantica* (Jezek et al., 2008), and *F. hepatica* (Rojas-Caraballo et al., 2014). In the case of *E. granulosus* s.l., several peptides have been proposed as vaccine candidates (Li et al., 2021; Miles et al., 2017; Pan et al., 2017; Wang et al., 2019), although no *in vivo* efficiency assays have been reported for any of them.

E. granulosus s.l. is a zoonotic cestode parasite that causes a cosmopolitan disease with high impacts on regional economies due to its effects on the human health as well as in livestock animals (Budke et al., 2006). Cystic echinococcosis develops in form of an ever-growing fluid-filled cyst, which can produce PSC by asexual reproduction, which are the infective parasite stage for the definitive host if ingested. Additionally, PSC can also develop into new cysts if accidentally seeded within the intermediate host after a cyst rupture (Heath, 1970). The WHO lists cystic echinococcosis as a neglected tropical disease, and besides its impact, limited information about the parasite biology is currently available. In this regard, we have recently identified seven novel potentially protective antigens, which are antibody targets in the control of the infection establishment (Miles et al., 2020a). Here we propose an easy, cheap and fast workflow for the *in silico* design of peptide-based vaccines

derived from such potentially protective antigens, overcoming most common difficulties. We also validated our design scheme by evaluating both *in vitro* and *in vivo* the efficiency of our vaccine candidates. Our results finally suggested a promising candidate (*"Vaccine 3"*) which is composed of a mixture of two KLH-peptide conjugates able to limit the establishment of *E. granulosus* s.l. in a murine model of secondary infection. However, further studies will be required to fully evaluate and improve our vaccine formulation.

Following our workflow, we selected six surface exposed linear B-cell epitopes (> 7 amino acids in length), free of PTMs and resembling a similar conformation to their parental native proteins. Then, selected peptides were commercially synthesized as covalent conjugates to KLH, a carrier protein. Peptide-specific antibodies were successfully induced after immunizing mice with KLH-peptide conjugates formulated with QuilA® as adjuvant (Figure 2), as it has already been proposed to be a plausible adjuvant for both helminth vaccines (Perera and Ndao, 2021) and other peptide-based vaccines (Azmi et al., 2014). Then, the generation of peptide-specific IgG antibodies (Figure 2.B.), and their cross-recognition of the native parental proteins (Figure 2.C.), was checked. Antibodies raised against peptides derived from the P2 and P3 proteins exhibited the highest levels of peptide-specific and PSEx cross-reacting IgG antibodies. Interestingly, P1A-specific IgG antibodies showed to be similar to the negative controls, both against the peptide and PSEx (Figure 2), suggesting that P1A-specific antibodies were not successfully generated and/or were unable to recognize their native parental protein.

After checking the peptides immunogenicity, the anti-parasite potential of the vaccine formulations was analyzed using both *in vitro* and *in vivo* strategies. For the *in vitro* studies, we evaluated different anti-PSC activities induced by peptide-specific antibodies. Of note, the obtained results showed that P3A- and P3B-specific antibodies were able to induce either the parasite death by direct interaction with PSC (Figure 3.A.), as well as the harmful classical activation of the complement system (Figure 3.C.). In this regard, PSC are well known to be susceptible to the attack by the complement system activation (Ferreira et al., 2000). Additionally, P3B-specific antibodies seemed also to interfere with certain metabolic processes in PSC increasing their death rate (Figure 3.B).

On the other hand, and for the *in vivo* evaluation of the vaccine candidates, peptides were grouped according to the *in vitro* results in three vaccine formulations: *"Vaccine 1"*, *"Vaccine 2"*, and *"Vaccine 3"*, reflecting low, medium and high anti-parasite activities *in vitro*, respectively. As expected from the *in vitro* results, *"Vaccine 1"* performed as a mock vaccine control showing no significant difference with the unvaccinated group of mice (Figure 4.A.). Additionally, and since the

three vaccine candidates contained KLH as a carrier protein, the negative results obtained with *"Vaccine 1"*, fortunately and indirectly, let us infer that KLH-induced immune responses do not influence *per se* the infection outcome in the murine model of secondary cystic echinococcosis. The *"Vaccine 3"* formulation successfully induced a 50% protection in the immunized mice (Figure 4.A.), as well as a significant reduction in the number of peritoneal hydatid cysts (Figure 4.B.).

Serendipitously, each formulated vaccine corresponded to a unique parental protein, and interestingly, the formulations that elicited some degree of protection (e.g. *"Vaccine 2"* and *"Vaccine 3"*), both contained peptide conjugates derived from parasite malate dehydrogenases (Table 1 and Figure 1). Within *E. granulosus* s.l. genome, there are three encoded malate dehydrogenases, being A0A068WS99 (a protein not used in this study) highly similar to protein P3, exhibiting 100% identity within their first 311 amino acids and their 35 extra C-terminal amino acids. The herein analyzed malate dehydrogenases (P2 and P3) showed only a 25% sequence identity between them; probably due to differences in their subcellular location, since P2 is mitochondrial while P3 corresponds to a cytoplasmic protein. Malate dehydrogenases have been previously tested as promising vaccine candidates against many pathogens, including bacteria (Arayan et al., 2019), fungi (Shibasaki et al., 2014), unicellular parasites (Liu et al., 2016), and also proposed as druggable targets against helminth parasites (Kayamba et al., 2021; Probert et al., 1981; Sanchez-Moreno et al., 1987). Thus, the present work may consolidate malate dehydrogenases as vaccine candidates against *E. granulosus* s.l., also suggesting at least two potential peptides (P3A and P3B) for such vaccine formulations.

In conclusion, our design and selection workflow for the identification of peptide-based vaccine candidates seems to be a valuable tool. By introducing two key analysis steps, our workflow substantially increased the rate of design success. Firstly, using mass spectrometry data assures the selection of peptide candidates free of post-translational modifications in their native parental protein, thus limiting the steric impairments that antibodies might encounter when recognizing the native structure. Secondly, using TSS as a way to select only peptides whose "in-solution" conformation resembles peptide conformation within the native parental protein, also increases the likelihood of antibody cross-reactivity. Thus, antigenic peptides can be selected in just six steps starting from mass spectrometry data obtained from a known vaccine candidate, and its amino acid sequence. Since we finally suggested six peptide candidates from seven initial proteins showing limited information besides their amino acid sequence, and a vaccine formulation composed of two of them induced a significant reduction in the infection rate and outcome, we conclude that the overall success rate of our designed workflow is quite high. We propose the present design and selection workflow as a potentially useful tool to be applied for other pathogens, thus greatly reducing R&D time and costs.

ACKNOWLEDGEMENTS

Agencia Nacional de Investigación e Innovación – ANII (Uruguay) and PEDECIBA – Química (Uruguay) are acknowledged for their general financial support. SM received a "*Iniciación a la Investigación"* research grant (n°279) from CSIC – Universidad de la República (Uruguay).

BIBLIOGRAPHY

Arayan, L.T., Huy, T.X.N., Reyes, A.W.B., Hop, H.T., Son, V.H., Min, W., Lee, H.J., Kim, S., 2019. Substantial protective immunity conferred by a combination of Brucella abortus recombinant proteins against Brucella abortus 544 infection in BALB/c mice. J. Microbiol. Biotechnol. 29, 330–338. https://doi.org/10.4014/jmb.1811.10066

Azmi, F., Al, A., Ahmad, H., Skwarczynski, M., Toth, I., 2014. Recent progress in adjuvant discovery for peptide-based subunit vaccines. Hum. Vaccin. Immunother. 778–796. https://doi.org/10.4161/hv.27332ferr

Bethony, J.M., Cole, R.N., Guo, X., Kamhawi, S., Lightowlers, M.W., Loukas, A., Petri, W., Reed, S., Valenzuela, J.G., Hotez, P.J., 2011. Vaccines to combat the neglected tropical diseases. Immunol. Rev. 239, 237–270. https://doi.org/10.1111/j.1600-065X.2010.00976.x

Budke, C.M., Deplazes, P., Torgerson, P.R., 2006. Global socioeconomic impact of cystic echinococcosis. Emerg. Infect. Dis. 12, 296–303. https://doi.org/10.3201/eid1202.050499

Dematteis, S., Baz, A., Rottenberg, M., Fernández, C., Örn, A., Nieto, A., 1999. Antibody and Th1/Th2-type responses in BALB/c mice inoculated with live or dead Echinococcus granulosus protoscoleces. Parasite Immunol. 21, 19–26. https://doi.org/10.1046/j.1365-3024.1999.00198.x

Di Natale, C., La Manna, S., De Benedictis, I., Brandi, P., Marasco, D., 2020. Perspectives in Peptide-Based Vaccination Strategies for Syndrome Coronavirus 2 Pandemic. Front. Pharmacol. 11, 1–16. https://doi.org/10.3389/fphar.2020.578382

Ferreira, A.M., Irigoín, F., Breijo, M., Sim, R.B., Díaz, A., 2000. How Echinococcus granulosus Deals with Complement. Parasitol. Today 16, 7387–7390.

Guex, N., Peitsch, M.C., 1997. SWISS-MODEL and the Swiss-PdbViewer: An environment for comparative protein modeling. Electrophoresis 18, 2714–2723. https://doi.org/10.1002/elps.1150181505

Heath, D.D., 1970. The development of Echinococcus granulosus larvae in laboratory animals. Parasitology 60, 449–456. https://doi.org/10.1017/S0031182000078252

Heath, D.D., Jensen, O., Lightowlers, M.W., 2003. Progress in control of hydatidosis using vaccination - A review of formulation and delivery of the vaccine and recommendations for practical use in control programmes. Acta Trop. 85, 133–143. https://doi.org/10.1016/S0001-706X(02)00219-X

Hebert, G.A., 1974. Ammonium Sulfate Fractionation of Sera: Mouse, Hamster, Guinea Pig, Monkey, Chimpanzee, Swine, Chicken, and Cattle. Appl. Microbiol. 27, 389–393. https://doi.org/10.1128/am.27.2.389-393.1974

Hernández, A., Nieto, A., 1994. Induction of protective immunity against murine secondary hydatidosis. Parasite Immunol. 16, 537–544. https://doi.org/10.1111/j.1365-3024.1994.tb00308.x

Hotez, P.J., 2018. The global fight to develop antipoverty vaccines in the anti-vaccine era. Hum. Vaccines Immunother. 14, 2128–2131. https://doi.org/10.1080/21645515.2018.1430542

Hotez, P.J., Bottazzi, M.E., Strych, U., 2016. New vaccines for the world's poorest people. Annu. Rev. Med. 67, 405–417. https://doi.org/10.1146/annurev-med-051214-024241

Huerta, M., De Aluja, A.S., Fragoso, G., Toledo, A., Villalobos, N., Hernández, M., Gevorkian, G., Acero, G., Díaz, A., Alvarez, I., Avila, R., Beltrán, C., Garcia, G., Martinez, J.J., Larralde, C., Sciutto, E., 2001. Synthetic peptide vaccine against Taenia solium pig cysticercosis: Successful vaccination in a controlled field trial in rural Mexico. Vaccine 20, 262–266. https://doi.org/10.1016/S0264-410X(01)00249-3

Ishihama, Y., Oda, Y., Tabata, T., Sato, T., Nagasu, T., Rappsilber, J., Mann, M., 2005. Exponentially Modified Protein Abundance Index (emPAI) for Estimation of Absolute Protein Amount in Proteomics by the Number of Sequenced Peptides per Protein*S.

Mol. Cell. Proteomics 4, 1265–1272. https://doi.org/https://doi.org/10.1074/mcp.M500061-MCP200

Jespersen, M.C., Peters, B., Nielsen, M., Marcatili, P., 2017. BepiPred-2.0: Improving sequence-based B-cell epitope prediction using conformational epitopes. Nucleic Acids Res. 45, W24–W29. https://doi.org/10.1093/nar/gkx346

Jezek, J., El Ridi, R., Salah, M., Wagih, A., Aziz, H.W., Tallima, H., El Shafie, M.H., Khalek, T.A., Abo Ammou, F.F., Strongylis, C., Moussis, V., Tsikaris, V., 2008. Fasciola gigantica cathepsin L proteinase-based synthetic peptide for immunodiagnosis and prevention of sheep fasciolosis. Biopolym. - Pept. Sci. Sect. 90, 349–357. https://doi.org/10.1002/bip.20788

Källberg, M., Wang, H., Wang, S., Peng, J., Wang, Z., Lu, H., Xu, J., 2012. Template-based protein structure modeling using the RaptorX web server. Nat. Protoc. 7, 1511–1522. https://doi.org/10.1038/nprot.2012.085

Kayamba, F., Faya, M., Pooe, O.J., Kushwaha, B., Kushwaha, N.D., Obakachi, V.A., Nyamori, V.O., Karpoormath, R., 2021. Lactate dehydrogenase and malate dehydrogenase: Potential antiparasitic targets for drug development studies. Bioorg. Med. Chem. 50, 116458. https://doi.org/10.1016/j.bmc.2021.116458

Lamiable, A., Thévenet, P., Rey, J., Vavrusa, M., Derreumaux, P., Tufféry, P., 2016. PEP-FOLD3: faster de novo structure prediction for linear peptides in solution and in complex. Nucleic Acids Res. 44, W449–W454. https://doi.org/10.1093/nar/gkw329

Larsen, J.E.P., Lund, O., Nielsen, M., 2006. Improved method for predicting linear B-cell epitopes. Immunome Res. 2, 2. https://doi.org/10.1186/1745-7580-2-2

Li, W., Joshi, M.D., Singhania, S., Ramsey, K.H., Murthy, A.K., 2014. Peptide vaccine: Progress and challenges. Vaccines 2, 515–536. https://doi.org/10.3390/vaccines2030515

Li, Y., Zhu, Y., Sha, T., Chen, Z., Yu, M., Zhang, F., Ding, J., 2021. A Multi-Epitope Chitosan Nanoparticles Vaccine of Canine Against Echinococcus granulosus. J. Biomed. Nanotechnol. 17, 910–920. https://doi.org/10.1166/jbn.2021.3065

Lightowlers, M.W., Jensen, O., Fernandez, E., Iriarte, J.A., Woollard, D.J., Gauci, C.G., Jenkins, D.J., Heath, D.D., 1999. Vaccination trials in Australia and Argentina confirm the effectiveness of the EG95 hydatid vaccine in sheep. Int. J. Parasitol. 29, 531–534. https://doi.org/10.1016/S0020-7519(99)00003-X

Lightowlers, M.W., Lawrence, S.B., Gauci, C.G., Young, J., Ralston, M.J., Maas, D., Heath, D.D., 1996. Vaccination against hydatidosis using a defined recombinant antigen. Parasite Immunol. 18, 457–462. https://doi.org/10.1111/j.1365-3024.1996.tb01029.x

Liu, Z., Yuan, F., Yang, Y., Yin, L., Liu, Y., Wang, Y., Zheng, K., Cao, J., 2016. Partial protective immunity against toxoplasmosis in mice elicited by recombinant Toxoplasma gondii malate dehydrogenase. Vaccine 34, 989–994. https://doi.org/10.1016/j.vaccine.2015.10.067

Malonis, R.J., Lai, J.R., Vergnolle, O., 2020. Peptide-Based Vaccines: Current Progress and Future Challenges. Chem. Rev. 120, 3210–3229. https://doi.org/10.1021/acs.chemrev.9b00472

McGuire, C., Chan, W.C., Wakelin, D., 2002. Nasal immunization with homogenate and peptide antigens induces protective immunity against Trichinella spiralis. Infect. Immun. 70, 7149–7152. https://doi.org/10.1128/IAI.70.12.7149-7152.2002

Miguez, M., Baz, A., Nieto, A., 1996. Carbohydrates on the surface of Echinococcus granulosus protoscoleces are immunodominant in mice. Parasite Immunol. 18, 559–569.

Miles, S., Magnone, J., Cyrklaff, M., Arbildi, P., Frischknecht, F., Dematteis, S., Mourglia-Ettlin, G., 2020a. Linking murine resistance to secondary cystic echinococcosis with antibody responses targeting Echinococcus granulosus tegumental antigens. Immunobiology 225. https://doi.org/10.1016/j.imbio.2020.151916

Miles, S., Magnone, J., García-Luna, J., Dematteis, S., Mourglia-Ettlin, G., 2022. Unraveling post-translational modifications in Echinococcus granulosus sensu lato. Acta Trop. 230, 106410. https://doi.org/10.1016/j.actatropica.2022.106410

Miles, S., Navatta, M., Dematteis, S., Mourglia-Ettlin, G., 2017. Identification of universal diagnostic peptide candidates for neglected tropical diseases caused by cestodes through the integration of multi-genome-wide analyses and immunoinformatic predictions. Infect. Genet. Evol. 54. https://doi.org/10.1016/j.meegid.2017.07.020

Miles, S., Velasco-de-Andrés, M., Lozano, F., Mourglia-Ettlin, G., 2020b. Interactome analysis of CD5 and CD6 ectodomains with tegumental antigens from the helminth parasite Echinococcus granulosus sensu lato. Int. J. Biol. Macromol. 164, 3718–3728. https://doi.org/10.1016/j.ijbiomac.2020.08.219

Monath, T.P., 2013. Vaccines against diseases transmitted from animals to humans: A one health paradigm. Vaccine 31, 5321–5338. https://doi.org/10.1016/j.vaccine.2013.09.029

Nakao, M., Yanagida, T., Okamoto, M., Knapp, J., Nkouawa, A., Sako, Y., Ito, A., 2010. State-of-the-art Echinococcus and Taenia: Phylogenetic taxonomy of human-pathogenic tapeworms and its application to molecular diagnosis. Infect. Genet. Evol. 10, 444–452. https://doi.org/10.1016/j.meegid.2010.01.011

Palarasah, Y., Nielsen, C., Sprogøe, U., Christensen, M.L., Lillevang, S., Madsen, H.O., Bygum, A., Koch, C., Skjodt, K., Skjoedt, M.O., 2011. Novel assays to assess the functional capacity of the classical, the alternative and the lectin pathways of the complement system. Clin. Exp. Immunol. 164, 388–395. https://doi.org/10.1111/j.1365-2249.2011.04322.x

Pan, W., Chen, D.-S., Lu, Y.-J., Sun, F.-F., Xu, H.-W., Zhang, Y.-W., Yan, C., Fu, L.-L., Zheng, K.-Y., Tang, R.-X., 2017. Bioinformatic prediction of the epitopes of Echinococcus granulosus antigen 5. Biomed. Reports 6, 181–187. https://doi.org/10.3892/br.2016.827

Perera, D.J., Ndao, M., 2021. Promising Technologies in the Field of Helminth Vaccines. Front. Immunol. 12, 1–21. https://doi.org/10.3389/fimmu.2021.711650

Probert, A.J., Sharma, R.K., Singh, K., Saxena, R., 1981. The effect of five fasciolicides on malate dehydrogenase activity and mortality of Fasciola gigantica, Fasciolopsis buski and Paramphistomum explanatum. J. Helminthol. 55, 115–122. https://doi.org/10.1017/s0022149x0002558x

Rojas-Caraballo, J., López-Abán, J., Pérez Del Villar, L., Vizcaíno, C., Vicente, B., Fernández-Soto, P., Del Olmo, E., Patarroyo, M.A., Muro, A., 2014. In vitro and in vivo studies for assessing the immune response and protection-inducing ability conferred by Fasciola hepatica-derived synthetic peptides containing B- and T-cell epitopes. PLoS One 9. https://doi.org/10.1371/journal.pone.0105323

Sanchez-Moreno, M., Salas Peregrin, J.M., Leon, P., Garcia-Ruiz, M.A., Lemaur, M., Monteoliva, M., 1987. Malate dehydrogenase in helminth parasites. Inhibition by benzimidazoles and pyrimidine derivatives. Arzneimittel-Forschung/Drug Res. 37, 1327–1331.

Sanchez-Trincado, J.L., Gomez-Perosanz, M., Reche, P.A., 2017. Fundamentals and Methods for T- and B-Cell Epitope Prediction. J. Immunol. Res. 2017, 1–14. https://doi.org/10.1155/2017/2680160

Shibasaki, S., Aoki, W., Nomura, T., Karasaki, M., Sewaki, T., Ueda, M., 2014. Evaluation of Mdh1 protein as an antigenic candidate for a vaccine against candidiasis. Biocontrol Sci. 19, 51–55. https://doi.org/10.4265/bio.19.51

Toledo, A., Larralde, C., Fragoso, G., Gevorkian, G., Manoutcharian, K., Hernández, M., Acero, G., Rosas, G., López-Casillas, F., Garfias, C.K., Vázquez, R., Terrazas, I., Sciutto, E., 1999. Towards a Taenia solium cysticercosis vaccine: An epitope shared by Taenia crassiceps and Taenia solium protects mice against experimental cysticercosis. Infect. Immun. 67, 2522–2530. https://doi.org/10.1128/iai.67.5.2522-2530.1999

Wang, L., Gao, J., Lan, X., Zhao, H., Shang, X., Tian, F., Wen, H., Ding, J., Luo, L., Ma, X., 2019. Identification of combined T-cell and B-cell reactive Echinococcus granulosus 95 antigens for the potential development of a multi-epitope vaccine. Ann. Transl. Med. 7, 652–652. https://doi.org/10.21037/atm.2019.10.87

Zhang, L., 2018. Multi-epitope vaccines: a promising strategy against tumors and viral infections. Cell. Mol. Immunol. 15, 182–184. https://doi.org/10.1038/cmi.2017.92

Zhang, Y., Skolnick, J., 2005. TM-align: A protein structure alignment algorithm based on the TM-score. Nucleic Acids Res. 33, 2302–2309. https://doi.org/10.1093/nar/gki524

TABLES

Table 1. Design of peptide candidates. Peptide candidates were selected from 7 parasite proteins following the workflow described in Materials and Methods. *"Protein Code"*, *"Protein name"* and *"Accession number"* columns refer to the parental proteins analyzed, while the rest of the columns reflect the number of selected peptides after each step. *"linear B-cell epitopes"* are the epitopes identified through Bepipred software. *"MS/MS"* and *"PTMomics"* clean epitopes correspond to peptides exhibiting any post-translational modification within their amino acid sequences. *"Unique Epitopes"* correspond to peptides whose exact sequence was not found in any mammalian protein. *"Superficial Epitopes"* correspond to peptides exposed on the surface of their parental proteins. *"original"* and *"modified"* High TSS epitopes correspond to peptides showing a high tertiary structure similarity between the "native" and the "in-solution" 3D-structure. *"Selected peptides"* correspond to the final number of epitopes selected from each protein, and used in the experimental studies.

FIGURES

Figure 1. Peptide candidates. Peptides suggested as vaccine candidates were selected following our novel herein described design workflow. In each figure, the 3D predicted structure of parental proteins P1, P2 and P3 is shown, highlighting in yellow the selected peptides within them. The protein names, accession numbers and amino acid sequences of their selected peptides are shown in the corresponding boxes.

Figure 2. Peptide-specific antibody responses. Specific IgG levels in the sera obtained from mice immunized with peptide-KLH conjugates, or their corresponding control groups, were assessed through ELISA. **(A)** In order to confirm the immunization success, each serum was analyzed for KLH-specific IgG levels. **(B)** Peptide-specific IgG responses were analyzed in comparison to the group of mice immunized with unconjugated KLH. **(C)** Cross-reactivity of peptide-specific antibodies with their parental native proteins was analyzed through the determination of PSEx-specific IgG levels. In all cases, specific IgG levels were reported as the absorbance values detected normalized by the sample dilution analyzed. Results are shown in *box-and-whiskers* style. In **(A)** and **(C)** the non-parametric Kruskal-Wallis test was used, and the asterisks correspond to statistical significance respect to the group immunized with unconjugated KLH. In **(B)** statistics were performed using the non-parametric Mann Whitney-Wilcoxon *U* test. In all cases, significant differences were regarded as p-value <0.05.

Figure 3. *In vitro* assessment of the anti-parasite activity of peptide-specific antibodies. Fold-increase in PSC killing activity induced by peptide-specific antibodies normalized to results obtained with P1A-specific antibodies (mock control). **(A)** Parasite death induced by the direct interaction between peptide-specific antibodies and PSC cultures in PBS during 48hs. **(B)** Parasite death induced by the metabolic interference of peptide-specific antibodies in PSC cultures in RPMI during 5 days. **(C)** Parasite death induced by the classical activation of the complement system through peptide-specific antibodies in PSC cultures in normal serum during 48hs. Results are shown as mean±SEM, and statistics were performed using the Student's t-test. Differences respect to results obtained with P1A-specific antibodies were regarded significant with p-value <0.05.

Figure 4. Efficacy of peptide-based vaccine candidates in the model of secondary infection. The efficacy potential of *"Vaccine 1"*, *"Vaccine 2"* and *"Vaccine 3"* formulations was assessed in the murine model of secondary cystic echinococcosis. To that end, groups of CD1 mice were s.c. immunized with each formulation following a priming-booster-booster scheme (days 0, 15 and 30). Then, every mice received an i.p. challenge, 45 days post-priming, with 2,000 highly viable PSC. At 6 months post infection, mice were euthanized, and the peritoneal hydatid cysts within each mouse were counted. Results are displayed as the percentage of infected mice **(A)**, and the number (mean±SEM) of peritoneal hydatid cysts per mouse **(B)**. In **(A)** the Fisher's exact test was used respect to either the unvaccinated and the *"Vaccine 1"* groups, while in **(B)** statistics were performed using the non-parametric Mann Whitney-Wilcoxon *U* test. Asterisks and numerals correspond to differences against the unvaccinated or the *"Vaccine 1"* groups, respectively. In all cases, significant differences were regarded as p-value <0.05.

Table 1

Protein Code	Protein Name	Accession Number	Linear B-cell epitopes	Clean epitopes		Unique Epitope	Superficial Epitopes	High TSS epitopes		Selected peptides
				MS/MS	PTMomics			Original	Modified	
P1	Severin/Gelsolin	U6IX85	11	3	3	6	6	1	1	2
P2	Malate dehydrogenase mitochondrial	A0A068X1L3	5	2	0	2	2	2	0	2
P3	Malate dehydrogenase cyotplasmatic	A0A068WYB8	7	0	5	4	4	1	1	2
P4	Actin	W6UMH9	8	4	2	2	2	0	0	-
P5	Vesicular amine transporter	A0A068X307	11	5	3	7	7	0	0	-
P6	Nucleoside diphosphate kinase	A0A068WL30	3	1	0	0	-	-	-	-
P7	Peptidyl-prolyl cis-trans isomerase	P14088	3	1	1	0	-	-	-	-

Figure 1

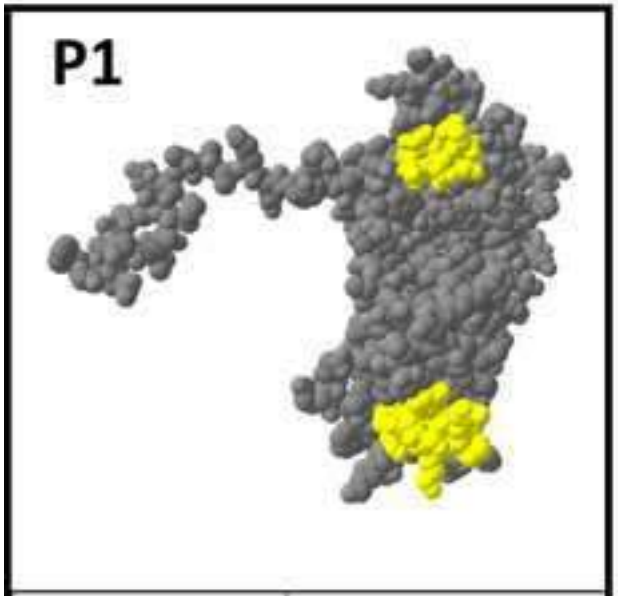

Protein Name	Gelosin
Accession Number	U6IX85
P1A	ANENERNS
P1B	ESPRFKSYF

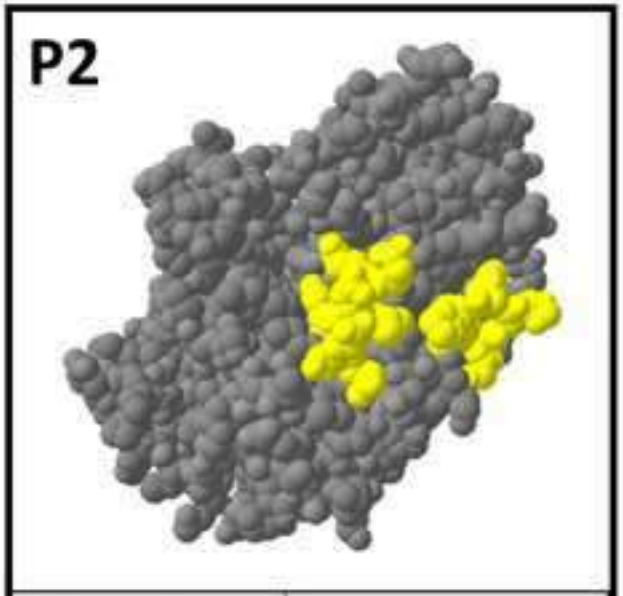

Protein Name	Malate dehydrogenase
Accession Number	A0A068X1L3
P2A	DELVDER
P2B	GDHTGAY

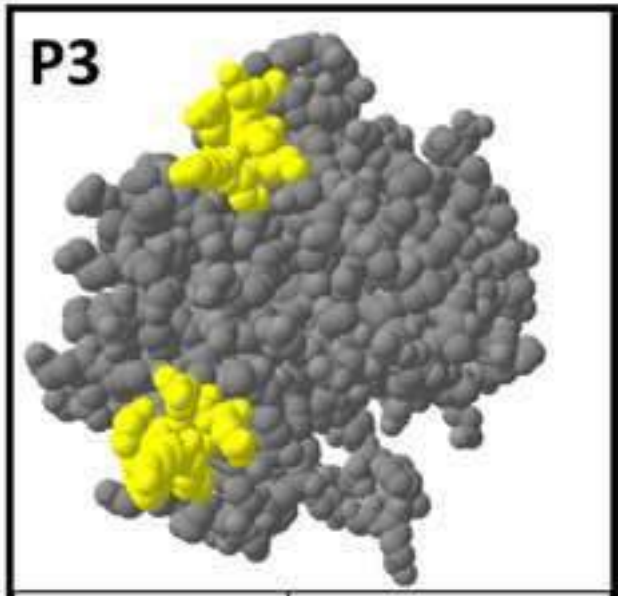

Protein Name	Malate dehydrogenase
Accession Number	A0A068WYB8
P3A	KSIKGKE
P3B	FAQKAREE

Figure 2

Click here to access/download;Figure;Figure 2.jpg

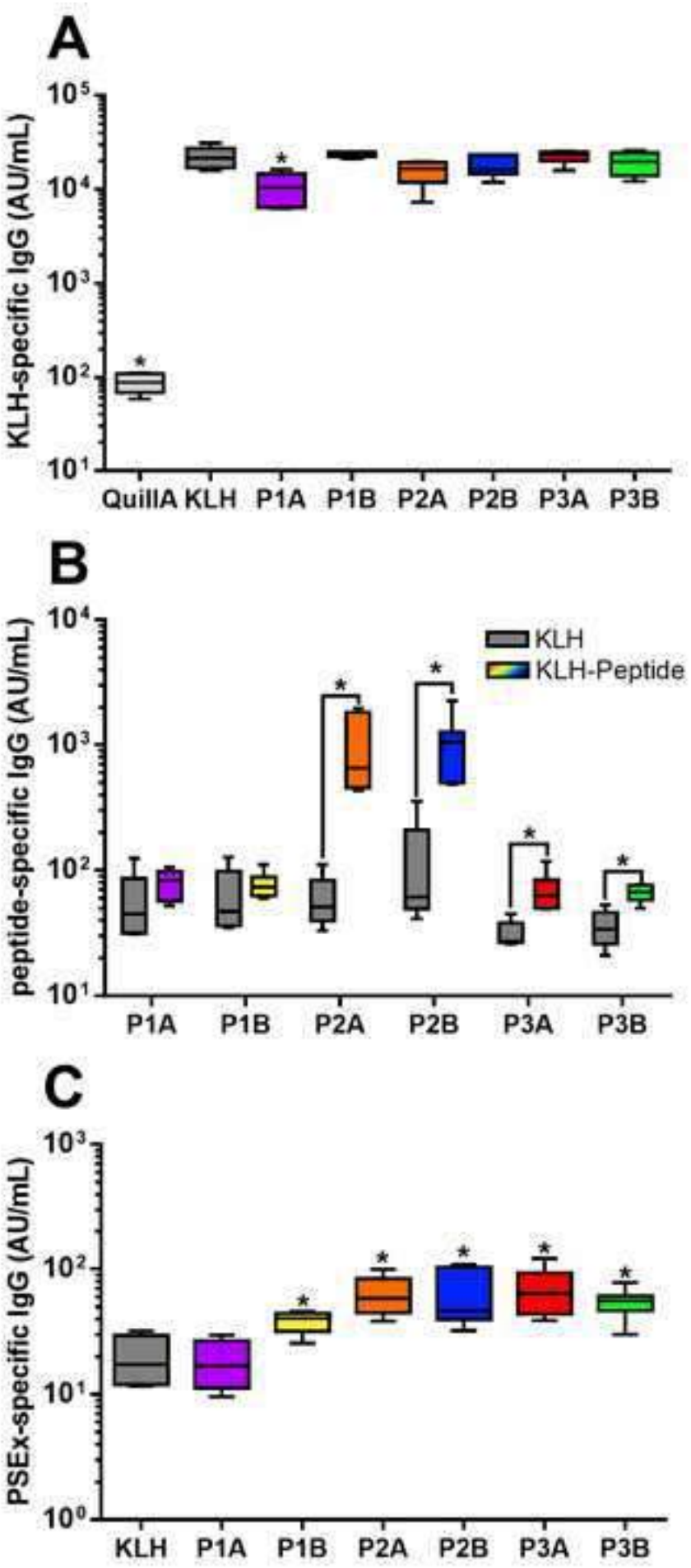

Figure 3

Click here to access/download;Figure;Figure 3.jpg

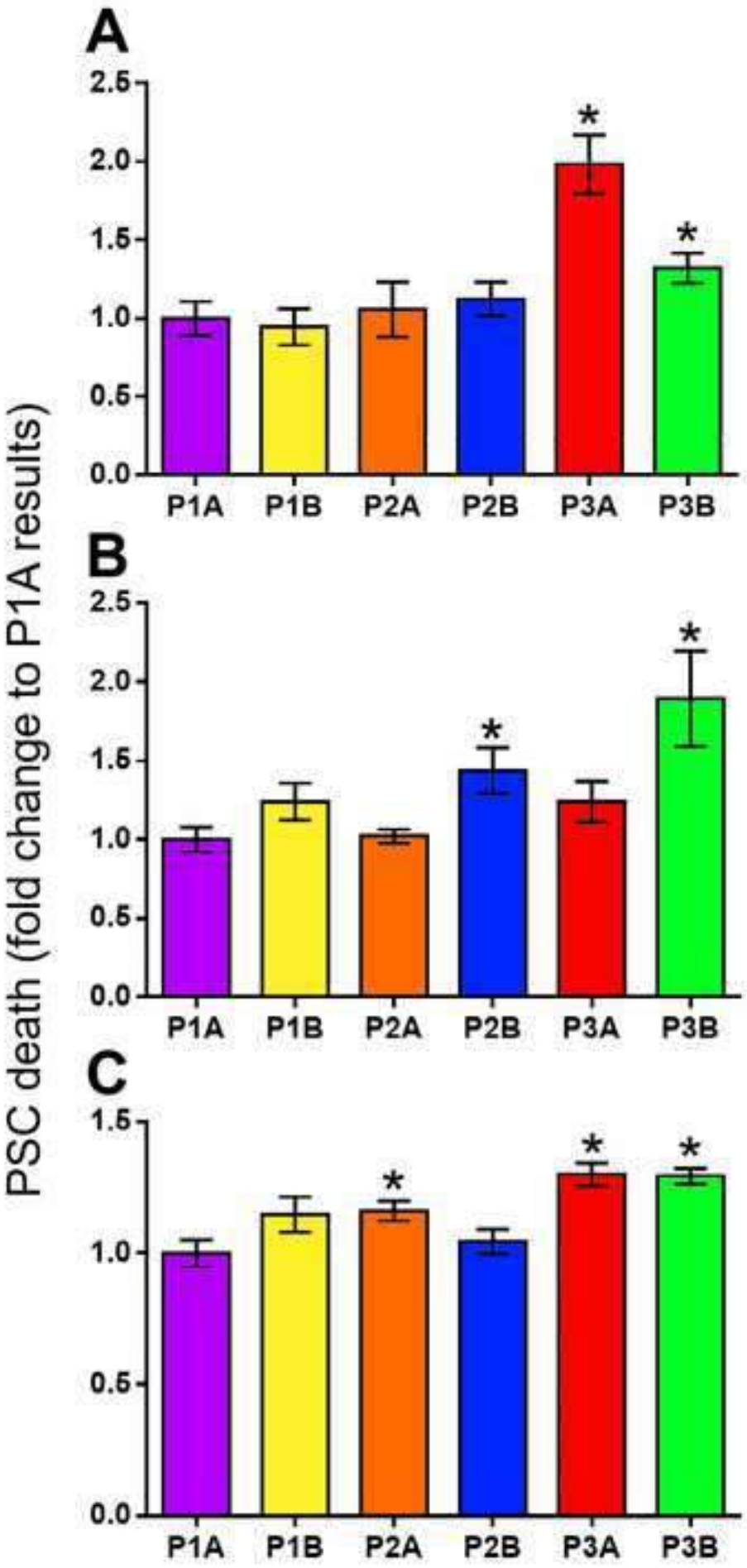

Figure 4

Click here to access/download;Figure;Figure 4.jpg

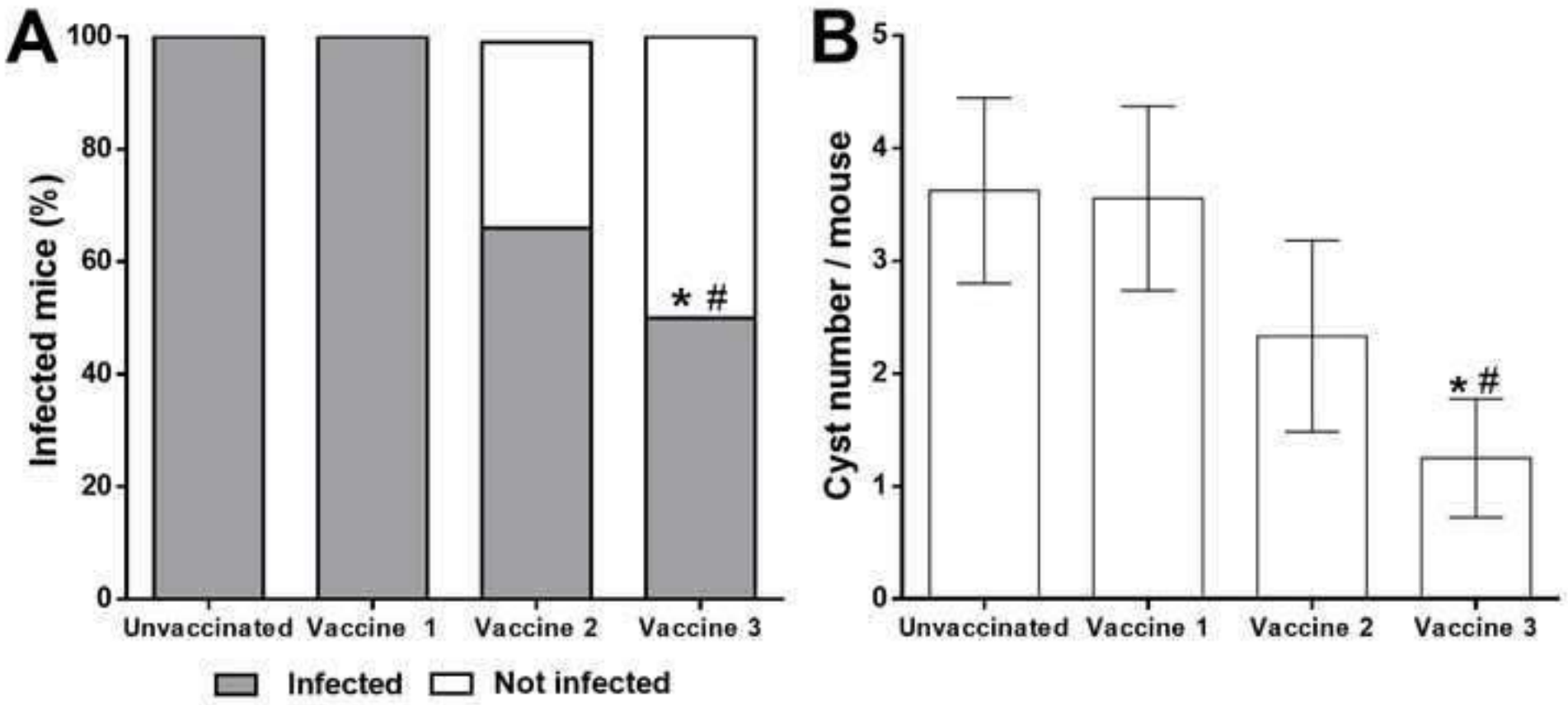

ANEXO 1

Interactome analysis of CD5 and CD6 ectodomains with tegumental antigens from the helminth parasite *Echinococcus granulosus*.

Miles S, Velasco-de-Andrés M, Lozano F, Mourglia-Ettlin G.

International Journal of Biological Macromolecules

2020

doi: 10.1016/j.ijbiomac.2020.08.219

International Journal of Biological Macromolecules 164 (2020) 3718–3728

Contents lists available at ScienceDirect

International Journal of Biological Macromolecules

journal homepage: http://www.elsevier.com/locate/ijbiomac

Interactome analysis of CD5 and CD6 ectodomains with tegumental antigens from the helminth parasite *Echinococcus granulosus sensu lato*

Sebastián Miles [a], María Velasco-de-Andrés [b], Francisco Lozano [b,c,d,*,1], Gustavo Mourglia-Ettlin [a,**,1]

[a] Área Inmunología, Facultad de Química/Facultad de Ciencias, DEPBIO/IQB, Universidad de la República, Montevideo, Uruguay
[b] Immunoreceptors del Sistema Innat i Adaptatiu, Institut d'Investigacions Biomèdiques August Pi i Sunyer (IDIBAPS), Barcelona, Spain
[c] Servei d'Immunologia, Centre de Diagnòstic Biomèdic, Hospital Clínic de Barcelona, Barcelona, Spain
[d] Departament de Biomedicina, Universitat de Barcelona, Barcelona, Spain

ARTICLE INFO

Article history:
Received 19 June 2020
Received in revised form 27 August 2020
Accepted 28 August 2020
Available online 04 September 2020

Keywords:
Echinococcus granulosus sensu lato
Interactome
Scavenger receptor
CD5
CD6
Ligand

ABSTRACT

Echinococcus granulosus sensu lato (s.l.) is a cestode parasite affecting both human and livestock health. Recombinant ectodomains of human scavenger receptors CD5 (rshCD5) and CD6 (rshCD6) were previously reported to bind its tegumental antigens and to exert prophylactic effects in a murine model of infection. Although the properties of mammalian scavenger receptors include the binding to diverse pathogen-derived structures, their interaction with helminth parasites has been scarcely explored. Therefore, we report here a search for CD5 and CD6 interactors within *E. granulosus* s.l. antigens. Mass spectrometry analysis of pull-downs from soluble tegumental components with biotinylated rshCD5 and rshCD6 resulted in 17 and 11 overrepresented interactors, respectively, 8 of which were shared. The interactors included previously reported protective molecules against *E. granulosus* s.l. and/or other helminths. Similar studies performed with 11-mer peptides mapping to each of the three extracellular scavenger domains of CD5 and CD6 allowed an estimated molecular topology of the interactions. In conclusion, the fact that most helminth interactors identified for rshCD5 and rshCD6 were already reported as vaccine candidates or pharmacological targets against different helminthiases, supports the view that their beneficial effects in experimental infection results from binding to multiple relevant tegumental antigens.

1. Introduction

Cystic echinococcosis (CE) is a cosmopolitan zoonosis caused by the larval stage of *Echinococcus granulosus sensu lato* (s.l.), a cestode parasite affecting both human and livestock health. Human incidence of CE is estimated to be as high as one million people worldwide, accompanied by annual livestock production losses reaching USD 2 billion [1]. Primary CE occurs in intermediate hosts (ungulates, accidentally humans) after ingestion of oncosphere-containing eggs, which develop into metacestodes (hydatid cysts) mainly in the host liver and lungs. Secondary CE occurs after spillage of protoscoleces (PSC) from a fertile cyst within an infected intermediate host, since PSC developmental plasticity allows them to become new cysts within intermediate hosts or adult worms if ingested by definitive hosts (usually dogs) [2].

Host-pathogen interaction is a highly dynamic process involving recognition of pathogen-associated molecular patterns (PAMPs) through pattern recognition receptors (PRRs) mainly expressed by innate immune cells [3]. Generally, PAMPs recognition by PRRs activates immediate host inflammatory responses with direct anti-pathogen activities. This is well exemplified by Scavenger Receptors (SRs), a structurally diverse group of PRRs with a wide range of biological functions (e.g. endocytosis, phagocytosis, adhesion and signaling) triggered upon binding to multiple non-self or altered-self ligands [4]. Some SRs (namely class A and class I) present single or multiple repeats of the ancient and highly conserved scavenger receptor cysteine-rich (SRCR) domain characteristic of a superfamily (SRCR-SF) comprising more than 30 different cell-surface or secreted proteins [5]. Although a high degree of structural conservation among SRCR-SF members is observed, not a single common unifying function has been reported. However, a steadily growing number of SRCR-SF members have been shown to interact with diverse microbial structures [4].

The lymphocyte cell surface receptors CD5 and CD6 are class I SRs exhibiting PRRs activities. Indeed, CD5 binds to β-glucans from saprophytic and pathogenic fungal species [6], and has been reported as a key receptor for human hepatitis C virus entry into T lymphocytes [7].

* Corresponding author.
** Correspondence to: Gustavo Mourglia-Ettilin, Área Inmunología, Facultad de Química, DEPBIO, Universidad de la República, Montevideo, Uruguay.
E-mail addresses: flozano@clinic.cat (F. Lozano), gmourglia@higiene.edu.uy (G. Mourglia-Ettlin).
[1] These authors are joint senior authors on this work.

https://doi.org/10.1016/j.ijbiomac.2020.08.219
0141-8130/

As for CD6, it binds to Gram-negative and Gram-positive bacteria through recognition of lipopolysaccharide (LPS) and lipotheichoic acid (LTA), respectively [8,9], and gp120 from HIV-1 [10]. Interestingly, the infusion of recombinant soluble forms of human CD5 (rshCD5) and CD6 (rshCD6) ectodomains show prophylactic and/or therapeutic actions in different murine models of bacterial [8,9,11] or fungal [6,12] infections.

Despite differences in PAMPs recognition, CD5 and CD6 receptors are highly homologous in terms of structure and functionality, since they are encoded by contiguous genes thought to derive from duplication of a common ancestor. The CD5 and CD6 ectodomains are exclusively composed of 3 consecutive SRCR domains showing extensive sequence identity, while their diverging cytoplasmic tails display several structural motifs compatible with signaling transduction functions [5]. Interestingly, CD5 and CD6 are physically associated with the clonotypic antigen-specific receptor of T (TCR) and B1a (BCR) cells, participating in the fine tuning of their activation and differentiation signals through still not fully understood mechanisms [13].

Besides CD5 and/or CD6 abilities to sense PAMPs from bacteria, fungi and viruses, their PRR activities were recently expanded to helminth parasites, a previously unexplored group of pathogens. Using the cestode *E. granulosus* s.l. as a helminth parasite model, CD5 and CD6 receptors were shown to interact mostly with tegumental protein antigens expressed in the PSC parasite stage. Furthermore, it was reported that rshCD5 and rshCD6 differentially modulated cytokine release upon peritoneal cells exposure to parasite tegumental components. Importantly, prophylactic infusion of rshCD5 or rshCD6 significantly ameliorated the outcome in a murine model of *E. granulosus* s.l. infection [14].

The present report aims at searching for rshCD5 and rshCD6 ligands within *E. granulosus* s.l. tegument since their blockade might be relevant for improving medical interventions in infected individuals. Additionally, a molecular topology of rshCD5 and rshCD6 interactors within their SRCR domains was performed through peptide mapping.

2. Materials and methods

2.1. Parasite antigens

PSC were obtained by aseptic puncture of pulmonary and fertile hydatid cysts from several bovine hosts collected at Uruguayan abattoirs. Viability of parasites was determined according to previous reports [15] after PSC from single hydatid cysts were extensively washed with phosphate buffered saline (PBS) pH 7.2 containing gentamicin (40 μg/mL). Only PSC exhibiting a viability ≥80% were used. Parasites obtained from different hydatid cysts were pooled, and PSC tegumental antigens (antigenic fraction termed PSEx) were extracted using a solution of MEGA-10 (1% w/v), EDTA (5 mM) and PMSF (2 mM) in PBS as originally reported [16]. PSEx obtained from several PSC batches were finally pooled and stored at −20 °C until use.

2.2. Recombinant receptors and synthetic peptides

Production of purified recombinant soluble proteins encompassing the whole ectodomains of human CD5 (rshCD5; from R^{25} to D^{345}) and CD6 (rshCD6; from D^{25} to R^{397}) receptors was performed based on previously reported methods [6,8] but using SURE CHO-M Cell line clones from the Selexis SURE-technology Platform (Geneva, Switzerland) and subjecting serum-free supernatants to size exclusion chromatography protocols developed at PX'Therapeutics (Grenoble, France). Proteins were biotinylated with EZ-Link PEO-maleimide-activated biotin (Pierce) following the manufacturer's instructions, and stored in PBS (10% glycerol, pH 7.4) at −80 °C until use. CD5 and CD6 intradomain peptide sequences homologous to the consensus 11-mer DMBT-1/SAG.pbs1 peptide sequence [17] were previously designed [18]. The sequence of such CD5- and CD6-derived peptides mapping at SRCR domains 1 to 3 were: CD5.P1 (GQLEVYLKDGW), CD5.P2 (GVVEFYSGSLG), CD5.P3 (GTVEVRQGAQW), CD6.P1 (GTVEVRLEASW), CD6.P2 (GRVEMLEHGEW), and CD6.P3 (GQVEVHFRGVW). Biotinylated peptides (≥80% purity) were synthesized by ProteoGenix (Schiltigheim, France) and stored at 5 mg/mL in water-diluted acetonitrile (1:3) at −80 °C until use.

2.3. Pull-down assays

Pull down experiments were performed following previously reported protocols [19], including a pre-cleaning step in order to minimize potentially unspecific bindings. Briefly, 8 mg of PSEx proteins (1 mg/mL in sterile PBS) were pre-cleaned using 200 μL of streptavidin agarose resin slurry (High Capacity Streptavidin Agarose Resin, Pierce®) during 90 min at RT with constant shaking followed by centrifugation at 2500*g* for 3 min at 4 °C. Pre-cleaned PSEx was transferred into 8 sterile microtubes (1 mL per tube) containing 100 μL of streptavidin agarose resin slurry pre-incubated with biotinylated receptors (rshCD5 or rshCD6) or synthetic peptides (CD5.P1, CD5.P2, CD5.P3, CD6.P1, CD6.P2 or CD6.P3). Such slurries were obtained from incubations with either biotinylated receptors (300 μg) or synthetic peptides (2 mg) following a similar protocol to PSEx pre-cleaning. Microtubes were then incubated during 18 h at 4 °C with constant shaking, and after centrifugation bound proteins were washed thrice with 1 mL of sterile PBS. Pellets were lyophilized and resuspended in SDS loading buffer (100 mM Tris-HCl, pH 6.8, 4% sodium dodecyl sulfate (w/v), 0.2% (w/v) bromophenol blue, 20% glycerol, 0.1 M dithiothreitol). SDS-PAGE gels (10%) were then shortly run, whole pieces upstream the running front line were cut without staining, and kept at −80 °C until protein digestion for mass spectrometry studies.

2.4. Mass spectrometry analyses

Protein digestion and mass spectrometry analyses were performed at the CEQUIBIEM Proteomics Core Facility (CONICET- National Research Council, Buenos Aires - Argentina) according to previously published protocols [20]. Briefly, protein samples were reduced and carbamidomethylated with 10 mM dithiothreitol or 20 mM iodoacetamide, respectively. Then, the protein solution was precipitated with trichloracetic acid at −20 °C, and after centrifugation pellets were washed twice with ice-cold acetone and finally dried at RT. Proteins were resuspended in 50 mM ammonium bicarbonate pH 8 and digested with trypsin. Resulting peptides were desalted with ZipTip C18 columns and then were analyzed by nanoLC-MS/MS in a Thermo Scientific Q Exactive Mass Spectrometer coupled to a nanoHPLC EASY-nLC 1000 (Thermo Scientific). MS equipment has a high collision dissociation cell (HCD) for fragmentation and an Orbitrap analyzer (Thermo Scientific, Q-Exactive). A voltage of 3.5 kV was used for Electro Spray Ionization (Thermo Scientific, EASY-SPRAY). XCalibur 3.0.63 software (Thermo Scientific) was used for data acquisition and equipment configuration that allows peptide identification at the same time of their chromatographic separation. Full-scan mass spectra were acquired in the Orbitrap analyzer. The scanned mass range was 400–1800 *m/z*, at a resolution of 70,000 at 400 m/z and the 12 most intense ions in each cycle were sequentially isolated, fragmented by HCD, and measured in the Orbitrap analyzer. Peptides with a charge of +1 or with unassigned charge state were excluded from fragmentation for MS2.

2.5. Analysis of MS data

Q Exactive raw data was processed using Proteome Discoverer software version 2.1.1.21 (Thermo Scientific) and searched against a database composed of *E. granulosus* s.l. and *Bos taurus* proteins -in addition to streptavidin from *Streptomyces avidinii* and CD5 and CD6 from *Homo sapiens*- sequences digested with trypsin with a maximum of one missed cleavage per peptide. Proteome Discoverer™ searches were performed with a precursor mass tolerance of 10 ppm and product

ion tolerance of 0.05 Da. Static modifications were set to carbamidomethylation of Cys, and dynamic modifications were set to oxidation of Met and N-terminal acetylation. Protein hits were filtered for high confidence peptide matches with a maximum protein and peptide false discovery rate of 1% calculated using a reverse database strategy. The exponentially modified protein abundance index (emPAI) was calculated automatically by Proteome Discoverer™.

2.6. Subcellular localization predictions

For each identified protein within PSEx and rshCD5/rshCD6 pull downs, subcellular localizations were predicted using DeepLoc software [21]. Proteins predicted to be either located in Golgi apparatus, Lysosome/Vacuole and/or Peroxisome were grouped into "Other" category.

2.7. ELISA binding assay

PSEx-binding ability of synthetic peptides (CD5.P1, CD5.P2, CD5.P3, CD6.P1, CD6.P2 or CD6.P3) was assessed following own published protocols [14] with minor modifications. Briefly, 96-well microtiter plates (Nunc, Roskilde, Denmark) were coated overnight at 4 °C with 100 μL/well of PSEx in PBS (20 μg/mL), and further blocked for 2 h at room temperature with 200 μL/well of PBS containing 1% (w/v) BSA. Increasing concentrations (0–40 mM) of biotinylated peptides (100 μL/well, triplicates) were then added to the wells and incubated overnight at 4 °C. Bound peptides were detected through incubation with HRP-labelled streptavidin (100 μL/well; 1:5000 dilution - Sigma) for 1 h at room temperature. Between incubation steps, unbound peptides were washed out thrice with PBS containing 0.05% (v/v) Tween-20. Enzymatic activity was developed during 20 min at room temperature by adding 100 μL/well of 3,3′,5,5′-tetramethylbenzidine reagent (Sigma) containing H_2O_2 substrate. After stopping the reaction with H_2SO_4 1.0 M (50 μL/well), absorbance values were read at 450 nm.

3. Results

3.1. Proteomic characterization of rshCD5 and rshCD6 interactomes

In an attempt to identify the parasite ligands interacting with the CD5 and CD6 lymphocyte receptors, we performed proteomic studies using PSEx as a model of soluble PSC tegumental antigens [22,23]. The analysis of the whole proteome of PSEx through nanoLC-MS/MS using an Orbitrap analyzer allowed us to successfully identify a total of 1252 proteins (Suppl. 1). The emPAI values for each protein were determined, thus enabling calculation of their relative abundance (RA) values (meaning percentage of each protein emPAI value relative to the overall sum of every proteins' emPAI values within PSEx) [24]. Moreover, given the bovine origin of PSC used for obtaining PSEx, a characterization in terms of *E. granulosus* s.l. vs. *B. taurus* proteins was also performed, thus showing that the PSEx proteome was composed of 1218 *E. granulosus* s.l. proteins (97.3%) and 34 *B. taurus* proteins (2.7%). Interestingly, the RA value of the most represented *B. taurus* protein was 0.19% (actin, alpha cardiac muscle 1 OS; ID: Q3ZC07), ranking as the 97th most abundant protein within PSEx proteome (Suppl. 1).

The potential parasite interactors for rshCD5 and rshCD6 were identified by means of pull down assays. This strategy has the limitation of identifying not only direct parasite interactors, but also proteins bonded to them. The analysis of pull down pellets by nanoLC-MS/MS provided the whole rshCD5 (Suppl. 2) and rshCD6 (Suppl. 3) interactomes. Both interactomes exhibited a lower number of proteins than PSEx (645 and 859 for rshCD5 and rshCD6, respectively), even though some proteins were solely found in interactomes (Suppl. 2 & 3). This fact might be either attributed to proteins having a RA value below the detection limit of the technique within PSEx but being enriched within interactomes, or to a dilution phenomenon within PSEx due to its high amount of proteins affecting the number of peptides used to assign, or not, a significant identification score. Interestingly, a higher proportion of host-derived proteins was found in both interactomes regarding whole PSEx proteome (11.8% and 13.0% for rshCD5 and rshCD6 interactomes, respectively). In this regard, tubulin alpha-1D chain (ID: Q2HJ86) and serum albumin (ID: A0A140T897) were the *B. taurus* proteins with the highest RA values in the rshCD5 (RA: 0.72%, ranking: 24th) and rshCD6 (RA: 0.54%, ranking: 38th) interactomes, respectively. In addition, streptavidin (ID: P22629) derived from the agarose resin used in pull down assays was highly represented in both interactomes as expected: in rshCD5 interactome its RA value was 1.94% (ranking: 4th), while in rshCD6 interactome its RA value was 1.23% (ranking: 10th). Also, hCD5 (ID: P06127 - RA value: 0.47%, ranking: 45th) and hCD6 (ID: P30203 - RA value: 0.58%, ranking: 33th) receptors were identified in their corresponding interactomes as expected (Suppl. 2 & 3). Further analyses were performed using only *E. granulosus* s.l. proteins, since *B. taurus*, streptavidin and hCD5/hCD6 proteins were considered contaminants lacking biological relevance in terms of interactors.

Parasite proteins with RA values ≥1% either within PSEx or both interactomes are shown in Table 1, while total parasite overlapping proteins are depicted in Fig. 1A. Predicted sub-cellular localization for *E. granulosus* s.l. proteins within PSEx showed mostly cytoplasmic proteins with a relevant contribution of mitochondrial, nuclear and cell membrane located proteins. A slightly higher proportion of cytoplasmic proteins was found within both interactomes compared with PSEx (Fig. 1B).

3.2. Identification of rshCD5 and rshCD6 specific interactors

The identification of specific interactors can be hindered by the fact that highly represented proteins within PSEx might also be highly represented in the interactomes simply due to a mass-action effect. Indeed, results in Table 1 show that 6 of the 15 top represented proteins within PSEx also corresponded to highly abundant proteins in rshCD5 and rshCD6 interactomes. Moreover, parasite proteins enriched within interactomes respect to PSEx might not necessarily correspond to top represented proteins within them. To overcome this issue we performed 95% prediction band analyses between PSEx and interactomes by selecting parasite proteins, and their respective RA values, present both within PSEx proteome and within each receptor interactome. Then, an XY graph was obtained and a linear regression plus a 95% prediction band were calculated. Such predictions represent a 95% probability a protein is similarly represented within PSEx and the corresponding interactome. Thus, selecting proteins outside the prediction bands allowed us to identify proteins effectively overrepresented within each interactome in comparison to PSEx, which are most likely direct rshCD5 and/or rshCD6 interactors. Results in Fig. 2 show the 95% prediction band analyses for both interactomes, exhibiting a total of 20 different parasite proteins outside bands (Table 2).

It is worth mentioning that 95% prediction band analyses were useful only for proteins identified within PSEx as well as within interactomes, since RA values from both samples were needed for the XY graph. Therefore, in order to analyze whether proteins solely found within interactomes were significantly overrepresented, or if their representation is just found among the 95% prediction band, we obtained the maximum RA values inside each prediction band for the rshCD5 and rshCD6 interactomes when RA value in PSEx corresponds to 0% (Fig. 2, dotted line). Then, proteins solely found within interactomes were compared with such threshold values, and those proteins with higher RA values were identified as overrepresented proteins. Accordingly, no *E. granulosus* s.l. proteins solely present within interactomes were assigned as overrepresented, although streptavidin (ID: P22629), hCD5 (ID: P06127) and hCD6 (ID: P30203) were identified as overrepresented proteins as expected, thus validating our approach.

Among the 20 overrepresented parasite proteins within rshCD5 and rshCD6 interactomes, 8 of them were identified as overrepresented in

Table 1
Top represented parasite proteins within PSEx proteome and rshCD5 and rshCD6 interactomes. *E. granulosus* s.l. proteins successfully identified showing RA values ≥1%. Proteins shared among proteomes are shown in bold letters.

Sample	ID	Protein name	Length	# Peptides	% Coverage	emPAI	%emPAI
PSEx	W6V2P2	Hydatid disease diagnostic antigen P-29	238	24	69	111.88	4.09
	W6UHV2	**Phosphoenolpyruvate carboxykinase**	628	52	79	80.11	2.93
	W6USI4	Eukaryotic translation initiation factor 5A	156	9	63	55.23	2.02
	W6V1T8	**Glyceraldehyde-3-phosphate dehydrogenase**	336	20	84	45.42	1.66
	W6UM50	**Heat shock protein HSP 90-alpha**	738	48	60	39.24	1.44
	U6JIC8	Heat shock 70 kDa protein 4	651	40	86	38.81	1.42
	U6IXV3	**Fructose-bisphosphate aldolase**	363	26	88	38.81	1.42
	U6JIM9	Annexin	331	20	71	37.99	1.39
	W6UDZ9	Paramyosin	892	70	66	37.66	1.38
	U6JIW0	Profilin	126	6	76	36.28	1.33
	U6IX85	**Gelsolin (Severin)**	364	24	72	32.25	1.18
	Q56J98	14-3-3 protein	247	18	61	30.62	1.12
	W6UHB1	**Dynein light chain 1, cytoplasmic**	102	8	79	30.62	1.12
	U6J1C5	Dynein light chain	89	4	52	30.62	1.12
	W6UFA4	Actin, cytoplasmic 2	377	20	69	29.08	1.06
rshCD5 pull-down	**W6UHV2**	**Phosphoenolpyruvate carboxykinase**	628	38	73	24.65	3.04
	W6V1T8	**Glyceraldehyde-3-phosphate dehydrogenase**	336	16	69	18.31	2.26
	W6UEU0	Major vault protein	253	13	62	16.78	2.07
	W6U2I8	Estradiol 17 beta-dehydrogenase	315	22	77	15.16	1.87
	U6IX85	**Gelsolin (Severin)**	364	18	62	13.93	1.72
	W6UHB1	**Dynein light chain 1, cytoplasmic**	102	6	62	13.68	1.69
	U6IXV3	**Fructose-bisphosphate aldolase**	363	20	73	11.02	1.36
	W6UTJ3	1,5-anhydro-D-fructose reductase	343	15	56	10.10	1.25
	W6UFA4	Actin, cytoplasmic 2	377	15	52	10.05	1.24
	U6J063	Calpain A	822	35	50	9.47	1.17
	W6UM50	**Heat shock protein HSP 90-alpha**	738	28	41	9.00	1.11
	U6JGI4	14-3-3 protein beta:alpha	248	16	55	9.00	1.11
	W6UMH9	Actin	393	14	49	9.00	1.11
	W6V798	Glucose-6-phosphate isomerase	422	15	41	9.00	1.11
	Q56J98	14-3-3 protein	247	12	42	9.00	1.11
rshCD6 pull-down	**U6IX85**	**Gelsolin (Severin)**	364	27	74	73.06	5.71
	U6IXV3	**Fructose-bisphosphate aldolase**	363	26	79	29.20	2.28
	W6U2I8	Estradiol 17 beta-dehydrogenase	315	27	82	27.73	2.17
	W6UHV2	**Phosphoenolpyruvate carboxykinase**	628	40	71	23.34	1.82
	W6UHB1	**Dynein light chain 1, cytoplasmic**	102	7	75	20.54	1.61
	W6UEU0	Major vault protein	253	14	67	16.78	1.31
	W6V1T8	**Glyceraldehyde-3-phosphate dehydrogenase**	336	18	80	16.30	1.27
	W6UM50	**Heat shock protein HSP 90-alpha**	738	38	48	16.08	1.26
	U6JGI4	14-3-3 protein beta:alpha	248	18	58	15.88	1.24
	W6V798	Glucose-6-phosphate isomerase	422	20	50	15.16	1.18

ID: Identification code. *Length*: number of amino acids composing each protein. *# Peptides*: number of matched MS/MS peptides. *% Coverage*: percentage of the identified protein covered by the peptides used to identify the protein. *emPAI*: exponentially modified protein abundance index. *%emPAI*: percentage of each protein emPAI value relative to the overall sum of every proteins' emPAI values within the proteome.

both cases, while 9 and 3 *E. granulosus* s.l. proteins were exclusively overrepresented in rshCD5 and rshCD6 interactomes, respectively (Table 2). However, since overrepresentation was assigned according to RA values within PSEx there is a lack of information regarding their abundance between interactomes. To overcome this issue we compared the RA values of the 8 shared overrepresented proteins through their normalization against an internal abundant protein present in both interactomes, following an already reported strategy [20]. We normalized the RA value of each shared protein against *E. granulosus* s.l. phosphoenolpyruvate carboxykinase (PEPCK; ID: W6UHV2) since it showed high and consistent RA values in both interactomes (Table 1). PEPCK Normalized Relative Abundance (PEPCK-NRA) was obtained for the 8 shared proteins according to each interactome, and then a ratio between PEPCK-NRA values in rshCD6 vs. rshCD5 interactomes was calculated. Proteins with a ratio ≥2 or ≤0.5 were considered either preferential rshCD6 or rshCD5 interactors, respectively. Results in Fig. 3 show that among the 8 shared overrepresented proteins, gelsolin (ID: U6IX85) showed to be a preferential rshCD6 interactor. Similar preferences -although to a lesser extent- were observed for glucose-6-phosphate isomerase (ID: W6V798), estradiol 17 beta-dehydrogenase (ID: W6U2I8), 14-3-3 protein beta:alpha (ID: U6JGI4), and dynein light chain (ID: W6UHB1). No preferential rshCD5 interactor among the 8 shared overrepresented proteins was identified (Fig. 3).

3.3. Topological analysis of rshCD5 and rshCD6 interactors

PAMPs binding properties of some SRCR-SF members have been accurately mapped through peptide-binding strategies [17,25,26]. Thus, biotinylated 11-mer peptides mapping within each of the three extracellular SRCR domains of CD5 and CD6 [18] were used to assess their specific PSEx-binding ability and the molecular topology of interactors within the SRCR domains. To that end, the PSEx-binding activity of peptides was firstly analyzed by solid phase assays in which PSEx-coated plates were incubated with increasing amounts of biotinylated peptides and then developed with HRP-streptavidin. Results showed that two CD5-derived peptides (CD5.P2 and CD5.P3) retained a concentration-dependent PSEx-binding ability (Fig. 4A), as well as two CD6-derived peptides (CD6.P1 and CD6.P2) (Fig. 4B). However, little or no PSEx-binding was observed for neither CD5.P1 (Fig. 4A) nor CD6.P3 (Fig. 4B) peptides. Since differences observed in our binding assays might be affected by several parameters, (e.g., peptide-ligand interaction affinity, number of total ligands per peptide, abundance of peptide ligand(s) within PSEx, dissimilar solid phase coating properties of ligands, among others) we performed analogous interactome studies to those performed with biotinylated rshCD5 and rshCD6. Pull down pellets derived from each biotinylated peptide were analyzed by nanoLC-MS/MS resulting in CD5.P1 (Suppl. 4), CD5.P2 (Suppl. 5), CD5.P3

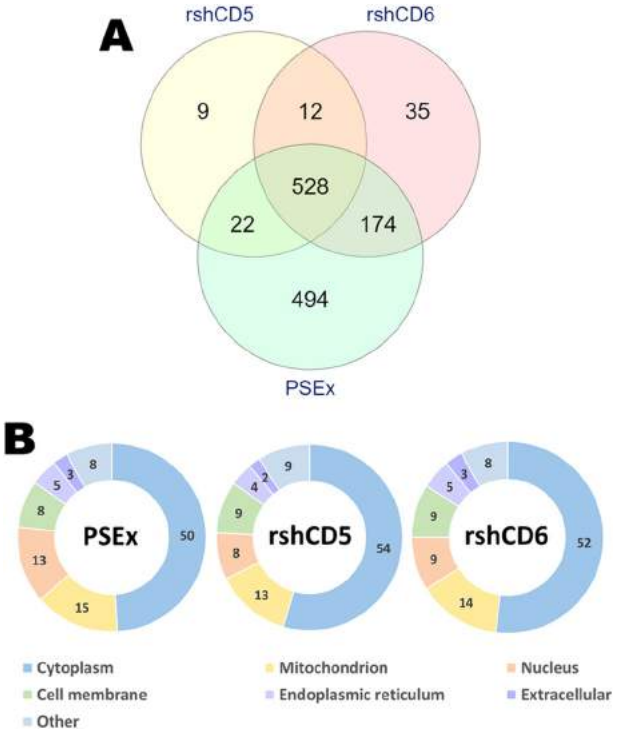

Fig. 1. PSEx proteome and rshCD5 and rshCD6 interactomes. Numbers of *E. granulosus* s.l. proteins successfully identified within PSEx proteome and rshCD5 as well as rshCD6 interactomes are depicted in Venn diagrams (A), while their subcellular localizations predicted using DeepLoc software are displayed in pie charts showing percentages of parasite proteins within each category (B). Proteins predicted to be either located in Golgi apparatus, Lysosome/Vacuole and/or Peroxisome were grouped into category termed "Other".

(Suppl. 6), CD6.P1 (Suppl. 7), CD6.P2 (Suppl. 8) and CD6.P3 (Suppl. 9) whole interactomes.

A highly diverse number of proteins were identified among the 6 peptide interactomes, ranging from 40 to 896 proteins (Suppl. 4–9). As expected, most identified proteins were from *E. granulosus* s.l. origin: CD5.P1 (96.6%), CD5.P2 (89.7%), CD5.P3 (95.2%), CD6.P1 (96.1%), CD6. P2 (86.9%), and CD6.P3 (96.2%). Among host contaminants, *B. taurus* proteins were also identified in every peptide interactome. The proteins with the highest RA were: actin alpha skeletal muscle (ID: P68138 - RA: 0.45% - ranking: 51st) for CD5.P1, keratin 10 (ID: A6QNZ7 - RA: 2.54% - ranking: 9th) for CD5.P2, keratin type II cytoskeletal 5 (ID: Q5XQN5 - RA: 0.33% - ranking: 66th) for CD5.P3, keratin 10 (ID: A6QNZ7 - RA: 0.19% - ranking: 109th) for CD6.P1, keratin type I cytoskeletal 14 (ID: F1MC11 - RA: 1.28% - ranking: 14th) for CD6.P2, and tubulin alpha-4A chain OS (ID: P81948 - RA: 0.33% - ranking: 57th) for CD6.P3. Streptavidin (ID: P22629) derived from the agarose resin used in pull down assays was significantly represented among peptide interactomes as expected: CD5.P1 (RA: 2.27% - ranking: 3rd), CD5.P2 (RA: 31.22% - ranking: 1st), CD5.P3 (RA: 2.29% - ranking: 4th), CD6.P1 (RA: 0.44% - ranking: 47th), CD6.P2 (RA: 6.30% - ranking: 1st), and CD6.P3 (RA: 0.52% - ranking: 40th).

As with rshCD5 and rshCD6 interactomes, peptide interactomes were further analyzed using only *E. granulosus* s.l. proteins, since *B. taurus* proteins and streptavidin were considered contaminants lacking biological relevance in terms of interactors. Among successfully identified *E. granulosus* s.l. proteins, many of them were shared between peptides and their parental receptor interactomes (Fig. 5). Therefore, similar analyses to those applied for identifying overrepresented proteins in rshCD5 and rshCD6 interactomes were performed, which allowed us to identify a total of 45 different parasite proteins overrepresented in at least one peptide interactome (Table 3). Among CD5-derived peptides, CD5.P2 showed the lowest number of parasite interactors (1), while CD5.P1 and CD5.P3 exhibited similar amounts of interactors (10 and 11, respectively). Meanwhile, CD6-derived peptides displayed overall more parasite interactors, since CD6.P1, CD6.P2 and CD6.P3 interactomes showed 29, 11 and 20 interactors, respectively (Table 3). Interestingly, one third of parasite proteins overrepresented in peptide interactomes (15 out of 45) were also found to be enriched in either rshCD5 and/or rshCD6 interactomes (Tables 2 and 3). Results in Table 3 show that among the 17 interactors recognized for rshCD5, 8 of them were also identified in the interactomes of CD5-derived peptides. Furthermore, 10 out of the 11 interactors recognized for rshCD6 were successfully identified in the interactomes of CD6-derived peptides (Table 3).

Finally, in order to suggest a topological estimate of SRCR domains involved in each ligand binding, rshCD5 and rshCD6 interactors were combined with peptide interactors (Table 4). In this way, CD5.P3 was shown to be potentially involved in binding most mapped rshCD5 interactors (6 out of 8 total ligands) in comparison to CD5.P1 (3 interactors) and CD5.P2 (1 interactor). Additionally, 2 out of the 8 total rshCD5 interactors identified in peptide interactomes were mapped in more than one different SRCR domain: gelsolin (ID:

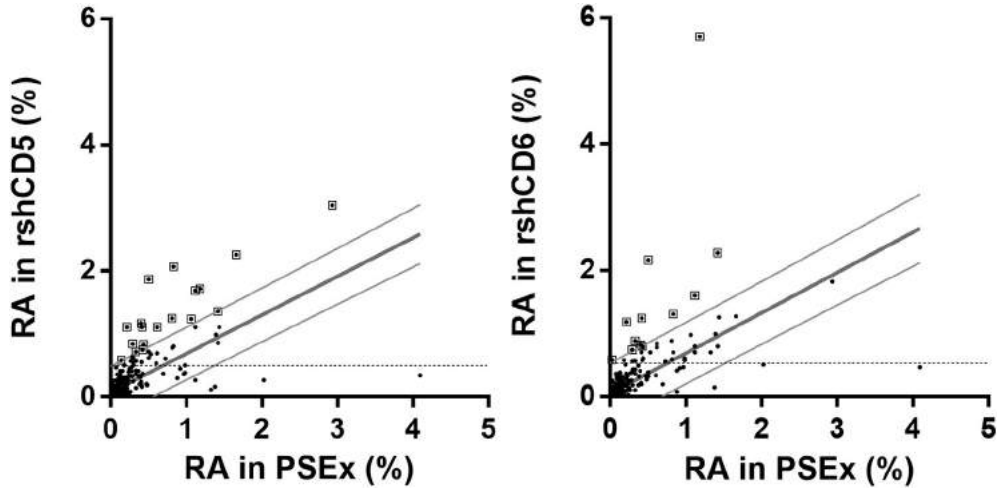

Fig. 2. Specific parasite interactors within rshCD5 and rshCD6 interactomes. XY graphs were obtained by selecting parasite proteins -and their respective RA values- present both within PSEx proteome and within each receptor interactome. Linear regressions plus 95% prediction bands were calculated. Proteins outside the prediction bands were identified as effectively overrepresented interactors within each interactome in comparison to PSEx proteome. Dotted lines indicate the maximum RA threshold within each band corresponding to a RA value of 0% within PSEx proteome.

Table 2
Specific parasite interactors within rshCD5 and/or rshCD6 interactomes. *E. granulosus* s.l. proteins overrepresented within rshCD5 and/or rshCD6 interactomes were identified through 95% prediction band analyses.

Overrepresented in	#	ID	Protein name	Length	# Peptides	% Coverage
rshCD5 only	1	U6JDG7	Tegumental protein	180	8	56
	2	O16058	Glutathione S-transferase	219	11	53
	3	W6V1T8	Glyceraldehyde-3-phosphate dehydrogenase	336	15	59
	4	W6UTJ3	1,5-anhydro-D-fructose reductase	343	15	56
	5	W6UFA4	Actin, cytoplasmic 2	377	15	52
	6	W6UMH9	Actin	393	14	49
	7	W6UBQ8	Lysosomal aspartic protease	425	9	20
	8	W6UB03	Alpha-1,4 glucan phosphorylase	611	22	45
	9	W6UHV2	Phosphoenolpyruvate carboxykinase	628	38	73
rshCD5 & rshCD6	10	W6UHB1	Dynein light chain	102	6/7	62/75
	11	U6JGI4	14-3-3 protein beta:alpha	248	15/18	52/58
	12	W6UEU0	Major vault protein	253	13/13	62/62
	13	W6U2I8	Estradiol 17 beta-dehydrogenase	315	21/26	77/82
	14	W6UNT9	Transaldolase	326	14/16	39/42
	15	U6IX85	Gelsolin (Severin)	364	19/27	63/74
	16	W6V798	Glucose-6-phosphate isomerase	422	16/20	41/50
	17	U6J063	Calpain-A	822	35/35	50/55
rshCD6 only	18	U6JEE0	14-3-3 protein epsilon	255	14	54
	19	W6UT22	glucose-1-phosphate uridylyltransferase	533	29	60
	20	U6IXV3	Fructose-bisphosphate aldolase	363	26	79

ID: Identification code. *Length*: number of amino acids composing each protein. *# Peptides*: number of matched MS/MS peptides. *% Coverage*: percentage of the identified protein covered by the peptides used to identify the protein.

U6IX85) in CD5.P1 and CD5.P3, and major vault protein (ID: W6UEU0) in CD5.P2 and CD5.P3 (Table 4). On the contrary, not a clear preference was observed for mapped rshCD6 interactors, since CD6.P1, CD6.P2 and CD6.P3 mapped 5, 6, and 7 interactors, respectively. Moreover, 6 out of the 10 total rshCD6 interactors identified in peptide interactomes were mapped in more than one different SRCR domain, and 2 interactors mapped on the three CD6 SRCR domains: gelsolin (ID: U6IX85) as well as estradiol 17 beta-dehydrogenase (ID: W6U2I8) (Table 4). Finally, among the 8 shared interactors between rshCD5 and rshCD6 all but one (dynein light chain - ID: W6UHB1) were also identified as potential interactors for at least 1 peptide derived from both receptors (Table 4).

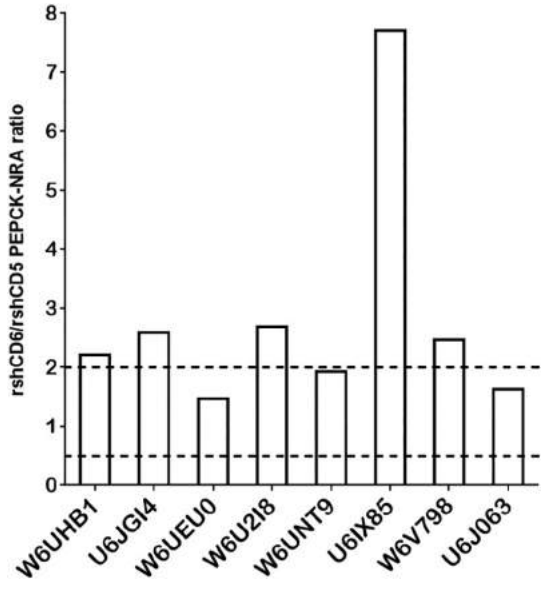

Fig. 3. Binding preference for shared rshCD5 and rshCD6 parasite interactors. RA values for the shared parasite interactors within rshCD5 and rshCD6 interactomes were compared through their normalization against *E. granulosus* s.l. phosphoenolpyruvate carboxykinase (PEPCK; ID: W6UHV2). PEPCK Normalized Relative Abundance (PEPCK-NRA) was obtained for the 8 shared proteins according to each interactome, and then a ratio between PEPCK-NRA values in rshCD6 vs. rshCD5 interactomes was calculated. Proteins with a ratio ≥2 or ≤0.5 were considered either preferential interactors of rshCD6 or rshCD5, respectively.

4. Discussion

Mammalian SRs are categorized into 10 different classes (SR-A to SR-L; excluding SR-C only present in *Drosophila melanogaster*), being class E (SR-E) the most important group in recognition of helminth-derived antigens, including Dectin-2 [27], Mannose Receptor/CD206 [28], CLEC4F/CLECSF13 [29], and DC-SIGN/CD209a [30]. However, the only molecular interaction reported between SRs and helminth-derived components is that of SR-AI (a class A member containing a single C-terminal SRCR domain [4]), calreticulin from *Heligmosomoides polygyrus* [31]. Regarding SR-I class members, no helminth interactions have been reported aside from those of CD5 and CD6 [14]. Notwithstanding, CD163 and WC1 expression by macrophages or certain lymphocyte subsets, respectively, has been reported of relevance in protozoan infections by *Theileria parva* [32], *Leishmania braziliensis* [33], *Trypanosoma vivax* [34] and *Neospora caninum* [35].

The human SR-I lymphocyte receptors CD5 and CD6 are known to exhibit PRR abilities to sense PAMPs from diverse pathogen groups, as well as prophylactic and/or therapeutic actions when infused in soluble form in different murine models of bacterial [8,9,11] fungal [6,12], and parasitic [14] infections. Regarding the latter, rshCD5 or rshCD6 were shown to interact with tegumental antigens from the cestode *E. granulosus* s.l. parasite and to differentially modulate the cytokine response of peritoneal cells exposed to them, as well as to ameliorate the infection outcome in a murine model of secondary cystic echinococcosis (CE) by reducing the proportion of infected mice, the number of developed hydatid cysts per mouse and their parasite loads. In the same study, few potential parasite ligands for both receptors were also suggested [14]. Therefore, the present work represents a step forward in the search for rshCD5 and rshCD6 ligands within *E. granulosus* s.l. tegument, and a molecular topology of the potential interactors within receptors' SRCR domains.

Human secondary CE is an important medical problem associated with the surgical removal of primary cysts, with high post-surgery reported rates [36]. In this regard, the intraperitoneal inoculation of viable PSC into mice constitutes the murine model of secondary CE, which has been widely used for several purposes, like studying basics of *E. granulosus* s.l. immunobiology or testing chemotherapeutics, vaccine candidates and diagnostic or follow-up tools [37]. Mouse secondary CE can be divided into two stages: an early pre-encystment stage (until day 20–30 post-inoculation) with PSC developing into hydatid cysts, and a late or post-encystment stage in which differentiated cysts grow

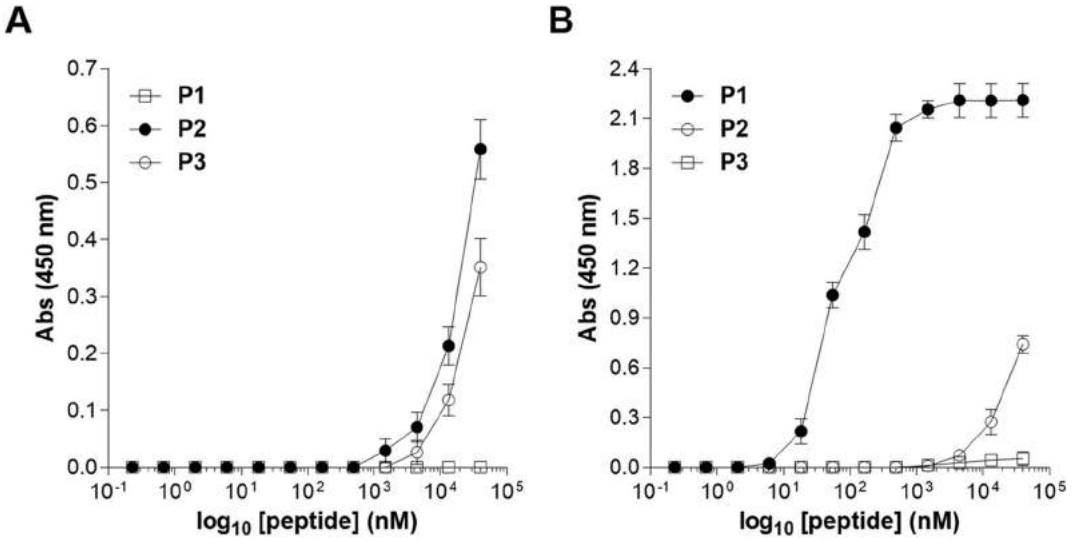

Fig. 4. PSEx-binding ability of CD5- and CD6-derived peptides. Biotinylated 11-mer peptides mapping the 3 extracellular SRCR domains of CD5 (A) and CD6 (B) were assessed for their PSEx-binding ability using an ELISA strategy. PSEx-coated plates were incubated with increasing amounts (0–40 mM) of biotinylated peptides and their binding was assessed using a HRP-streptavidin probe.

and eventually become fertile cysts [38]. Such a sequential developmental process is associated with a strong local control of inflammation during the initial phase of PSC differentiation into hydatid cysts, and after parasite encystment immune effectors are mostly inefficient [39]. Thus, the immune response during the pre-encystment stage is of outstanding importance for an efficient parasite clearence; and rshCD5 as well as rshCD6 infusion has been shown to be prophylactically active at that time point [14]. Therefore, identification of rshCD5 and rshCD6 *E. granulosus* s.l. ligands is highly relevant, to better understand the pathophysiology of the pre-encystment phase and to identify effective targets against the parasite.

PSC from *E. granulosus* s.l. possess an outer acellular tegumental layer involved in parasite nutrition, morphological maintenance and defense. Components of such tegumental layer might initially interact with the host immune system during secondary CE influencing the infection outcome. In this regard, our group previously reported that Balb/c and C57Bl/6 mice not only show differences in susceptibility to secondary CE [15], but also induce early antibody responses targeting different PSC tegumental antigens [23] suggesting their relevance during the pre-encystment immune response. Additionally, an antigenic fraction enriched in tegumental PSC components -termed PSEx- was shown to induce host protection when used as an immunizing agent [16], and several components within PSEx were recently suggested as potential vaccine candidates [22,23]. Therefore, in order to search for potential rshCD5 and rshCD6 tegumental interactors, we firstly performed a PSEx proteome characterization, successfully identifying 1218 *E. granulosus* s.l. proteins (Suppl. 1). This proteomic analysis allowed us to obtain not only a more complete PSEx proteome than the one previously reported [20], but also novel information regarding the relative abundance of each protein within it (Table 1 and Suppl. 1). Thanks to pull down assays the rshCD5 or rshCD6 interactomes were identified, resulting in 571 and 749 parasite proteins, respectively (Fig. 1A).

Results show that rshCD5 interactome and PSEx proteome shared 550 *E. granulosus* s.l. proteins, while rshCD6 interactome shared 702 proteins (Fig. 1A). Therefore, the identification of specific interactors needed a deeper analysis to overcome potential mass-action effects due to the pull down strategy performed. Most likely interactors were supposed to show higher RA values within interactomes than in the original PSEx proteome, and through 95% prediction band analyses a total of 20 parasite proteins were found overrepresented within interactomes: 17 and 11 proteins in rshCD5 and rshCD6 interactomes, respectively (Fig. 2 and Table 2). Interestingly, none of the previously suggested potential interactors for rshCD5 (thioredoxin peroxidase

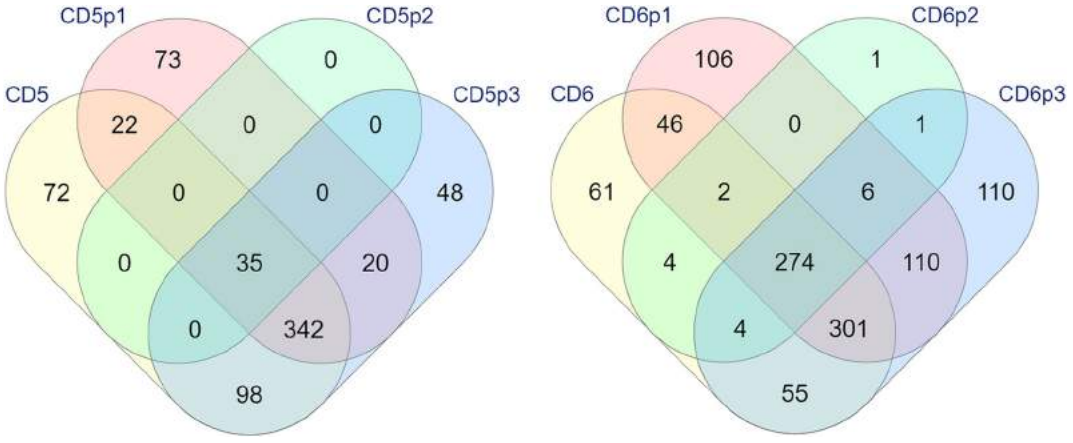

Fig. 5. Interactomes for rshCD5 and rshCD6 and their 11-mer derived peptides. Numbers of *E. granulosus* s.l. proteins successfully identified within interactomes either from rshCD5 and rshCD6 and their respective 11-mer derived peptides mapping the 3 extracellular SRCR domains are depicted in Venn diagrams.

Table 3
Specific parasite interactors within CD5- and/or CD6-derived peptide interactomes. *E. granulosus* s.l. proteins overrepresented within CD5- and/or CD6-derived peptide interactomes were identified through 95% prediction band analyses.

#	ID	Protein name	Overrepresented in					
			CD5-derived			CD6-derived		
			P1	P2	P3	P1	P2	P3
1	U6IX85	Gelsolin (Severin)	+	−	+	+	+	+
2	U6IUN6	Thioredoxin peroxidase	+	−	−	+	+	+
3	Q56J98	14-3-3 protein	+	−	+	+	−	+
4	W6U2I8	Estradiol 17 beta-dehydrogenase	−	−	+	+	+	+
5	W6UEU0	Major vault protein	−	+	+	−	+	−
6	W6UNT9	Transaldolase	−	−	+	+	+	−
7	W6UTJ3	1,5-anhydro-D-fructose reductase	−	−	−	+	+	+
8	W6UT22	glucose-1-phosphate uridylyltransferase	+	−	+	−	−	+
9	U6J063	Calpain-A	+	−	−	−	+	+
10	W6UHB1	Dynein light chain	−	−	−	−	+	+
11	W6UM65	Thioredoxin domain-containing protein	+	−	−	−	−	+
12	W6UT00	Translationally-controlled tumor protein	−	−	−	+	−	+
13	U6JDG7	Tegumental protein	−	−	−	+	−	+
14	W6UHX6	Adenylate kinase	−	−	−	+	+	−
15	O16058	Glutathione S-transferase	−	−	−	+	−	+
16	U6JGI4	14-3-3 protein beta:alpha	+	−	−	+	−	+
17	U6JEE0	14-3-3 protein epsilon	+	−	−	+	−	−
18	W6UW09	Heterogeneous nuclear ribonucleoprotein A2	−	−	−	+	−	+
19	W6UN54	UDP-glucose 4-epimerase	−	−	+	+	−	−
20	U6JI56	Sarcoplasmic calcium-binding protein	−	−	−	+	−	+
21	W6V798	Glucose-6-phosphate isomerase	−	−	+	−	−	+
22	W6UDZ9	Paramyosin	+	−	−	−	−	+
23	W6U3G1	Dynein light chain	−	−	+	−	−	−
24	W6UGV8	Fatty acid-binding protein	+	−	−	−	−	−
25	U6JIW0	Profilin	−	−	+	−	−	−
26	U6JRP2	Peptidyl-prolyl cis-trans isomerase	−	−	−	−	+	−
27	U6JB79	Sulfhydryl oxidase	−	−	−	+	−	−
28	U6JCG1	Glutathione S-transferase	−	−	−	+	−	−
29	W6UCY9	Lactamase_B domain-containing protein	−	−	−	+	−	−
30	U6JN02	Triosephosphate isomerase	−	−	−	+	−	−
31	U6JH31	Proteasome subunit alpha type	−	−	−	+	−	−
32	U6JM50	Proteasome subunit alpha type	−	−	−	+	−	−
33	W6U1C9	Thioredoxin-dependent peroxide reductase	−	−	−	−	+	−
34	W6ULQ6	Annexin	−	−	−	+	−	−
35	U6JIM9	Annexin	−	−	−	+	−	−
36	W6V1T8	Glyceraldehyde-3-phosphate dehydrogenase	−	−	−	−	−	+
37	U6IUI1	cAMP dependent protein kinase regulatory	−	−	−	+	−	−
38	W6V6R7	Serine protease inhibitor	−	−	−	+	−	−
39	W6UFA4	Actin, cytoplasmic 2	−	−	−	+	−	−
40	W6USW1	Annexin	−	−	−	−	−	+
41	U6JGN1	Elongation factor 1-gamma	−	−	−	+	−	−
42	U6J0K5	Citrate synthase	−	−	−	+	−	−
43	W6UMA5	Asparaginyl-tRNA synthetase, cytoplasmic	−	−	−	+	−	−
44	W6UHV2	Phosphoenolpyruvate carboxykinase	−	−	+	−	−	−
45	W6UEU2	Spectrin alpha chain	−	−	−	−	−	+

ID: Identification code.

- ID: U6IUN6) or rshCD6 (peptidyl-prolyl cis-trans isomerase - ID: U6JRP2, and endophilin B1 - ID: W6V2P2) [14] were found among them. Although differences in methodological and technical approaches used might explain such inconsistencies, previously suggested interactors were indeed found within the corresponding interactomes: thioredoxin peroxidase showed a RA value of 0.69% (ranking 28th) in rshCD5 interactome (Suppl. 2), while peptidyl-prolyl cis-trans isomerase and endophilin B1 exhibited RA values of 0.45% (ranking 45th) and 0.46% (ranking 44th), respectively, within rshCD6 interactome (Suppl. 3).

Table 4
Molecular topology of rshCD5 and srhCD6 parasite interactors within their peptide-derived interactomes. *E. granulosus* s.l. proteins overrepresented within CD5- and/or CD6-derived peptide interactomes were related with the overall parasite interactors identified within rshCD5 and/or rshCD6 interactomes. Proteins shared among interactomes are shown in bold letters.

Interactome	ID	Name	Peptide		
			P1	P2	P3
rshCD5	U6IX85	**Gelsolin**	+	−	+
	W6UEU0	**Major vault protein**	−	+	+
	U6JGI4	**14-3-3 protein beta:alpha**	+	−	−
	U6J063	**Calpain-A**	+	−	−
	W6U2I8	**Estradiol 17 beta-dehydrogenase**	−	−	+
	W6UNT9	**Transaldolase**	−	−	+
	W6V798	**Glucose-6-phosphate isomerase**	−	−	+
	W6UHV2	Phosphoenolpyruvate carboxykinase	−	−	+
	W6UHB1	**Dynein light chain**	−	−	−
	U6JDG7	Tegumental protein	−	−	−
	O16058	Glutathione S-transferase	−	−	−
	W6V1T8	Glyceraldehyde-3-phosphate dehydrogensae	−	−	−
	W6UTJ3	1,5-anhydro-D-fructose reductase	−	−	−
	W6UFA4	Actin, cytoplasmic 2	−	−	−
	W6UMH9	Actin	−	−	−
	W6UBQ8	Lysosomal aspartic protease	−	−	−
	W6UB03	Alpha-1,4 glucan phosphorylase	−	−	−
rshCD6	W6U2I8	**Estradiol 17 beta-dehydrogenase**	+	+	+
	U6IX85	**Gelsolin**	+	+	+
	W6UHB1	**Dynein light chain**	−	+	+
	U6J063	**Calpain-A**	−	+	+
	W6UNT9	**Transaldolase**	+	+	−
	U6JGI4	**14-3-3 protein beta:alpha**	+	−	+
	U6JEE0	14-3-3 protein epsilon	+	−	−
	W6UEU0	**Major vault protein**	−	+	−
	W6UT22	UTP–glucose-1-phosphate uridylyltransferase	−	−	+
	W6V798	**Glucose-6-phosphate isomerase**	−	−	+
	U6IXV3	Fructose-bisphosphate aldolase	−	−	−

ID: Identification code.

In accordance to own previously reported suggestion on partial ligands overlapping between both receptors [14], here we found that 8 out of the 20 identified interactors were shared (Table 2). It is important to highlight on this regard that although rshCD5 and rshCD6 exhibited prophylactic effects in the murine model of secondary CE, the former showed a relatively higher degree of protection [14]. Since shared ligands might be responsible for a common basal level of induced protection, specific interactors may account for enhanced protection ability. Therefore, besides the specific interactors identified for each receptor (Table 2), we further characterized shared interactors regarding their potential preference against any receptor through normalization of their RA values against an internal abundant protein [20]. Although none of the 8 shared overrepresented proteins showed to be a special rshCD5 interactor, gelsolin (ID: U6IX85) -among other less evident ligands- exhibited a clear preference towards rshCD6 (Fig. 3).

More than half of the 20 different interactors identified for rshCD5 and/or rshCD6 have been previously reported as potential protective molecules against *E. granulosus* s.l. and/or other helminth parasites, either as vaccine candidates and/or pharmacological targets. In order to simplify their description, we categorized them into interactors previously suggested/tested as targets against *Echinococcus* spp. parasites, and interactors already tested against other helminth parasites except *Echinococcus* spp. Accordingly, 6 out of the 20 identified interactors belonged to the first category. Among them, the most characterized examples are the 14-3-3 proteins, which belong to an eukaryotic family of highly conserved proteins involved in several basic cellular events (e.g., cellular proliferation, differentiation, and survival). The 14-3-3 proteins have successfully been used as vaccine candidates in different pre-clinical settings against either *E. granulosus* s.l. or *E. multilocularis* [40]. Additional vaccine candidates already tested among rshCD5 and/or rshCD6 interactors include glyceraldehyde-3-phosphate

dehydrogenase, which successfully induced protection against *E. multilocularis* in immunized mice [41], and glutathione-S-transferase, which probed to be very effective in mouse immunization protocols against *E. granulosus* s.l. infection [42]. Besides vaccine candidates, other identified interactors showed relevant functions in *Echinococcus* spp. immunobiology. Tegumental proteins (TegPs) usually coat the surface of many worms, and are mainly involved in ion uptake and immune evasion mechanisms. Though *Echinococcus* spp. have many TegPs, they have been poorly studied reporting immunomodulatory and/or immunosuppressive roles in *E. granulosus* s.l. [43] as well as in *E. multilocularis* [44] infections. The last member of interactors within this category is phosphoenolpyruvate carboxykinase, a key enzyme in glucose metabolism shown to be a possible chemotherapeutic target against *E. granulosus* s.l. [45].

Regarding the second category, 5 out of the 20 identified interactors have already been suggested/tested as targets against other helminth parasites except *Echinococcus* spp. Among them, lysosomal aspartic protease from *Necator americanus* is a promising vaccine immunogen, which induces antibodies neutralizing hemoglobin proteolysis in the gut of the worm [46]. The remaining interactors within this category -actin, gelsolin and fructose-bisphosphate aldolase- are either directly or indirectly involved in cytoskeleton dynamics. Helminth parasites exhibit high cytoskeletal plasticity, likely as an acquired strategy to allow them to enter, settle and develop into their hosts. Therefore, cytoskeleton components have been proposed as interesting therapeutic targets. The interference of actin dynamics in *Schistosoma mansoni* by cytochalasins was shown to indirectly affect other functions than movement, like glucose uptake from the host [47] or tegumental shedding needed for optimal immune evasion [48]. Actin filaments assembly/disassembly is regulated by a variety of actin-binding proteins, among which gelsolin superfamily members are highly relevant. Also in *S. mansoni*, gelsolin was shown to be involved in tegumental disruption induced by praziquantel [49]. Though functional studies regarding gelsolin and related proteins in *E. granulosus* are lacking, potential relevant roles could be assigned based on the highly organized F-actin cytoskeleton recently described in the parasite [50]. Finally, the glycolytic enzyme fructose-bisphosphate aldolase has been described as a complex multifunctional protein that may perform non-glycolytic moonlighting functions. *E. granulosus* fructose-bisphosphate aldolase has been shown to bind F-actin filaments suggesting it has alternative multifunctional properties [51]. Therefore, blocking parasite fructose-bisphosphate aldolase might also influence actin dynamics, as above suggested for gelsolin and actin itself. Moreover, parasite fructose-bisphosphate aldolase has been tested as a promising vaccine candidate against *Onchocerca volvulus* [52], *S. mansoni* [53], and *Trichinella spiralis* [54]. Taken together, the reported data support the hypothesis that blockade of relevant tegumental antigens by rshCD5 or rshCD6 infusion might be beneficial during the pre-encystment stage of *E. granulosus* s.l. infection.

Binding properties for PAMPs in some members of the SRCR-SF have been accurately mapped through peptide-binding strategies within SRCR domains. The prototypical member of the SRCR-SF displaying PAMPs binding properties is deleted in malignant brain tumors-1 (DMBT-1), also known as salivary agglutinin (SAG) or gp340 [55]. DMBT-1/SAG/gp340 is a soluble glycoprotein containing 14 SRCR -among other- domains, whose bacterial-binding properties have been accurately mapped within them to an 11-mer consensus peptide sequence (termed pbs1, GRVEVLYRGSW) containing a 9-mer motif (VEVLxxxxW) identified in 13 out of its 14 SRCR domains [17]. Similar functional peptide mappings performed for other SRCR-SF members exhibiting bacterial-binding properties include MARCO [25] and CD163 [26]. Regarding CD5 and CD6, functional studies involving similar 11-mer peptides were performed only for CD6-derived peptides, which showed high binding affinities for PAMPs either from Gram-negative (LPS) or Gram-positive (LTA) bacteria [18]. Therefore, here we used such biotinylated-peptides (3 from CD5 and 3 from CD6 ectodomains) to evaluate their PSEx-binding ability. Additionally, since different SRCR domains within receptors' ectodomains might interact with specific *E. granulosus* s.l. molecules, a potential molecular topology of the interactions was also assessed. NanoLC-MS/MS analyses from pull down experiments provided the corresponding peptide interactomes (Suppl. 4 to 9, and Fig. 5), allowing the identification of 45 different parasite proteins overrepresented in at least one peptide interactome (Table 3). A topological estimate of SRCR domains involved in each ligand binding was suggested by combining rshCD5 and rshCD6 interactors with peptide interactors. CD5.P3 was shown to be involved in binding most mapped rshCD5 interactors, while not a clear preference was observed for mapped rshCD6 interactors (Table 4). It is important to highlight that although the three CD6-derived peptides showed high bacterial PAMPs binding affinities, only the peptide mapped at its SRCR domain 3 exhibited broad bacterial-agglutination properties and improved survival of mice undergoing polymicrobial sepsis in a dose- and time-dependent manner [18], suggesting that functional studies do not necessarily reflect ligand binding abilities. Therefore, CD5- and CD6-derived peptides -independently of their identified interactors- deserve further functional studies to assess their prophylactic and/or therapeutic potential in the context of *E. granulosus* s.l. infection.

5. Conclusion

The present work successfully identified several helminth-derived interactors for the ectodomains of the human lymphocyte scavenger receptors CD5 and CD6, and a potential molecular topology of parasite interactors within receptors' SRCR domains was also suggested. Most identified interactors were previously reported as potential protective molecules against *Echinococcus* spp. and/or other helminth parasites, either as vaccine candidates or pharmacological targets. This fact supports the view that multiple binding to relevant tegumental parasite components by either rshCD5 or rshCD6 is beneficial for the experimental host during the pre-encystment stage of mouse secondary CE. Additionally, since several identified interactors were previously reported as protective molecules against other helminthiases than CE (i.e. lysosomal aspartic protease, gelsolin and fructose-bisphosphate aldolase), our present results might support their further exploration as novel vaccine candidates and/or pharmacological targets against CE. Finally, further work will be required to ascertain the prophylactic/therapeutic potential of rshCD5 and rshCD6, and their sequence-derived peptides, in other helminthiases, as well as to explore whether additional SRCR-SF members might also exhibit similar activities.

Supplementary data to this article can be found online at https://doi.org/10.1016/j.ijbiomac.2020.08.219.

CRediT authorship contribution statement

Conceptualization: SM, FL, GM-E. Funding acquisition: FL, GM-E. Investigation: SM, MV-d-A, GM-E. Writing manuscript: SM, MV-d-A, FL, GM-E.

Data availability statement

The data that support the findings of this study are available from the corresponding author upon reasonable request.

Declaration of competing interest

The authors have declared that no competing interests exist.

Acknowledgements

The work by GM-E's group is supported by a grant from Uruguayan Agencia Nacional de Investigación e Innovación (ANII, FCE-1-2017-1-135537), and general financial funding from CSIC (Universidad de la

República, Uruguay) and PEDECIBA-Química (Uruguay). SM is recipient of a pre-doctoral fellowship from Comisión Académica de Posgrado (CAP, Universidad de la República, Uruguay). GM-E received a short-stage post-doctoral fellowship from Spanish Fundación Carolina. The work by FL's group is supported by grants from Spanish Ministerio de Economía y Competitividad (MINECO, Plan Nacional I+D+i, SAF2016-80535-R and PCIN-2015-070 under the project SRecognite Infect-ERA/0003/2015 - cofinanced by European Development Regional Fund "A way to achieve Europe" ERDF) and Agència de Gestiò d'Ajuts Universitaris i de Recerca (AGAUR; 2017/SGR/1582) from Generalitat de Catalunya. MV-d-A is recipient of a pre-doctoral fellowship from Spanish MINECO (BES-2014-069237). The funders had no role in study design, data collection and analysis, decision to publish, or preparation of the manuscript.

References

[1] C.M. Budke, P. Deplazes, P.R. Torgerson, Global socioeconomic impact of cystic echinococcosis, Emerg. Infect. Dis. 12 (2) (2006) 296–303.
[2] R.C. Thompson, The taxonomy, phylogeny and transmission of Echinococcus, Exp. Parasitol. 119 (4) (2008) 439–446.
[3] C.A. Janeway Jr., R. Medzhitov, Innate immune recognition, Annu. Rev. Immunol. 20 (2002) 197–216.
[4] I.A. Zani, S.L. Stephen, N.A. Mughal, et al., Scavenger receptor structure and function in health and disease, Cells 4 (2) (2015) 178–201.
[5] V.G. Martínez, S.K. Moestrup, U. Holmskov, et al., The conserved scavenger receptor cysteine-rich superfamily in therapy and diagnosis, Pharmacol. Rev. 63 (4) (2011) 967–1000.
[6] J. Vera, R. Fenutría, O. Cañadas, et al., The CD5 ectodomain interacts with conserved fungal cell wall components and protects from zymosan-induced septic shock-like syndrome, Proc. Natl. Acad. Sci. U. S. A. 106 (5) (2009) 1506–1511.
[7] M.A. Sarhan, T.N. Pham, A.Y. Chen, T.I. Michalak, Hepatitis C virus infection of human T lymphocytes is mediated by CD5, J. Virol. 86 (7) (2012) 3723–3735.
[8] M.R. Sarrias, M. Farnós, R. Mota, et al., CD6 binds to pathogen-associated molecular patterns and protects from LPS-induced septic shock, Proc. Natl. Acad. Sci. U. S. A. 104 (28) (2007) 11724–11729.
[9] M. Martínez-Florensa, M. Consuegra-Fernández, V.G. Martínez, et al., Targeting of key pathogenic factors from gram-positive bacteria by the soluble ectodomain of the scavenger-like lymphocyte receptor CD6, J. Infect. Dis. 209 (7) (2014) 1077–1086.
[10] E. Carrasco, C. Escoda, C. Alvarez-Fernández, et al., A role for scavenger-like lymphocyte receptor CD6 in HIV-1 viral infection, AIDS Res Hum Retrov 30 (S1) (2014) A49–A50 (abstract).
[11] Martínez-Florensa M, Consuegra-Fernández M, Aranda F, et al. Protective effects of human and mouse soluble scavenger-like CD6 lymphocyte receptor in a lethal model of polymicrobial sepsis. Antimicrob. Agents Chemother.. 2016; 61(1): e01391-16.
[12] M. Velasco-de-Andrés, C. Català, S. Casadó-Llombart, et al., The lymphocyte scavenger receptor CD5 plays a nonredundant role in fungal infection, Cell Mol Immunol (2020)https://doi.org/10.1038/s41423-020-0434-7.
[13] J.H. Cho, J. Sprent, TCR tuning of T cell subsets, Immunol. Rev. 283 (1) (2018) 129–137.
[14] G. Mourglia-Ettlin, S. Miles, M. Velasco-De-Andrés, et al., The ectodomains of the lymphocyte scavenger receptors CD5 and CD6 interact with tegumental antigens from *Echinococcus granulosus sensu lato* and protect mice against secondary cystic echinococcosis, PLoS Negl. Trop. Dis. 12 (11) (2018), e0006891.
[15] G. Mourglia-Ettlin, M. Cucher, P. Arbildi, et al., Natural and induced antibodies contribute to differential susceptibility to secondary cystic echinococcosis of Balb/c and C57Bl/6 mice, Immunobiology 221 (1) (2016) 103–115.
[16] A. Hernández, A. Nieto, Induction of protective immunity against murine secondary hydatidosis, Parasite Immunol. 16 (10) (1994) 537–544.
[17] F.J. Bikker, A.J. Ligtenberg, C. End, et al., Bacteria binding by DMBT1/SAG/gp-340 is confined to the VEVLXXXXW motif in its scavenger receptor cysteine-rich domains, J. Biol. Chem. 279 (46) (2004) 47699–47703.
[18] M. Martínez-Florensa, C. Català, M. Velasco-de-Andrés, et al., Conserved bacterial-binding peptides of the scavenger-like human lymphocyte receptor CD6 protect from mouse experimental sepsis, Front. Immunol. 9 (2018) 627.
[19] Y. Hamma-Kourbali, O. Bermek, I. Bernard-Pierrot, et al., The synthetic peptide P111-136 derived from the C-terminal domain of heparin affin regulatory peptide inhibits tumour growth of prostate cancer PC-3 cells, BMC Cancer 11 (2011) 212.
[20] T. Masson, M.L. Fabre, M.L. Ferrelli, et al., Protein composition of the occlusion bodies of *Epinotia aporema* granulovirus, PLoS One 14 (2) (2019) e0207735.
[21] J.J. Almagro-Armenteros, C.K. Sønderby, S.K. Sønderby, et al., DeepLoc: prediction of protein subcellular localization using deep learning, Bioinformatics 33 (21) (2017) 3387–3395.
[22] S. Miles, M. Portela, M. Cyrklaff, et al., Combining proteomics and bioinformatics to explore novel tegumental antigens as vaccine candidates against *Echinococcus granulosus* infection, J. Cell. Biochem. 120 (9) (2019) 15320–15336.
[23] S. Miles, J. Magnone, M. Cyrklaff, et al., Linking murine resistance to secondary cystic echinococcosis with antibody responses targeting *Echinococcus granulosus* tegumental antigens, Immunobiology 225 (3) (2020), 151916.
[24] Y. Ishihama, Y. Oda, T. Tabata, et al., Exponentially modified protein abundance index (emPAI) for estimation of absolute protein amount in proteomics by the number of sequenced peptides per protein, Mol. Cell. Proteomics 4 (9) (2005) 1265–1272.
[25] A. Brännström, M. Sankala, K. Tryggvason, T. Pikkarainen, Arginine residues in domain V have a central role for bacteria-binding activity of macrophage scavenger receptor MARCO, Biochem. Biophys. Res. Commun. 290 (5) (2002) 1462–1469.
[26] B.O. Fabriek, R. van Bruggen, D.M. Deng, et al., The macrophage scavenger receptor CD163 functions as an innate immune sensor for bacteria, Blood 113 (4) (2009) 887–892.
[27] M. Ritter, O. Gross, S. Kays, et al., *Schistosoma mansoni* triggers Dectin-2, which activates the Nlrp3 inflammasome and alters adaptive immune responses, Proc. Natl. Acad. Sci. U. S. A. 107 (47) (2010) 20459–20464.
[28] R.A. Paveley, S.A. Aynsley, J.D. Turner, et al., The mannose receptor (CD206) is an important pattern recognition receptor (PRR) in the detection of the infective stage of the helminth *Schistosoma mansoni* and modulates IFNγ production, Int. J. Parasitol. 41 (13–14) (2011) 1335–1345.
[29] T.L. Hsu, G. Lin, A. Koizumi, et al., The surface carbohydrates of the *Echinococcus granulosus* larva interact selectively with the rodent Kupffer cell receptor, Mol. Biochem. Parasitol. 192 (1–2) (2013) 55–59.
[30] H.E. Ponichtera, M.J. Stadecker, Dendritic cell expression of the C-type lectin receptor CD209a: a novel innate parasite-sensing mechanism inducing Th17 cells that drive severe immunopathology in murine schistosome infection, Exp. Parasitol. 158 (2015) 42–47.
[31] J. Rzepecka, S. Rausch, C. Klotz, et al., Calreticulin from the intestinal nematode *Heligmosomoides polygyrus* is a Th2-skewing protein and interacts with murine scavenger receptor-A, Mol. Immunol. 46 (6) (2009) 1109–1119.
[32] L.M. Fry, D.A. Schneider, C.W. Frevert, et al., East Coast fever caused by *Theileria parva* is characterized by macrophage activation associated with vasculitis and respiratory failure, PLoS One 11 (5) (2016), e0156004.
[33] H.A. Silva, G.S. Lima, M.C. Boité, et al., Expression of annexin A1 in *Leishmania*-infected skin and its correlation with histopathological features, Rev. Soc. Bras. Med. Trop. 48 (5) (2015) 560–567.
[34] P.B. Bassi, F.F. de Araújo, G.C. Garcia, et al., Parasitological and immunological evaluation of cattle experimentally infected with *Trypanosoma vivax*, Exp. Parasitol. 185 (2018) 98–106.
[35] R.K. Peckham, R. Brill, D.S. Foster, et al., Two distinct populations of bovine IL-17$^+$ T-cells can be induced and WC1$^+$IL-17$^+$γδ T-cells are effective killers of protozoan parasites, Sci. Rep. 4 (2014) 5431.
[36] Q. Pang, H. Jin, Z. Man, et al., Radical versus conservative surgical treatment of liver hydatid cysts: a meta-analysis, Front Med 12 (3) (2018) 350–359.
[37] M. Siles-Lucas, A. Hemphill, Cestode parasites: application of in vivo and in vitro models for studies on the host-parasite relationship, Adv. Parasitol. 51 (2002) 133–230.
[38] A. Baz, G.M. Ettlin, S. Dematteis, Complexity and function of cytokine responses in experimental infection by *Echinococcus granulosus*, Immunobiology 211 (1–2) (2006) 3–9.
[39] F. Tamarozzi, M. Mariconti, A. Neumayr, E. Brunetti, The intermediate host immune response in cystic echinococcosis, Parasite Immunol. 38 (3) (2016) 170–181.
[40] M. Siles-Lucas, M. Merli, B. Gottstein, 14-3-3 proteins in *Echinococcus*: their role and potential as protective antigens, Exp. Parasitol. 119 (4) (2008) 516–523.
[41] V. Müller-Schollenberger, W. Beyer, P. Schnitzler, et al., Immunisation with *Salmonella typhimurium*-delivered glyceraldehyde-3-phosphate dehydrogenase protects mice against challenge infection with *Echinococcus multilocularis* eggs, Int. J. Parasitol. 31 (13) (2001) 1441–1449.
[42] M. Zhu, X. Wang, H. Wang, et al., Mechanism of protective immunity by vaccination with recombinant *Echinococcus granulosus* glutathione S-transferase (Chinese strain) in mice, Exp Ther Med 10 (3) (2015) 1127–1132.
[43] E. Ortona, P. Margutti, F. Delunardo, et al., Screening of an *Echinococcus granulosus* cDNA library with IgG4 from patients with cystic echinococcosis identifies a new tegumental protein involved in the immune escape, Clin. Exp. Immunol. 142 (3) (2005) 528–538.
[44] Y. Zheng, X. Guo, M. Su, et al., Identification of emu-TegP11, an EF-hand domain-containing tegumental protein of *Echinococcus multilocularis*, Vet. Parasitol. 255 (2018) 107–113.
[45] S.H. Xiao, J.J. Feng, H.F. Guo, et al., Effects of mebendazole, albendazole, and praziquantel on fumarate hydratase, pyruvate kinase, and phosphoenolpyruvate carboxykinase of *Echinococcus granulosus* cyst wall harbored in mice, Zhongguo Yao Li Xue Bao 15 (1) (1994) 69–72.
[46] M.S. Pearson, D.A. Pickering, L. Tribolet, et al., Neutralizing antibodies to the hookworm hemoglobinase Na-APR-1: implications for a multivalent vaccine against hookworm infection and schistosomiasis, J. Infect. Dis. 201 (10) (2010) 1561–1569.
[47] P.J. Skelly, J.W. Kim, J. Cunningham, C.B. Shoemaker, Cloning, characterization, and functional expression of cDNAs encoding glucose transporter proteins from the human parasite *Schistosoma mansoni*, J. Biol. Chem. 269 (6) (1994) 4247–4253.
[48] W.M. Kemp, P.R. Brown, S.C. Merritt, R.E. Miller, Tegument-associated antigen modulation by adult male *Schistosoma mansoni*, J. Immunol. 124 (2) (1980) 806–811.
[49] E. Linder, C. Thors, *Schistosoma mansoni*: praziquantel-induced tegumental lesion exposes actin of surface spines and allows binding of actin depolymerizing factor, gelsolin. Parasitology 105 (Pt1) (1992) 71–79.
[50] S. La-Rocca, J. Farias, C. Chalar, et al., *Echinococcus granulosus*: insights into the protoscolex F-actin cytoskeleton, Acta Trop. 199 (2019) 105122.
[51] K.R. Lorenzatto, K.M. Monteiro, R. Paredes, et al., Fructose-bisphosphate aldolase and enolase from *Echinococcus granulosus*: genes, expression patterns and protein interactions of two potential moonlighting proteins, Gene 506 (1) (2012) 76–84.

[52] J.S. McCarthy, M. Wieseman, J. Tropea, et al., *Onchocerca volvulus* glycolytic enzyme fructose-1,6-bisphosphate aldolase as a target for a protective immune response in humans, Infect. Immun. 70 (2) (2002) 851–858.

[53] M. Saber, T. Diab, O. Hammam, et al., Protective and anti-pathology effects of Sm fructose-1,6-bisphosphate aldolase-based DNA vaccine against *Schistosoma mansoni* by changing route of injection, Korean J Parasitol 51 (2) (2013) 155–163.

[54] Y. Yang, X. Bai, C. Li, et al., Molecular characterization of Fructose-1,6-bisphosphate Aldolase from *Trichinella spiralis* and its potential in inducing immune protection, Front. Cell. Infect. Microbiol. 9 (2019) 122.

[55] A.J. Ligtenberg, N.G. Karlsson, E.C. Veerman, Deleted in malignant brain tumors-1 protein (DMBT1): a pattern recognition receptor with multiple binding sites, Int. J. Mol. Sci. 11 (12) (2010) 5212–5233.